Control theory for infinite dimensional dynamical systems and applications to falling liquid film flows

A thesis submitted for the Imperial College London degree of

Doctor of Philosophy in Mathematics

by

Susana Teresa Noronha Moreira Antunes Gomes

Department of Mathematics

Imperial College London

2016

I certify that this thesis, and the research to which it refers, are the product of my own work, and that any ideas or quotations from the work of other people, published or otherwise, are fully acknowledged in accordance with the standard referencing practices of the discipline.

Signed: Susana Gomes

Copyright

"O caos é uma ordem por decifrar"

José Saramago

"Chaos is merely order waiting to be deciphered"

José Saramago

To my parents, Teresa and Agostinho,
and my sister, Inês.

Acknowledgements

First and foremost, I want to thank my supervisors, Professors Greg Pavliotis and Demetrios Papageorgiou, for giving me the great opportunity to work here and introducing me to control theory and fluid dynamics. They were always supportive and encouraging during my PhD, giving me the time to learn when I needed and the freedom to choose my research directions and work in my pace and in my own way. Their help was and is invaluable on the pursuit of my career goals.

Professor Serafim Kalliadasis from the Chemical Engineering Department was also a source of support and encouragement. I wish to thank him for all the suggestions and comments that improved my work, and for including me in his group and giving me the opportunity to present my work for them and their visitors. Alice Thompson and Marc Pradas were a great source of help during the last years of my PhD. They taught me everything I know about hydrodynamic stability, thin films and bifurcation/continuation theory and also helped me with some of the numerics used in this thesis. Most importantly, they were always available every time I needed help or advice.

I would also like to thank everyone in the Department of Mathematics of the University of Coimbra, who one way or another contributed for me getting this far. In particular, Professors M. Paula de Oliveira, José Augusto Ferreira and Luís Nunes Vicente offered invaluable advice and guidance during my Masters years and the PhD application process, and before and during my first few weeks in London.

During the last 3.5 years I got to meet and interact with many people that made my experience in London much more enjoyable. Anna, Elena, Elias and Radu were a great initial support and source of many interesting discussions, as well as great travel companions. Adam, Alex, Hannah, Julius, Lisa, Michael and Vikas never let life in the office become boring. They were always available to discuss work, but also for non-academic discussions during endless coffee breaks and lunches. I am also very grateful to Marina, for reminding

me of home, and Eliza, for many stress-releasing runs and yoga adventures.

My friends in Portugal always make time for me in their busy lives when I go home, and always make me feel like I've never left. Special thanks to Ana Luísa, Bruno Filipe, Catarina, Fábio, Joana, Rui and Vânia.

Finally, I am also grateful to my family for their support and for always trying to understand what I am doing here. Most importantly, I am very grateful to my parents for their constant support and understanding, and for doing everything they can so that I can pursue my goals.

This research was funded by the Department of Mathematics, Imperial College London through a Roth PhD Scholarship. I would like to acknowledge additional funding by the American Physical Society for a travel grant to attend the 68^{th} APS-DFD Meeting in Boston and the Institute for Mathematics and its Applications in the University of Minnesota for funding my visit there to attend their Workshop on Computational Methods for Control of Infinite-dimensional Systems.

Susana Gomes

Abstract

In this thesis, we study the problem of controlling the solutions of various nonlinear PDE models that describe the evolution of the free interface in thin liquid films flowing down inclined planes. We propose a control methodology based on linear feedback controls, which are proportional to the deviation between the current state of the system and a prescribed desired state. We first derive the controls for weakly nonlinear models such as the Kuramoto-Sivashinsky equation and some of its generalisations, and then use the insight that the analytical results obtained there provide us to derive suitable generalisations of the controls for reduced-order long-wave models. We use two long-wave models to test our controls: the first order Benney equation and the first order weighted-residual model, and compare some linear stability results with the full 2-D Navier–Stokes equations. We find that using point actuated controls it is possible to stabilise the full range of solutions to the generalised Kuramoto-Sivashinsky equation, and that distributed controls have a similar effect on both long-wave models. Furthermore, point-actuated controls are efficient when stabilising the flat solution of both long-wave models. We extend our results to systems of coupled Kuramoto-Sivashinsky equations and to stochastic partial differential equations that arise by adding noise to the weakly nonlinear models.

List of Publications

The material presented in this thesis is the outcome of a collaboration between the author, Susana N. Gomes, and her supervisors, Professors Grigorios A. Pavliotis and Demetrios T. Papageorgiou. Parts of the thesis resulted from further collaborations with Dr Marc Pradas, Dr Alice B. Thompson, Dr Stephen J. Tate and Professor Serafim Kalliadasis. The following publications and articles in preparation are the result of this work:

[90] Susana N. Gomes, Marc Pradas, Serafim Kalliadasis, Demetrios T. Papageorgiou and Grigorios A. Pavliotis. Controlling Spatiotemporal Chaos in Active Dissipative-Dispersive Nonlinear Systems. *Phys. Rev. E*, 92:022912 (2015).

[89] Susana N. Gomes, Demetrios T. Papageorgiou and Grigorios A. Pavliotis. Stabilising nontrivial solutions of the generalised Kuramoto-Sivashinsky equation using feedback and optimal control. *IMA J. Appl. Math.*, doi:10.1093/imamat/hxw011 (2016)

[205] Alice B. Thompson, Susana N. Gomes, Grigorios A. Pavliotis and Demetrios T. Papageorgiou. Stabilising falling liquid film flows using feedback control. *Phys. Fluids*, 28:012107 (2016)

[91] Susana N. Gomes, Marc Pradas, Serafim Kalliadasis, Demetrios T. Papageorgiou and Grigorios A. Pavliotis. Controlling roughening processes in the stochastic Kuramoto-Sivashinsky equation. *Submitted to Physica D.*

[92] Susana N. Gomes and Stephen. J. Tate. Solution of a Lyapunov type matrix equation arising in the control of stochastic partial differential equations. *Submitted to IMA J. Appl. Math.*.

Table of contents

List of Tables

List of Figures

Chapter 1

Introduction

In this chapter we introduce the problems studied in this thesis. We start with an introduction and motivation for the control of thin film flows and for the introduction of noise in our models. We will then take a closer look at the hierarchy of models for the description of thin film flows and explain how we are going to use it to construct our controls. We will also review the relevant results in the literature, summarising the existing techniques for both long-wave models and weakly nonlinear models, with and without noise. Finally, we outline the objectives of the thesis, discuss the main results of our work and describe the structure of the thesis.

1.1 Overview of the subject and applications

The ability to control a desired particular dynamic state in systems exhibiting chaos is a challenging and fundamental problem in nonlinear science that has attracted considerable attention over the last decades [27, 43, 166, 192]. Chaos and its control are pertinent in a wide variety of natural phenomena and technological applications, from turbulent flows [65], coating processes [95], and reaction-diffusion systems [145] to spatiotemporal instabilities in lasers [114] and cardiac arrhythmias [41], to name but a few. Not surprisingly, many different approaches have been proposed to control, up to some extent, different aspects of chaotic dynamics. Most of these approaches were attempted for the case of maps or ordinary differential equations (ODEs), and this case has been thoroughly explored - see [27] for a review of the subject. In particular, it is known how to find strange chaotic attractors [94], stabilise unstable periodic orbits in low dimensional systems [198], direct chaotic trajectories to any desired state using small perturbations [166, 192] and how to control chaos in a high dimensional chaotic time signal, without assuming any knowledge of the dynamics [11].

Despite the considerable attention that chaos control for maps or ODEs has received, several important problems, such as the control of spatiotemporal chaos for partial differential equations (PDEs), which are infinite dimensional dynamical systems, have not yet been resolved. In this thesis, we will focus on the control of PDEs whose solutions exhibit spatiotemporal chaotic behaviour, systems of coupled PDEs of this type, and also stochastic partial differential equations (sPDE) that are obtained from these equations by the addition of noise. The common factor between all the equations we present is that they are all obtained in different asymptotic limits when modelling falling liquid films flowing down an inclined planar wall - see Fig. 1.1. This is a classical problem in fluid mechanics, and it is well known that the solution corresponding to a flat film, which is known as Nusselt solution, is stable when the film layer is sufficiently thin. However, it becomes unstable when the Reynolds number is above a critical value which depends on the inclination angle θ. In our case, the Reynolds number depends on the undisturbed interface flow speed, and is going to be defined later in this Chapter. The development of thin film models for this system, and the behaviour exhibited therein, has recently been reviewed in [54, 120].

In addition to acting as a paradigm for understanding transitions between different types of dynamical behaviour, the flow of thin films has a broad range of industrial applications. We note particularly coating flows [227], where a uniform coating of a flat or shaped sub-

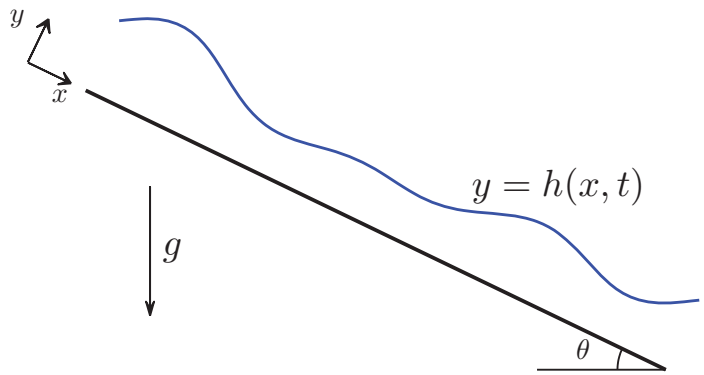

Figure 1.1: Sketch of a thin liquid film falling down a planar wall. We consider a fluid layer bounded on $y = 0$ by a rigid wall inclined at an angle θ to the horizontal, and at $y = h(x)$ by a free surface.

strate is desired, and heat and mass transfer, which is typically enhanced by mixing associated with interfacial waves [120]. These contrasting applications lead naturally to the desire to control the system dynamics, and in an ideal situation we would like to be able to drive the system into the full range of regimes.

After the onset of instability, the system initially exhibits waves that propagate down the slope, followed by more complicated behaviour that can eventually lead to three-dimensional (3-D) spatiotemporal chaos (see Fig. 1.2), which is precisely the behaviour we want to suppress. In order to do that, we will apply linear feedback controls [234], which represent our ability of injecting/removing fluid through a finite number of slots in the wall. Intuitively, if we can remove fluid from places where the fluid layer is too thick, or inject it where it is too thin, we will be able to obtain the desired state.

The first instability to develop as the film thickness increases is in the form of long-wave perturbations which propagate down the slope, and have no transverse component. The long-wave, streamwise nature of the instability means that thin film flows are often studied using reduced-dimensional models based on long-wave assumptions and neglecting variation in the transverse direction (and hence also neglecting any effect of side walls). A number of different models are available, which differ most fundamentally in the manner in which inertial effects are incorporated. Despite the fact that these are reduced-dimensional models, and therefore much easier to solve than the full Navier–Stokes system, the nonlinearities present in the equations make it hard to obtain analytical results for these models, and there-

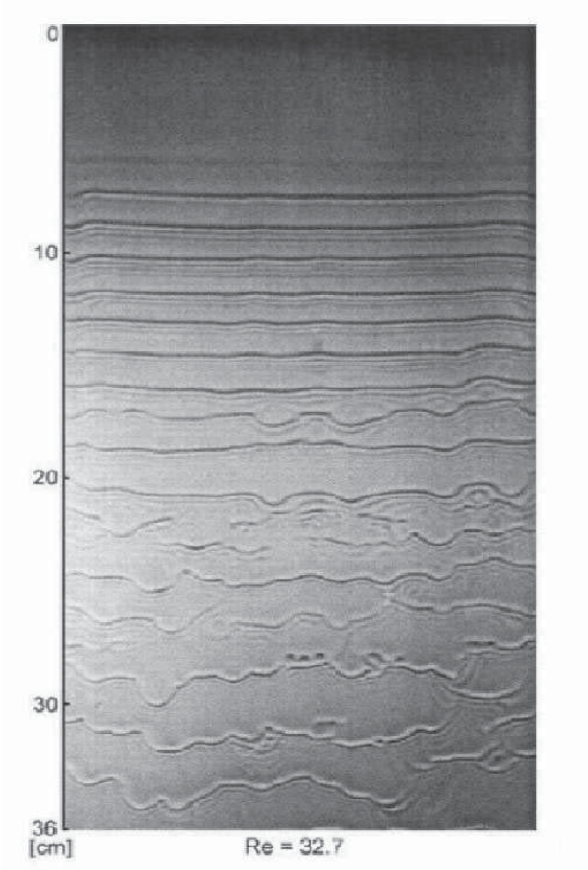

Figure 1.2: Shadow image of waves naturally occurring on a falling film at $R = 32.7$ without controlled perturbations imposed on the film flow. Reproduced from [173].

fore a weakly nonlinear asymptotic analysis can be performed, obtaining a simpler prototype model which provides a good description of the dynamics of the interface of thin films close to criticality. We consider two different first-order long-wave models: the Benney equation and the weighted-residual (WR) equation, which were extended by [206] to include the effect of suction and injection through the planar wall. These two long-wave models are identical at zero Reynolds number, and both agree with the Navier–Stokes system regarding the critical Reynolds number for the onset of instability. Furthermore, both models reduce to the well known Kuramoto-Sivashinsky (KS) equation under weakly nonlinear analysis - see Section 1.2 for further details. However, the structures of these models differ significantly, in particular the number of degrees of freedom. The Benney and KS equations are single evolution equations for the interface height $h(x,t)$, while the weighted-residual model comprises coupled equations for $h(x,t)$, and the independently-evolving down-slope flux $q(x,t)$. It is important to notice, however, that the Navier–Stokes equations at finite Reynolds number

allow evolution of $h(x,t)$ together with evolution of the vector-valued velocity field at every point within the fluid.

The controls we will apply in the systems studied here model blowing and suction of fluid through the planar wall. We will consider two cases: in the simplest scenario, the controls are distributed along the domain, which allows us to obtain linear stability results for both the flat solution and nontrivial steady states and travelling wave solutions, even in the case of long wave models; but in more realistic cases, the control actuation is only possible at a finite number of points in the domain and we consider the effect of this type of controls on the flat solution of long-wave models and in both the flat and nontrivial solutions of the Kuramoto-Sivashinsky equation. Furthermore, observations of the current state are not available everywhere and we will also take this into account in our analysis.

Physical systems are naturally susceptible to the effects of random noise. In the case of thin films, this is usually an effect of thermal noise [60, 96], but in control systems it can also be an effect of noise in the observations of the system state, the application of the controls or uncertainty in parameters of the system. There are many ways in which the effects of noise can be studied for thin films, and we will focus on the case of roughening processes, which are characterised by a time-fluctuating 'rough' interface, the dynamics of which is described in terms of a stochastic partial differential equation. Examples are found in a broad range of applications, which include surface growth dynamics such as surface erosion by ion sputtering processes [31, 32, 106, 110], fluid flow in porous media [4, 177, 199], fracture dynamics [29]; and, as mentioned before, thin film dynamics [24, 60, 96, 120], to name but a few. Understanding the dynamics of the fluctuating interface in terms of its roughening properties, which often exhibit scale-invariant universal features, has become an important problem in statistical physics which has received considerable attention over the last decades [14].

1.2 Governing equations and hierarchy of models

We will now present the equations that we will consider in this thesis. The full details on the derivation of the long-wave equations are in [206], where the authors extended the Benney [21] and weighted-residual [187] methodologies to the controlled case. We consider a thin layer of fluid, with mean thickness h_s, flowing down a plane inclined at an angle θ to the horizontal. We adopt a coordinate system such that x is the down-slope coordinate, and

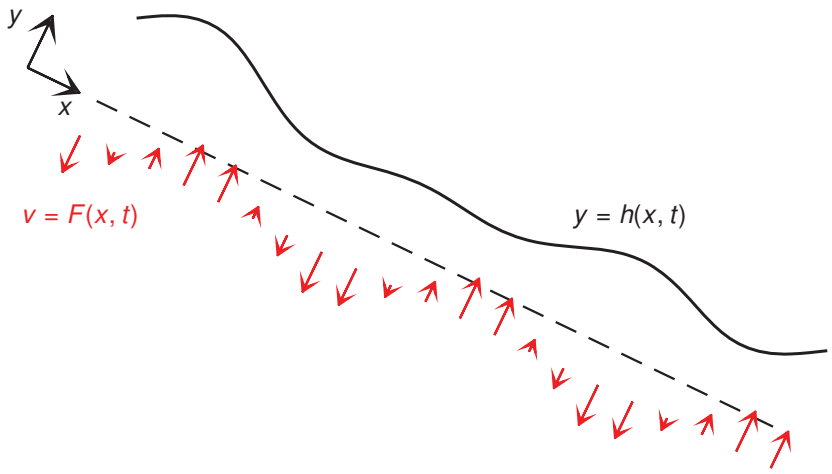

Figure 1.3: Sketch of flow domain showing coordinate system. We consider a fluid layer, with mean height h_s, bounded on $y = 0$ by a rigid wall inclined at an angle θ to the horizontal, and at $y = h(x)$ by a free surface. Fluid is injected through the wall, with velocity $v = F(x, t)$ which changes in time in response to fluctuations of the free surface.

y is the perpendicular distance from the wall, as shown in Fig. 1.3. The upper interface of the fluid is a free surface, located at $y = h(x, t)$. The lower boundary of the fluid is a rigid wall, through which fluid may be injected or removed.

The two-dimensional (2-D) Navier–Stokes equations admit a solution which is uniform in the streamwise direction, known as the Nusselt solution [162], for which the surface velocity is $U_s = \frac{\rho g h_s^2 \sin\theta}{2\eta}$, where ρ is the fluid density, g the acceleration due to gravity, h_s the mean film thickness and η the dynamic viscosity of the fluid. We non-dimensionalise the problem based on the length scale h_s and the velocity scale U_s, and define the Reynolds number R and the capillary number C based on the velocity U_s:

$$R = \frac{\rho h_s U_s}{\eta}, \quad C = \frac{\eta U_s}{\gamma}, \tag{1.1}$$

where γ is the coefficient of surface tension at the air-fluid interface. Subsequent equations are all dimensionless.

The main goal of a successful control methodology would be to solve the 2-D Navier–Stokes equations, with velocity $\mathbf{u}(x, y, t) = (u, v)$, and fluid pressure $p(x, y, t)$. In this case,

the momentum and continuity equations are

$$R\left(u_t + uu_x + vu_y\right) = -p_x + 2 + u_{xx} + u_{yy}, \tag{1.2a}$$

$$R\left(v_t + uv_x + vv_y\right) = -p_y - 2\cot\theta + v_{xx} + v_{yy} \tag{1.2b}$$

and

$$u_x + v_y = 0. \tag{1.3}$$

The boundary conditions at the wall are given by

$$u = 0, \quad v = F(x,t). \tag{1.4}$$

Here the function $F(x,t)$ represents the injection velocity normal to the wall, $y = 0$. Note that we assume that the injection of fluid does not affect the no-slip boundary condition on the wall. At the interface, $y = h(x,t)$, the tangential and normal components of the dynamic stress balance condition yield

$$\left(v_x + u_y\right)\left(1 - h_x^2\right) + 2h_x\left(v_y - u_x\right) = 0, \tag{1.5}$$

$$p - p_a - \frac{2}{1+h_x^2}\left(v_y + u_x h_x^2 - h_x\left(v_x + u_y\right)\right) = -\frac{1}{C}\frac{h_{xx}}{(1+h_x^2)^{3/2}}, \tag{1.6}$$

where p_a is the atmospheric pressure, assumed constant. The system is closed by the kinematic boundary condition at the free surface

$$h_t = v - uh_x. \tag{1.7}$$

Defining the down slope flux q

$$q(x,t) = \int_0^h u(x,y,t)\,\mathrm{d}y, \tag{1.8}$$

integrating (1.3), and applying the boundary conditions (1.4) and (1.7), yields the mass conservation equation in terms of q:

$$h_t - F(x,t) + q_x = 0. \tag{1.9}$$

1.2.1 Long-wave models for thin film flows

In the long wave limit, the solutions are characterised by having large wavelength when compared to its mean thickness, and therefore when deriving the models it is usual to look for solutions with wavelength $L \gg 1$ and define the long-wave parameter $\epsilon = 1/L$. The first step then is to rescale the Navier–Stokes equations (1.2)-(1.7) according to

$$X = \epsilon x, \quad T = \epsilon t, \quad v = \epsilon V, \quad C = \epsilon^2 \widehat{C}, \quad F = \epsilon f, \tag{1.10}$$

where $\epsilon \ll 1$, obtaining

$$\epsilon R \left(u_T + u u_X + V u_y\right) = -\epsilon p_X + 2 + \epsilon^2 u_{XX} + u_{yy}, \tag{1.11a}$$

$$\epsilon^2 R \left(V_T + u V_X + V V_y\right) = -p_y - 2\cot\theta + \epsilon^3 V_{XX} + \epsilon V_{yy} \tag{1.11b}$$

$$u_x + v_y = 0. \tag{1.11c}$$

The boundary conditions at the wall are given by

$$u = 0, \quad V = f(x,t), \tag{1.12}$$

and at the interface $y = h(X,T)$ we have

$$\left(\epsilon^2 V_X + u_y\right)\left(1 - \epsilon^2 h_X^2\right) + 2\epsilon h_X \left(\epsilon V_y - \epsilon u_X\right) = 0, \tag{1.13}$$

$$p - p_a - \frac{2}{1+\epsilon^2 h_x^2}\left(\epsilon V_y + \epsilon^3 u_X h_X^2 - \epsilon h_X \left(\epsilon^2 V_X + u_y\right)\right) = -\frac{1}{\hat{C}} \frac{h_{XX}}{(1+\epsilon^2 h_X^2)^{3/2}} \tag{1.14}$$

The rescaled equation (1.9) is

$$h_T - f(X,T) + q_X = 0. \tag{1.15}$$

First order Benney equation

After expanding u, V, p and q in powers of ϵ,

$$u = u_0 + \epsilon u_1 + O(\epsilon^2), \qquad V = V_0 + \epsilon V_1 + O(\epsilon^2), \tag{1.16}$$

$$p = p_0 + \epsilon p_1 + O(\epsilon^2), \qquad q = q_0 + \epsilon q_1 + O(\epsilon^2), \tag{1.17}$$

and substituting in (1.11)-(1.15), we obtain the following leading order solution

$$u_0 = y(2h - y), \quad V_0 = f(X,T) - y^2 h_X, \quad p_0 = p_a - \frac{h_{XX}}{\hat{C}} + 2(h-y)\cot\theta, \tag{1.18}$$

with the flux being

$$q_0 = \int_0^h u_0 \, dy = \frac{2h^3}{3}, \tag{1.19}$$

which leads to the equation

$$h_T - f(X,T) + 2h^2 h_X = O(\epsilon). \tag{1.20}$$

We then substitute the leading order solution into the $O(\epsilon)$ part of the rescaled equations and integrate to obtain u_1:

$$u_1 = \frac{y}{2}(y-2h)\left(2h\cot\theta - \frac{h_{XX}}{\hat{C}}\right)_X + \\ + R\left[(h_T - f)\left(\frac{y^3}{3} - h^2 y\right) + \frac{2hh_X}{3}\left(\frac{y^4}{4} - h^3 y\right) + hy(y-2h)f\right]. \tag{1.21}$$

We can then find the first order correction for q:

$$q_1 = \int_0^h u_1 \, dy = -\frac{h^3}{3}\left(2h\cot\theta - \frac{h_{XX}}{\hat{C}}\right)_X + R\left(-\frac{5h_T h^4}{12} - \frac{3h^6 h_X}{10} - \frac{h^4 f}{4}\right). \tag{1.22}$$

We eliminate h_T from (1.22) using (1.20) and obtain the Benney equation for q:

$$q(X,T) = q_0 + \epsilon q_1 + O(\epsilon^2) = \\ \frac{2h^3}{3} + \epsilon\left[\frac{h^3}{3}\left(-2h_X\cot\theta + \frac{h_{XXX}}{\widehat{C}}\right) + R\left(\frac{8h^6 h_X}{15} - \frac{2h^4 f}{3}\right)\right] + O(\epsilon^2), \tag{1.23}$$

which can be recasted into the original variables to obtain

$$q(x,t) = \frac{h^3}{3}\left(2 - 2h_x\cot\theta + \frac{h_{xxx}}{C}\right) + R\left(\frac{8h^6 h_x}{15} - \frac{2h^4 F}{3}\right) = Z(h,F), \tag{1.24}$$

where Z is a (nonlinear) differential operator, which is applied to h and F. The coupling of (1.24) to (1.9) yields a closed system for the evolution of the interface height $h(x,t)$. We note that the appearance of terms involving F in (1.24) is a consequence of the choice of F

with respect to the long wave scaling. By supposing F to be an order smaller with respect to ϵ, we can replace (1.24) with the simpler version:

$$q(x,t) = \frac{h^3}{3}\left(2 - 2h_x \cot\theta + \frac{h_{xxx}}{C}\right) + \frac{8Rh^6 h_x}{15}. \tag{1.25}$$

In this limit, the only effect of F on the system dynamics is via the mass conservation equation (1.9).

First order weighted-residual model

In the Benney model, the flux q is slaved to the interface height h. Alternatively, following the weighted-residual methodology developed by [187], the flux q gains its own evolution equation, so that time derivatives of both h and q appear in the equations. In this methodology, ϵ is considered as an ordering parameter, rather than being a variable with respect to which the solutions are expanded: for the first order weighted residuals equations we retain terms up to order ϵ in equations (1.11)-(1.15), obtaining

$$\epsilon R\left(u_T + uu_X + Vu_y\right) = -\epsilon p_X + 2 + u_{yy}, \tag{1.26a}$$

$$0 = -p_y - 2\cot\theta + \epsilon V_{yy} \tag{1.26b}$$

The mass conservation equation and boundary conditions at the wall remain the same, while the boundary conditions at $y = h(X,T)$ become

$$u_y = 0, \tag{1.27}$$

$$p = p_a + 2\epsilon u_X - \frac{h_{XX}}{\hat{C}}, \tag{1.28}$$

where we used mass conservation to write $V_y = -u_X$. We can then integrate the rescaled $y-$momentum equation (1.26b) to obtain an expression for p:

$$p = p_a + 2(h-y)\cot\theta - \frac{h_X X}{\hat{C}} - \epsilon u_X - 2\epsilon h_x u_y, \tag{1.29}$$

which we can then substitute in the $x-$momentum equation (1.26a).

The weighted-residual methodology then assumes that u can be expanded in terms of basis functions ϕ_j satisfying the no-slip boundary condition on the wall and zero tangential

stress in the interface,

$$u = \sum_j a_j(X,T)\phi_j(\bar{y}), \quad \phi_j(z) = z^{j+1} - \left(\frac{j+1}{j+2}\right) z^{j+2}, \quad \bar{y} = \frac{y}{h(X,T)}. \tag{1.30}$$

We can then use the functions ϕ_j as test functions and integrate. We obtain

$$\epsilon R \int_0^h \phi_n(\bar{y})(u_{0T} + u_0 u_{0X} + V_0 u_{0y})\, dy = \\ = \left(-\epsilon\left(2h\cot\theta - \frac{h_{XX}}{\bar{C}}\right)_X + 2\right)\int_0^h \phi_n(\bar{y})\, dy + \int_0^h \phi_n(\bar{y}) u_{yy}\, dy,$$

where

$$u_0(X,y,T) = \frac{3q}{h}\phi_0(\bar{y}), \quad V_0(X,y,T) = f(X,T) - \int_0^y u_{0X}(X,y',T)\, dy'. \tag{1.31}$$

We then set $n = 0$ and integrate by parts to obtain

$$\epsilon R\left(\frac{2}{5}q_T - \frac{23}{40}\frac{qh_T}{h} + \frac{111}{280}\frac{qq_X}{h} - \frac{18}{35}\frac{q^2 h_X}{h} + \frac{3qf}{8h}\right) = \left(-\epsilon\left(2h\cot\theta - \frac{h_{XX}}{\bar{C}}\right)_X + 2\right)\frac{h}{3} - \frac{q}{h^2}. \tag{1.32}$$

We can now use (1.20) again to eliminate h_T and obtain the equation for q:

$$\frac{2\epsilon R h^2}{5} q_T + q = \frac{2h^3}{3} + \epsilon\left[\frac{h^3}{3}\left(-2h_X\cot\theta + \frac{h_{XXX}}{\widehat{C}}\right) + R\left(\frac{18q^2 h_X}{35} - \frac{34hqq_X}{35} + \frac{hqf}{5}\right)\right], \tag{1.33}$$

which can be rescaled back to the original variables, to obtain

$$\frac{2}{5}Rh^2 q_t + q = \frac{h^3}{3}\left(2 - 2h_x\cot\theta + \frac{h_{xxx}}{C}\right) + R\left(\frac{18q^2 h_x}{35} - \frac{34hqq_x}{35} + \frac{hqF}{5}\right) = Z(h,q,F), \tag{1.34}$$

which when coupled to (1.9) yields a closed system for $h(x,t)$ and $q(x,t)$. Initial conditions are required for both h and q. The Benney and weighted-residual models are identical when $R = 0$, and can be shown to agree at $O(1)$ and $O(\epsilon)$ in the long-wave limit [206].

1.2.2 Weakly nonlinear models

The long-wave models presented in the previous subsection represent good low-order approximations of thin film flows down inclined planes, but the complicated nonlinearities that

are present in the models make the task of obtaining analytical results practically impossible. This motivated the development of weakly nonlinear models of thin film flows. Weakly nonlinear models are a significant development in nonlinear dynamics and are widely used in fluid mechanics, plasma physics or reaction-diffusion systems. In the context of thin film flows, the validity of the models obtained depends on certain *a priori* assumptions (e.g., the derivation of these models assumes small amplitude waves) and therefore these models are only valid in limited regions of the parameter space. Nevertheless, the simplicity of the equations obtained makes them amenable to mathematical analysis, which allows for a better understanding of the dynamics in the appropriate parameter regime.

The weakly nonlinear model obtained for thin film flows down inclined planes is the so-called Kuramoto-Sivashinsky (KS) equation. This equation was derived in the context of reaction-diffusion systems by Kuramoto [132] and for flame front propagation by Sivashinsky [157, 195]. In the context of thin film flows, it is studied for the case of vertical walls by Sivashinsky and Michelson [194] and for the interface between two fluids by Hooper and Grimshaw [101]. The KS equation is a fourth order dissipative PDE, which has a Burgers nonlinearity. Its controlled version can be obtained from both equations (1.24) and (1.34). Starting from (1.24), we write $h(x,t) = 1+\epsilon U(\xi,\tau)$, $f(x,t) = \epsilon^2 g(\xi,\tau)$, where we rescaled the time and space variables so that the equations sit in the moving frame, $\xi = x - t$, $\tau = \epsilon t$, so that we obtain

$$U_\tau + 4UU_\xi + \left(\frac{8R}{15} - \frac{2}{3}\cot\theta\right)U_{\xi\xi} + \frac{1}{3\hat{C}}U_{\xi\xi\xi\xi} = g,$$

and after a new change of variables

$$U = \frac{1}{60}\sqrt{\frac{3\hat{C}\left(8R - 10\cot\theta\right)^3}{15}}U, \qquad \xi = \sqrt{\frac{5}{\hat{C}(8R - 10\cot\theta)}}X,$$
$$g = \frac{\hat{C}^2(8R - 10\cot\theta)^5}{16\cdot 3^3\cdot 5^5}G, \qquad \tau = \frac{75}{\hat{C}(8R - 2\cot\theta)^2}T$$

we obtain

$$u_T + u_{XXXX} + u_{XX} + uu_X = G, \tag{1.35}$$

where $X \in (0, L)$, $T > 0$ and L is the original wavelength of the perturbations. This equation can then be rescaled to different domain lengths: rescaling it to $x \in (0, 2\pi)$ peri-

odic domains introduces the instability parameter ν that we will discuss in Chapter 2, while rescaling it to $x \in (0,1)$ introduces the parameter λ that we will discuss below. The latter case is commonly seen in the context of boundary control problems, where the usual boundary conditions are Dirichlet, Neumann or mixed, rather than periodic.

It is important to notice that dispersion effects can be included in this equation [120] if when deriving the Benney equation we retain terms up to order ϵ^2 and/or derive a second order weighted-residual model. Furthermore, other effects such as electric fields can be included in the derivation [217].

Similarly to the uncontrolled case, even though the KS equation is not valid everywhere in the parameter space, it still provides us with (analytical) information about the behaviour of the system in certain parameter regions. We can therefore derive controls for this equation and hope that we can learn enough so that we can generalise these controls in order to apply them to the more complicated long-wave models, or to other models which we describe below.

Weakly nonlinear models are also useful for the analysis of multiphase flows in channels. For the case of three fluids confined in a channel and driven by gravity and/or a streamwise pressure gradient, Papaefthymiou *et al* [169] derived systems of coupled equations of the form

$$u_{it}+\sum_{j=1}^{2}\left[q_{ij}u_{jx}+\sum_{k=1}^{2}\epsilon\beta_{ijk}(u_ju_k)_x+\epsilon(Rs_{ij}+\cot\theta g_{ij})u_{jxx}+\frac{\epsilon}{C_i}d_{ij}u_{jxxxx}\right]=0, \quad (1.36)$$

for $i = 1, 2$, and where ϵ is again the long-wave parameter and all of the coefficients are rational polynomial functions of the physical parameters. This is a quite general system of PDEs, which was studied by extensive numerical experiments in [168] but for which there are no known analytical results. We study two particular cases of this system in Chapter 5.

1.2.3 The stochastic Kuramoto-Sivashinsky equation

We will also consider the stochastic Kuramoto-Sivashinsky (sKS) equation,

$$u_t = -\nu u_{xxxx} - u_{xx} - uu_x + \sigma\xi(x,t), \quad (1.37)$$

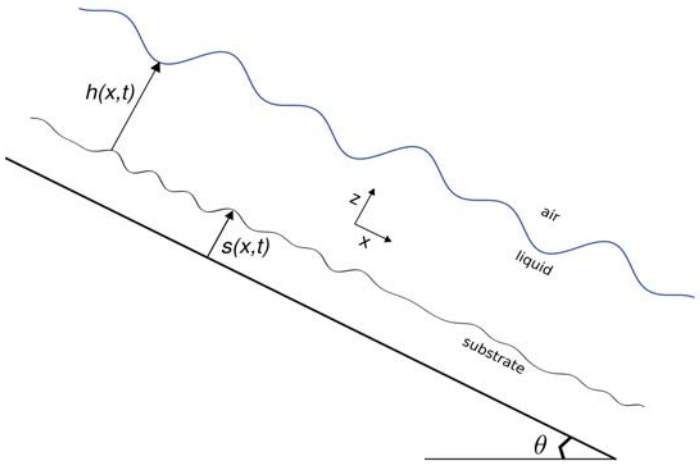

Figure 1.4: Sketch of a liquid film falling down an inclined plane with a vibrating disordered wall. The thickness of the film is denoted as $h(x,t)$ and the disordered wall position is denoted as $s(x,t)$. Reproduced from [179].

which has been derived in [179] as a weakly nonlinear asymptotic model for a liquid film falling down an inclined plane with a vibrating disordered wall - see Fig. 1.4. The term $\xi(x,t)$ denotes a Gaussian mean-zero spatiotemporal noise, which is taken to be white in time, and whose strength is controlled by the parameter σ:

$$\langle \xi(x,t)\xi(x',t')\rangle = \mathcal{G}(x-x')\delta(t-t'), \tag{1.38}$$

where $\mathcal{G}(x-x')$ represents its spatial correlation function.

The quadratic nonlinearity in Eq. (1.37) is typically referred to as Burgers nonlinearity. We note that an alternative version of Eq. (1.37) is found by making the change of variable $u=-h_x$, giving rise to

$$h_t = -\nu h_{xxxx} - h_{xx} + \frac{1}{2}(h_x)^2 + \sigma\eta(x,t), \tag{1.39}$$

where $\xi(x,t) = \partial_x \eta(x,t)$.

The main effect of this transformation is to change the dynamics of the mass $u_0(t) = \frac{1}{2\pi}\int_0^{2\pi} u(x,t)\,dx$ of the solution. Indeed, Eq. (1.37) with PBCs preserves the value of u_0 whereas as a consequence of the nonlinear term $(h_x)^2$, Eq. (1.39) does not conserve the mass $h_0(t) = \frac{1}{2\pi}\int_0^{2\pi} h(x,t)\,dx$. Both equations have received a lot attention over the last decades, with Eq. (1.37) being more appropriate in mass-conserved systems such as the dynamics of

thin liquid films [24, 60, 96, 120, 179], and Eq. (1.39) relevant in modeling surface growth processes such as surface erosion by ion sputtering processes [31, 32, 55, 56, 135, 151, 186].

It is also worth mentioning that the quadratic nonlinearity appearing in equation (1.39) is the same as that in the Kardar-Parisi-Zhang (KPZ) equation [97, 122]

$$h_t = h_{xx} + \frac{1}{2}(h_x)^2 + \sigma\eta(x,t). \tag{1.40}$$

In fact extensive work indicates that Eq. (1.39) and Eq. (1.40) are asymptotically equivalent, something referred to as the “Yakhot conjecture" [66, 182, 230]. Throughout the remainder of this thesis we will refer to Eq. (1.37) as the sKS equation with Burgers nonlinearity and Eq. (1.39) as the sKS equation with KPZ nonlinearity.

1.3 Stability and control of thin film flows

For flat homogeneous walls, a trivial solution of all of the models for thin film flows is a steady uniform flow, known as the Nusselt solution, in which the free interface is flat. As we mentioned already, this solution can be unstable in certain parameter regimes, e.g., if the inclination angle is too steep, or the fluid layer is too thick. This instability, and therefore the existence of other, possibly non-steady, states of the system, can be explored to achieve certain states that can be of benefit for different applications. Much of the thin-film literature focuses on the additional instabilities and flow modes that can occur in flows with heating and cooling [13], or on flows over steady non-uniform topography; both have direct applications in heat exchangers. Thermal effects and topography are often combined with each other [25, 189] or with electric fields [83, 213, 214, 217, 222].

The introduction of steady but spatially-varying topography can be used to create patterned steady states, which have slightly different stability properties to the corresponding unpatterned system. The steady states and dynamics of systems with wavy walls have been studied using various combinations of full computations, long-wave models, and experiments [81, 98, 174, 176, 190, 212]. The effect of topographical patterning on flow stability is quite subtle, and the critical Reynolds number can be increased or decreased depending on the system parameters and the choice of topography amplitude and wavelength. It is generally only possible to obtain significant modification to the critical Reynolds number by introducing large-amplitude topographical variations, and hence also large-amplitude defor-

mation of the free surface and flow. Steady topographical patterning falls into the category of open-loop control, where the controls to be applied are pre-determined.

Steady heating of the planar wall, either by heating the substrate uniformly [13, 210], locally [119], in an oscillating manner [189], or by point heaters [207] has a more direct effect in the stability of thin films. It is shown that local or point heating induce gradients of surface tension, which in turn promote the formation of waves or bumps in the heated region, which travel downstream. Similarly, distributed heating leads to steady state deformations, which enhance heat transfer. When combined with topography, Blyth and Bassom [25] have shown that for zero Reynolds number, small Péclet number and small amplitude topography, sinusoidal heating can flatten the interface, while large enough steady uniform heating induces the interface to be in phase with the wall shape, which would otherwise be out of phase. An important thing to notice, however, is that too much heating may lead to evaporation, which in turn can induce film breakup [13].

Thompson *et al* [206] used long wave models to study the effect of imposed, steady, spatially-periodic suction/injection on thin-film flow down an inclined plane. They found that the imposed suction always leads to non-uniform states, enables a non-trivial bifurcation structure and complicated time-dependent behaviour, and significantly alters the trajectories of particles in the flow, but has a relatively small effect on flow stability. Suction is, however, the only mechanism by which the net system mass can be modified, and so suction controls are the only way in which perturbations of infinite wavelength can be made better than neutrally stable.

Other physical mechanisms that have been investigated within the context of thin-film flow down inclined planes include chemical coatings or microstructure to induce effective slip [121], surfactants [26], porous [163, 204] or deformable [82] walls and magnetic fields [5]. All of these previous studies consider passive, predetermined, modifications to the system, rather than active feedback, and therefore their effect is on introducing additional solution states of the system, rather than affecting the stability of the existing ones.

It is well known from a control theory perspective that controls chosen in response to real-time observations of the system state are able to have a much stronger effect on flow stability than that caused by open-loop controls, and furthermore can do so without changing the nature of the steady state itself. Therefore we will consider this more efficient way of affecting the stability of a given system state by using feedback controls [234]. Feedback

control consists of a set of control actuators and response functions, where the response functions are constructed based on hypotheses regarding the dynamics of the uncontrolled system and its response to the control actuators. We will use linear feedback controls, in which the response functions are linear functions of the deviation of the observed state from the desired state. This agrees with the intuition that removing fluid from thicker areas, or injecting it in thinner regions will drive the system towards the desired state. We note that the main advantage of using (closed-loop) feedback controls is that the controls actively respond to the evolution of the system, as opposed to the passive (open-loop) control, such as varying topography, or prescribed uniform heating, which have been used before. This in turn means that if/once the desired state is achieved, then the controls do not need to be active anymore. The advantages of this fact will become clearer in Chapters 2 and 3.

Feedback control methodologies rely on the ability of shifting the eigenvalues of a linear operator to the complex left half-plane, *ie*, to make the eigenvalues of this operator have negative real part. This is called pole placement and we state the algorithms we will use in Appendix A.2. These are based on results on robustness and invariance concepts, which are presented in, e.g., [19, 45, 46, 57, 58, 87, 123].

In order to obtain the response functions, the control methodology requires real-time observations of at least some components of the system state, and we will build our control strategies around observations of the film height. These can be obtained in experiments in several ways: Liu and Gollub [142] investigated experimentally the dynamics of thin films within the context of the onset of chaos; they used a fluorescence imaging process to measure the two-dimensional film thickness in real time, and also used laser beam deflection to obtain local measurements of the interface slope; Vlachogiannis and Bontozoglou [223] examined the flow of thin films over a wavy wall, and used interferometry calibrated against needle-point measurements to obtain the interface height; Heining, Pollak and Sellier [99] showed that the free surface shape and topography profile can be obtained from measurements of the surface velocity, and implemented this both in Navier–Stokes simulations and experiments; and Schörner, Reck and Aksel [190] used experiments with visualization by laser reflection to study the effect of differently shaped topographical configurations with the same basic amplitude and wavelength on the flow down an inclined plane; they were able to infer the streamwise growth rate of small-amplitude perturbations by comparing the magnitude of interfacial fluctuations at two streamwise locations.

Feedback control in the form of suction and blowing is used in aeronautics [86] and proves to be a useful tool for the delay of transition to turbulence. It is shown that strong, localised, or point actuated suction can weaken or completely suppress the secondary instabilities created by cross-flow vortices [76, 77]. Furthermore, numerical studies [111] show that suction is an efficient way of reducing drag, while downstream blowing in small amplitudes improves lift and drag characteristics. These are useful tools for reducing fuel consumption. Feedback control strategies have also been implemented for the two-dimensional Navier–Stokes equations in the context of data assimilation [68], in which controls applied towards known observations are used to overcome incomplete knowledge of the initial state in the forecasting of hurricanes and typhoons, and also to suppress noise-induced unsteadiness on flow over a round backward facing step [15]. However, in the case of long-wave models for thin film flows, we are only aware of the use of feedback controls in applications such as the use of thermal perturbations in liquids spreading over a solid substrate to suppress the contact line instability [95] or the delay of the onset of long-wavelength Marangoni-Bénard convection [164] in systems with zero Reynolds number.

There is extensive work on the use of feedback control to suppress waves in the weakly nonlinear model of thin film flows - see, e.g. [42, 63, 136]. Christofides [42] used point actuated controls modelling blowing and suction to stabilise the zero solution of the Kuramoto-Sivashinsky equation. Armaou and Christofides [8, 9] also claim that stabilisation of the flat state can be achieved by using only 5 control actuator functions, independently of the domain length (which affects the number of unstable eigenvalues of the system); they argue that this is possible due to the multiplicity of the eigenvalues of the linear operator of the KS equation being less than or equal to 4. Furthermore, using a similar argument, they prove that the response function can be built based on only a finite number of observations of the interface height, and they do that by using static (where the controls are based on only the most recent set of observations) or dynamic (where the controls are based on an approximation of the system which evolves over time) output feedback controls (see Chapter 3 and Appendix A.2 for more details), either using linear or nonlinear feedback controls. Moreover, when using nonlinear feedback controls, efforts have been made to optimise the placement of actuators and sensors when stabilising the zero solution of the KS equation [10, 149]. This is done by defining an appropriate cost functional and either by analysing a large number of runs or using the optimisation software MINOS, which uses reduced gradient techniques; a proof of

the existence of these optimal positions was not given, however.

In the works mentioned above, the Kuramoto-Sivashinsky equation is assumed to satisfy periodic boundary conditions. If this is not the case, then it is possible to use both distributed and boundary controls for the control of the resulting system. In non-periodic domains, x is usually rescaled to be in a domain of length 1, $x \in (0, 1)$, thus defining an instability parameter λ, which is proportional to the original domain length. In [144], the authors stabilise the zero solution for small λ (*ie*, small domains) by using nonlinear boundary feedback control in both boundaries. Cerpa [35] uses a problem of moments approach and spectral analysis to prove that the linear KS equation with both Dirichlet and Neumann boundary conditions can be controlled using one boundary control on the first derivative at $x = 0$; the system is controllable if the parameter λ does not belong to a specific countable set. A similar result is proved for distributed controls in [37].

For the full nonlinear case, Cerpa and Mercado [38] use two boundary controls applied at $x = 0$ to steer the solutions of the Kuramoto-Sivashinsky equation to any given trajectory. They use a Carleman estimate to obtain the null controllability of the linearised system, followed by a local inversion theorem to prove local controllability of all the trajectories of the KS equation. Hu and Temam [104] formulate and solve the problem of robust control of the KS equation through the boundary in the finite time horizon, by considering the finite component of the worst case disturbance aggravating the system. Their results are not only valid for the zero solution but also for any target flow U. They apply their results to a data assimilation problem, where the control to be determined is the initial condition. Sakthivel and Ito [188] consider the same problem, with Neumann and Dirichlet boundary control, but in the case where there is uncertainty in the parameters of the system; they use a spatially dependent scaling function, which provides them with controllers of less control effort. Byrnes *et al* [33] consider the different problem of tracking regulation for systems governed by the Kuramoto-Sivashinsky equation. They use boundary controls applied in both boundaries which force the system to remain bounded while at the same time all outputs are driven to track time dependent reference signals. Furthermore, they only consider a finite number of observations (outputs) of the system, by using a dynamic compensator (or dynamic output feedback control). Finally, Kobayashi [128] uses adaptive stabilisation techniques based on high-gain nonlinear output feedback controls and proves global asymptotic stability of the zero solution. Other examples of adaptive or input-output feedback control

applied to fluid dynamics are its application to convectively unstable flows [67], where the authors apply both linear-quadratic regulators and model-free adaptive methods to the linearised Kuramoto-Sivashinsky equation, spatially developing flows [12], where the controls are applied to the Ginzburg-Landau equation, and general dissipative PDEs [220].

Some authors also consider the case when a generalisation of the Kuramoto-Sivashinsky equation that includes effects of dispersion is coupled with a heat equation that models the temperature of the thin film. In [39], the authors prove that these systems can be forced to rest (*ie*, to the zero solution) by using boundary control in both equations. Furthermore, in [40] the authors prove that the same system can be controlled by using a localised control that acts in an open subset of the domain and only in one of the equations. In a recently submitted paper [34], this result is generalised to the control of any given trajectory.

The optimal control problem for the weakly nonlinear models with Dirichlet/Neumann boundary conditions was also considered: Gao [79] proves a Pontryagin's maximum principle for a forced Kuramoto-Sivashinsky equation, where both the solution and the (distributed) control have pointwise constraints, while Sun [200] investigates the problem for optimal boundary control, presenting first order necessary conditions for both fixed and free final time horizons. When the equations include the effects of dispersion, Zheng [238] established a bang-bang principle for an optimal control, by obtaining a relationship between the null controllability and the time optimal control problem with the help of Carleman estimates.

1.4 Roughening processes

As was mentioned before, roughening processes are characterised by a time-fluctuating rough interface which is described in terms of a stochastic partial differential equation. An important feature of systems involving dynamics of rough surfaces is that one often observes the emergence of scale invariance both in time and space, *i.e.*, the statistical properties of quantities of interest are described in terms of algebraic functions of the form $f(t) \sim t^{\beta}$ or $g(x) \sim x^{\alpha}$, where α and β are referred to as scaling exponents. An example of this is the surface roughness, or variance of $u(x,t)$, which is defined as

$$r(t) = \sqrt{\frac{1}{2\pi}\int_0^{2\pi} \left[u(x,t) - u_0(t)\right]^2 \, dx}, . \tag{1.41}$$

We remark that u_0 may or may not depend on time, depending on whether we consider the Burgers or the KPZ nonlinearities. Usually the above quantity grows in time until it reaches a saturated regime, in which the fluctuations become statistically independent of time and are scale-invariant up to some typical length scale of the system, say ℓ_s. This behavior can be expressed as:

$$\langle r(t) \rangle \sim \begin{cases} t^{\beta} & \text{if } t \ll t_s, \\ r_s & \text{if } t \gg t_s, \end{cases} \tag{1.42}$$

where $\langle \dots \rangle$ denotes average over different realizations, β is the so-called growth exponent [14], and t_s and r_s are the saturation time and saturated roughness value, respectively, which depend on the length scale ℓ_s. In particular, at a given time $t < t_s$, the correlation of these fluctuations are on a spatial length scale which grows in time as $\ell_c \sim t^{1/z}$. Therefore, saturation occurs whenever $\ell_c = \ell_s$ from which we find $r_s \sim \ell_s^{\alpha}$ with $\alpha = \beta z$. In this context, the exponents α and z are the roughness and dynamic exponent, respectively, and their particular values determine the type of universality class [130]. For example, it is known that the long-time behavior of the KPZ equation Eq. (1.40), is characterized by the KPZ universality class with $\alpha = 1/2$ and $z = 3/2$, while its linear version, which is referred to as the Edwards-Wilkinson (EW) equation, is characterized by the EW universality class with $\alpha = 1/2$ and $z = 2$ [14, 52, 97, 160, 183].

The ability to control not only the dynamics of the surface roughness (*i.e.* the growth rate) but also its convergence towards a desired saturated value has recently seen an increased interest due to the large amount of different technological applications. We notice particularly the work by Lou and Chtistofides [146, 150, 151], where the authors use nonlinear (distributed) feedback controls to control the solutions of the sKS equation to a desired saturated value of the surface roughness. These authors also use kinetic Monte-Carlo methods to predict the future state variance in order to design controls that minimise an objective function that penalises the discrepancy between the predicted state variance of the solution and that of a desired trajectory [152, 153]. The same method is also applied to equations that consider the system coupled to a gas phase [147, 148]. Finally, similar techniques are used and combined with dynamic output feedback control in [106, 107] and applied to the control of other statistical properties such as film porosity, film thickness and surface mean slope in [105, 108, 109, 237].

It is important to note that these control strategies address not only the control the surface

roughness but also other face values, such as the film porosity and film thickness, and also consider various linear dissipative models, including the stochastic heat equation, the linear stochastic KS equation, and the Edwards-Wilkinson (EW) equation. However, it should be pointed out that most of these works involve the use of nonlinear feedback controls which change the dynamics of the system and requires knowledge of the nonlinearity at all times, something that may be difficult to achieve. This is because the nonlinear terms are included implicitly in the controls, which makes the system dynamics essentially linear.

In addition to these works, we note [184], where the authors use nonlinear model predictive control to drive the system towards a desired mean value and surface roughness, and estimates the system state based on the substrate temperature; Hu and Mao [110] address the use of feedback controls both on the drift and the diffusion part of the sPDE and investigate the almost-sure stabilisation problem, rather than the mean-square stabilisation problem, which is equivalent to control the surface roughness; finally, Block *et al* [23] derive a method to control the surface roughness of the KPZ equation by using time delayed feedback controls.

Still considering the sKS equation but focussing on the trajectories of the solutions rather than their statistical properties, Pradas *et al* [179, 180] showed that in the parameter regime where the system is close to criticality (*i.e.*, for ν close to 1), if the noise present in the equation is highly degenerate, it forces the system to undergo several transitions, eventually stabilising the zero solution for strong enough noise intensities. This is because in this parameter regime the system can be described by the dynamics of the first mode only, and therefore the authors can use multiscale analysis to obtain an amplitude equation for the first mode. Gao *et al* [80] discuss observability estimates and also the null controllability of the linear stochastic KS equation, as well as the same equation when considered backwards in time *i.e.*, with a minus sign in front of the time derivative.

Feedback control problems are also studied for general stochastic PDEs and mostly involve the inverse problem of the generation of the stationary covariance matrix of the associated system. This problem is solved in [6] by identifying each possible system with the solution of a quadratic matrix inequality.

1.5 Objectives and structure of this thesis

In this thesis, we study the problem of using feedback controls to stabilise different solutions to equations modelling thin films flowing down inclined planes. The main objective is to derive controls based either on the reduced-order long-wave models or the weakly nonlinear models that would be effective in the full Navier–Stokes system. Ideally, we would like to derive controls for the Kuramoto-Sivashinsky equation, which would then work for both the long-wave models and the full Navier–Stokes system. The difficulty in applying the KS controls to these more complicated systems is twofold: the nonlinearities, even in the simplest case of the Benney equation (when the linear operator is the same as in the KS case, and therefore controls that stabilise the KS equation should stabilise at least the linear operator of the Benney equation) are more complicated, and so there is no guarantee that controls that stabilise the linear operator will work in the full nonlinear dynamics; and secondly, the structure of the weighted-residual and Navier–Stokes models, when applied at finite wavelength, is significantly different to that of the KS equation. On the other hand, since the linear operators are similar for the KS and the Benney equations, we can carefully build a control strategy for the Kuramoto-Sivashinsky equation, for which we can obtain analytic results, and extract information on the behaviour of the system and its reaction to the controls at least in a region of the parameters where this equation is valid. This will in turn build our intuition on how the controls should behave in the long-wave models.

We therefore start in Chapter 2 by studying the control problem applied to the Kuramoto-Sivashinsky equation and some of its generalisations that include the effects of dispersion and/or of an electric field applied perpendicular to the undisturbed surface. We apply point-actuated feedback controls and prove that with the right choice of response functions, which depend on the difference between the current state of the system and the state we wish to achieve, we can drive the system towards any chosen state, either the zero state, or steady state or travelling wave solutions of the KS equation. The solution can also be driven to any periodic state of our choosing by using point actuated controls combined with the right choice of distributed controls. We proceed to prove that the controls obtained are robust with respect to changes in the parameters of the system and small changes in the number of control actuators used, and finally we present our results on the existence of an optimal distributed control, and an algorithm to compute the optimal position for the control actuators in the various cases considered.

We then consider the effect of feedback controls in the long-wave models. Using insight from the weakly nonlinear models, we know that proportional controls are likely to stabilise the linear operator of the long-wave models, and we show that in fact, a proportional control scheme in which fluid is injected at each streamwise location in proportion to the observed deviation of the interface height at that location from uniform, has a stabilising effect on nearly-uniform flow in both the long-wave models. Furthermore, by solving an Orr-Sommerfeld equation for the linear stability of the Navier–Stokes equations, we also find that proportional controls have a stabilising effect in the full system. We also consider control strategies based on a finite number of point actuators and when the system can only be observed at a small number of locations in the domain, by using dynamic observers. For non uniform states, we discuss linear stability and nonlinear behaviour of the controlled system when using distributed, proportional controls. We note that the property of a given non-uniform state being an exact solution of the equations is model dependent and therefore can never be perfectly satisfied. It is therefore reasonable to suspect that a control strategy carefully optimised for one model may be ineffective in another, and so we focus on the use of relatively simple control schemes, and investigate their robustness to variations in the model details.

Chapter 4 is dedicated to the stochastic Kuramoto-Sivashinsky equation. We will make use of the controls obtained for the deterministic KS equation to derive a splitting methodology that will allow us to control the saturated value of the surface roughness of the solutions to the stochastic KS equation with both the Burgers and the KPZ nonlinearities: we split the equation into a linear stochastic PDE, of which we know how to control the surface roughness, and a nonlinear deterministic KS-type equation, which we can then control to zero. This splitting method allows us to build linear feedback controls with smaller cost, with the additional advantage that we can control the deterministic equation towards any desired shape, which allows us to also control the solution trajectories. It improves the existing results since we neither need to assume knowledge of the nonlinearity at all times nor need to change the dynamics of the system in the way that it was done before. We then extend the controls to be point actuated, which, to our knowledge, has not been done for stochastic PDEs. This extension makes the problem considerably harder to solve, due to the fact that the resulting system of linear stochastic ODEs is not decoupled. This leads to the need to solve a new matrix problem, which is similar to a matrix Lyapunov equation, but that to our

knowledge has not been addressed. We develop an algorithm to solve the resulting matrix problem, and note that its complexity makes it harder to solve for a large N. However, we obtained satisfactory results when controlling towards a range of surface roughness values for moderately small N.

Finally, in chapter 5 we consider systems of coupled KS equations. We consider two particular cases of the system described in equation (1.36): the first one considers that there are no first order derivatives and the coupling comes through the second derivatives only, and in the second case, which represents a vanishing viscosity limit of a conservation law, there are no second derivatives (*i.e.* inertia) involved and the coupling is only via the first derivatives. There are no analytical results known for these systems and therefore we begin in both cases by trying to find bounds on their solutions. We use the so-called background flow method to bound the solutions to the first particular case and we find that both the solutions to these systems and their derivatives are bounded in L^2. This provides us with the necessary estimates to be able to prove the applicability of feedback controls to the system, as well as to prove existence of an optimal distributed control. In the second case, we use the entropy method proposed by Giacomelli and Otto [84] for the scalar KS equation in the system obtained. We were able to generalise most of the results in this reference to the particular system that we are considering. However, the crucial step on bounding the system depends on the existence of viscosity solutions for the Burgers equation, which does not generalise to our case and therefore we were not able to obtain the desired bounds for the system. We discuss some ideas on how to overcome this problem.

We summarise the main results and outcomes of our research, and discuss possible future work directions in Chapter 6.

Chapter 2

Controlling weakly nonlinear models

In this chapter we study the problem of controlling and stabilising solutions of the Kuramoto-Sivashinsky equation, which is an example of a general class of infinite-dimensional dynamical systems exhibiting low-dimensional spatiotemporal chaos. We consider a generalised form of the equation in which the effects of an electric field and dispersion are included.

We show that using a finite number of linear, time dependent, point actuated feedback controls we are able to stabilise and/or control all stable or unstable solutions, including steady solutions, travelling waves (single and multipulse ones, which we refer to as bound states) and spatiotemporal chaos. Both the feedback and optimal control problems are studied. Furthermore, the proposed control methodology is shown to be robust with respect to changing the parameters in the equation, e.g. the viscosity coefficient or the intensity of the electric field.

The main results of this chapter are published in references [89, 90].

2.1 The generalised Kuramoto-Sivashinsky equation

The starting point of our analysis of the control of thin film flows down inclined planes is the weakly nonlinear model for the perturbations of the flow's interface, the well-known Kuramoto-Sivashinsky (KS) equation. More than modelling such interfaces, the Kuramoto-Sivashinsky equation on $L-$periodic domains

$$\begin{aligned} u_t + u_{xxxx} + u_{xx} + uu_x = 0, \\ u(x,t) = u(x+L,t), \end{aligned} \tag{2.1}$$

is a paradigm evolution equation that has received considerable attention in recent years due to its wide applicability as well as the rich and complex dynamics that it supports. The KS equation arises in many physical problems including falling film flows [21, 101, 193, 196], two-fluid core-annular flows [53, 170], flame front instabilities and reaction-diffusion-combustion dynamics [194, 195], propagation of concentration waves in chemical physics applications [132, 133, 134], and trapped ion mode dynamics in plasma physics, [48]. The KS equation (2.1) is one of the simplest partial differential equations (PDEs) that can produce complex dynamics including chaos - see for example the numerical experiments in [112, 113, 117, 127, 172, 197, 228, 229]. Routes to chaos have been shown numerically to follow a Feigenbaum period-doubling cascade - see [197] where the two universal Feigenbaum constants are also computed for the KS equation with three-digit accuracy. A detailed knowledge of the stationary, travelling and time-oscillatory solutions (typically chaotic) of (2.1) is significant in technological applications that seek to enhance heat or mass transfer, for example. In this sense certain solutions are better than others and a description of the solution phase space is a crucial step in constructing relevant control strategies that can access unstable states, for instance, that may be desirable in applications.

In many studies equation (2.1) is scaled to $2\pi-$periodic domains according to the rescaling

$$x^* = \frac{2\pi}{L}x, \quad t^* = \left(\frac{2\pi}{L}\right)^2 t, \quad u^* = \frac{L}{2\pi}u, \tag{2.2}$$

to take the form (we drop the stars and use the same symbols for dependent and independent

variables)

$$u_t + \nu u_{xxxx} + u_{xx} + uu_x = 0, \qquad (2.3)$$
$$u(x,t) = u(x+2\pi,t),$$

where $\nu = (2\pi/L)^2$ is a positive parameter that decreases as the system size L increases. The mathematical interest in the KS equation and related models resides in the fact that it is a simple, one-dimensional equation exhibiting complex dynamics making it amenable to analysis and also a good case study in the area of infinite-dimensional dynamical systems and their control. The equation is of the active-dissipative type and instabilities are present depending on the value of ν. If $\nu > 1$, it is well known [185, 191, 202, 203] that the zero solution, representing a flat film, is unique. However, when $\nu < 1$ the zero solution is linearly unstable and bifurcates into nonlinear states including steady states, travelling waves and solutions exhibiting spatiotemporal chaos - the dynamical complexity increasing as ν decreases. Some of these solutions are stable, and others are unstable [127]. In [78, 127, 171], one can find studies of the stability of steady states of the KS equation.

In the context of falling film flows there have been several studies to extend the KS equation by including additional physical effects. Of most interest to the present study are the derivations in [217, 219] for film flow over flat walls in the presence of electric fields applied perpendicular to the undisturbed interface. The resulting equation, that also incorporates the effects of dispersion, is a generalisation of (2.3) and takes the form

$$u_t + \nu u_{xxxx} + \mu\mathcal{H}[u_{xxx}] + \delta u_{xxx} + u_{xx} + uu_x = 0, \qquad (2.4)$$
$$u(x,t) = u(x+2\pi,t), \qquad u(x,0) = u_0(x),$$

where $\mu \geq 0$ measures the strength of the applied electric field and the parameter δ measures dispersive effects. These parameters have also been rescaled in the form $\delta^* = \frac{2\pi}{L}\delta$, $\mu^* = \frac{2\pi}{L}\mu$. The linear operator $\mathcal{H}$ is the Hilbert transform operator (see Appendix A.1) and represents flow destabilisation due to the electric field. On $2\pi-$periodic domains the definition of $\mathcal{H}$ is

$$\mathcal{H}[u](x) = \frac{1}{2\pi} PV \int_0^{2\pi} u(\xi) \cot\left(\frac{x-\xi}{2}\right) d\xi, \qquad (2.5)$$

where PV stands for the Cauchy principal value integral. In the model analysed, the electric field needs to be found by solving a harmonic problem above the film and calculating the Dirichlet to Neumann map of the solution to construct the Maxwell stresses that interact with the hydrodynamics - see [217, 219] for the details. In fact, for the linearised problem the eigenvalues λ corresponding to the eigenfunctions $\exp(ikx)$ are

$$\lambda = k^2 + \mu k^2|k| - \nu k^4 + i\delta k^3, \tag{2.6}$$

showing that the presence of the electric field destabilises the flow and increases the number of linearly unstable modes. Note that instability is possible if $|k| < k_c = \frac{\mu+\sqrt{\mu^2+4\nu}}{2\nu}$, and so there are $2l+1$ unstable modes where l is the integer part of k_c. This additional destabilisation is important in what follows and makes the control problem more challenging. The modified

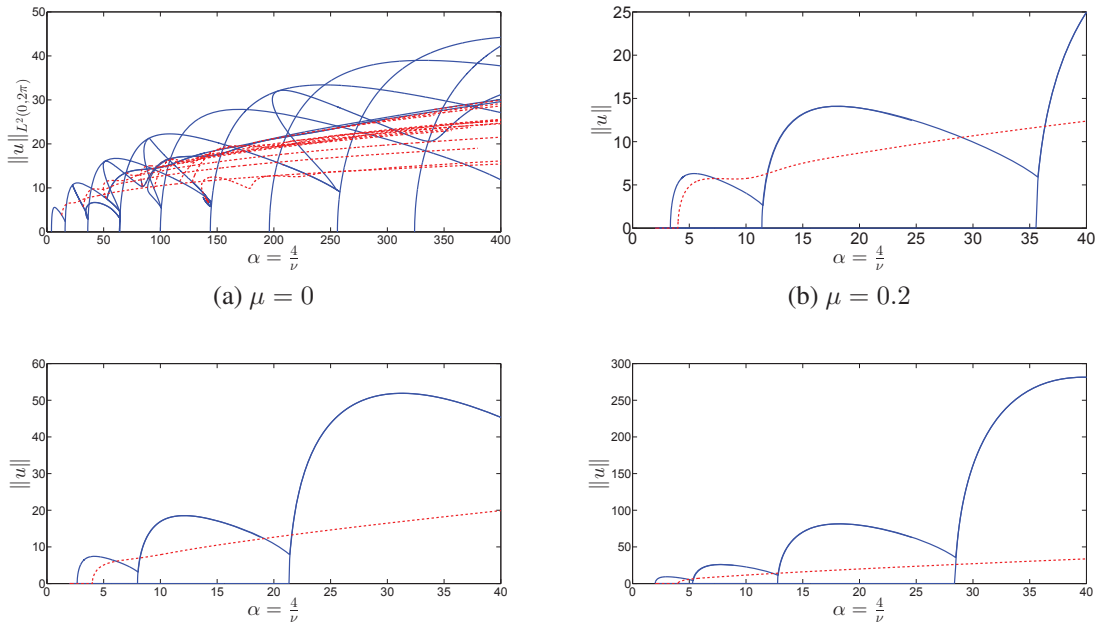

(a) $\mu = 0$ (b) $\mu = 0.2$

(c) $\mu = 0.5$ (d) $\mu = 1$

Figure 2.1: Bifurcation diagram of the L^2-norm of the steady state solutions (blue solid curves) and travelling wave solutions (red dashed curves) to the gKS equation (2.4) (with $\delta = 0$) in the presence of an electric field for $0.01 \leq \nu \leq 1$, and $\mu = 0$ (2.1a), and $0.1 \leq \nu \leq 1$ and $\mu = 0.2$ (2.1b), $\mu = 0.5$ (2.1c), and $\mu = 1$(2.1d). Note that for $\mu \neq 0$, only a few of the branches are shown in these diagrams.

equation (2.4) in the absence of dispersion ($\delta = 0$), has a similar dynamical behaviour to the KS equation (2.3) but with chaotic dynamics appearing at higher values of ν as μ increases

- see Fig. 2.1.

On the other hand, in the absence of an electric field but with dispersion present, it is established that sufficiently large values of δ act to regularise the dynamics (even chaotic ones) into nonlinear travelling wave pulses - see [3, 124, 125]. However, in a regime of moderate values of δ travelling waves or pulses appear to be randomly interacting with each other giving rise to what is widely known as weak/dissipative turbulence (in the "Manneville sense" [120, 126, 155]) - see [178, 216] for a weak interaction theory between pulses that are sufficiently separated.

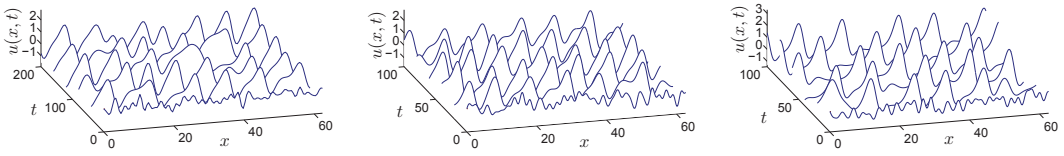

(a) $\delta = 0$ (b) $\delta = 0.01$ (c) $\delta = 0.05$

Figure 2.2: Time evolution of the gKS equation for $\nu = 0.01$ ($L = 20\pi$), $\mu = 0$. The left panel shows the chaotic behaviour in the absence of dispersion, while the middle panel shows the weak/dissipative turbulent behaviour for small values of δ and the right panel shows the chaotic regularisation with relatively large values of dispersion.

2.1.1 Existence, uniqueness and bounds on solutions

There is extensive literature on the behaviour of the solutions to the KS equation. Well posedness of solutions is studied, for instance, in [185, 202, 203]. It was proved in [51] that the long time dynamics of the KS equation are finite dimensional in the sense that they are governed by a dynamical system of finite dimension which is at least as large as the number of linearly unstable modes (this number scales with L or $\nu^{-1/2}$ for (2.1) or (2.3), respectively); these authors also proved that the solutions are attracted by a global attractor, a set of finite dimension. Boundedness of solutions for general initial conditions was proved independently and by using distinct methods by [50, 93, 115]. These studies also focussed on finding bounds for the dimension of the global attractor by estimating L^2-norms of the solutions, starting with the odd-parity results of [159] and those for general initial data by [50] along with more recent improvements in [30] and [167]. We will summarise the existing bounds and the methods used to obtain them below - see Table 2.1. Analyticity of solutions

in a strip in the complex plane around the real axis was also proved in [1] and [49] using different methods.

For the generalised Kuramoto-Sivashinsky equation case the literature is less extensive, but one can find a detailed analysis of the spatiotemporal dynamics of the solutions to the case when $\mu > 0$, detailing the various attractors and their stability in [217], as well as a study of the boundedness of solutions and an estimate of the dimension of the global attractor [218] for a class of more general operators whose symbols in Fourier space are such that the electric field term in (2.6) is $|k|^\alpha$ with $3 \leq \alpha < 4$. When $\delta > 0$, and in fact for a more general linear operator, Frankel and Roytburd [74] proved that there exist an absorbing set and a compact attractor of finite Hausdorff dimension and a stability analysis for the same operators can be found in [75]. For the gKS equation with $\mu = 0$, studies of the stability of travelling waves are available at [16, 17]. Finally, the general case ($\mu > 0, \delta > 0$) was studied numerically by Tseluiko and Papageorgiou in [219]. The authors carried out extensive numerical experiments to characterise the solutions to this equation and study the interactions between dispersion and the electric fields applied. To our knowledge, there are no analytical bounds explicitly dependent on ν and μ on the solutions for this particular equation, although Frankel and Roytburd [75] found bounds for a more general case, when $\nu u_{xxxx} + \mu\mathcal{H}[u_{xxx}]$ is replaced by $\mathcal{P}(D)u$, where $\mathcal{P}(D)$ is an elliptic pseudo-differential operator. In this case, the authors found that the norm of the solutions is bounded by a constant, as long as ν is larger than a constant ν_0 that depends on $\mathcal{P}(D)$, and therefore on ν and μ, or bounded by $\nu^{-17/4}$ otherwise.

The goal of this chapter is to stabilise non-uniform unstable steady states or travelling wave solutions of equation (2.4). For the theoretical analysis of the feedback control problem for the gKS equation we need L^∞ bounds on the solution and its derivatives and for this reason we present a survey of the many bounds obtained for the solutions of the gKS equation for various cases, depending on whether one, both or none of the coefficients μ or δ are positive. These bounds are presented in Table 2.1 below.

We will use some of the L^2 bounds summarised in Table 2.1, as well as existing bounds for the derivatives of the solutions, together with the Sobolev embedding theorem - see Appendix A.1 - to establish the necessary L^∞ estimates. We now outline the chosen estimates. Optimal estimates for the solution of the KS equation (2.1) in $(0, L)$ were obtained by Otto [167], and for the rescaled $2\pi-$periodic KS equation (2.3) these estimates can be

Paper	Bound	Method
Case $\nu > 0,\ \mu = \delta = 0$		
Nicolaenko *et al*, [159]	ν^{-1}	Uses background flow method, only valid for odd functions
Il'yashenko, [115]	ν^{-72}	Approximates KS equation as perturbation of Hamilton-Jacobi equation; removes parity assumption
Goodman, [93]	ν^{-1}	Uses Lyapunov method and is valid for general periodic solutions
Collet *et al*, [50]	$\nu^{-\frac{11}{20}}$	Uses background flow method, valid for all mean zero functions
Jolly *et al*, [118]	$\nu^{-\frac{1}{2}}$	Modified the method in [50]
Bronski and Gambill, [30]	$\nu^{-\frac{1}{2}}$	Generalises [50] for general boundary conditions
Giacomelli and Otto, [84]	$\nu^{-\frac{1}{4}}$	Uses entropy method
Otto, [167]	$\nu^{-\frac{1}{6}}$	Uses Besov spaces
Goldman *et al*, [88]	$\nu^{-\frac{1}{6}}$	Simplifies and improves bounds in [167]
Wittenberg and Holmes, [229]	$\nu^{\frac{1}{4}}$	Found numerically
Case $\nu > 0,\ \delta > 0,\ \mu = 0$		
Frankel and Roytburd, [75]	$\nu^{-\frac{17}{4}}$	Combines the methods in [50] and [93]
Case $\nu > 0,\ \mu > 0,\ \delta = 0$		
Tseluiko and Papageorgiou, [218]	$C(\nu, \mu, \varphi)$	Uses background flow method, φ is the background flow
	$\mathcal{O}(\mu^3)$	Found numerically for $\nu = 0.5$, estimated to be valid for all values of ν
General case		
Frankel and Roytburd, [75]	Constant or $\nu^{-\frac{17}{4}}$	if $\nu \geq \nu_0 = \nu_0(\nu, \mu)$ if $\nu < \nu_0$ Combines the methods in [50] and [93].

Table 2.1: Various bounds established for the gKS equation.

expressed in terms of $\nu = \left(\frac{2\pi}{L}\right)^2$ to find

$$\limsup_{t\to\infty} \|u(\cdot,t)\| \leq \mathcal{O}(\nu^{-1/6}), \tag{2.7a}$$

$$\limsup_{t\to\infty} \|u_x(\cdot,t)\| \leq \mathcal{O}\left(\nu^{1/2}\ln^{5/3}\left(\nu^{-1/2}\right)\right), \tag{2.7b}$$

$$\limsup_{t\to\infty} \|u_{xx}(\cdot,t)\| \leq \mathcal{O}\left(\nu\ln^{5/3}\left(\nu^{-1/2}\right)\right), \tag{2.7c}$$

where $\|\cdot\| = (\int_0^{2\pi}(\cdot)^2\ dx)^{1/2}$ denotes the L^2-norm of the solution. For the generalised

equation (2.4) but in the absence of dispersion ($\delta = 0$), Tseluiko & Papageorgiou [218] used the background flow method to obtain similar estimates in the presence of an electric field. Their estimates are of the form

$$\|u\| \leq (\|u_0\| + \|\varphi\|)\, e^{-Dt} + C(\nu, \mu) + \|\varphi\|, \tag{2.8}$$

where C and D are constants depending on μ and ν, and φ is a constructed function with finite L^2-norm (we do not need to give it here). They also proved that for $u_0 \in \dot{H}^1_p(0, 2\pi)$, the first and second derivatives of the solution are bounded, and therefore, $u \in \dot{H}^2_p(0, 2\pi)$, where $\dot{H}^s_p$ is the Sobolev space of $s-$times differentiable functions that are periodic and have zero mean - see Appendix A.1.

It is also important to remark that in the case of the generalised KS equation (2.4), with both δ and μ non-zero, it was proved in [74, 75] that the L^2 norm of the solution is also bounded. In fact

$$\limsup_{t\to\infty} \|u(\cdot, t)\| \leq \begin{cases} \mathcal{O}(\nu^{-17/4}), & \text{if } \nu < \nu_0, \\ C, & \text{if } \nu \geq \nu_0, \end{cases} \tag{2.9}$$

where ν_0 depends on the symbol of the linear operator. Note that these are not optimal bounds. The authors also prove boundedness in L^2 of spatial derivatives of u up to order 4. The estimates (2.7)-(2.9) together with the fact that the solutions to all the equations belong to the Sobolev spaces $\dot{H}^s_p$ with $s \geq 2$, imply (by use of the Sobolev embedding theorem) that there exist constants $C_1,\ C_2$ that depend only on ν and μ such that

$$\|u\|_\infty \leq C_1 \|u\|_{H^2}, \quad \|u_x\|_\infty \leq C_2 \|u_x\|_{H^1}, \tag{2.10}$$

where u is a solution of equation (2.4), which provides us with the necessary L^∞ bounds.

2.1.2 Stabilisation of the zero solution of the KS equation

Recently, a few research groups [7, 9, 42, 43, 44, 63, 136, 149] showed how to stabilise the zero solution of the Kuramoto-Sivashinsky equation by using state feedback controls. When using linear feedback controls, it was shown that it is possible to stabilise the zero solution using only 5 point actuated controls. In addition, in [42], Christofides also proves that the stabilisation is possible using only a certain number of observations of the solution instead of full knowledge of the solution at all times, as long as the number of observations is equal

to or exceeds the number of unstable modes. These results, however, seem to only be valid for relatively large values of ν ($\nu \geq 1/49$), and for smaller ν the authors suggest the use of more control actuators or a change in the location of the actuators and observers. In further work utilising nonlinear feedback controls [7, 43], Armaou and Christofides formulated optimisation techniques and computed possible optimal states by analysing a large number of runs; a proof of the existence of these optimal positions was not given, however.

An example of the stabilisation of the zero solution for relatively large values of ν ($\nu = 0.2$ and $\nu = 0.4$, which have 5 and 3 unstable modes, respectively) using the same number of point actuated controls as unstable modes, and assuming full knowledge of the solution at all times is plotted in Fig. 2.3. Our results are in good agreement with those obtained in [44].

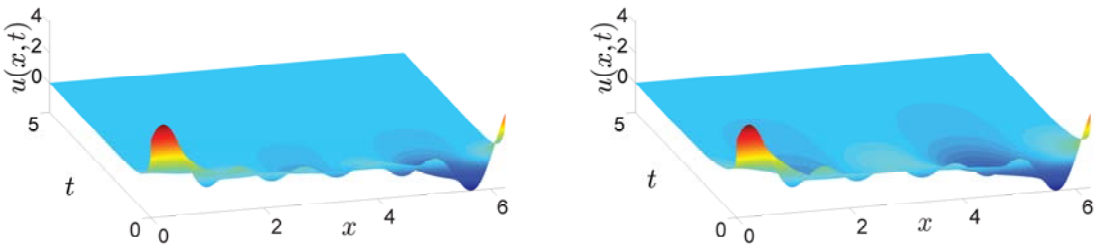

(a) $\nu = 0.2$ (b) $\nu = 0.4$

Figure 2.3: Spatiotemporal evolution showing stabilisation to the zero solution of the KS equation for (a) $\nu = 0.2$ ($\alpha = 20$), and (b) $\nu = 0.4$ ($\alpha = 10$).

2.2 Stabilisation of nontrivial solutions to the gKS equation

We can now introduce the controlled generalised KS equation, which will form the basis of our analysis and computations. This consists of a forced version of (2.4) and reads

$$\begin{cases} u_t + \nu u_{xxxx} + \mu \mathcal{H}[u_{xxx}] + \delta u_{xxx} + u_{xx} + u u_x &= \displaystyle\sum_{i=1}^{m} b_i(x) f_i(t), & x \in (0, 2\pi),\ t > 0, \\ u(x,0) &= u_0(x), & x \in (0, 2\pi), \\ \dfrac{\partial^j u}{\partial x^j}(x + 2\pi, t) &= \dfrac{\partial^j u}{\partial x^j}(x,t), & x \in (0, 2\pi),\ t > 0, \\ f_i(t) &\in L^2(0,T). \end{cases} \tag{2.11}$$

We assume that the initial condition satisfies $u_0 \in \dot{H}^2_p(0, 2\pi)$, m denotes the number of controls, $b_i(x)$, $i = 1, \ldots, m$ are the control actuator functions and $f_i(t)$, $i = 1, \ldots, m$ are the controls. We will use point actuator functions, which means that the functions $b_i(x)$ are delta functions centered at positions x_i, i.e. $b_i(x) = \delta(x - x_i)$, or a smooth approximation of such delta functions.

We use an argument similar to [8, 42, 44] to prove that it is possible to stabilise nontrivial steady states of the generalised KS equation (2.4). Using the Galerkin representation of u,

$$u(x,t) = \frac{u_0(t)}{\sqrt{2\pi}} + \sum_{n=1}^{\infty} u_n^s(t)\frac{\sin(nx)}{\sqrt{\pi}} + \sum_{n=0}^{\infty} u_n^c(t)\frac{\cos(nx)}{\sqrt{\pi}}, \tag{2.12}$$

substituting into (2.11), and taking the inner product with the functions $\frac{1}{\sqrt{2\pi}}$, $\frac{\sin(nx)}{\sqrt{\pi}}$ and $\frac{\cos(nx)}{\sqrt{\pi}}$, $n = 1, \ldots, \infty$, we obtain the following infinite system of ODEs (dots denote time derivatives):

$$\begin{cases} \dot{u}_n^s &= \left(-\nu n^4 + \mu n^3 + n^2\right) u_n^s + \delta n^3 u_n^c + g_n^s + \sum_{i=1}^{m} b_{in}^s f_i(t), \quad n = 1, \ldots, \infty, \\ \dot{u}_n^c &= \left(-\nu n^4 + \mu n^3 + n^2\right) u_n^c - \delta n^3 u_n^s + g_n^c + \sum_{i=1}^{m} b_{in}^c f_i(t), \quad n = 0, \ldots, \infty, \end{cases} \tag{2.13}$$

where $b_{in}^s = \int_0^{2\pi} b_i(x)\sin(nx)dx$ and $b_{in}^c = \int_0^{2\pi} b_i(x)\cos(nx)dx$. The nonlinearities g_n^s and g_n^c are given by (see [2] and Appendix B.1)

$$g_n^s = \frac{n}{4\sqrt{\pi}} \sum_{j+k=n} (u_j^c u_k^c - u_j^s u_k^s) + \frac{n}{2\sqrt{\pi}} \sum_{j-k=n} (u_j^c u_k^c + u_j^s u_k^s), \quad n = 1, \ldots, \infty,$$

$$g_n^c = -\frac{n}{2\sqrt{\pi}} \sum_{j+k=n} u_j^c u_k^s + \frac{n}{2\sqrt{\pi}} \sum_{j-k=n} (u_j^c u_k^s - u_j^s u_k^c), \quad n = 0, \ldots, \infty.$$

In deriving the system (4.16) we used $\mathcal{H}[\sin(x)](x) = -\cos(x)$ and $\mathcal{H}[\cos(x)](x) = \sin(x)$; these formulas can be derived using contour integrations in the complex plane, for example.

We now define $z^u = \begin{bmatrix} z_u^u & z_s^u \end{bmatrix}^T$, where $z_u^u = \begin{bmatrix} u_0^c & u_1^s & u_1^c & \cdots & u_l^s & u_l^c \end{bmatrix}^T$ contains the coefficients of the (slow) unstable modes and $z_s^u = \begin{bmatrix} u_{l+1}^s & u_{l+1}^c & \cdots \end{bmatrix}^T$ those of the (fast) stable modes. In addition,

$$G = \begin{bmatrix} 0 \\ g_1^s \\ g_1^c \\ g_2^s \\ g_2^c \\ \vdots \end{bmatrix}, \qquad D = \begin{bmatrix} 0 & 0 & 0 & 0 & \cdots & 0 & \cdots \\ 0 & 0 & \delta & 0 & 0 & 0 & \cdots \\ 0 & -\delta & 0 & 0 & 0 & 0 & \cdots \\ 0 & 0 & 0 & \cdots & 0 & \delta n^3 & \cdots \\ 0 & 0 & 0 & \cdots & -\delta n^3 & 0 & \cdots \\ \vdots & \vdots & \vdots & \vdots & \vdots & \vdots & \ddots \end{bmatrix}, \qquad F = \begin{bmatrix} f_1(t) \\ f_2(t) \\ \vdots \\ f_m(t) \end{bmatrix}.$$

Furthermore, we introduce the notation

$$A = \begin{bmatrix} A_u & 0 \\ 0 & A_s \end{bmatrix} \quad \text{and} \quad B = \begin{bmatrix} B_u \\ B_s \end{bmatrix}, \tag{2.14}$$

where

$$A_u = \mathrm{diag}(0, -\nu + \mu + 1, -\nu + \mu + 1, \cdots, -l^4\nu + \mu l^3 + l^2, -l^4\nu + \mu l^3 + l^2),$$

$$A_s = \mathrm{diag}(-(l+1)^4\nu + \mu(l+1)^3 + (l+1)^2, -(l+1)^4\nu + \mu(l+1)^3 + (l+1)^2, \cdots),$$

and

$$B_u = \begin{bmatrix} b_{10}^c & b_{20}^c & \cdots & b_{m0}^c \\ b_{11}^s & b_{21}^s & \cdots & b_{m1}^s \\ b_{11}^c & b_{21}^c & \cdots & b_{m1}^c \\ \vdots & \vdots & \cdots & \vdots \\ b_{1l}^s & b_{2l}^c & \cdots & b_{ml}^c \\ b_{1l}^s & b_{2l}^s & \cdots & b_{ml}^s \end{bmatrix}, \qquad B_s = \begin{bmatrix} b_{1(l+1)}^s & b_{2(l+1)}^s & \cdots & b_{m(l+1)}^s \\ b_{1(l+1)}^c & b_{2(l+1)}^c & \cdots & b_{m(l+1)}^c \\ \vdots & \vdots & \cdots & \vdots \end{bmatrix}, \tag{2.15}$$

discretise the stable and unstable parts of the linear operator $\mathcal{A}$ and the delta functions, respectively. We can rewrite the infinite dimensional system of ODEs (4.16) as

$$\dot{z}^u = Az^u + Dz^u + G + BF. \tag{2.16}$$

We have the following result.

Proposition 1. *Let $\bar{u}$ be a linearly unstable steady state or travelling wave solution of* (2.4)

and let $2l+1$ *be the number of unstable eigenvalues of the system*

$$u_t = -\nu u_{xxxx} - \mu\mathcal{H}[u_{xxx}] - u_{xx}, \tag{2.17}$$

i.e., $l+1 \geq \frac{\mu+\sqrt{\mu^2+4\nu}}{2\nu} > l$. *If* $m = 2l+1$ *and there exists a matrix* $K \in \mathbb{R}^{m\times m}$ *such that all of the eigenvalues of the matrix* $A_u + B_u K$ *have negative real part, then the state feedback controls*

$$[f_1 \ \cdots \ f_m]^T = F = K(z_u^u - z_u^{\bar{u}}) \tag{2.18}$$

stabilise $\bar{u}$.

Proof. Let $u = \bar{u} + v$ be a solution to (2.4). Substituting into (2.4) and using the fact that $\bar{u}$ is a steady state or travelling wave solution of (2.4), we obtain the following PDE for the perturbation v,

$$v_t + \nu v_{xxxx} + \mu\mathcal{H}[v_{xxx}] + \delta v_{xxx} + v_{xx} + vv_x + (\bar{u}v)_x = 0, \tag{2.19}$$

and in controlled form we have

$$v_t + \nu v_{xxxx} + \mu\mathcal{H}[v_{xxx}] + \delta v_{xxx} + v_{xx} + vv_x + (\bar{u}v)_x = \sum_{i=1}^{m} b_i(x) f_i(t). \tag{2.20}$$

First we will prove that the given controls stabilise the zero solution of

$$v_t = -\nu v_{xxxx} + \mu\mathcal{H}[v_{xxx}] + v_{xx}. \tag{2.21}$$

Note that the dispersion term does not affect instability due to it being an antisymmetric operator in a periodic domain and therefore it is not necessary to include it in this part of the analysis. After applying a Galerkin truncation and the controls given by (2.18), we obtain

$$\dot{z}^v = \begin{bmatrix} A_u + B_u K & 0 \\ B_s K & A_s \end{bmatrix} z^v = C z^v. \tag{2.22}$$

Since the eigenvalues of $A_u + B_u K$ have negative real part and the matrix C multiplying z^v is triangular by blocks, it follows that the zero solution to (2.22) is exponentially stable.

Next, following [8, 42, 44], we use a Lyapunov argument to show that these controls stabilise the zero solution to equation (2.19). We first use the fact that exponential stability

of the system (2.22) implies that there exists a positive constant a such that the operator $\mathcal{L}(v) = -\nu v_{xxxx} - \mu\mathcal{H}[v_{xxx}] - v_{xx} + \sum_{i=1}^{m} b_i(x)K_{i\cdot}z_u^v$, where $K_{i\cdot}$ denotes the $i-$th row of the matrix K, satisfies

$$(\mathcal{L}v, v) \leq -a\|v\|^2. \tag{2.23}$$

Defining $\mathcal{E}(v) = \int_0^{2\pi} \frac{v^2}{2}\, dx$, it is easy to verify that $\mathcal{E}(0) = 0$ and $\mathcal{E}(v) > 0, \forall v > 0$. Multiplying (2.19) by v and integrating gives

$$\frac{d}{dt}\int_0^{2\pi} \frac{v^2}{2}\, dx = \int_0^{2\pi} vv_t\, dx = (\mathcal{L}v, v) - \delta\int_0^{2\pi} v_{xxx}v\, dx - \int_0^{2\pi} v^2 v_x\, dx - \int_0^{2\pi} v(\bar{u}v)_x\, dx. \tag{2.24}$$

Integration by parts and use of periodicity shows that the first two integrals on the right-hand side of (2.24) are zero. It remains to obtain an estimate for the third integral. Again using integration by parts and periodicity gives

$$-\int_0^{2\pi} (\bar{u}v)_x v\, dx = -\int_0^{2\pi} \bar{u}v_x v\, dx - \int_0^{2\pi} \bar{u}_x v^2\, dx = -\frac{1}{2}\int_0^{2\pi} \bar{u}_x v^2\, dx$$

$$\leq -\frac{\inf \bar{u}_x}{2}\int_0^{2\pi} v^2\, dx = -\frac{\inf \bar{u}_x}{2}\|v\|^2. \tag{2.25}$$

Adding everything up, we obtain

$$\frac{1}{2}\frac{d}{dt}\|v\|^2 \leq -\left(a + \frac{\inf \bar{u}_x}{2}\right)\|v\|^2. \tag{2.26}$$

If the eigenvalues of the matrix $A_u + B_u K$ are chosen such that $2a + \inf \bar{u}_x \geq 0$, we obtain that $\frac{d}{dt}\mathcal{E}(v(t)) \leq 0$, which proves that V is a Lyapunov function for the system at $v = 0$ and therefore the zero solution is stable.

Using the controls given by (2.18), we can therefore stabilise the nontrivial steady state $\bar{u}$ of the original equation. □

Using Proposition 1, we can conclude that in order to stabilise the steady state $\bar{u}$ of equation (2.4) we should solve the PDE

$$u_t + \nu u_{xxxx} + \mu\mathcal{H}[u_{xxx}] + \delta u_{xxx} + u_{xx} + uu_x = \sum_{i=1}^{m} b_i(x)K_{i\cdot}(z_u^u - z_u^{\bar{u}}). \tag{2.27}$$

Remark 1. *Since the solutions to the generalised Kuramoto-Sivashinsky equation are taken*

to be periodic with zero mean, it follows that $\inf \bar{u}_x < 0$*. Therefore, the constant* a *in* (2.26) *must be chosen large enough so that* $a + \frac{\inf \bar{u}_x}{2}$ *is positive. In the case when* $\delta > 0$*, we also need to account for the fact that the amplitude of the solutions (and therefore the absolute value of their derivatives) grows with* δ *[3, 126]. Further details can be found in Section 2.3.*

Remark 2. *The above proposition is clearly valid for the case when* $\bar{u} = 0$*, in which case the controls are* $f_i(t) = K_i . z^u_u$*, as presented in [8, 42, 44]. In the case when* $\bar{u}$ *is a travelling wave, the result follows using a time dependent* $z^{\bar{u}}$*. See Section 2.3 and in particular Equation* (2.41)*.*

Remark 3. *From estimates* (2.7)*, it follows that the value* $\inf |\bar{u}_x|$ *is finite and therefore we can conclude* (2.26)*.*

Remark 4. *Christofides et al. [8, 42, 44] argued that due to the multiplicity of the eigenvalues of the Kuramoto-Sivashinsky equation being less or equal than* 4*, one would only need* 5 *controls to stabilise the zero solution of that equation. The same holds in our case: the multiplicity of the eigenvalues of the linear operator in* (2.21) *is also less than or equal to 4, but numerical results suggest that we need to use* $m = 2l + 1$ *controls, or at best* $m = 2l - 1$ *controls, see Fig. 2.5 and the discussion below.*

Remark 5. *The fact that we are separating the system between stable and unstable modes implies that the matrix* B_u *is square (*$B_u \in \mathbb{R}^{m \times m}$*), and using* $b_i(x) = \delta(x - x_i)$ *means that* B_u *has full rank. It follows that the Kalman rank condition ([234] and Appendix A.2) is automatically verified and the matrix* K *needed for the stabilisation will always exist.*

2.2.1 Controls applied to general PDEs

The framework we present here is valid for general infinite dimensional dynamical systems described by PDEs considered in a bounded domain with periodic boundary conditions of the form

$$u_t = \mathcal{A}u + \mathcal{D}u + \mathcal{N}(u), \tag{2.28}$$

where $\mathcal{A}$ and $\mathcal{D}$ are linear spatial differential operators with constant coefficients, $\mathcal{A}$ being a long-wave unstable operator, which we assume to be self adjoint in L^2 so that its eigenfunctions, denoted as $\{w_j\}_{j=0}^{\infty}$, form a basis of L^2, and $\mathcal{D}$ being a dispersive operator which has the same eigenfunctions as $\mathcal{A}$, and $\mathcal{N}$ is a nonlinear operator. Writing

$u(x,t) = \sum_{j=0}^{\infty} u_j(t)w_j(x)$, all of the analysis follows, as long as the operator $\mathcal{D}$ is anti-symmetric or can be bounded and we can bound the nonlinearity $\mathcal{N}(u)$ in a similar way to equation (2.25).

Furthermore, it should be noted that with our methodology not only nontrivial solutions but also arbitrary periodic functions, say $g(x,t)$, which are not necessarily solutions of Eq. (2.28), can be stabilised by adding an extra forcing term as follows:

$$u_t - \mathcal{A}u - \mathcal{D}u + \mathcal{N}(u) = \sum_{i=1}^{m} b_i(x) f_i(t) + \mathcal{G}(g), \tag{2.29}$$

where $\mathcal{G}(g) = g_t - \mathcal{A}g - \mathcal{D}g + \mathcal{N}(g)$. This makes $u = g$ a solution of equation (2.29) and the same argument described above for (2.11) is still valid for (2.29). For example, we can choose to stabilise the solution of (2.4) with $\mu = 0$ to a sinusoidal function $g(x) = \sin(x)$ for which case we have $\mathcal{G}(g) = (\nu - 1)\sin(x) - \delta\cos(x) + \frac{1}{2}\sin(2x)$ - see Section 2.3.

2.2.2 Robustness of controls

A natural and important question is whether the proposed control methodology is robust with respect to changes (or uncertainty) in the parameters ν, μ and δ that appear in the equation. The robustness of our method can be proved rigorously using techniques from control theory, e.g. [123, Thm. 6], and we take this up next.

Proposition 2. ([123, Thm. 5]) *Let λ_i, $i = 1, \ldots, N$ be the eigenvalues of the matrix C appearing in* (2.22)*, X be the matrix of eigenvectors of C , and let $\kappa(\cdot)$ denote the condition number. Then we have*

$$\|K\|_2 \leq \frac{\left(\|A\|_2 + \max_j \left(|\lambda_j|\right)\kappa(X)\right)}{\sigma_m(B)} \tag{2.30}$$

where $\sigma_m(B)$ is the m-th smallest singular value of B, which is defined in Equations (2.14) *and* (2.15)*, and the solution z^v to equation* (2.22) *satisfies*

$$\|z^v(t)\| \leq \kappa(X)\max_j \left(|e^{\lambda_j t}|\right)\|z^v(0)\|. \tag{2.31}$$

Proposition 3. (Thm. 6, [123]) *If the feedback matrix K is such that Equation* (2.22) *is exponentially stable, then the perturbed closed loop system matrix $A + BK + \Delta$ remains*

stable for all disturbances Δ which satisfy

$$\|\Delta\|_2 < \min_{s=i\omega} \sigma_N \left(sI - (A + BK)\right) =: \zeta(K), \tag{2.32}$$

where

$$\zeta(K) \geq \min_j Re\left(\frac{-\lambda_j}{\kappa(X)}\right),$$

and $Re(\cdot)$ denotes the real part.

In particular, if there is an error in the estimation of the parameters ν and μ, then the feedback matrix K will still stabilise the zero solution as long as the error in the parameter estimation is bounded by $\zeta(K)$. We have studied the robustness of the controls for stabilising steady states and travelling waves by combining Propositions 2 and 3. We now present a summary of our results.

Variations in δ

As seen from the dispersion relation (2.6), variations in δ do not affect the stability of the solutions and consequently so they do not affect the matrix K. This implies that the matrix Δ is zero, and the zero solution to system (2.22) is still stable. In the case when we are interested in stabilising travelling waves, we need to take into account the fact that the amplitude of the travelling waves increases with δ - see for example [126, Fig. 1]. Hence, if we overestimate the value of $\inf \bar{u}_x$ and take this into account when choosing the new eigenvalues, the stabilised solution should remain close to the desired travelling wave as demonstrated by our numerical experiments in Fig. 2.4.

Variations in ν and μ

As seen from (2.6) variations in ν and μ can affect the stability of the solutions and the number of unstable modes. An increase in unstable modes in turn affects the number of controls needed since our theoretical results support that we need the same number of controls as unstable modes as stated in Remark 4. However, we have performed numerical experiments (see Fig. 2.5) that show that using two less controls than predicted theoretically does not affect the stability of the solutions.

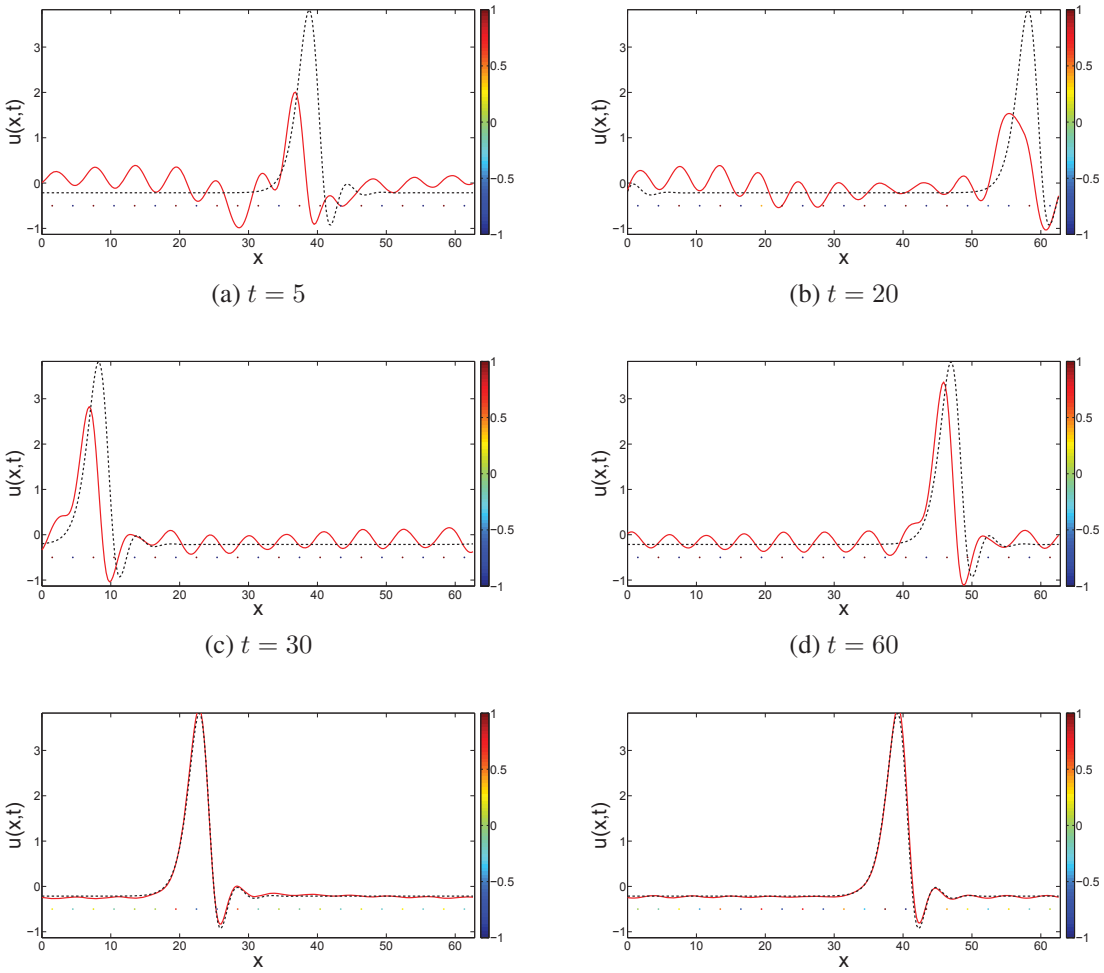

(a) $t = 5$ (b) $t = 20$

(c) $t = 30$ (d) $t = 60$

(e) $t = 90$ (f) $t = 200$

Figure 2.4: Snapshots of the time evolution of a stabilised travelling wave solution for $\mu = 0$, $\nu = 0.01$ and assuming uncertainty in the parameter δ. Black dashed line is the desired travelling wave (which is the correct solution for $\delta = 0.03$), red full line is the controlled solution assuming $\delta = 0.04$ and the dots represent the controls locations and their intensity.

Now we consider the case where we have some uncertainty of amplitude ϵ_1 and ϵ_2 in the values of ν and μ, respectively,

$$u_t = -(\nu + \epsilon_1)u_{xxxx} - (\mu + \epsilon_2)\mathcal{H}[u_{xxx}] - u_{xx} - uu_x + \sum_{i=1}^{m} b_i(x)K_i.\left(z^u - z^{\bar{u}}\right). \quad (2.33)$$

The controls have been chosen so that the solution to the equation is stabilised when $\epsilon_1 =$

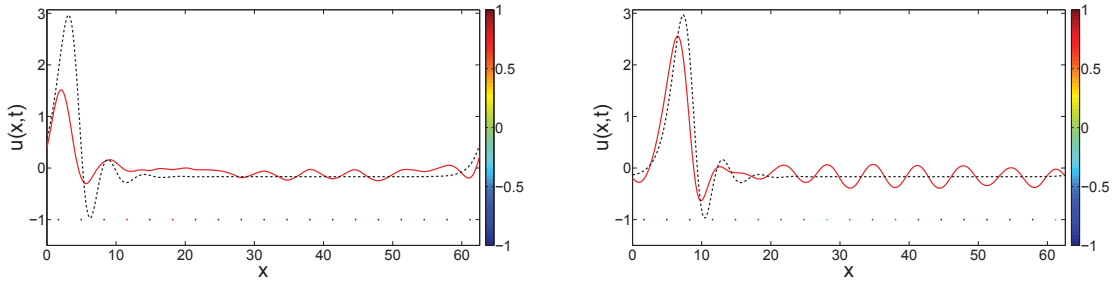

(a) $t = 1$

(b) $t = 3$

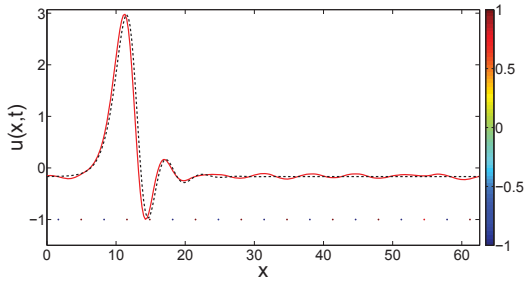

(c) $t = 5$

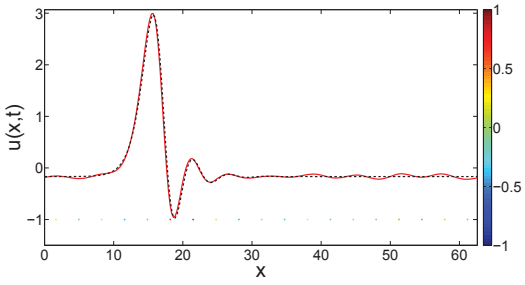

(d) $t = 7$

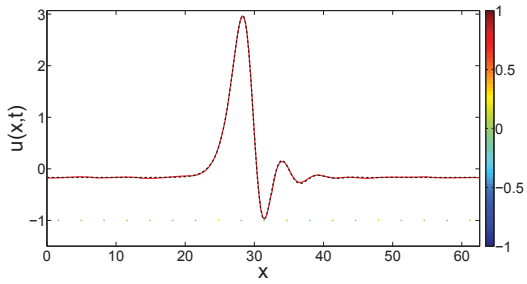

(e) $t = 13$

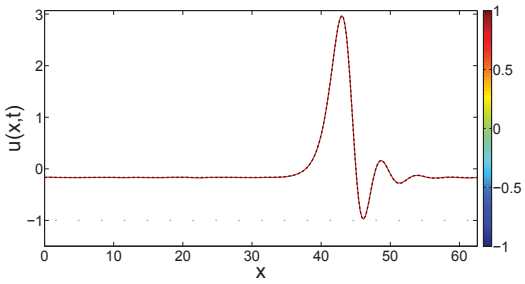

(f) $t = 20$

Figure 2.5: Snapshots of the time evolution of the stabilised travelling wave solution in Fig. 2.12b using $m = 19$ controls instead of $m = 21$ at different times. Red full line is the controlled solution, black dashed line is the desired travelling wave and the dots represent the controls and their intensity.

$\epsilon_2 = 0$. Multiplying (2.33) by u, integrating by parts and using Young's inequality, we find

$$\frac{1}{2}\frac{d}{dt}\|u(\cdot,t)\|^2 \leq -\kappa\|u\|^2 - \epsilon_1\|u_{xx}\|^2 + \frac{\epsilon_2}{2}\left(\|u_x\|^2 + \|u_{xx}\|^2\right),$$

where $\kappa = a + \frac{\inf \bar{u}_x}{2}$ is a constant. On the other hand, the perturbation $-\epsilon_1 u_{xxxx} - \epsilon_2 \mathcal{H}[u_{xxx}]$ can be discretised and written as

$$\Delta = \mathrm{diag}(0, -\epsilon_1 k^4 + \epsilon_2 k^3, -\epsilon_1 k^4 + \epsilon_2 k^3), \tag{2.34}$$

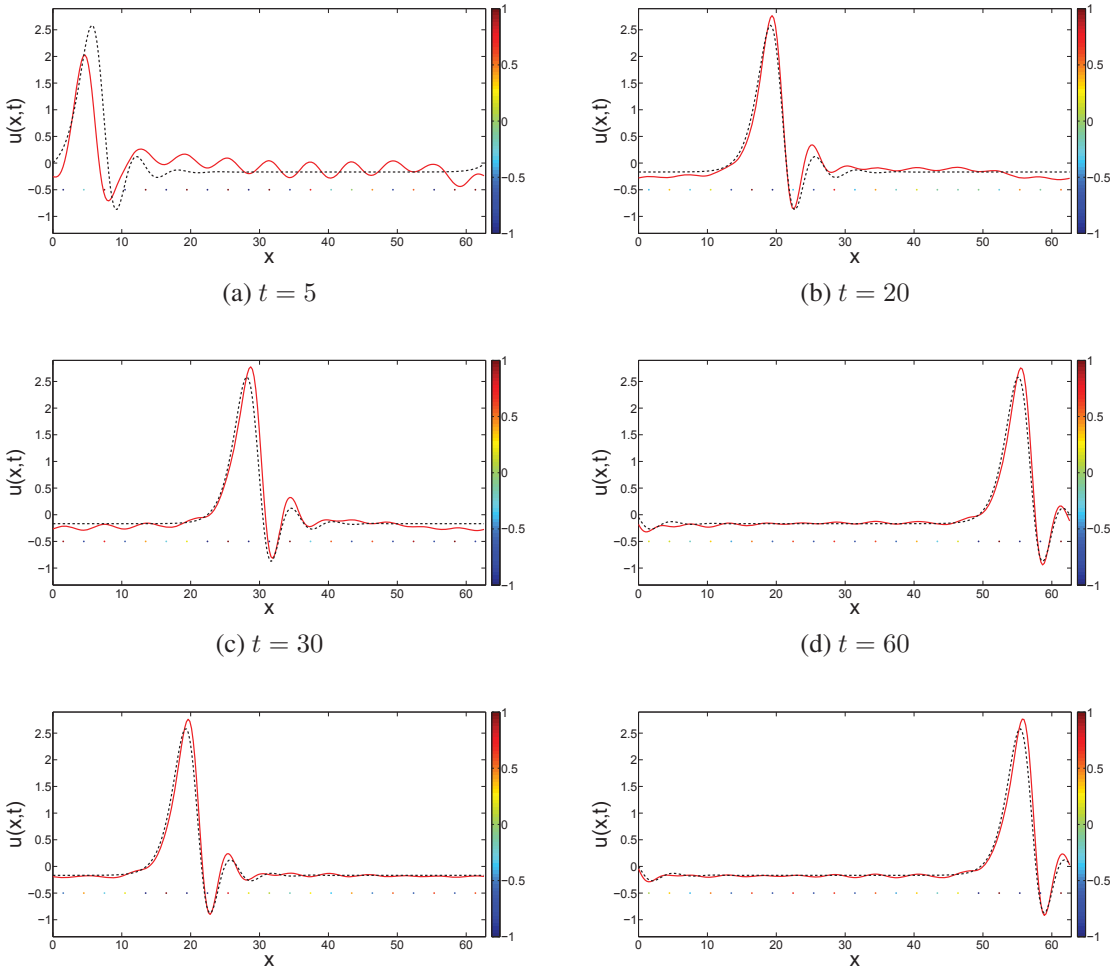

(a) $t = 5$ (b) $t = 20$

(c) $t = 30$ (d) $t = 60$

(e) $t = 90$ (f) $t = 200$

Figure 2.6: Snapshots of the time evolution of a stabilised travelling wave solution for $\delta = \mu = 0$ and assuming uncertainty in the parameter ν. Black dashed line is the desired travelling wave (which is the correct solution for $\nu = 0.013 \Leftrightarrow L \approx 55$) and red full line is the controlled solution assuming $\nu = 0.01 \Leftrightarrow L \approx 62$. The dots represent the controls' locations and their colours represent each control's amplitude.

$k = 1, \ldots, N/2$, and it follows that its Fröbenius norm is given by

$$\|\Delta\|_2^2 = 2\sum_{k=1}^{N/2} k^6 \left(-\epsilon_1 k + \epsilon_2\right)^2 = 2\sum_{k=1}^{N/2} k^6 \left(\epsilon_1^2 k^2 - 2\epsilon_1\epsilon_2 k + \epsilon_2^2\right). \tag{2.35}$$

For stability we need (2.35) to satisfy estimate (2.32) - see Proposition 3. Therefore, we have the following proposition.

Proposition 4. *Let K be a matrix such that $A_u + B_u K$ has the prescribed (negative real*

part) eigenvalues, $\lambda_1, \ldots, \lambda_m$*, with* $m = 2l + 1$*, and let*

$$BK = \begin{bmatrix} B_u K & 0 \\ B_s K & 0 \end{bmatrix}.$$

Then the perturbed system $A + BK + \Delta$*, where* Δ *is given by* (2.34)*, is stable provided that*

$$\left(2 \sum_{k=1}^{N/2} k^6 \left(\epsilon_1^2 k^2 - 2\epsilon_1 \epsilon_2 k + \epsilon_2^2 \right) \right)^{1/2} \leq \min_{s=i\omega} \sigma_N \left(sI - (A + BK) \right).$$

We have performed numerical experiments to test the robustness of the controls, and in particular we focussed on robustness with respect to the parameters δ and ν. Numerical results are presented in Figs. 2.4-2.6 (results in these figures are shown in the original unscaled domain of length L - see (2.2) for the transformations). In Fig. 2.5 we use the same parameter values as in Fig. 2.12b but we use 19 controls instead of 21, i.e. two controls less than the number of unstable eigenvalues. The black dashed curve is the desired travelling wave solution and the red solid curve is the controlled solution with 19 controls. We conclude, therefore, that our control methodology is robust with respect to a slight decrease in the number of controls. Note however, that the number of controls cannot be significantly smaller than the number of unstable eigenvalues - for example, running the same numerical experiment with 17 controls did not yield satisfactory results in the sense that wavy perturbations observed in panels (b) and (c) were not suppressed.

A robustness test with respect to changes in ν (with $\delta = \mu = 0$) is depicted in Fig. 2.6. We begin with an unstable travelling wave at $\nu = 0.013$ and wish to control it but by solving the KS equation with a reduced value of $\nu = 0.01$, i.e. we impose an uncertainty in the value of the parameter ν or equivalently in the shape of the desired solution. The results again show robust behaviour with the two solutions being almost indistinguishable. Finally in Fig. 2.4 we present robustness experiments for $\mu = 0$, $\nu = 0.01$ and changes in the dispersion parameter δ from 0.03 to 0.04, with equally accurate performance as before.

2.3 Numerical Results

Section 2.2 was devoted to proving rigorously that steady states and travelling wave solutions of the generalised KS equation can be stabilised using linear feedback controls. The

number of controls is predicted to be as large as the number of linearly unstable modes, and robustness with respect to uncertainty in the parameters ν, μ and δ was also proved. In this section we implement the linear feedback controls numerically and undertake an extensive computational study of the stabilisation and control in practical situations.

2.3.1 Computation of non-uniform steady states and travelling waves

One of the main objectives of our work is the stabilisation of unstable solutions of the gKS equation. To obtain steady state solutions $\bar{u}(x)$ (in the absence of dispersion), we need to solve the equation

$$\nu\bar{u}_{xxxx} + \mu\mathcal{H}[\bar{u}_{xxx}] + \bar{u}_{xx} + \bar{u}\bar{u}_x = 0, \tag{2.36}$$

in the interval $[0, 2\pi]$, subject to periodic boundary conditions. Travelling waves of speed c are found by looking for solutions of the form $\bar{u}(x,t) = U(x-ct) = U(\xi)$ and solving

$$-cU' + \nu U'''' + \mu\mathcal{H}[U'''] + \delta U''' + U'' + UU' = 0, \tag{2.37}$$

subject to periodic boundary conditions, where primes denote differentiation with respect to ξ. We note that equation (2.36) is a particular case of (2.37). Expressing the solutions in Fourier series

$$U(\xi) = \sum_{n=1}^{\infty} U_n^s \frac{\sin(n\xi)}{\sqrt{\pi}} + U_n^c \frac{\cos(n\xi)}{\sqrt{\pi}}, \tag{2.38}$$

and substituting into (2.36) and (2.37) we obtain an infinite system of nonlinear algebraic equations for the coefficients U_n^s, U_n^c, $n = 1, \ldots, \infty$, or for the coefficients and the velocity c, in the case of travelling waves. The resulting system of equations for steady states is

$$(\nu n^4 - \mu n^3 - n^2)U_n^c + g_n^c = 0, \qquad n = 1, \ldots, \infty, \tag{2.39a}$$

$$(\nu n^4 - \mu n^3 - n^2)U_n^s + g_n^s = 0, \qquad n = 1, \ldots, \infty. \tag{2.39b}$$

For travelling waves we can assume, without loss of generality due to translation invariance, that $U_1^s = 0$, to obtain

$$-(cn+\delta n^3)U_n^s+(\nu n^4-\mu n^3-n^2)U_n^c+g_n^c=0, \qquad n=1,\ldots,\infty, \tag{2.40a}$$

$$(cn+\delta n^3)U_n^c+(\nu n^4-\mu n^3-n^2)U_n^s+g_n^s=0, \qquad n=2,\ldots,\infty, \tag{2.40b}$$

$$(c+\delta)U_1^c+g_1^s=0. \tag{2.40c}$$

The systems were truncated and solved using a nonlinear solver (e.g. MATLAB's *fsolve*) to find solutions to system (2.39) by first setting $\mu = 0$ and carrying out a numerical continuation on ν, and secondly by fixing a value of ν and varying μ. Additional computations were done using the continuation software AUTO-07p [61]. For travelling waves we used continuation on ν, μ and δ. Without loss of generality we also impose $c > 0$: if $U(x-ct)$ is a solution of (2.37) with $c < 0$, then $-U(-x-(-c)t)$ is also a solution with $c > 0$.

Given the Fourier coefficients and the velocity of a travelling wave, we can write the soluton of the KS equation as

$$\begin{aligned}\bar{u}(x,t)=U(x-ct)= \;& \textstyle\sum_{n=1}^{\infty}\left(U_n^s\cos(nct)+U_n^c\sin(nct)\right)\sin(nx)+\\ & \textstyle\sum_{n=1}^{\infty}\left(U_n^c\cos(nct)-U_n^s\sin(nct)\right)\cos(nx).\end{aligned} \tag{2.41}$$

Our computational results are presented in the bifurcation diagram in Fig. 2.1 that depicts the variation of the L^2-norm with ν of the steady states and travelling wave solutions of the gKS equation (2.4) in the absence of dispersion ($\delta = 0$). Panels (a)-(d) correspond to $\mu = 0,\ 0.2,\ 0.5,\ 1.0$; steady-states are plotted with solid blue curves and travelling waves with dashed red curves. We observe that the presence of the Hilbert transform increases the value of ν for which instability arises [217], but it does not change the shape of the bifurcation diagram. This is because the Hilbert transform term acts as a negative diffusion, see Equation (2.6), and therefore its presence acts to shift the bifurcation diagram to higher ν, i.e. lower $\alpha = 4/\nu$ as seen in the figure. We emphasise the fact that the bifurcation diagrams in Fig. 2.1 are not complete and we expect additional unstable branches, in analogy with known results for the KS equation [127]. This is not a restriction here, since we are interested in demonstrating the stabilisation of unstable steady or travelling wave solutions, rather than the stabilisation of all such branches. For the branches computed here, we analysed their stability numerically by adding a small perturbation to the initial condition (about 10% or smaller of the amplitude of the steady state solution) and studied the time evolution to ensure

that we identified unstable steady solutions to be stabilised using linear feedback controls.

2.3.2 Time dependent simulations and feedback control

We used a Galerkin truncation [208] for the spatial discretisation of the PDE, with the number of modes varying between 32, 64 and 128 depending on the number of unstable modes. Time integration is carried out using second order implicit-explicit backward differentiation formulae (BDF) schemes [2, 3].

To construct the matrix K necessary for the stabilisation of the steady states, we used MATLAB's command *place* (see Appendix A.2 for description). Given the matrices A and B, we sought a matrix K such that the eigenvalues of the matrix $A + BK$ were:

- -1 if it is the eigenvalue corresponding to the constant eigenfunction $\frac{1}{\sqrt{2\pi}}$.
- $\pm\lambda$ if λ is an eigenvalue of A with negative/positive real part.
- $-10\delta\lambda$ instead of $-\lambda$ if $\delta > 0$. We do this because the amplitude of the solutions grows with δ - [126], so we need to account for this when building the controls.

Controlling towards steady state solutions

We begin by comparing our numerical results in the absence of electric fields and dispersion ($\mu = 0, \delta = 0$) and for two values of $\nu = 0.2$ and $\nu = 0.4$ with those obtained by Christofides in [44] (note that the number of unstable eigenvalues is $2l + 1$ where $l = [\nu^{-1/2}]$, and $[\cdot]$ denotes the integer part). The number of controls used is 5 and 3, respectively, i.e. equal to $2l + 1$; these are placed equidistantly and the initial condition is

$$u_0(x) = \frac{1}{\sqrt{2\pi}} + \frac{1}{\sqrt{\pi}} \sum_{n=1}^{5} \left(\sin(nx) + \cos(nx)\right).$$

The results are presented in Fig. 2.3 and clearly show that the system is controlled to the zero solution long before the final computed time of $t = 5$.

With our methodology we can also stabilise the zero solution for small values of ν (i.e., a large domain length), which support rather complex chaotic behaviour. As an example, we plot in Fig. 2.7 the results of the stabilisation of the zero solution for $\nu \approx 9 \times 10^{-4}$, which corresponds to $L = 200$, and $\delta = \mu = 0$. We used $m = 63$ equidistant controls and

random initial conditions. For a video of the time evolution shown in this Figure, see the Supplemental material of [90]. The dots in the video represent the control actuator positions, while their colour varies with the amplitude of the controls.

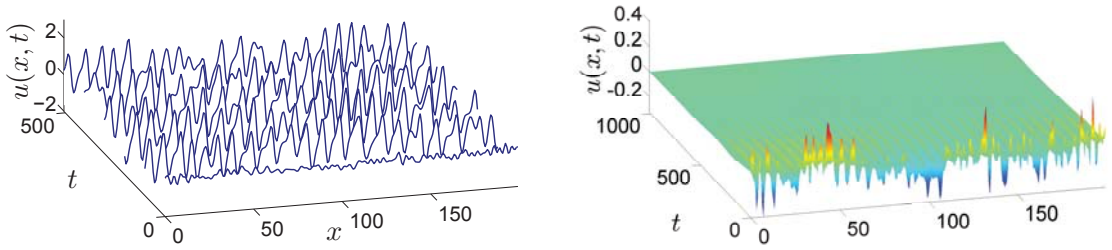

(a) Uncontrolled Solution (b) Controlled Solution

Figure 2.7: Spatiotemporal evolution of the KS equation ($\delta = \mu = 0$). The left panel shows the uncontrolled solution, while the right panel shows the stabilised zero solution, using $m = 63$ equidistant controls.

Results analogous to those presented in Fig. 2.3 were found regarding the stabilisation of the zero solution to the KS equation in the presence of an electric field. In what follows we use the following initial condition unless stated otherwise:

$$u_0(x) = \frac{1}{\sqrt{\pi}} \left(\sin(x) + \cos(x)\right). \tag{2.42}$$

Note that the number of unstable modes is $2l+1$ where $l = \left[\frac{\mu+\sqrt{\mu^2+4\nu}}{2\nu}\right]$: see Proposition 1- and this is the number of controls used in the numerical experiments. The numerical results for $\nu = 0.2$ and $\mu = 0.5$ with 5 equidistant controls are shown in Fig. 2.8, where we again clearly observe stabilisation to the zero solution.

Having shown the stabilisation of zero states for small values of ν, we turn next to the stabilisation of nontrivial steady states of the generalised KS equation (2.4), in the absence of dispersion. We illustrate the feasibility of our control methodology for two typical cases that yield unstable steady states as computed in the bifurcation diagram of Fig. 2.1. In the first case we use $\nu = 0.1115$, $\mu = 0$, and in the second $\nu = 0.35$, $\mu = 0.3$. In both cases we used $2l + 1$ equidistant controls, i.e., the same as the number of unstable eigenvalues of the system. The results of our numerical experiments are presented in Figs. 2.10 and 2.11, respectively. When $\nu = 0.1115$, $\mu = 0$, i.e. $\alpha \approx 35.87$, both stable and unstable steady states coexist and the solution of the PDE with a given initial condition, e.g. (2.42), evolves to the

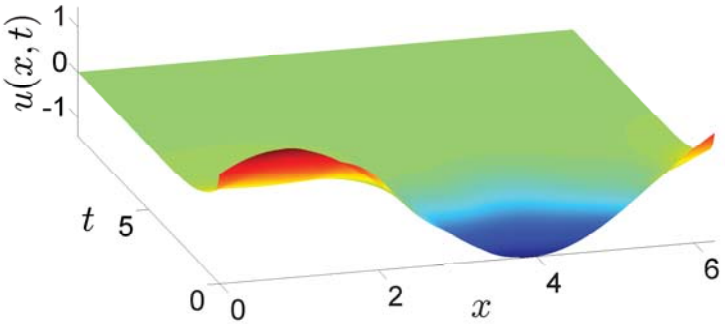

Figure 2.8: Spatiotemporal evolution showing stabilisation to the zero solution of the KS equation in the presence of an electric field with $\mu = 0.5$ and $\nu = 0.2$ ($\alpha = 20$).

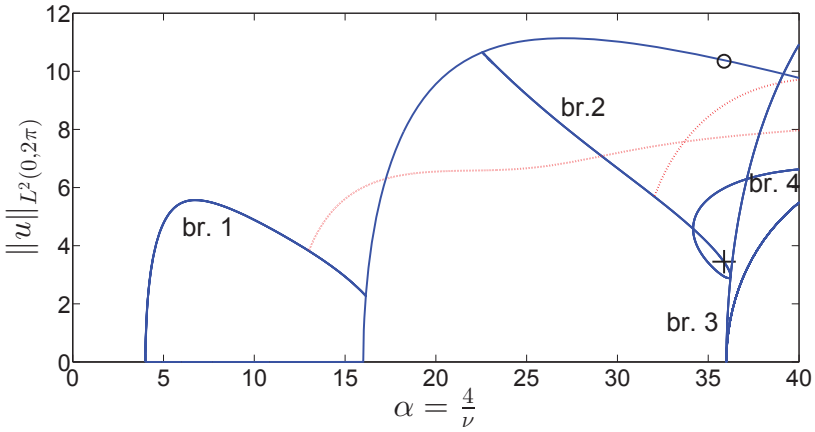

Figure 2.9: Zoom in of Panel 2.1(a) with $\nu \in [0.1, 1]$. Branches are labelled as used in Tables 2.5-2.7: Branch 1 - unimodal steady states; branch 2 - bimodal steady states; branch 3 - trimodal steady states; branch 4 - tetramodal steady states. The cross and open circle symbols indicate the steady states (stable and unstable, respectively) that are shown in Fig. 2.10.

most attracting stable state. This is shown in Fig. 2.10(a) where it is seen that the solution evolves to a stable bimodal steady state, marked with a circle in Fig. 2.9. We are interested in using feedback control to stabilise one of the coexisting unstable steady states, and the results of achieving this are presented in Figs. 2.10(b)-(c); panel 2.10(b) shows the evolution of the initial condition (2.42) using $2l + 1 = 5$ equidistant controls and stabilisation of the steady state marked with a $+$ in Fig. 2.9 is achieved relatively quickly after approximately 2 time units. The evolution of the amplitudes of the 5 applied controls is shown in Fig. 2.10(c), and we see that the required energy tends to values very close to zero as time evolves. Note that the control amplitudes remain small and close to zero once the unstable controlled state is reached, but they cannot be identically zero due to the unstable nature of the controlled

solution. Fig. 2.11 shows the results for $\nu = 0.35$, $\mu = 0.3$. The solution we choose to

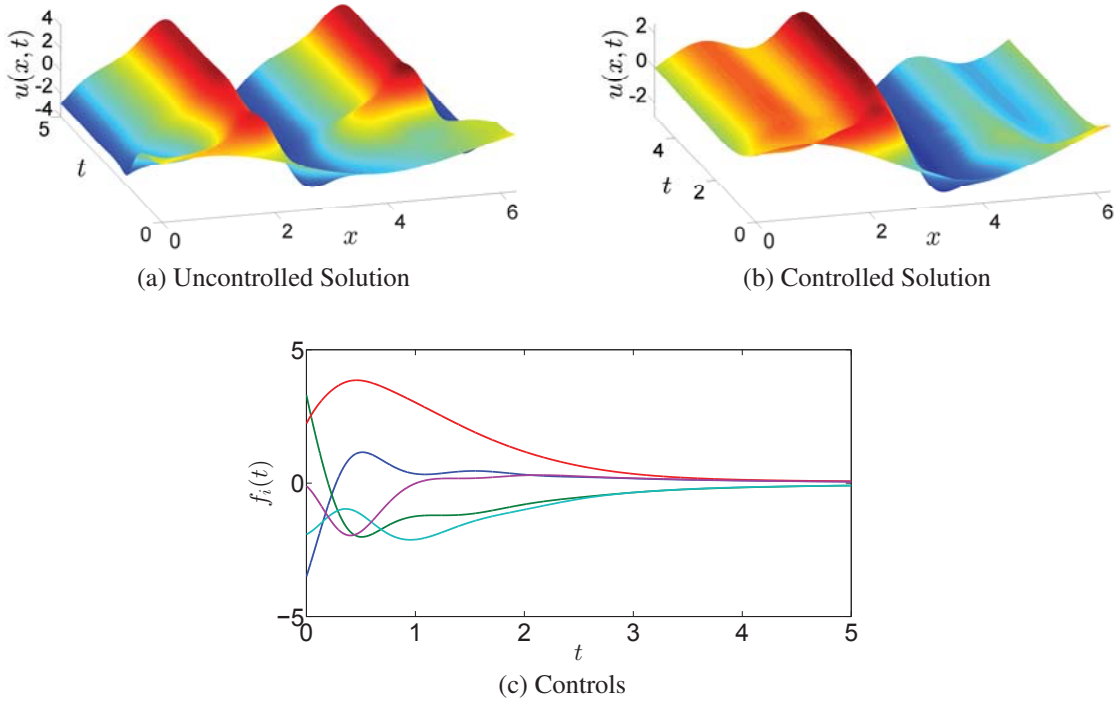

(a) Uncontrolled Solution

(b) Controlled Solution

(c) Controls

Figure 2.10: Control of non-uniform solutions of the KS equation for $\nu = 0.1115$; panel (a) spatiotemporal evolution without controls (solution belongs to branch 1 of the bifurcation diagram in Fig. 2.1a); panel (b) controlled to the steady state in branch 4 of the bifurcation diagram in Fig. 2.1a; panel (c) evolution of the amplitude of the 5 applied controls.

stabilise at these values is an unstable bimodal steady state and Fig. 2.11 shows how it is stabilised using $2l + 1 = 5$ controls.

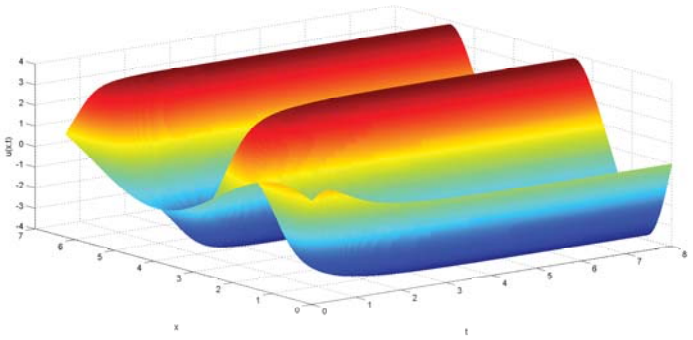

Figure 2.11: Spatiotemporal evolution of the stabilised steady state of the Kuramoto-Sivashinsky equation for $\nu = 0.35$ ($\alpha \approx 11.43$), $\mu = 0.3$.

Controlling towards travelling wave solutions

Our next task is to stabilise travelling wave solutions of the equation with and without dispersion and electric field. Fig. 2.12 illustrates the stabilisation of three different travelling wave

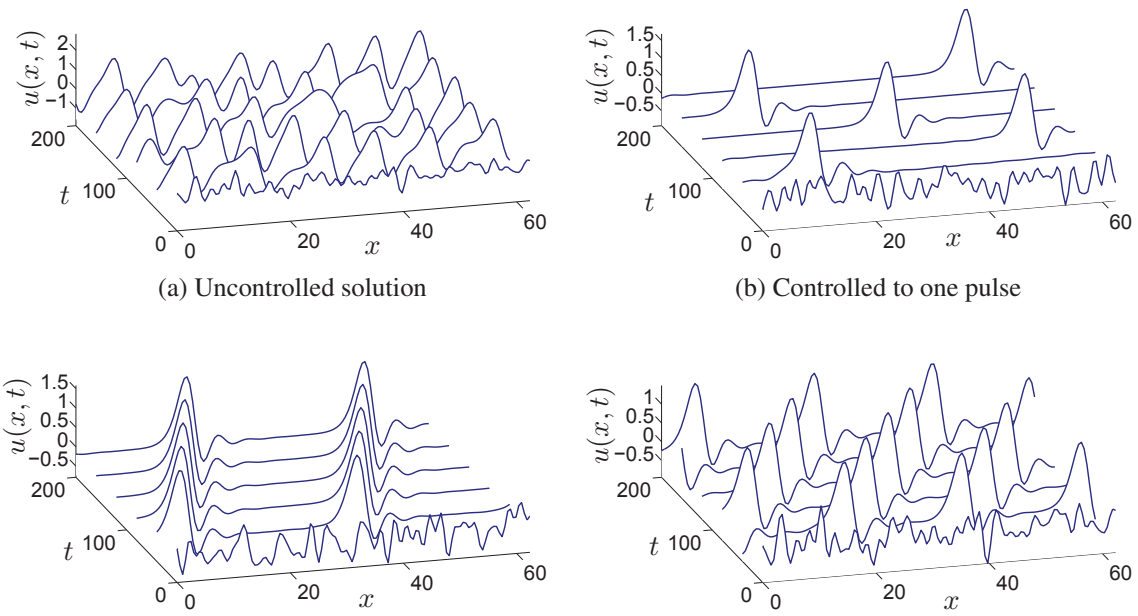

(a) Uncontrolled solution

(b) Controlled to one pulse

(c) Controlled to two pulses

(d) Controlled to three pulses

Figure 2.12: Solution to the KS equation for $\nu = 0.01$ (2.12a) with no controls, and controlled to (2.12b) one solitary pulse, (2.12c) two solitary pulses and (2.12d) three solitary pulses.

solutions to the KS equation (2.4) with no dispersion or electric field ($\delta = \mu = 0$) and for a small value of ν ($\nu = 0.01$) which corresponds to a very large domain ($L = 20\pi \approx 62$) that enables the existence of single pulse travelling waves as well as two- or three-pulse bound states. However, due to the small value of ν, when solving the PDE the initial condition evolves to a solution that exhibits the spatiotemporal chaotic behaviour that is characteristic of this equation. Panel 2.12(a) shows this chaotic behaviour while Panels (b)-(d) show the evolution of the controlled solution to 1, 2 and 3 pulses, respectively. We used $m = 21$ equidistant controls and random initial conditions in each case.

As mentioned before, the presence of dispersion regularises the chaotic behaviour of the solutions, trapping its dynamics into spatially periodic travelling waves that appear to be randomly interacting with each other. However, it is also possible to control the solutions in the presence of dispersion to desired travelling waves or bound states. Figs. 2.13 and 2.14

show this stabilisation for $\nu = 0.01$, $\mu = 0$ and $\delta = 0.01$ and $\delta = 0.05$, respectively. These values correspond to original values of $L = 20\pi$ and $\delta = 0.1$ and 0.5. We again used $m = 21$ controls.

Fig. 2.13 plots the results for $\delta = 0.01$. This is a relatively small value of δ and as we can see in panel (2.13a), we can observe the weak/dissipative turbulent behaviour characteristic of the gKS equation with small dispersion. Panels (2.13b), (2.13c) and (2.13d) show the successful stabilisation of travelling waves/bound states with 1, 2 and 3 pulses, respectively.

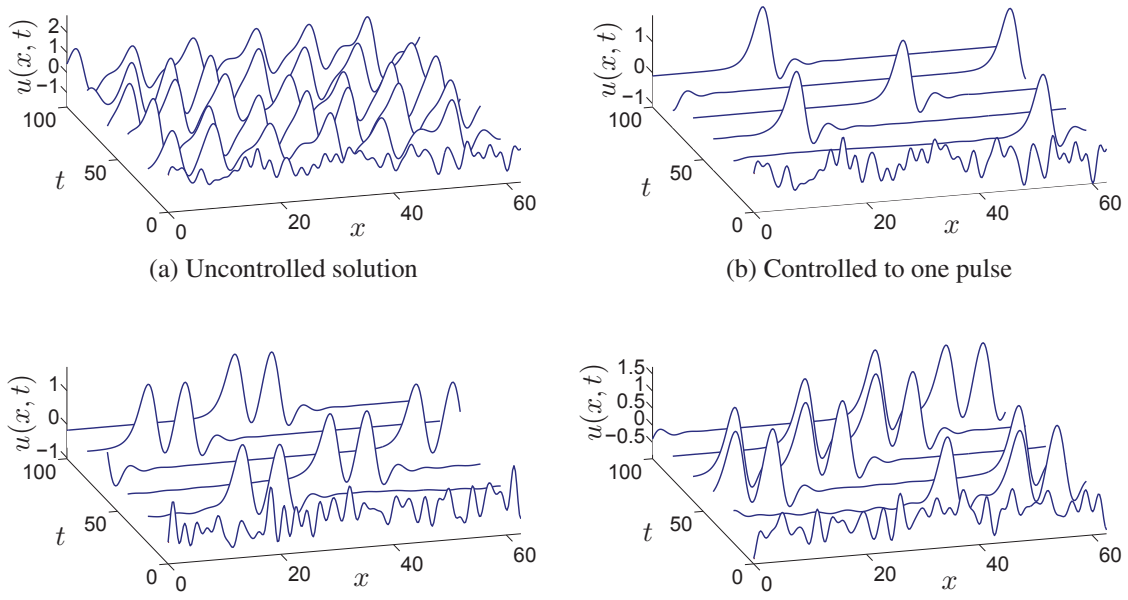

(a) Uncontrolled solution

(b) Controlled to one pulse

(c) Controlled to two pulses

(d) Controlled to three pulses

Figure 2.13: Solution to the gKS equation for $\nu = 0.01$, $\delta = 0.01$ ($L = 20\pi$, $\delta = 0.1$ in the original variables) (2.13a) with no controls, and controlled to (2.13b) one solitary pulse, (2.13c) two solitary pulses and (2.13d) three solitary pulses.

Similarly, Fig. 2.14 plots the results for $\delta = 0.05$. As this is a larger value of δ, we expect the chaotic dynamics to be regularised, and we observe that in panel (2.14a). Again, panels (2.14b), (2.14c) and (2.14d) show the successful stabilisation of travelling waves/bound states with 1, 2 and 3 pulses, respectively. All the travelling wave figures are rescaled to the original domains for clarity. Animations of the time evolution of these examples, as well as the robustness tests presented in Section 2.2.2 are available in the supplemental material of [90], where we plot the uncontrolled and stabilised solutions, together with $m = 21$ dots that

represent the control actuators locations and whose colours represent their amplitude.

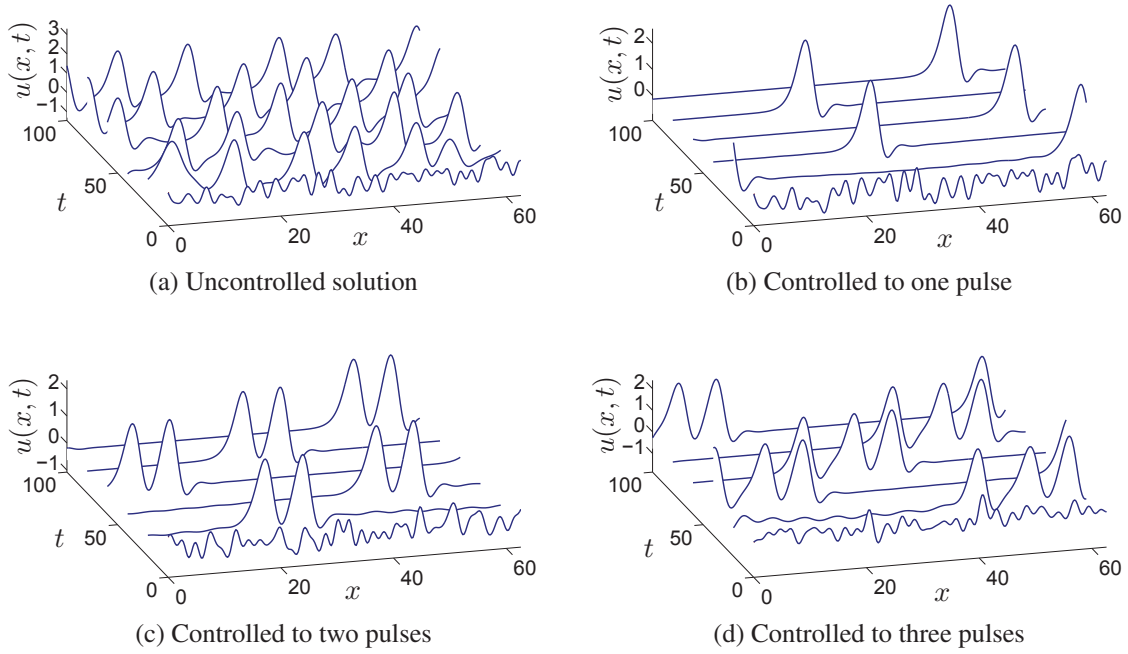

(a) Uncontrolled solution

(b) Controlled to one pulse

(c) Controlled to two pulses

(d) Controlled to three pulses

Figure 2.14: Solution to the gKS equation for $\nu = 0.01$, $\delta = 0.05$ ($L = 20\pi$, $\delta = 0.5$ in the original variables) (2.13a) with no controls, and controlled to (2.13b) one solitary pulse, (2.13c) two solitary pulses and (2.13d) three solitary pulses.

Controlling towards steady states that are not solutions

Finally, we plot the numerical results of the stabilisation of periodic steady states that are not solutions of the gKS equation, as was presented in Section 2.2.1. We control the solution of the gKS equation with $\nu = 0.01$, $\mu = 0$ and $\delta = 0.05$ towards the steady state $g(x,t) = \sin\left(\frac{2\pi}{L}x\right) = \sin(\sqrt{\nu}x)$. We notice, however, that in this case, we need to force the system with the right hand side $\mathcal{G}(g(x,t))$ and the controls are no longer point actuated. This is necessary, however, so that $g(x,t)$ is a solution to the equation. We point out that the gKS equation with $\delta > 0$ does not admit steady non zero solutions. The stabilised solution is presented in Fig. 2.15.

Energy spent with the controls

When controlling different solutions to the gKS equation, one of the factors to take into account is the energy spent with the controls: in a practical application it is useless to be able

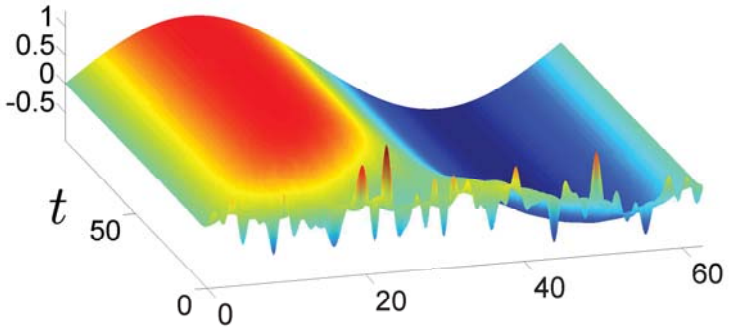

Figure 2.15: Spatiotemporal evolution of the gKS equation controlled towards $g(x,t) = \sin(\sqrt{\nu}x)$ for $\nu = 0.01$, $\mu = 0$, $\delta = 0.05$.

to stabilise a chosen state if the energy spent with the stabilisation process, and therefore its cost, outweighs the advantages of achieving such state. Since our controls are proportional to the difference between the current state of the solution and the desired state, we know that once the desired state is reached the amplitudes of the controls will become practically zero. In most of the computations presented in this section for travelling waves, we kept track of the energy spent with the controls, which we plot in Fig. 2.16, by tracking their L^2 norms over time:

$$E_1(t) = \sum_{i=1}^{m} f_i(t)^2. \tag{2.43}$$

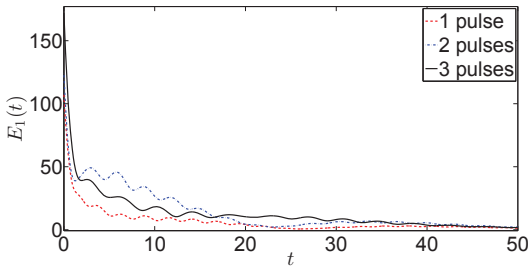

(a) $\delta = 0.01$

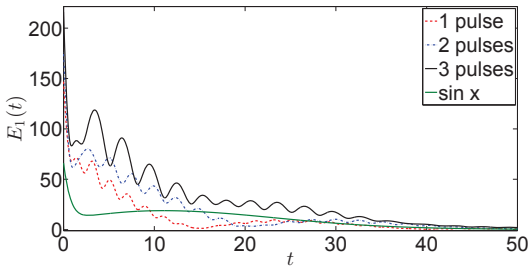

(b) $\delta = 0.05$

Figure 2.16: Energy $E_1(t)$ spent when stabilising the travelling waves in Figs. 2.13 and 2.14 and the periodic solution $g(x,t)$ in Fig. 2.15 for $\nu = 0.01$ and (a) $\delta = 0.01$ and (b) $\delta = 0.05$.

In Section 2.4 we will be concerned with how to optimise the energy spent in the control process, where we measure the cost of the controls by three different ways (given by different Sobolev norms of the solutions).

2.4 Optimal control for the generalised Kuramoto-Sivashinsky equation

In practical applications it is important to apply controls that minimise the cost associated with their use, and this leads to considerations of an optimal control problem based on some measure of the energy cost of the controls. In what follows we consider the energy of the controls given by their L^2-norm. Since the controls decay to almost zero relatively fast in time (see Figs. 2.11 or 2.16, for instance), we expect that minimising their L^2-norm should decrease their amplitude.

The objective, then, is to achieve control of the zero solution or other unstable steady-state or travelling wave solutions of the gKS equation, and to do this while spending the least energy possible. To that end, we consider a cost functional that includes the distance between the solution and the desired state, as well as the L^2-norm of the controls used. Different distance norms $\|u - \bar{u}\|$ can be used and in our computations we employ the L^2, H^1 or H^2 norms. The reason we consider different norms is that the solutions are expected to belong to $H^2(0, 2\pi)$, and we wish to analyse the effects of the regularity and the oscillations of the solutions on the cost functional.

In flow control it is possible to use point actuator functions [7, 43, 44, 63], implying that we can take $b_i(x) = \delta(x - x_i)$. Assuming that the cost of placing a control at x_i is the same for all actuator positions $x \in (0, 2\pi)$, it makes sense to seek a solution that minimises the norms of the control functions $f_i(t)$. Since the delta functions in the feedback controls are not L^2 functions, the standard results of constrained optimisation for PDEs [141, 211] do not apply. Because of this hurdle we will first prove existence of optimal controls for the case of general controls, $f(x,t) \in L^2(0,T;\dot{L}^2(0,2\pi))$, i.e. mean zero spatially periodic controls in $L^2(0,2\pi)$ that are also L^2 functions of time, and focus on the case of feedback controls where we can apply standard optimisation techniques.

We consider cost functionals of the form

$$\mathcal{C}\,(u,F) = \frac{1}{2}\int_0^T \|u(\cdot,t) - \bar{u}\|^2\,dt + \frac{1}{2}\|u(\cdot,T) - \bar{u}\|^2 + \frac{\gamma}{2}\int_0^T \sum_{i=1}^{m} f_i(t)^2\,dt \qquad (2.44)$$

where $\bar{u}$ is the desired steady state, $F = [f_1\ \cdots\ f_m]$, and the norm (e.g. L^2, H^1 or H^2) is left unspecified. The choice of the parameter γ depends on how large we are willing to allow the norm of the controls to become: if we need to maintain a small norm of the

controls while allowing the solution to be considerably different from the steady state, then we use $\gamma > 1$. If, on the other hand, we have a very large amount of energy to spend on the controls and want the solution to be as close as possible to the desired steady state, then we choose $\gamma \ll 1$ so that the weight of the controls does not influence significantly the value of the cost functional. The terminal time term $\frac{1}{2}\|u(\cdot,T)-\bar{u}\|^2$ is introduced to provide us with a condition for the final-value problem obtained when solving the adjoint equation for the optimisation problem. Before proceeding to the optimisation problem it is useful to introduce the following definitions.

Definition 1. *We denote the space of admissible controls by F_{ad}. F_{ad} is usually a bounded convex subset of $L^2(0,T;\dot{L}^2(0,2\pi))$.*

Definition 2. *A control $f^* \in F_{ad}$ is said to be optimal, and $u^* = u(f^*)$ is the associated optimal state, if $\mathcal{C}(u(f^*),\bar{u},f^*) \leq \mathcal{C}(u(f),\bar{u},f)\ \forall f \in F_{ad}$.*

Our numerical experiments, which we will present in Section 2.4.2, suggest that, given an initial condition and a desired steady state, there exists at least one optimal placement of the control actuators for every value of ν and μ. However, here we prove existence of an optimal control in the case of an open-loop control using the quadratic cost functional

$$\mathcal{C}\,(u,f) = \frac{1}{2}\int_0^T \|u(\cdot,t)-\bar{u}\|_{L^2}^2\,dt + \frac{1}{2}\|u(\cdot,T)-\bar{u}\|_{L^2}^2 + \frac{\gamma}{2}\int_0^T\int_0^{2\pi} f(x,t)^2\,dx\,dt. \tag{2.45}$$

The point actuated controls in the form of delta functions are not in L^2 and hence an analogous proof in this case requires distribution theory which is beyond the scope of the present study. The optimisation problem is:

$$\begin{aligned}
\text{minimise} \quad & \mathcal{C}\,(u,f) && \text{(2.46a)}\\
\text{subject to} \quad & u_t + \nu u_{xxxx} + u_{xx} + uu_x = f(x,t), && \text{(2.46b)}\\
& u(x,0) = u_0(x) \in \dot{H}_p^2(0,2\pi), && \text{(2.46c)}\\
& \frac{\partial^j u}{\partial x^j}(x+2\pi) = \frac{\partial^j u}{\partial x^j}(x), \quad j=0,1,2,3, && \text{(2.46d)}\\
& f \in F_{ad}. && \text{(2.46e)}
\end{aligned}$$

The main result of this section is the following.

Theorem 1. *Assume that $F_{ad} \subset L^2(0,T;\dot{L}^2(0,2\pi))$. Then* (2.46) *has at least one optimal control f^* with associated optimal state u^*.*

Remark 6. *Since the Hilbert transform and third derivative terms are linear functionals of u, Theorem 1 can be easily generalised to the case when $\mu, \delta > 0$.*

Remark 7. *The presence of the Burgers nonlinearity in the PDE makes the optimisation problem no longer convex. Consequently, we do not expect the solution of the optimal control problem to be unique.*

The nonlinearity in our problem, defined by $\mathcal{N}(u) = uu_x$, is twice Fréchet differentiable (see Appendix A.1) with respect to u but is neither an increasing functional of u, nor is it globally Lipschitz continuous. Furthermore, it depends explicitly on the derivative u_x. Consequently, the well developed theory of optimal control for systems of reaction-diffusion equations [141, 211] does not apply to our problem.

Proof of Theorem 1. Let $X = H^1(0,T;\dot{H}^2_p(0,2\pi)) \times F_{ad}$ and $e(\cdot,\cdot)$ be a functional defined in X by

$$e(u,f) = \begin{bmatrix} u_t + \nu u_{xxxx} + u_{xx} + uu_x - f \\ u(\cdot,0) - u_0(x) \end{bmatrix}. \tag{2.47}$$

Our optimisation problem is that of minimising the cost functional $\mathcal{C}$ subject to $e(u,f) = 0$, periodic boundary conditions and $(u,f) \in X$; see Equation (2.46).

Let $(u,f) \in X$ satisfy $e(u,f) = 0$. Since $\mathcal{C}$ is a function of the sum of the norms of u and f, it is clear that $\mathcal{C}$ is nonnegative and

$$\mathcal{C}(u,f) \to \infty \quad \text{for} \quad \|(u,f)\|_X \to \infty. \tag{2.48}$$

Therefore, there exists a constant $c \geq 0$ such that

$$c = \inf_{e(u,f)=0} \mathcal{C}(u,f) = \lim_{n\to\infty} \mathcal{C}(u^n, f^n),$$

where (u^n, f^n) is a minimising sequence in X, which exists due to the reflexivity of L^2. From Equation (2.48) we can conclude that $\{(u^n,f^n)\}_{n\in\mathbb{N}}$ is bounded, and therefore there exists $(u^*,f^*) \in X$ such that $(u^n,f^n) \rightharpoonup (u^*,f^*) \quad \text{for} \quad n \to \infty$. This means that all the linear functionals of u^n and f^n, and in particular their derivatives, also converge weakly to

the same functionals of u^* and f^* in the appropriate space. Hence, we only need to prove the convergence of the nonlinearity.

Following an argument similar to that in [225] for the Burgers equation, we notice that since for every $t \in [0,T]$ we have $u^*(\cdot,t) \in \dot{H}^2_p(0,2\pi)$, then $u^*(\cdot,t) \in C([0,2\pi])$ and therefore if $\varphi \in X$, $(u^*\varphi)(\cdot,t) \in L^2([0,2\pi])$. Hence, $u^*\varphi \in H^1(0,T;L^2(0,2\pi))$ and

$$\int_0^T \int_0^{2\pi} (u^n - u^*)_x u^* \varphi \, dx \, dt \xrightarrow[n\to\infty]{} 0, \quad \forall \varphi \in H^1(0,T;\dot{H}^2_p(0,2\pi)). \tag{2.49}$$

Finally, from the estimates (2.7) we know that $\|u^n_x\|$ is bounded, and since $H^2(\Omega)$ is compactly embedded in $L^2(\Omega)$, we deduce that

$$\int_0^T \int_0^{2\pi} (u^n - u^*) u^n_x \varphi \, dx \, dt \leq \|u^n - u^*\| \|u^n_x\| \|\varphi\|_{L^\infty(0,2\pi)} \xrightarrow[n\to\infty]{} 0, \quad \forall \varphi \in \dot{H}^2_p(0,2\pi). \tag{2.50}$$

Hence, by adding and subtracting appropriate terms we have

$$\int_0^T \int_0^{2\pi} (u^n u^n_x - u^* u^*_x)\varphi \, dx \, dt = \int_0^{2\pi} \left((u^n - u^*)u^n_x \varphi + (u^n - u^*)_x u^* \varphi\right) \, dx \xrightarrow[n\to\infty]{} 0, \quad \forall \varphi \in \dot{H}^2_p(0,2\pi), \tag{2.51}$$

and therefore the nonlinearity $u^n u^n_x$ is weakly convergent to $u^* u^*_x$ in X. Now, noticing that u^* and u^*_x are continuous in $[0,2\pi] \times [0,T]$, we observe that u^* satisfies the periodic boundary conditions and the initial condition. If we now consider $\varphi \in X$ satisfying $\varphi(x,T) = 0$, and use the weak convergence of the derivatives of u and equation (2.51), we conclude that (u^*, f^*) is a weak solution of the state equation. The optimality of the pair (u^*, f^*) follows from the weak lower semi-continuity of $\mathcal{C}$ (cf. proof of Theorem 4.15 in [211]). □

2.4.1 Algorithm and Numerical Experiments

We note that the dependence of the cost functional on the positions x_i, $i = 1, \ldots, m$ is in the controls, since the matrix K necessary to define them depends on the positions chosen. However, when defining the Lagrangian we will assume that only the functions $b_i(x)$ depend on x_i, and treat the controls $f_i(t)$ as if they were independent of the positions x_i. Under

this assumption we are able to obtain very satisfactory results, as evidenced by the results presented in the tables below. We begin by introducing the Lagrangian for this problem (see Appendix A.3)

$$\begin{aligned}\mathcal{L}\left(u,p,[x_1,x_2,\ldots,x_m]^T\right) = \; & \frac{1}{2}\int_0^T \|u(\cdot,t)-\bar{u}\|^2\,dt + \frac{1}{2}\|u(\cdot,T)-\bar{u}\|^2 \\ & + \frac{\gamma}{2}\int_0^T \sum_{i=1}^m f_i(t)^2\,dt \\ & - \int_0^T\int_0^{2\pi} \left(u_t + \nu u_{xxxx} + u_{xx} + uu_x\right) p(x,t)\,dx\,dt \\ & + \int_0^T\int_0^{2\pi} \sum_{i=1}^m \delta(x-x_i)_i f_i(t) p(x,t)\,dx\,dt.\end{aligned} \tag{2.52}$$

Integrating by parts in space and time and computing the Fréchet derivative with respect to u (with test functions $\varphi(x,t)$ satisfying $\varphi(x,0)=0$), we obtain the adjoint equation

$$\begin{cases} -p_t + \nu p_{xxxx} + p_{xx} - up_x &= \sum_{i=1}^m \delta(x-x_i)K_i.z^p + u - \bar{u}, \\ p(x,T) &= u(x,T), \\ \frac{\partial^j p}{\partial x^j}(x+2\pi) &= \frac{\partial^j p}{\partial x^j}(x), \end{cases} \tag{2.53}$$

where $x \in [0,2\pi]$ and $t \in [0,T]$. This PDE is backwards in time but is well-posed since it is a final value problem. To solve it, we obtain the discretised ODE system $-\dot{z}^p = \mathcal{A}z^p + G^{adj}(z^p,z^u) + z^u - z^{\bar{u}}$, where the elements of $G^{adj}(z^p,z^u)$ are given by (see Appendix B.2)

$$\begin{aligned} g^s_{n,adj} &= \frac{1}{2\sqrt{\pi}}\sum_{j+k=n} k(u^s_j p^s_k - u^c_j p^c_k) + \frac{1}{2\sqrt{\pi}}\sum_{j-k=n}\left(k(u^s_j p^s_k + u^c_j p^c_k) - j(u^s_k p^s_j + u^c_k p^c_j)\right), \\ g^c_{n,adj} &= \frac{1}{2\sqrt{\pi}}\sum_{j+k=n} k(u^c_j p^s_k + u^s_j p^c_k) + \frac{1}{2\sqrt{\pi}}\sum_{j-k=n}\left(k(u^c_j p^s_k - u^s_j p^c_k) + j(u^c_k p^s_j - u^s_k p^c_j)\right), \end{aligned}$$

and we have used the Fourier series representation $p(x,t) = \frac{p^c_0}{\sqrt{2\pi}} + \sum_{n=1}^\infty p^s_n(t)\frac{\sin(nx)}{\sqrt{\pi}} + \sum_{n=1}^\infty p^c_n(t)\frac{\cos(nx)}{\sqrt{\pi}}$.

Differentiating with respect to the positions of the control actuators, we also obtain a descent direction using the variational inequality, or first variation

$$\int_0^T \left[f_1(t)p_x(\bar{x}_1,t)\cdots f_m(t)p_x(\bar{x}_m,t)\right]^T\cdot(x-\bar{x})\,dt \geq 0, \quad \forall x = [x_1\cdots x_m]^T, \tag{2.54}$$

where $\bar{x} = [\bar{x}_1, \ldots, \bar{x}_m]$ are the optimal positions. To proceed with the optimisation, we will use a gradient descent method, see [211, Sec. 5.9], and consider $F_{ad} = (0, 2\pi)^m$. The algorithm is as follows.

Algorithm for optimal control for the KS equation

Given ν, μ, γ, T, $u_0(x)$, A, x^0, B^0, $\bar{u}$, compute the matrix K^0.

while $\mathcal{C}$(current iteration) $<$ $\mathcal{C}$(previous iteration) **do**

1. Solve the state equation to obtain u^{k-1} and compute $\mathcal{C}(u^{k-1}, \bar{u}, F(x^{k-1}))$;
2. Solve the adjoint equation to obtain p^{k-1};
3. Define $P_x = \left[p_x^{k-1}(x_1^{k-1}, t) \cdots p_x^{k-1}(x_m^{k-1}, t)\right]$, $P_{k-1} = \displaystyle\int_0^T K^{k-1}(z^{u^{k-1}} - z^{\bar{u}})P_x \, dt$ and $h_k = -P_{k-1}$;
4. Find $s = \min_{s>0} \left\{C(u(x^{k-1} + sh_k), \bar{u}, F(x^{k-1} + sh_k))\right\}$;
5. Project $x^{k-1} + sh_k$ into $(0, 2\pi)^m$, obtaining x^k;
6. Compute the matrix B^k;
7. Compute the matrix K^k with MATLAB's command *place*.

end

Figure 2.17: Algorithm for optimal control of the KS equation.

Note that as mentioned earlier we consider the following three different cost functionals:

$$\mathcal{C}_1(u, \bar{u}, f) = \frac{1}{2}\int_0^T \|u(\cdot, t) - \bar{u}\|^2 \, dt + \frac{1}{2}\|u(\cdot, T) - \bar{u}\|^2 + \frac{\gamma}{2}\sum_{i=1}^m \|f_i(t)\|_{L^2(0,T)} \tag{2.55}$$

$$\begin{aligned} \mathcal{C}_2(u, \bar{u}, f) = \; & \tfrac{1}{2}\textstyle\int_0^T \left(\|u(\cdot, t) - \bar{u}\|^2 + \|u_x(\cdot, t) - \bar{u}_x\|^2\right) dt \\ & + \frac{1}{2}\left(\|u(\cdot, T) - \bar{u}\|^2 + \|u_x(\cdot, T) - \bar{u}_x\|^2\right) \\ & + \frac{\gamma}{2}\sum_{i=1}^m \|f_i(t)\|_{L^2(0,T)} \end{aligned} \tag{2.56}$$

$$\begin{aligned}\mathcal{C}_3\left(u,\bar{u},f\right) = \; & \tfrac{1}{2}\int_0^T \left(\|u(\cdot,t)-\bar{u}\|^2+\|u_x(\cdot,t)-\bar{u}_x\|^2+\|u_{xx}(\cdot,t)-\bar{u}_{xx}\|^2\right)\,dt \\ & +\frac{1}{2}\left(\|u(\cdot,T)-\bar{u}\|^2+\|u_x(\cdot,T)-\bar{u}_x\|^2+\|u_{xx}(\cdot,T)-\bar{u}_{xx}\|^2\right) \\ & +\frac{\gamma}{2}\sum_{i=1}^{m}\|f_i(t)\|_{L^2(0,T)}.\end{aligned} \tag{2.57}$$

2.4.2 Numerical Experiments

Computations were carried out using the algorithm presented in Fig. 2.17 for various values of ν and μ. The number of controls used was equal to the number of unstable eigenvalues, and m equidistant points were used as an initial guess for the position of the controls. In all the computations the initial condition is $u_0(x)=\frac{\sin(x)}{\sqrt{\pi}}+\frac{\cos(x)}{\sqrt{\pi}}$, and the final time is $T=10$.

For $\mu=\delta=0$, the numerical results are presented in Tables 2.2-2.4 for the stabilisation of the zero solution of the KS equation, and in Tables 2.5-2.7 for the stabilisation on non-trivial unstable steady states as computed in the bifurcation diagram of Fig. 2.9. Each entry in Tables 2.2-2.4 contains the value of ν, the value of the cost functional ($\mathcal{C}_1$, $\mathcal{C}_2$ and $\mathcal{C}_3$ for tables 2.2, 2.3 and 2.4, respectively), the cost of the controls $\sum_{i=1}^{m}\|f_i(t)\|_{L^2(0,T)}$, the number of iterations required to obtain an optimal state, and in the last column the spatial distribution of the controls over the domain $[0,2\pi]$ - a heavy dot is placed where a control acts. Tables 2.5-2.7 are presented in an analogous manner, with the difference that the first column provides information on the unstable solution that is being controlled, and in particular the branch on Fig. 2.1a where the solution was taken from is stated along with the value of ν. As the results indicate, several distinct unstable solutions at a given value of ν are controlled (e.g. for $\nu=0.1$, three solutions are stabilised coming from branches 1, 3 and 4 respectively).

ν	Cost $\mathcal{C}_1$	Cost of Controls	Iterations	Optimal Positions
0.9	8.9647	0.5592	3	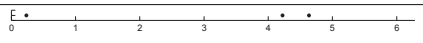
0.8	6.5012	1.1274	6	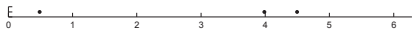
0.7	5.5760	1.7204	4	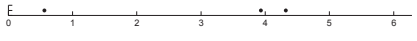
0.6	5.2803	2.3018	3	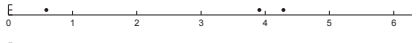
0.5	5.2230	2.8204	5	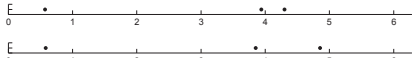
0.4	5.9339	3.8404	5	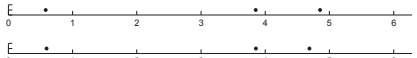
0.3	6.2152	3.9813	2	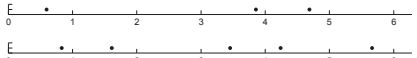
0.2	6.3127	4.5261	2	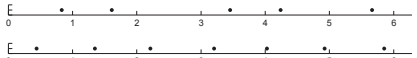
0.1	7.1652	5.5759	2	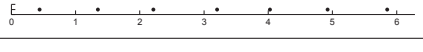

Table 2.2: Optimal positions and value of the cost functional considered in the L^2-norm for different values of ν when stabilising the zero solution to the KS equation.

ν	Cost $\mathcal{C}_2$	Cost of Controls	Iterations	Optimal Positions
0.9	17.6354	0.9698	3	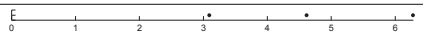
0.8	12.2553	1.5486	6	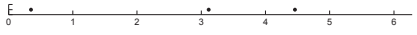
0.7	10.8270	2.0016	2	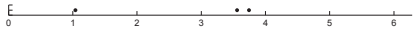
0.6	10.2340	4.0181	6	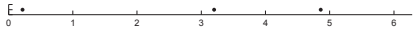
0.5	10.1517	4.5407	4	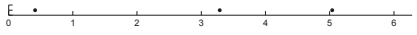
0.4	9.3345	4.2298	2	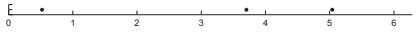
0.3	10.9671	4.8110	2	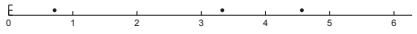
0.2	10.7154	5.5308	3	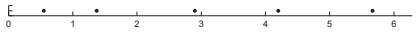
0.1	9.7088	5.6463	1	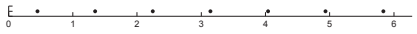

Table 2.3: Optimal positions and value of the cost functional considered in the H^1-norm for different values of ν when stabilising the zero solution to the KS equation.

ν	Cost $\mathcal{C}_3$	Cost of Controls	Iterations	Optimal Positions
0.9	27.2098	1.1313	3	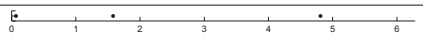
0.8	19.3431	2.3490	5	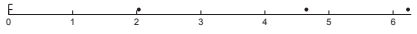
0.7	15.8522	2.5815	4	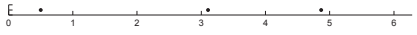
0.6	14.0865	3.3384	5	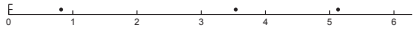
0.5	17.0462	6.4166	1	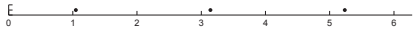
0.4	20.7720	8.3217	1	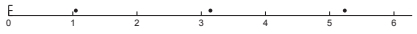
0.3	14.4393	5.3865	3	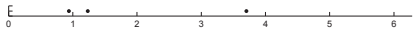
0.2	21.5856	6.1456	1	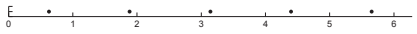
0.1	21.1636	5.6463	1	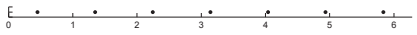

Table 2.4: Optimal positions and value of the cost functional considered in the H^2-norm for different values of ν when stabilising the zero solution to the KS equation.

As expected we observe that the value of the cost functionals $\mathcal{C}_1$, $\mathcal{C}_2$, $\mathcal{C}_3$ given by (2.55)-(2.57), increases as ν decreases. Furthermore, the value of the cost functional also increases as we increase the desired regularity of the solution from L^2 to H^1 to H^2-norms. Comparing the results and in particular the positions of the optimal controls for the three different cost functionals in Tables 2.2-2.4, we can conclude that for the stabilisation of the zero steady states, the optimal control problem is more robust (in the sense that the optimal positions of the controls do not change much as ν is reduced) when the L^2 cost functional $\mathcal{C}_1$ is used.

Turning now to the results of Tables 2.5-2.7 that deal with the stabilisation of unstable nonuniform steady states, we observe once again that there is an increase in the cost functionals as ν decreases. We also observe that in this case (and in contrast to the stabilisation of the zero solution) the higher order norms give optimal controls that are more robust, with respect to changing ν, in comparison to utilising the L^2 cost functional.

ν	Cost $\mathcal{C}_1$	Cost of Controls	Iterations	Optimal Positions
0.3	14.3164	9.7419	5	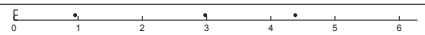
0.2,br.1	30.0588	21.8691	1	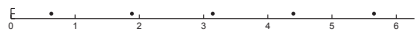
0.2,br.3	24.0520	16.2832	2	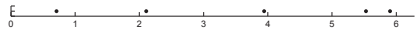
0.1,br.1	28.5591	32.9859	2	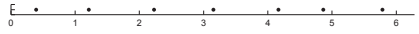
0.1,br.3	37.8902	32.4264	1	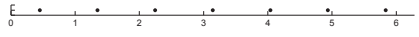
0.1,br.4	62.3916	51.6820	4	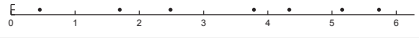

Table 2.5: Optimal positions and value of the cost functional considered in the L^2-norm for different values of ν when stabilising some of the nontrivial steady states from the bifurcation diagram 2.1a.

ν	Cost $\mathcal{C}_2$	Cost of Controls	Iterations	Optimal Positions
0.3	24.6922	9.6582	3	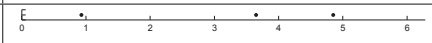
0.2,br.1	53.7672	17.9929	2	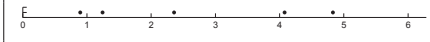
0.2,br.3	52.2630	15.4089	3	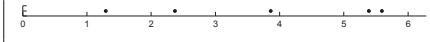
0.1,br1	87.1636	35.2169	1	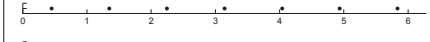
0.1,br.3	83.9787	33.7581	2	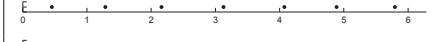
0.1,br.4	171.6040	62.1381	2	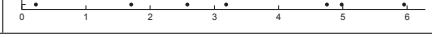

Table 2.6: Optimal positions and value of the cost functional considered in the H^1-norm for different values of ν when stabilising some of the nontrivial steady states from the bifurcation diagram 2.1a.

ν	Cost $\mathcal{C}_3$	Cost of Controls	Iterations	Optimal Positions
0.3	54.5441	13.8436	2	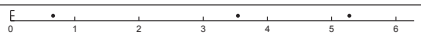
0.2,br.1	262.7363	21.1679	3	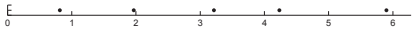
0.2,br.3	266.0515	32.4603	3	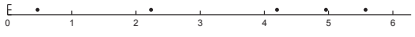
0.1,br.1	702.4697	35.2169	1	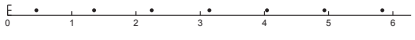
0.1,br.3	745.6007	32.4264	1	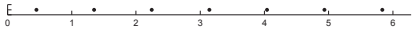
0.1,br.4	1384.6689	63.1272	2	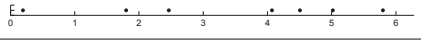

Table 2.7: Optimal positions and value of the cost functional considered inthe H^2-norm for different values of ν when stabilising some of the nontrivial steady states from the bifurcation diagram 2.1a.

We performed the same computations for the case when $\mu > 0$, and the numerical results are presented in the same manner in Tables 2.8-2.13 (zero solution in Tables 2.8-2.10 and steady states in Tables 2.11-2.13). However, now we fix $\nu = 0.5$ and each entry in Tables 2.8-2.13 contains the value of μ, the value of the cost functional, the cost of the controls $\sum_{i=1}^{m} \|f_i(t)\|_{L^2(0,T)}$, the number of iterations required to obtain an optimal state, and in the last column the spatial distribution of the controls over the domain $[0, 2\pi]$.

The results are quite similar to the ones for the KS equation: with few exceptions, an

μ	Cost	Cost of Controls	Iterations	Optimal Positions
0.1	5.9009	3.8021	6	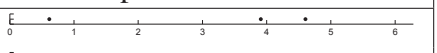
0.2	6.6360	4.7441	4	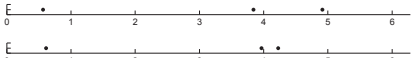
0.3	6.2167	4.3916	2	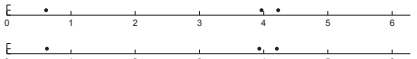
0.4	6.9673	4.8854	2	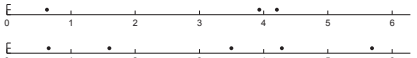
0.5	7.9267	6.4703	2	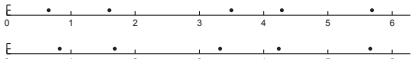
0.6	8.1923	6.7510	2	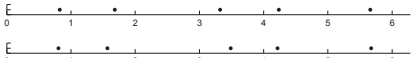
0.7	8.6480	7.4013	4	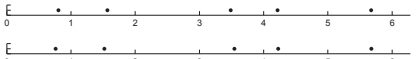
0.8	9.2724	8.1103	5	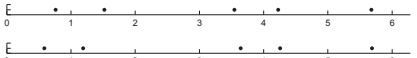
0.9	9.3181	8.1963	5	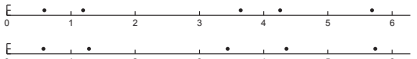
1	9.9345	8.8975	5	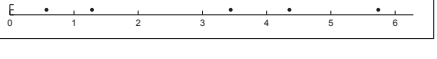

Table 2.8: Optimal positions and value of the cost functional considered in the L^2-norm for $\nu = 0.5$ and different values of μ when stabilising the zero solution to the gKS equation.

μ	Cost	Cost of Controls	Iterations	Optimal Positions
0.1	10.0252	4.9799	2	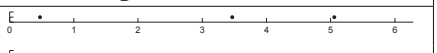
0.2	9.3949	4.9606	3	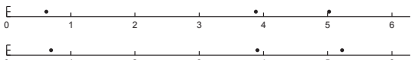
0.3	10.2386	6.0085	4	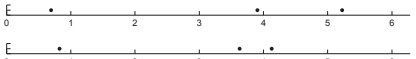
0.4	9.5283	5.7364	2	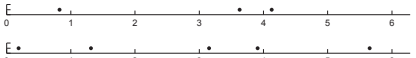
0.5	9.7414	6.7310	4	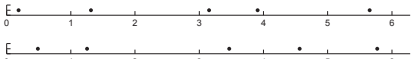
0.6	10.2817	6.5249	3	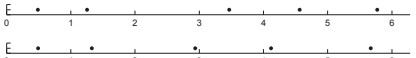
0.7	11.3514	8.4107	3	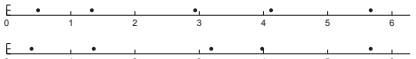
0.8	10.7201	8.1917	2	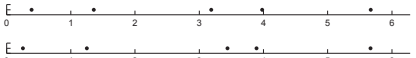
0.9	11.1564	8.5838	2	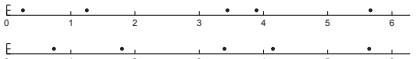
1	12.8182	9.8639	4	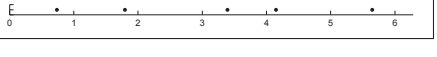

Table 2.9: Optimal positions and value of the cost functional considered in the H^1-norm for $\nu = 0.5$ and different values of μ when stabilising the zero solution to the gKS equation.

μ	Cost	Cost of Controls	Iterations	Optimal Positions
0.1	18.8787	8.1662	1	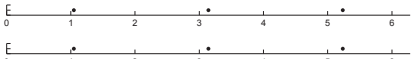
0.2	23.1180	10.1904	1	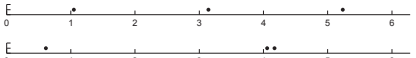
0.3	18.7295	4.4576	3	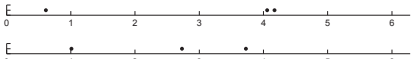
0.4	17.4085	90.484	2	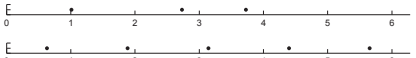
0.5	13.4211	8.1216	1	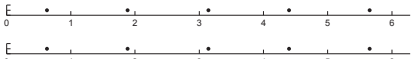
0.6	19.0901	8.2441	1	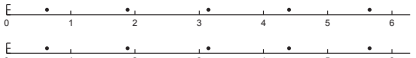
0.7	16.9693	9.9604	1	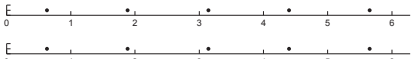
0.8	17.5729	11.3804	1	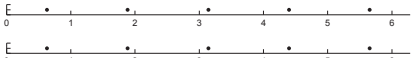
0.9	19.3294	12.6604	1	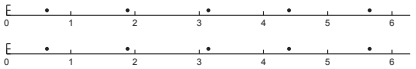
1	23.6598	13.9538	1	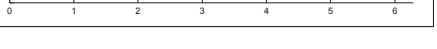

Table 2.10: Optimal positions and value of the cost functional considered in the H^2-norm for $\nu = 0.5$ and different values of μ when stabilising the zero solution to the gKS equation.

increase in the intensity of the electric field parameter μ increases the cost of the controls. In addition, it is found that the optimal controls for stabilising zero steady states are more robust, with respect to changes in μ, when using the L^2 cost functional. Similarly, when stabilising nontrivial steady states, more robust optimal positions for the controls arise when the H^1 and H^2 cost functionals are used.

μ	Cost	Cost of Controls	Iterations	Optimal Positions
0.4	1.1036	0.7239	24	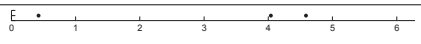
0.5	77.3429	68.9036	2	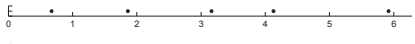
0.6	24.1021	16.5390	3	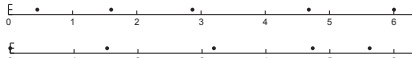
0.7	64.4793	57.1950	6	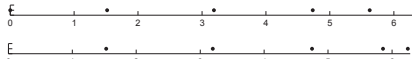
0.8	121.3373	114.4435	5	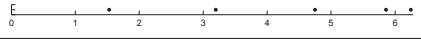

Table 2.11: Optimal positions and value of the cost functional considered in the L^2-norm for $\nu = 0.5$ and different values of μ when stabilising unstable nontrivial steady states of the gKS equation.

μ	Cost	Cost of Controls	Iterations	Optimal Positions
0.4	2.4294	0.9982	10	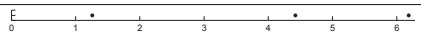
0.5	104.0632	78.0547	3	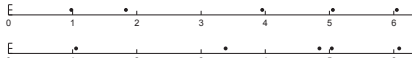
0.6	56.4254	21.3122	2	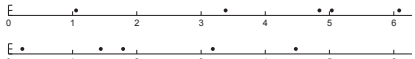
0.7	99.3032	58.1332	4	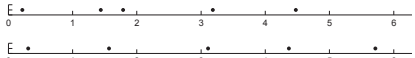
0.8	190.9989	144.7036	2	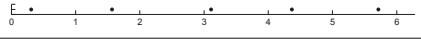

Table 2.12: Optimal positions and value of the cost functional considered in the H^1-norm for $\nu = 0.5$ and different values of μ when stabilising unstable nontrivial steady states of the gKS equation.

μ	Cost	Cost of Controls	Iterations	Optimal Positions
0.4	14.8599	2.7471	1	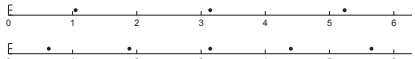
0.5	169.7523	86.2344	1	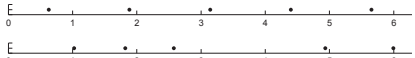
0.6	194.5729	27.3814	2	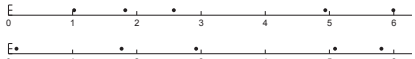
0.7	298.9302	109.7305	2	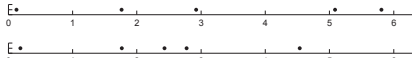
0.8	489.1133	199.6977	2	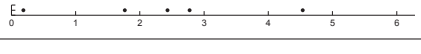

Table 2.13: Optimal positions and value of the cost functional considered in the H^2-norm for $\nu = 0.5$ and different values of μ when stabilising unstable nontrivial steady states of the gKS equation.

A more detailed comparison of the energy required to control different solutions using equidistant actuators or optimally computed positions as described above, is provided in

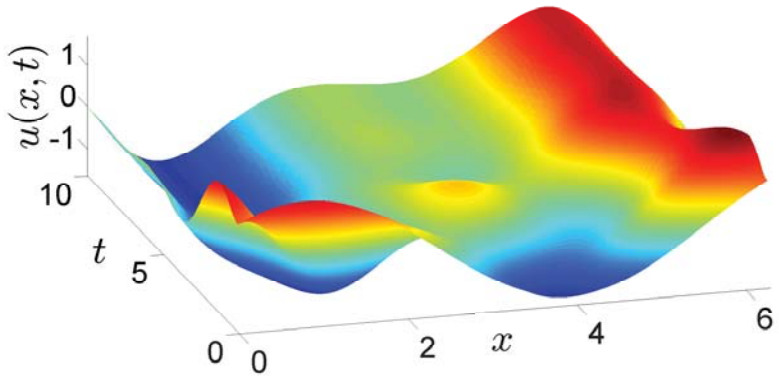

(a) Controlled solution

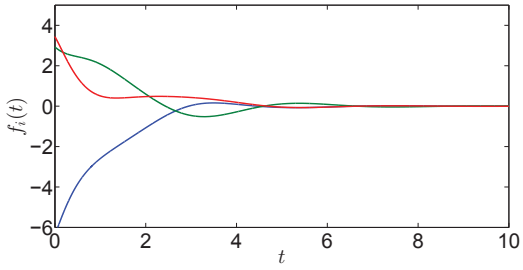

(b) Equidistant controls

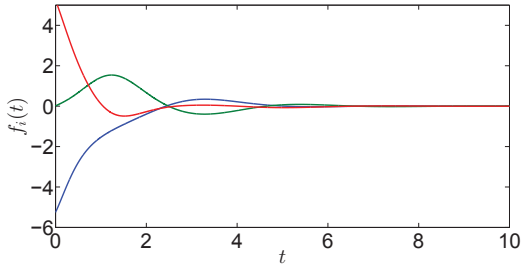

(c) Optimal controls

Figure 2.18: Controlled steady state of the KS equation for $\nu = 0.3$ (2.18a) and controls applied: (2.18b) equidistant and (2.18c) optimal.

Figs. 2.18 and 2.19. Fig. 2.18 shows the stabilisation of a nonuniform steady state for the KS equation, $\nu = 0.3$ and $\mu = 0$, while Fig. 2.19 shows analogous results but for the electrified problem with parameters $\nu = 0.5$ and $\mu = 0.4$ (in both cases dispersion is absent, $\delta = 0$). Panel (a) shows the spatiotemporal evolution to the desired state in the presence of controls, while panels (b) and (c) depict the evolution of the control amplitudes (there are three controls in each case) for equidistant or optimally positioned actuators, respectively. The results show that the amplitudes of optimally placed controls decay to zero faster than those of the equidistantly placed ones.

Optimal control of travelling waves

We also performed similar numerical experiments to find the optimal position of the control actuators when stabilising travelling waves. We found that in most cases, we cannot do better than equidistant controls.

We believe that this is due to the following reasons. First, the length of the domain needed

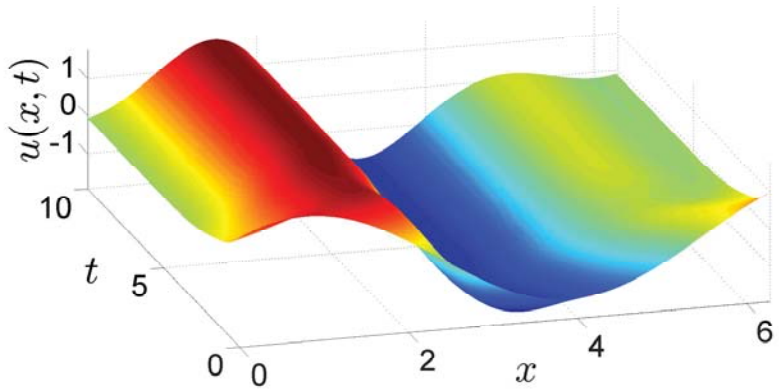

(a) Controlled solution

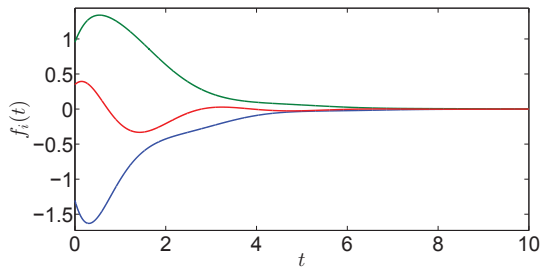

(b) Equidistant controls

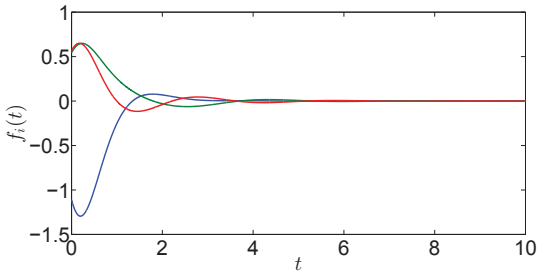

(c) Optimal controls

Figure 2.19: Controlled steady state of the KS equation for $\nu = 0.5$, $\mu = 0.4$ (2.19) and controls applied: (2.19b) equidistant and (2.19c) optimal.

for the existence of (unstable) travelling waves is long, and therefore the number of unstable modes (and hence of the number of controls) is large (e.g., in the example of Fig. 2.12 we are using $m = 21$ controls); thus, shifting the position of the controls in a relatively large domain should not have a big effect on their amplitudes. Second, solitary pulses on long domains necessarily have large flat regions which are susceptible to linear instabilities leading to the nonlinear wavy perturbations seen in panels (b) and (c) in Fig. 2.5. It is interesting to note that there are 10 wavy structures corresponding to the number of linearly unstable modes; thus, we expect optimality when the controls are approximately equally spaced thus guaranteeing one control under each wavy structure. Shifting the controls can introduce instability and nonlinear growth to a different state.

2.5 Discussion

In this chapter we took our first step towards controlling falling liquid films by studying the effect of point actuated feedback controls on the Kuramoto-Sivashinsky equation and some of its generalisations that include physical effects such as dispersion and an electric field. These are weakly nonlinear models for the interface of thin film flows and are the simplest models that can be obtained in the rational hierarchy of models presented in Section 1.2.

We extended previous results by Christofides *et al.* [8, 9, 42, 44] for the stabilisation of the zero solution to the Kuramoto-Sivashinsky equation ($\mu = \delta = 0$) and are now able to stabilise all types of solutions: we can use point actuated feedback controls to suppress the spatiotemporal chaotic behaviour that is characteristic to this equation for large domains (or small values of ν) and drive the solutions towards any chosen steady state or travelling wave solution of the equations (with both $\mu = \delta = 0$ or positive values of these parameters) and can also drive the solutions of this equation to arbitrary periodic solutions by adding an extra forcing term. The number of controls is related to the number of unstable modes in the system, and their amplitudes quickly decay to zero, which is due to the fact that they are proportional to the distance between the current solution and the desired state. These, however, cannot be exactly zero since the desired solutions are unstable, and therefore even numerical error can destabilise them if the controls are not applied. Finally, we also showed that the controls are robust with respect to variations in the parameters of the system. This means that they are robust to uncertainties. In particular, these uncertainties can change the number of unstable modes (by being present in the parameter ν or μ), and we showed that we can still achieve stabilisation if the number of controls differs by the predicted number by two. This is in agreement with the results by Armaou and Christofides [8] for the zero solution of the KS equation, where the authors claim that they can use $m = 5$ controls as long as $\nu \geq \frac{1}{49}$, which corresponds to 7 unstable eigenmodes.

Furthermore, we studied the optimal control problem for this equation by both proving the existence of an optimal control when considering general distributed and periodic controls $f(x,t) \in L^2(0,T;\dot{L}^2(0,2\pi))$, and by developing an algorithm that enables us to compute the optimal position for the control actuators, both for the zero solution and nontrivial steady states. We consider three different cost functionals; all of the chosen cost functionals penalised the L^2 norm of the controls in time, while measuring the distance between the current solution and the desired steady state in the L^2, H^1 and H^2 norms. We found that,

in general, the L^2 norm is more efficient when stabilising the zero solution, while higher regularity norms are better when stabilising nontrivial steady states. We also found that we cannot usually do better than equidistant controls when we are trying to stabilise travelling wave solutions, and we think that this is due to the fact that these only occur in very large domains and have large flat regions that are susceptible to linear instabilities, and therefore having equidistant controls increases our chances of suppressing these instabilities.

For the results presented here, we assumed that complete information about the solution of the gKS equation is available. In e.g. [7], the authors considered that information about the solution $u(x,t)$ to the KS equation was only available at a finite number of points and proved that one can still achieve stabilisation of the zero solution by approximating the solution using these observations. They used static (that only use the latest information available) and dynamic (which construct an approximation of the system that evolves in time) observers. This extension is trivially valid for our case and therefore we chose not to apply it here. However, we will use similar techniques in Chapter 3 for the control of more complicated long wave models.

There are several directions in which the results presented here can be extended. Since the KS equation is a simplified model for thin film flows obtained using weakly nonlinear analysis and valid close to criticality [54, 120], we can apply the control methodologies studied here to simplified long wave models that are closer to the full 2D Navier–Stokes dynamics, such as the Benney equation and the weighted-residual model and we will do that in Chapter 3. Similar controls are expected to work at least for the Benney equation, since the linear operators of both equations have the same structure. However, we cannot apply the controls derived here directly, since the KS equation sits in a moving frame, and having point actuated controls in a moving frame is not realisable. Nevertheless, we find that proportional controls (both distributed and point actuated) work surprisingly well in the Benney equation, and the controls obtained for this equation can also be applied to stabilise solutions of the weighted-residual model. A more detailed discussion will be given in Chapter 3. We will also extend these techniques so that they apply to the stochastic KS equation. Given that the noise itself can sometimes stabilise linearly unstable solutions [179, 180], the interaction between noise and controls can lead to very interesting dynamic phenomena. We think that this is a particularly interesting direction for further research, since the stochastic KS equation is closely related to the KPZ equation, which is a universal model for weakly asymmetric

processes [97], and we will present our results concerning this equation in Chapter 4. Finally, we will also show how to extend our results to systems of coupled KS equations and systems of conservation laws used to model interfaces of multi-phase flows in Chapter 5.

Chapter 3

Control of long-wave models

The aim of this chapter is to study the application of feedback controls similar to those obtained in Chapter 2 for weakly nonlinear models to long-wave models such as the first order Benney equation or the first order weighted-residual model. These models are more realistic and provide a good approximation for the Navier–Stokes equations in the long wave limit, when modelling thin films flowing down inclined planes.

We will use feedback control in the form of perpendicular injection and suction of fluid through the wall, and the feedback is based on observations of the film height. We study both distributed and point actuated feedback controls when stabilising the solution corresponding to a flat film and compare the results obtained between the two models and, in the distributed control case, to the linear stability results for the Navier–Stokes equations. We also study the effect of displacement between observers and actuators and show that when using a finite number of point actuated controls the system can still be stabilised when only a small number of observations are available, using static (where the controls are based on only the most recent set of observations) and dynamic (where the controls are based on an approximation of the system which evolves over time) control schemes. Furthermore, we study the effect of distributed controls on the stabilisation of travelling wave solutions, steady states, and non-solutions.

The main results of this chapter are published in [205]

3.1 The Benney and weighted-residual equations

The next step towards controlling thin film flows is to go one step higher in our hierarchy of models and control the solutions to long-wave approximations of such flows. Long-wave models were developed in order to obtain a reduced-dimensional description of thin film flows down inclined planes and they take advantage of the fact that the first instabilities to develop in these flows are in the form of long-wave perturbations. The main difference between the various models is in the manner in which inertial effects are incorporated.

The long-wave methodology was derived by Benney [21], but in his work the author neglected the effects of surface tension; these were later included by Gjevik [85]. The Benney equation captures the critical conditions for the onset of instability exactly, as well as the neutral stability conditions and interfacial dynamics close to criticality. However, it fails to describe the dynamics within the actual thin film; for example, the solutions exhibit unphysical behaviour as the Reynolds number is increased. Eventually, the increase of Reynolds number will lead to finite-time blow-up solutions. Some of these issues can be delayed by introducing higher order terms in the derivation of the Benney equation, but cannot be suppressed.

This motivated the need to develop models that are more accurate for moderate and high Reynolds numbers. Several models are available in the literature (e.g. a very widely used model, obtained using different scalings of the variables to that we will consider, is the well-known Shkadov model), and here we choose to consider the first order weighted-residual equations. The weighted-residual methodology was introduced by Ruyer-Quil and Manneville [187] and consists of expanding the velocity u in terms of basis functions satisfying the boundary conditions at the interface and then obtaining the relevant coefficients by averaging the bulk equations. This model is identical to the Benney equation at zero Reynolds number and also captures the onset of instability exactly, but remains in good agreement with the Orr-Sommerfeld linear stability results for the Navier–Stokes equations. It consists of two coupled equations (higher order models will have more equations) for the interface height, h and the flow rate q.

The methodologies for deriving both types of models (the Benney and first order weighted-residual methodologies) are described in e.g. [120]. The application of suction/injection controls for both models was introduced in [206] and we summarise the derivation of the relevant equations in Chapter 1.

We will now consider the controlled versions of these two models. Both models satisfy a mass conservation equation

$$h_t - F(x,t) + q_x = 0, \tag{3.1}$$

which is coupled with an equation for $q(x,t)$. For the Benney equation, the equation for $q(x,t)$ is

$$q(x,t) = \frac{h^3}{3}\left(2 - 2h_x \cot\theta + \frac{h_{xxx}}{C}\right) + R\left(\frac{8h^6 h_x}{15} - \frac{2h^4 F}{3}\right) = Z(h,F), \tag{3.2}$$

or, if we assume F to be small with respect to the long-wave scaling (see Section 1.2),

$$q(x,t) = \frac{h^3}{3}\left(2 - 2h_x \cot\theta + \frac{h_{xxx}}{C}\right) + \frac{8Rh^6 h_x}{15}. \tag{3.3}$$

Both these equations, when coupled with (3.1), yield an evolution equation for $h(x,t)$. The fact that the whole dynamics of the system are enclosed in one equation for $h(x,t)$ is the main reason why the Benney model fails to describe the physics of these flows for large Reynolds numbers.

In the weighted-residual model, $q(x,t)$ gains its own evolution equation

$$\frac{2}{5}Rh^2 q_t + q = \frac{h^3}{3}\left(2 - 2h_x \cot\theta + \frac{h_{xxx}}{C}\right) + R\left(\frac{18q^2 h_x}{35} - \frac{34hqq_x}{35} + \frac{hqF}{5}\right) = Z(h,q,F), \tag{3.4}$$

which when coupled to (3.1) yields a closed system for $h(x,t)$ and $q(x,t)$.

As far as we are aware, no attempts of controlling long-wave models for falling film flows using injection and suction were made before. However, our results for the weakly nonlinear models in Chapter 2 motivated us to explore the same methodology here since, when linearised, the Benney equation shows similar behaviour to that of the KS equation, in the sense that its eigenvalues have the same structure. Therefore, the stabilisation of the linear operator for the Benney equation using feedback controls such as the ones we derived in Chapter 2 should be straightforward. We cannot simply apply the controls derived for the weakly nonlinear models: the KS equation sits in a moving frame, and therefore, unless we consider controls that are also moving, we cannot expect them to work without any change. Moreover, the nonlinearities here are more complicated, and so there is no global existence theory; this reduces our hopes to prove any analytical results concerning the controllability of the full system, but nevertheless our numerical experiments show that we can achieve

stabilisation of the flat state and other solutions using fairly simple controls. Another difficulty is that the structure of the weighted-residual and Navier–Stokes models, when applied at finite wavelength, is significantly different to that of the KS equation (and also the Benney equation). It is reasonable to suspect that a control strategy carefully optimised for one model may be ineffective in another, and so we will focus on the use of relatively simple control schemes, and investigate their robustness to variations in the model details.

3.1.1 Choice of controls

Our focus is on the application of suction as a linear control mechanism in response to observations of the interface height. Given the fact that there are no existence or uniqueness results for these models, and also that there is no reason why we should expect the behaviour of the linear operator of these systems to govern the full nonlinear evolution, we do not know *a priori* that linear proportional feedback controls will work for long-wave models. However, since the Kuramoto-Sivashisnky equation is obtained as an approximation for these models (see Section 1.2) and proportional feedback controls work remarkably well for all types of solutions of this equation, we will explore several different control mechanisms based on our experience with the weakly nonlinear models: our controls will be linear and proportional to the difference between the current and desired solutions, but we will allow them to be not only point actuated but also distributed throughout the whole domain. We will also consider separately the cases of controlling towards the flat solution ($h(x,t) = 1$) and nontrivial solutions such as travelling waves or nontrivial steady states (which are not solutions to these equations in the absence of any kind of forcing). We will therefore begin in Sec. 3.2 by considering the case of controlling towards the uniform Nusselt state, based only on observations of h, and using distributed controls. To achieve this, we set

$$F(x,t) = -\alpha[h(x,t) - 1], \tag{3.5}$$

where α is a real constant to be chosen; in most cases we find that the uniform state becomes increasingly stable for large positive α. Note that if $h = 1$ everywhere, then the controls have zero magnitude.

The control scheme (3.5) requires perfect knowledge of the instantaneous interface shape $h(x,t)$, and the ability to impose any continuous $F(x,t)$. In practice, we expect neither of

these assumptions to hold. Instead, fluid is injected via a number of localised actuators, or slots, in the substrate, and interface observations are available at a small number of locations in the flow domain. This, and our results for the weakly nonlinear models, motivated us to investigate, in Section 3.3, control schemes based on point actuated controls

$$F(x,t) = \sum_{m=1}^{M} f_m(t) b_m(x). \tag{3.6}$$

As discussed in Section 2.5, for the long-wave models we will consider both the case when we have full information of the current system state, and also the case where the M coefficients $f_m(t)$ are to be determined from P discrete localised observations $y_p(t)$ of the interface height:

$$y_p(t) = \int_0^L \Phi_p(x)(h(x,t) - 1)\,\mathrm{d}x. \tag{3.7}$$

Depending on the way we determine $f_m(t)$ from the observations, we will say that the control scheme uses either static observations or dynamic observers.

We then will consider the stabilisation of nontrivial solutions. In Sec. 3.4, we consider controlling towards either nonuniform travelling waves of permanent form or nonuniform steady states. Travelling waves can be written as $h = H(\zeta)$, where $\zeta = x - Ut$ and U is the constant propagation speed. By direct analogy to (3.5), we set

$$F(\zeta,t) = -\alpha[h(\zeta,t) - H(\zeta)]. \tag{3.8}$$

We note that if $h(x,t) = H(x - Ut)$ for all time, then $F = 0$, so that the travelling wave $h = H(x - Ut)$, is also a solution of the controlled equations.

Remark 8. *We note that travelling waves with permanent shape and constant speed correspond to both steady state and travelling wave solutions of the Kuramoto-Sivashinsky equation, since this model is obtained by a Galilean transformation from the long-wave models. Steady states of the KS equation correspond to waves travelling at the same speed as that of the moving frame of reference for the Galilean transformation, while travelling waves in the weakly nonlinear framework are those which travel at a different speed than the Galilean transformation one.*

Nonuniform steady interface shapes $H(x)$ are not steady states of the equations when $F = 0$, but [206] showed that imposing a steady suction component $S(x)$ enables non-

uniform steady states. This is a similar approach to that taken in Section 2.2.1 and exemplified for the gKS equation in Fig. 2.15. Combining with proportional controls, we obtain

$$F(x,t) = -\alpha[h(x,t) - H(x)] + S(x). \tag{3.9}$$

For non-uniform states, the calculation of $S(x)$ to obtain an exact steady state, or of the travelling wave solution $H(\zeta)$, requires detailed knowledge of the governing equations. For example, these states differ even between the Benney and weighted-residual models, let alone the Navier–Stokes equations. Therefore, we cannot expect that the controls obtained for a specific solution for one of the models to work for another model. Nevertheless, we will consider, in Section 3.4.3, the robustness of our control schemes when the model details are not well known; we do so by controlling towards a finite-amplitude non-uniform state $H(x)$, but setting $S(x) = 0$, so that the target state is not a steady solution of any of our models. As a result, the control parameter α has a role to play in setting both the shape of any steady states obtained, as well as their stability.

3.2 The effect of proportional controls on the stability of a uniform film

The uniform film state $h = 1$, known as the Nusselt solution, is a steady solution to all three sets of equations (Navier–Stokes, Benney and weighted-residual) in the absence of suction. The base state is

$$h = 1, \quad q = 2/3, \quad u = y(2-y), \quad v = 0, \quad p = 2(1-y)\cot\theta. \tag{3.10}$$

In 2-D Navier–Stokes [20, 233], Benney [21] and weighted-residual models [187], this solution is linearly stable to perturbations of all wavelengths if

$$R < R_0 \equiv \frac{5}{4}\cot\theta. \tag{3.11}$$

As R is increased across this threshold, the first perturbations to become unstable are those with infinite wavelength, and in fact the long-wavelength nature of the instability was the physical motivation for the development of long-wave models.

The application of linear proportional controls $F = -\alpha(h-1)$ affects the linear stability of the Nusselt solution. As the system is invariant under translation in x, the eigenmodes are

proportional to $\exp(ikx)$, and so we write

$$h = 1 + \epsilon\hat{h}e^{ikx+\lambda t}, \quad q = \frac{2}{3} + \epsilon\hat{q}e^{ikx+\lambda t} \tag{3.12}$$

and seek a solution for $\epsilon \ll 1$. We aim to compute $\lambda(k)$; solutions are stable to perturbations of all wavelengths if the real part of λ, $\Re(\lambda)$, is negative for all real k. In what follows we calculate λ for each of the models including linear proportional feedback control in order to establish that the constant α can be chosen to stabilise the uniform flow (3.10). In the case of Benney and weighted-residual models this can be performed analytically, whereas for the Navier–Stokes equations we compute the eigenvalues numerically.

3.2.1 Benney equation

The linearised mass conservation equation (3.1) yields

$$\lambda\hat{h} + \alpha\hat{h} + ik\hat{q} = 0. \tag{3.13}$$

Substituting (3.12) into (3.2) gives

$$\hat{q} = \left(2 - \frac{2ik\cot\theta}{3} - \frac{ik^3}{3C} + \frac{8ikR}{15} + \frac{2\alpha R}{3}\right)\hat{h}, \tag{3.14}$$

and combining (3.14) with (3.13) yields a single eigenvalue λ:

$$\lambda = -\alpha\left(1 + \frac{2Rik}{3}\right) - 2ik + \frac{8k^2}{15}\left(R - \frac{5\cot\theta}{4} - \frac{5k^2}{8C}\right). \tag{3.15}$$

We assume that α is real and independent of k, and taking $\alpha > 0$ in (3.15) is seen to have a stabilising effect on the Benney system. If $R < R_0$, the Nusselt solution is linearly stable for all real k in the absence of controls, and becomes more so as α increases. However, if $R > R_0$, there is a finite k with maximum growth rate, and it is easy to show that

$$\max_k \Re(\lambda) = -\alpha + \frac{16C(R - R_0)^2}{75}. \tag{3.16}$$

Hence we can stabilise the uniform film state against perturbations of all wavelengths by

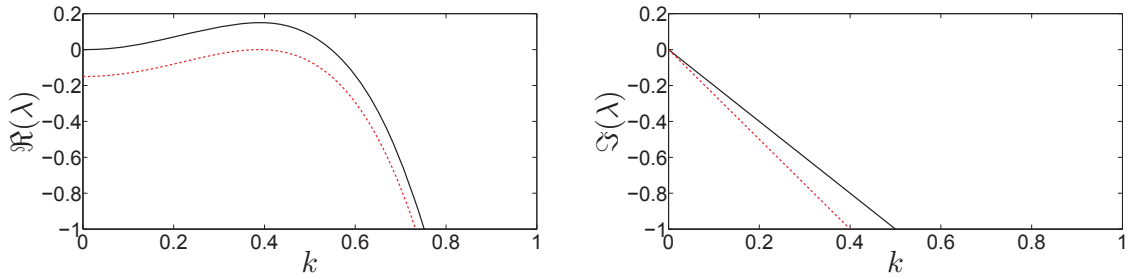

(a) Real part (b) Imaginary part

Figure 3.1: Real (left) and imaginary (right) part of the Benney eigenvalue λ as a function of k, for $R = 5$, $C = 0.05$, $\theta = \pi/4$ and $\alpha = 0$ (black solid line), and $\alpha = \alpha_B = 0.15$ (red dashed line) from (3.17).

choosing $\alpha > \alpha_B$, where

$$\alpha_B = \frac{16C(R - R_0)^2}{75}. \tag{3.17}$$

The dispersion relation (3.15) is plotted with and without controls in Fig. 3.1, for parameters at which the uncontrolled solution is unstable. In the absence of controls, the real part of λ is positive for small k, with a finite cutoff wavenumber k, above which the real part rapidly becomes increasingly negative. Setting $\alpha = \alpha_B$ shifts the real part of the entire spectrum by $-\alpha_B$. This means that perturbations of very small wavenumber decay with a finite growth rate of approximately $-\alpha_B$, rather than having a small positive growth rate in the absence of controls. The maximum growth rate occurs at the same k as in the absence of controls, and for $\alpha = \alpha_B$, this maximum growth rate is exactly zero. We can also compare the imaginary part of λ; we find that setting $\alpha = \alpha_B$ slightly increases the magnitude of the imaginary part, and hence the downstream propagation speed of small perturbations is slightly increased.

3.2.2 Weighted-residual equations

The linearised version of the weighted-residual equations (3.4) yields

$$\frac{2\lambda R}{5}\hat{q} + \hat{q} = \left(2 - \frac{2ik\cot\theta}{3} - \frac{ik^3}{3C} + \frac{8ikR}{35} - \frac{2R\alpha}{15}\right)\hat{h} - \frac{68ikR}{105}\hat{q}. \tag{3.18}$$

We combine (3.18) with (3.13) to obtain a quadratic equation for λ:

$$\frac{2R\lambda^2}{5} + \lambda\left(1 + \frac{68ikR}{105} + \frac{2\alpha R}{5}\right) + \alpha\left(1 + \frac{18ikR}{35}\right) + 2ik + \frac{8k^2R_H}{15} - \frac{8k^2R}{35} = 0, \tag{3.19}$$

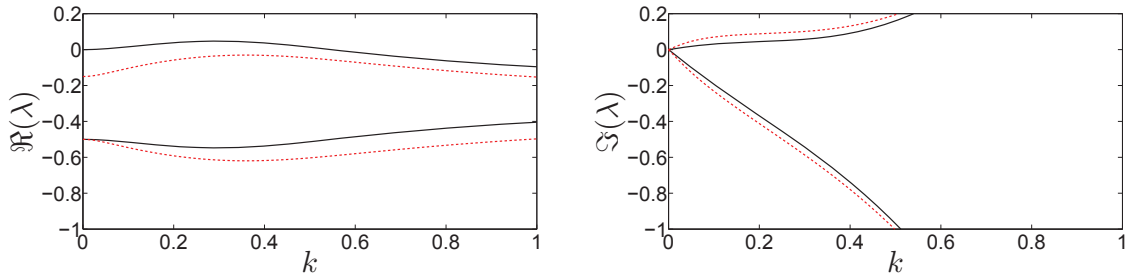

(a) Real part (b) Imaginary part

Figure 3.2: Real (left) and imaginary (right) part of both the weighted-residual eigenvalues λ as a function of k, for $R = 5$, $C = 0.05$, $\theta = \pi/4$ and $\alpha = 0$ (black solid lines), and $\alpha = \alpha_B$ (red dashed lines) from (3.17).

where

$$R_H = \frac{5}{4}\cot\theta + \frac{5k^2}{8C} = R_0 + \frac{5k^2}{8C}. \tag{3.20}$$

The characteristic equation (3.19) has complex coefficients, and so its two roots for λ are not complex conjugates. We calculate the two roots for λ numerically to determine the effect of imposing controls; Fig. 3.2 shows λ as a function of k, with and without controls. The eigenvalues of the weighted-residual equation display relatively little variation with respect to k in comparison to the Benney results, but the two systems share the same cutoff wavenumber in the absence of feedback controls. With the addition of feedback controls, we find that positive α decreases the real part of λ for both eigenvalues of the weighted-residual system, with the exception of the most stable eigenmode at $k = 0$, which is independent of α (see below). The effect of the controls in the imaginary part of λ is similar to that observed for the Benney equation. Choosing the critical $\alpha = \alpha_B$ for the Benney equation, given by (3.17), is more than sufficient to stabilise the uniform state against perturbations of all wavenumbers in the weighted-residual equations.

In the long-wave limit $k \ll 1$, (3.19) becomes

$$(\lambda + \alpha)\left(1 + \frac{2R\lambda}{5}\right) = 0 \tag{3.21}$$

which has roots at $\lambda = -\alpha$ and $\lambda = -5/(2R)$. Choosing non-zero α affects the stability of the first root, and means that we must choose $\alpha > 0$ to obtain a stable solution. The second root is unaffected by α, and as a consequence, the maximum real part of λ across all k is always greater than $-5/(2R)$, regardless of the value of α.

Although the effect of α on λ is more complicated than that for the Benney equation, we can still calculate the critical control amplitude α needed to ensure that $\Re(\lambda) \leq 0$ for all k. Perturbations with very large wavenumber are always stabilised by surface tension, so have negative real part. If the uniform state is unstable to perturbations for some k, then there is at least one cutoff value of k for which $\Re(\lambda) = 0$. We therefore investigate the conditions for which there is a purely imaginary root, writing for convenience $\lambda = -2ik\Omega$. We solve the imaginary part of (3.19) to obtain

$$\Omega = \frac{1 + \dfrac{9\alpha R}{35}}{1 + \dfrac{2\alpha R}{5}}. \tag{3.22}$$

Since Ω is independent of k, we can rewrite the real part of (3.19) as a quadratic equation in k^2:

$$\frac{k^4}{3C} + k^2\left(-\frac{8R\Omega^2}{5} + \frac{136R\Omega}{105} - \frac{8R}{35} + \frac{8R_0}{15}\right) + \alpha = 0. \tag{3.23}$$

The roots of this equation correspond to wavenumbers where $\Re(\lambda(k)) = 0$. When α is insufficient to stabilise perturbations of all wavelengths, there are two roots for k^2, and one root at the critical value of α. The uniform state is stable to perturbations of all wavelengths if there are no real roots for k^2, i.e. when (3.23) has negative determinant. This condition can be rewritten using the definition of Ω to obtain that the uniform state is stable if

$$\left(R\left[\frac{1 + \dfrac{71\alpha R}{245} + \dfrac{3\alpha^2R^2}{175}}{1 + \dfrac{4\alpha R}{5} + \dfrac{4\alpha^2R^2}{25}}\right] - R_0\right)^2 < \frac{75\alpha}{16C}. \tag{3.24}$$

The term in square brackets is monotonically decreasing in αR for $\alpha R > 0$. When α is small, we find

$$R \approx R_0 + \sqrt{\frac{75\alpha}{16C}}, \tag{3.25}$$

which is exactly the Benney result. At large α,

$$R \approx \frac{28}{3}\left(R_0 + \sqrt{\frac{75\alpha}{16C}}\right) \tag{3.26}$$

and so the maximum R for which the uniform solution is stable at large, fixed α in the

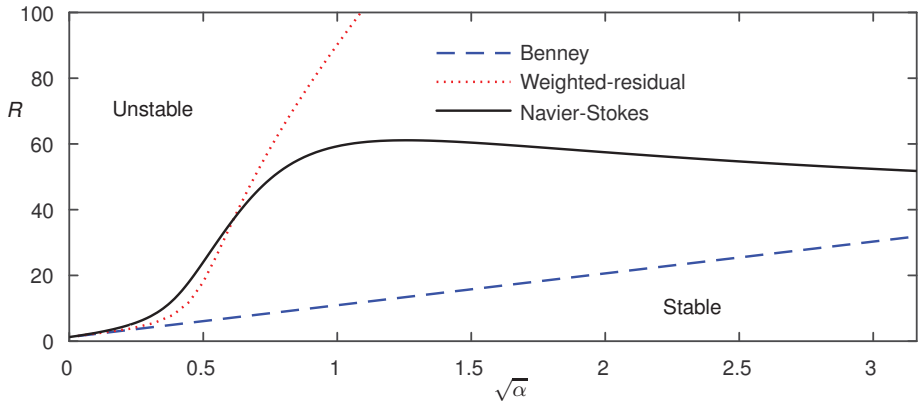

Figure 3.3: The boundaries for stability to perturbations of all wavelengths, for $\theta = \pi/4$, $C = 0.05$. The stable region emanates from the $\sqrt{\alpha}$ axis.

weighted-residual model is nearly 10 times larger than predicted by the Benney model. The stability boundaries for the Benney and weighted-residual results are given by (3.17) and (3.24), and are plotted in the $\sqrt{\alpha}$-R plane in Fig. 3.3, together with the corresponding Navier–Stokes results as we will discuss below; it appears that the stable region of the Benney equation is always a subset of the stable region according to the weighted-residual equation, so the critical α predicted by (3.17) is indeed a conservative estimate of the necessary α required to stabilise the uniform film to perturbations of all wavelengths.

3.2.3 Navier–Stokes equations

We can compute the linear stability of the Nusselt state in the two-dimensional Navier–Stokes equations, subject to distributed feedback controls, by a normal mode analysis. This analysis is well known in the absence of controls [73]. The addition of suction controls changes only one boundary condition in the resulting Orr-Sommerfeld system, and so only a brief description of the equations is presented here.

We perturb about the uniform state, writing

$$\begin{aligned} h &= 1 + \epsilon\hat{H}\exp(ikx+\lambda t) \\ u &= \bar{u}(y) + \epsilon\hat{U}(y)\exp(ikx+\lambda t) \\ v &= 0 + \epsilon\hat{V}(y)\exp(ikx+\lambda t) \\ p &= \bar{p}(y) + \epsilon\hat{P}(y)\exp(ikx+\lambda t), \end{aligned} \tag{3.27}$$

where $\bar{u}(y) = y(2-y)$ and $\bar{p}(y)$ correspond to the uniform film solution described in (3.10),

and then linearise with respect to ϵ. The perturbation velocity components $\hat{U}(y)$ and $\hat{V}(y)$ can be expressed in terms of a streamfunction $\psi(y)$, so that

$$\hat{U}(y) = -\psi'(y), \quad \hat{V}(y) = ik\psi(y), \tag{3.28}$$

which immediately satisfies the mass conservation equation (1.3). The two components of the momentum equation (1.2a) and (1.2b) can then be combined to yield the Orr-Sommerfeld equation, which is a linear ordinary differential equation for ψ in $0 < y < 1$:

$$\left(\frac{d^2}{dy^2} - k^2\right)^2 \psi = R[\lambda + ik\bar{u}(y)]\left(\frac{d^2}{dy^2} - k^2\right)\psi - ik\bar{u}''(y)R\psi. \tag{3.29}$$

The boundary conditions at the free surface are unaffected by α, and after some manipulation involving (1.2a) to eliminate the fluid pressure, we obtain three boundary conditions at the free surface:

$$-\psi'''(1) + (R\lambda + ikR - 3k^2)\psi'(1) = 2ik\hat{H}\cot\theta + \frac{ik^3\hat{H}}{C}, \tag{3.30a}$$

$$\psi''(1) = -2\hat{H} - k^2\psi(1), \tag{3.30b}$$

$$ik\psi(1) = (\lambda + ik)\hat{H}. \tag{3.30c}$$

The no-slip boundary condition on the wall yields

$$\hat{U}(0) = -\psi'(0) = 0 \tag{3.31}$$

and the responsive flux through the wall becomes the boundary condition

$$\hat{V}(0) = ik\psi(0) = -\alpha\hat{H}. \tag{3.32}$$

When $k = 0$, we can solve the system (3.29)-(3.32) for $\psi(y)$ and λ analytically, and enumerate the eigenmodes. There is a single eigenmode that involves perturbations to the interface height (i.e. $\hat{H} \neq 0$), and for this eigenmode $\lambda = -\alpha$ at $k = 0$. There are also an infinite number of shear eigenmodes which leave the interface position unperturbed. These eigenmodes are all stable, and the eigenvalue with the largest real part satisfies $\lambda R = -(\pi/2)^2$, irrespective of α.

For $k \neq 0$, we solve the system (3.29)-(3.32) numerically. We can formulate the system

as a generalised eigenvalue problem for ψ, $\hat{H}$ and λ, discretise the derivative operators on ψ using finite differences or Chebyshev polynomials, and solve the resulting generalised eigenvalue problem using standard MATLAB routines.

Results for $\lambda(k)$ are shown in Fig. 3.4 for the two least stable eigenmodes. In the absence of controls, the Navier–Stokes results show a smaller cutoff wavenumber than the Benney and weighted-residual results. As was the case for the weighted-residual equations, we find that introducing positive α decreases the real part of both eigenvalues shown, but has vanishing effect when $k = 0$ on all but the least stable eigenmode. Furthermore, the critical α computed according to the Benney result (3.17) is again sufficient to stabilise the uniform state against perturbations of all wavelengths.

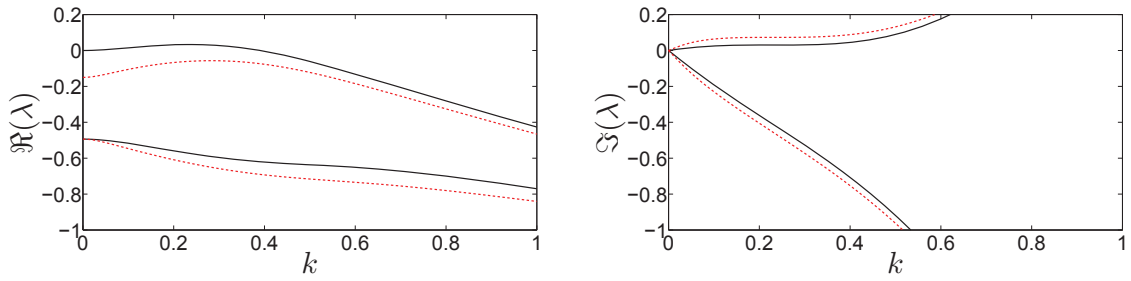

(a) Real part (b) Imaginary part

Figure 3.4: Real (left) and imaginary (right) part of the two Navier–Stokes eigenvalues λ with largest real part as a function of k, for $R = 5$, $C = 0.05$, $\theta = \pi/4$, $\alpha = 0$ (black solid lines), and $\alpha = \alpha_B$ (red dashed lines) from (3.17).

In Fig. 3.3, we show the critical α required so that $\Re(\lambda) \leq 0$ for all k in the Navier–Stokes equations. This is computed in AUTO-07P, with the condition that $\Re(\lambda)$ has both a turning point and a zero at the same value of k. When $\alpha < 0.5$, this stability boundary is in good agreement with the weighted-residual results, with both predicting that the critical Reynolds number is increased substantially, from its uncontrolled value of 1.25 to around 50. Beyond this point, the weighted-residual results predict that the critical R should continue to increase rapidly with α. However, the Navier–Stokes results show a turning point in $R(\alpha)$, followed by a very slow decrease in R as α is increased. This eventual deviation is not entirely unexpected, given the wide range of Reynolds numbers spanned in this calculation.

3.2.4 Time dependent calculations

Although we have demonstrated that the control parameter α can be chosen to make the uniform state linearly stable to perturbations of all wavelengths, it is not necessarily the case that the system will converge to the uniform state in nonlinear simulations. In Fig. 3.5, we show results of an initial value calculation of the weighted-residual system, starting from a finite-amplitude state that is neither a steady nor travelling wave solution of the weighted-residual equations. We initially allow this state to evolve without controls, and find that

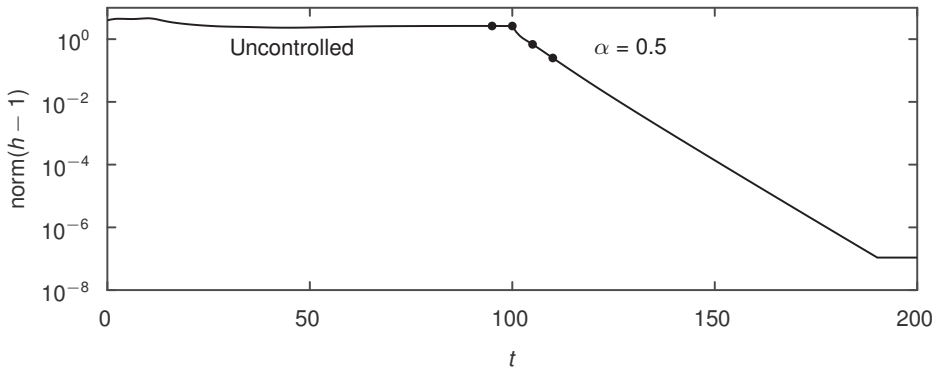

Figure 3.5: Results of an initial value calculation using the weighted-residual equations, starting from a non-uniform, non-equilibrium state, which evolves without suction until $t = 100$. For $t > 100$, we enable feedback controls with $F = -0.5(h-1)$, and the system converges towards the uniform state. Flow fields for the four instants marked with black dots are shown in Fig. 3.6

the system moves towards a travelling wave state of finite amplitude. We then activate the feedback controls with $\alpha = 0.5$, which is large enough that the uniform state is linearly stable. Instantaneous flow fields are shown in Fig. 3.6 just before and after the application of controls. After the decay of transient behaviour, we observe that the distance of the solution to the desired state decays exponentially with respect to time, which is consistent with the expectation that the largest deviation is due to a single eigenmode which decays at constant rate. As the imposed injection is proportional to $h-1$, the control magnitude also decays exponentially with time and the flow becomes increasingly laminar. However, although the amplitude of the applied injection and suction becomes vanishingly small at late times, the feedback control scheme is still required to suppress the growth of small perturbations, and thus to ensure the linear stability of the system.

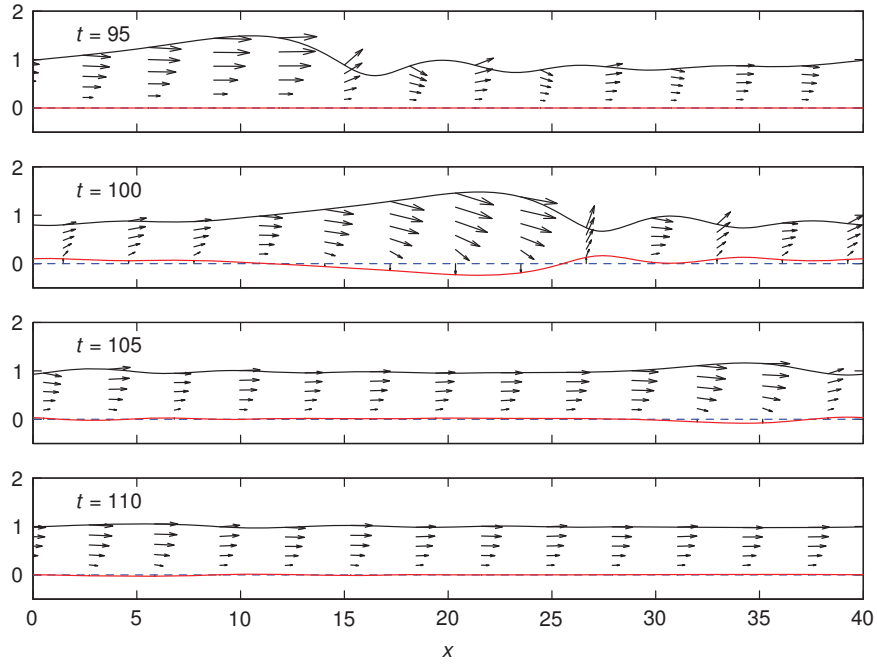

Figure 3.6: Instantaneous flow fields at moments just before and after the application of controls for the same calculation as Fig. 3.5. At $t = 95$, the system has reached a travelling wave state. Controls are activated at $t = 100$, and the magnitude of controls is largest there. At subsequent times, the interface is closer to the flat state, so smaller controls are needed.

3.2.5 Effect of phase-shifted controls

As an initial step towards designing a more efficient system for feedback control, we can investigate the effect of shifting observations relative to actuators, still using a normal mode analysis. We replace the control scheme (3.5) with a scheme based on shifted observers:

$$F(x,t) = -\alpha[h(x-\xi,t) - 1]. \tag{3.33}$$

Here the real parameter ξ is the distance between observer and actuator. Positive ξ means that the observers are displaced upstream relative to the position at which the injection is applied. This scheme introduces no favoured x locations, and so the eigenmodes can still be written as

$$h = 1 + \epsilon\hat{h}\exp(ikx + \lambda t) + O(\epsilon^2), \quad q = 2/3 + \epsilon\hat{q}\exp(ikx + \lambda t) + O(\epsilon^2). \tag{3.34}$$

We then find

$$F = -\alpha e^{-ik\xi}\epsilon\hat{h}\exp(ikx + \lambda t). \tag{3.35}$$

We thus simply replace α by $\alpha\exp(-ik\xi)$ in (3.15) and (3.19) to understand the effect of ξ on the eigenvalues of the Benney and weighted-residual models respectively. For both models, we can perform a numerical search to calculate the boundary of the region in α-ξ space where the uniform state is stable to perturbations of arbitrary wavelengths, as shown in Fig. 3.7; for the parameters in this figure, we find that choosing $\xi \approx 2$ has the best stabilising effect in both models, in the sense that a stable uniform state is obtained at the lowest value of α. There are some differences between the results for the two models: the effect of positive ξ is less pronounced in the weighted-residual model than in the Benney equation, and in fact for the weighted-residual model, choosing positive ξ eventually becomes less stabilising as α is increased.

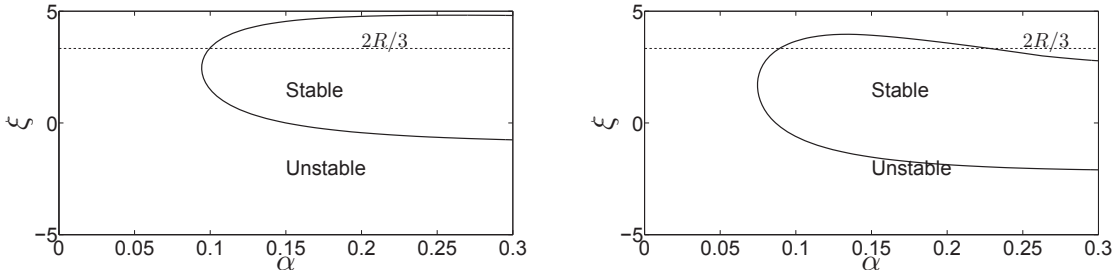

(a) Benney (b) Weighted-residual

Figure 3.7: Linear stability properties of the uniform state as a function of the control strength α and the displacement ξ between observer and actuator, with the control scheme (3.33) for $R = 5$, $\theta = \pi/4$, $C = 0.05$. Stability results refer to perturbations of all wavelengths. The lowest α is required at a finite positive value of ξ. The dashed line shows the $O(k^2)$ optimiser in the Benney equations: $\xi = 2R/3$.

In order to understand why the control scheme is most effective when actuators are displaced upstream by a finite distance, we can expand the Benney eigenvalue under the assumption that $k\xi$ is small, to reach

$$\Re(\lambda) = -\alpha\left(1 + k^2\xi\left[\frac{2R}{3} - \frac{\xi}{2}\right]\right) + \frac{8k^2}{15}\left(R - \frac{5\cot\theta}{4} - \frac{5k^2}{8C}\right). \tag{3.36}$$

To maximise the effect of α, we should choose $\xi = 2R/3$, which provides a reasonable estimate of the optimal ξ, as shown in Fig. 3.7. This should become a better estimate as

$R \to R_0$, so that the unstable k move towards zero.

3.2.6 Linear stability for non translationally invariant systems

For a translationally invariant system, as occurs for distributed controls towards a uniform film state, the linear stability of the uniform film state can be calculated via a normal mode analysis, as was shown throughout this section. However, if the base state for the stability analysis is not uniform, or the feedback control system has localised actuators or observers, then the system is no longer translationally invariant, and so the eigenmodes of the system are no longer normal modes. In that case, we can compute the discretised eigenmodes of the system by formulation and numerical solution of a generalised eigenvalue problem for linear stability, as described below.

We consider the evolution of a small perturbation $\hat{h}$:

$$h = H(x) + \epsilon\hat{h}e^{\lambda t}, \quad q = Q(x) + \epsilon\hat{q}e^{\lambda t}, \quad F = S(x) - \epsilon e^{\lambda t}\alpha\hat{h} \tag{3.37}$$

and recall the Benney equation:

$$h_t + q_x - F = 0, \quad q = Z(h, F), \tag{3.38}$$

where $Z(h, F)$ is defined in (3.2), and expand for small ϵ. The equations at $O(1)$ in ϵ must be satisfied by the base state $H(x)$, $Q(x)$, $S(x)$. At $O(\epsilon)$, we obtain a generalised eigenvalue problem for $\hat{h}$, $\hat{q}$ and λ:

$$\lambda \begin{pmatrix} I & 0 \\ 0 & 0 \end{pmatrix} \begin{pmatrix} \hat{h} \\ \hat{q} \end{pmatrix} = \begin{pmatrix} -\alpha I & -\partial_x \\ Z_h - Z_F\alpha I & -I \end{pmatrix} \begin{pmatrix} \hat{h} \\ \hat{q} \end{pmatrix} \tag{3.39}$$

where ∂_x is the derivative operator, I is the identity matrix, and the blocks Z_h and Z_F are linear operators; for example from (3.2) we have

$$Z_h = \left[H^2\left(2 - 2\cot\theta H_x + \frac{H_{xxx}}{C}\right) + \frac{16RH^5H_x}{5} - \frac{8H^3RS}{3}\right] I + \left[-\frac{2H^3}{3}\cot\theta + \frac{8R}{15}H^6\right]\partial_x + \frac{H^3}{3C}\partial_{xxx}. \tag{3.40}$$

We can eliminate $\hat{q}$ to obtain a smaller eigenvalue problem for $\hat{h}$ alone:

$$\lambda\hat{h} = -\partial_x Z_h \hat{h} - [I - \partial_x Z_F]\alpha\hat{h}. \tag{3.41}$$

For the uniform state, $H = 1$, $Q = 2/3$, and $S = 0$, the blocks Z_h and Z_F simplify considerably; in fact, we can calculate the eigenvalues analytically in that case. For non-uniform base states, we calculate the eigenvalues by replacing the derivative operators with pseudo-spectral derivative matrices, and solving the eigenvalue problem numerically using standard algorithms available in MATLAB.

We can also write the flux equation of the weighted-residual system in a similar form:

$$\frac{2}{5}Rh^2 q_t + q = Z(h, q, F). \tag{3.42}$$

We again obtain a generalised eigenvalue problem for $\hat{h}$, $\hat{q}$ and λ in the weighted-residual equations:

$$\lambda \begin{pmatrix} I & 0 \\ 0 & \frac{2}{5}RH^2 I \end{pmatrix} \begin{pmatrix} \hat{h} \\ \hat{q} \end{pmatrix} = \begin{pmatrix} -\alpha I & -\partial_x \\ Z_h - Z_F\alpha I & Z_q - I \end{pmatrix} \begin{pmatrix} \hat{h} \\ \hat{q} \end{pmatrix}, \tag{3.43}$$

where the blocks Z_h, Z_q and Z_F can be obtained by differentiating (3.4). We note that there are twice as many eigenmodes in the weighted-residual equations as in the Benney equation.

3.3 Point actuated controls

The physically important question that we wish to address next is the application of suction controls using point actuators, and based on a limited number of observations of the system state. Here we consider only behaviour within a spatial period of length L, and only stabilisation of the uniform state.

We are given the localised actuator functions $b_m(x)$, so that

$$F(x,t) = \sum_{m=1}^{M} f_m(t) b_m(x), \tag{3.44}$$

where the M coefficients $f_m(t)$ are to be determined from P discrete observations $y_p(t)$ of the interface height:

$$y_p(t) = \int_0^L \Phi_p(x)(h(x,t) - 1)\,\mathrm{d}x. \tag{3.45}$$

We note that the explicit x-dependence of the system that arises from localised actuators and observers means that the system is no longer translationally invariant in x, and so linear stability properties of even a uniform film in the Navier–Stokes equations cannot be obtained by a normal mode analysis. Instead, we derive most of our control strategies using the Benney model, and use the weighted-residual model as a black box experiment to represent the additional complexities of the full physical system subject to controls derived using a low order model.

As a starting point, we suppose that the controls are a linear function of the observations available at a given instant, which is known as a static observation scheme. In the most general form, we can then write

$$F = BK\Phi(h-1). \tag{3.46}$$

Here the operator Φ describes observations of the system, B represents the shape of the actuators, and K is the control operator which we are free to choose based on our knowledge of Φ, B and the system dynamics. We will use M linearly independent actuators and P observations, which are the ranks of B and Φ respectively. In a discretised form, B and Φ are matrices of size $N \times M$ and $P \times N$ respectively. The matrix K has size $M \times P$, and we may choose all of its entries. Given this form for F, we can compute the linear stability of a given steady state by replacing α with $-BK\Phi$ in the eigenvalue problems described in Section 3.2.6.

3.3.1 Choice of point actuators and observers

We choose to use M equally-spaced actuators, which are each periodic with period L and locally behave as Dirac δ-functions, so that

$$b_m(x) = \delta(x - x_m), \quad x_m = mL/M. \tag{3.47}$$

We similarly use P equally-spaced observer functions, which are displaced upstream by a distance ξ from the actuator positions, so that

$$\Phi_p(x) = \delta(x - x_p), \quad x_p = pL/P - \xi. \tag{3.48}$$

For our numerical calculations, we replace $\delta(x)$ in (3.47) and (3.48) by the smoothed, periodic function $d(x)$, defined by

$$d(x) = \exp\left[\frac{\cos(\frac{2\pi x}{L}) - 1}{w^2}\right]. \tag{3.49}$$

One such actuator shape function is plotted in Fig. 3.8 for $w = 0.1$. We normalise the smoothed functions $d(x)$ so that each actuator and observer shape function has integral 1 over the interval $[0, L]$, and so $d(x) \to \delta(x)$ as $w \to 0$.

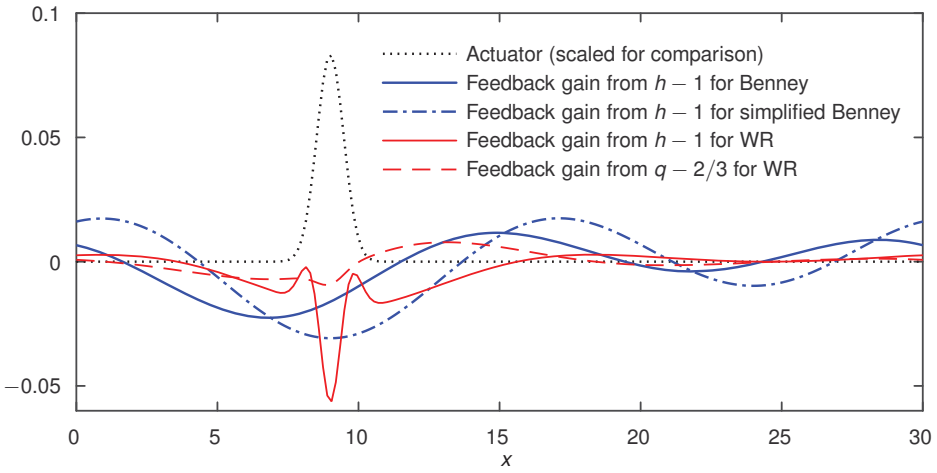

Figure 3.8: A typical row of the matrix K, or feedback gain, obtained by the LQR algorithm, with 5 equally spaced actuators, with shape smoothed according to (3.49) with $w = 0.1$, and shown by the dotted line here. The cost parameter for (3.51) is $\varsigma = 0.1$, and for the weighted-residual equation, the same cost weighting is associated with $q - 2/3$ as for $h - 1$.

3.3.2 Proportional control

If the number of actuators is equal to the number of observers, one of the simplest methods to choose the suction/injection profile is to link each actuator to a neighbouring observer, setting

$$f_m(t) = -\alpha y_m(t) \tag{3.50}$$

where the positive control amplitude α acts analogously to the control parameter α in Sec. 3.2. In terms of the generalised eigenvalue problems, we simply set $K = -\alpha I$. If all actuators, and all observers, are equally spaced, the control scheme is specified entirely by α and the displacement ξ between actuator and observer. In Sec. 3.2, we considered the continuous

analogue of this scheme, with feedback at every point proportional to the interface height at that point only. We found that positive α had a stabilising effect on the system dynamics according to both long-wave models and also in the Navier–Stokes equations.

When applying the proportional control scheme (3.50) with localised observers and actuators, the eigenmodes are not sinusoidal, and so we calculate the linear stability properties numerically by solving an eigenproblem; note that this calculation only allows for perturbations with wavelength at most L. We find that increasing α has a stabilising effect on the uniform film, and that the value of α required to obtain a linearly stable state decreases when increasing the number of actuators M and observers P (see Fig. 3.9).

We can also investigate the effect of the displacement ξ between the observers and actuators on the linear stability of the uniform state. As discussed in Sec. 3.2.5, the uniform state is most easily stabilised by distributed controls when $\xi \approx 2$, and when R is close to R_0, this best choice for ξ is given by $\xi \sim 2R/3$. However, the use of localised observers and actuators introduces a natural lengthscale L/M, which is the distance between neighbouring actuators or observers, and for the analysis in this section, we also have the lengthscale L of the imposed periodicity. We can numerically calculate the effect of the displacement ξ on the linear stability of the uniform film, subject to the control scheme (3.50), by solving an eigenvalue problem for each ξ and α. Fig. 3.9 shows the stability boundaries in α-ξ space for $M = P = 3, 5, 7, 9$. We find that a stable state can be obtained at the smallest α when $\xi \approx 2$, which is comparable to the results of the calculations for distributed controls and observations shown in Fig. 3.7, despite the additional lengthscales present in the system with localised observers and controls. The magnitude of α required to stabilise the uniform state generally decreases as $M = P$ is increased, but even for just three actuators, we can stabilise the uniform film state by choosing a sufficiently large α with $\xi \approx 3$.

3.3.3 Linear-quadratic regulator (LQR) with full observations

The control scheme described in the previous subsection only allows each actuator to communicate with a single observer. We should be able to obtain better control by allowing data from all observers to be combined before determining the control amplitudes; we will still consider linear control, but allow all entries of the $M \times P$ matrix K to be non-zero. This more general scheme can also encompass situations where $M \neq P$.

The statement that the full system state can be observed is a stringent constraint; for

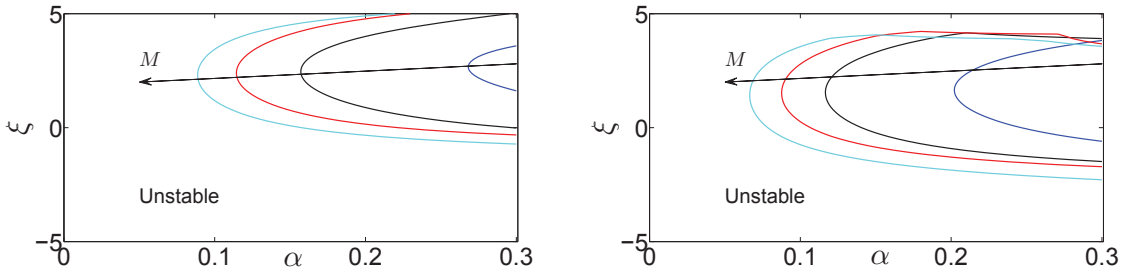

(a) Benney (b) Weighted-residual

Figure 3.9: Stability results as the control amplitude α is varied, with a phase shift ξ between actuator and observer. There are M equally-spaced actuators, and $P = M$ equally-spaced observers, each smoothed according to (3.49) with $w = 0.1$, and results are shown for $M = P = 3, 5, 7, 9$. The largest stable region occurs for $M = 9$. As is the case for distributed actuators (see Section 3.2.5 and Fig. 3.7), the best stabilisation occurs at a moderate, positive value of ξ, so that the observers are positioned upstream relative to the actuators.

the weighted-residual model this requires simultaneous information regarding $h(x,t)$ and $q(x,t)$, and in the Navier–Stokes system, the full system state includes two components of the velocity field along with the interface height. Notwithstanding the difficulties of obtaining full observations, if we are somehow able to observe the full system state, a variety of algorithms from control theory can be used to compute the controls. Here we choose to use the linear-quadratic regulator (LQR) algorithm [234] (see Appendix A.2 for a description of the algorithm), which determines K so as to minimise a cost functional associated with control amplitudes and the deviation of the system from the flat state.

We use the following cost functional, in terms of our variables,

$$\kappa = \int_0^\infty \int_0^L \left\{ \varsigma (h-1)^2 + (1-\varsigma) F^2 \right\} \, \mathrm{d}x \, \mathrm{d}t. \tag{3.51}$$

For a given physical system, the control scheme is a function of the single parameter $\varsigma \in (0,1)$. The choice of K and the resulting system eigenvalues are dependent on ς, but a stable system should be obtained for any $0 < \varsigma < 1$. Row m of the matrix K determines the amplitude of actuator m:

$$f_m(t) = \sum_{n=1}^{N} K_{mn}(h_n(t) - 1), \tag{3.52}$$

where $h_n(t)$ is the value of h at the position x_n.

Fig. 3.8 shows one such row, or feedback gain, computed using the LQR algorithm,

as implemented using the MATLAB LQR function, for the Benney and weighted-residual equations. The LQR algorithm gives very smooth control input functions for the Benney equation. The largest part of the input function is localised slightly upstream of the actuator location when using the full Benney equation (3.2), or more centrally when using the simplified version (3.3). We can insert the Benney controls directly into the weighted-residual model, and in fact still obtain a stable state.

We can also use the LQR algorithm to calculate controls for the weighted-residual model, but the controls require observations of both h and q. We also note that the control input functions (Fig. 3.8) have relatively sharp edges near the width of the actuator. The full LQR controls are able to stabilise the uniform state in the weighted-residual model, and for our test case the maximum real part of any eigenvalue is -5.62×10^{-2}. Realistically, we are unlikely to have access to observations of both h and q, and so it would be desirable to approximate q from our observations of h using a low order model. The simplest method is to suppose that $q = 2/3$, in effect discarding the control component from q. We find that this yields a linearly stable system, but the maximum real part of any eigenvalue is then -5.09×10^{-3}, so that convergence towards the uniform state would be very slow. We can recover the information regarding the q controls by supposing that $q = 2h^3/3$ (which is the leading order term in the long-wave flux (3.2)), and so $\hat{q} = 2\hat{h}$. The largest growth rate is then -5.64×10^{-2}, which is comparable to the growth rate obtained when the flux q can be fully observed.

3.3.4 Dynamical observers for a finite number of observations

For the LQR methodology described above, full observations of the system state are assumed to be available. The system is specified by the interface shape in the Benney equation, but in the weighted-residual equations we also require full knowledge of the total downstream flux at each streamwise location. Furthermore, for the Navier–Stokes equation we would need to know the instantaneous velocity at every point within the fluid. Such knowledge is unrealistic, and so we now consider the case where the only system observations available are those of the interface height, h, at only a finite number of points within the periodic domain. In the previous subsection, we showed that if full observations are available, standard algorithms, such as LQR, can be used to construct a control matrix K for the instantaneous control scheme (3.46) so that localised actuators can be used to stabilise the uniform state. Alternatively, if distributed actuators can be applied, the LQR algorithm can also be used to

calculate a control scheme subject to localised observers. However, if there are restrictions on both actuators and observers, it is not always possible to construct a control scheme based on (3.46) so that the uniform state is linearly stable. Instead, we turn to a system of dynamical observers, in which both current and historical observations are used to determine the controls.

The principle of the approach described here is to construct an approximation of the system state which is continually corrected based on the observations available. We focus our effort on approximating the coefficients of those modes which are unstable in the uncontrolled system. We use the dynamic method described by [234] and applied for the KS equation in [9], where the predictions evolve in time according to our understanding of the linearised system behaviour in the form of its Jacobian matrix, J, and the system amplitudes, and the predicted amplitudes are corrected according to our observations. This is in contrast to a static observation scheme (3.46), where the controls are calculated only from the most recent set of observations.

After transformation to Fourier space, we can describe the evolution of a small perturbation $\tilde{h}$ in the (simplified) Benney equation (3.3) by

$$\frac{d\tilde{h}}{dt} = \tilde{J}\tilde{h} + \tilde{F}. \tag{3.53}$$

In the absence of controls, the system has no preferred positions, and so the eigenvectors of J are Fourier modes, and the transformed Jacobian matrix $\tilde{J}$ is diagonal. We reorder the wavenumbers so that the unstable eigenmodes of J appear first:

$$\frac{d\tilde{h}}{dt} = \tilde{J}\tilde{h} + \tilde{F} = \begin{pmatrix} \tilde{J}_u & 0 \\ 0 & \tilde{J}_s \end{pmatrix} \tilde{h} + \tilde{F}, \tag{3.54}$$

where the subscripts u and s correspond to unstable and stable modes, respectively. We wish to control to the state $\tilde{h} = 0$.

To stabilise the zero state of this system, we would ideally leave the stable modes untouched, while choosing F to react to the unstable modes. This can be achieved by letting

$$\tilde{F} = \tilde{B}\tilde{K}\tilde{h}_u = \begin{pmatrix} \tilde{B}_u \\ \tilde{B}_s \end{pmatrix} \tilde{K}\tilde{h}_u, \tag{3.55}$$

so that

$$\frac{d}{dt}\begin{pmatrix}\tilde{h}_u\\ \tilde{h}_s\end{pmatrix} = \begin{pmatrix}\tilde{J}_u & 0\\ 0 & \tilde{J}_s\end{pmatrix}\begin{pmatrix}\tilde{h}_u\\ \tilde{h}_s\end{pmatrix} + \begin{pmatrix}\tilde{B}_u\tilde{K} & 0\\ \tilde{B}_s\tilde{K} & 0\end{pmatrix}\begin{pmatrix}\tilde{h}_u\\ \tilde{h}_s\end{pmatrix} = \begin{pmatrix}\tilde{J}_u + \tilde{B}_u\tilde{K} & 0\\ \tilde{B}_s\tilde{K} & \tilde{J}_s\end{pmatrix}\begin{pmatrix}\tilde{h}_u\\ \tilde{h}_s\end{pmatrix}. \quad (3.56)$$

The matrix on the right-hand side of this eigenvalue problem is lower triangular by blocks, and the block $\tilde{J}_s$ is diagonal. The eigenvalues and eigenvectors corresponding to $\tilde{J}_s$ are thus unchanged by $\tilde{F}$.

The remaining task is to stabilise the subsystem

$$\frac{d\tilde{h}_u}{dt} = \tilde{J}_u\tilde{h_u} + \tilde{B}_u\tilde{K}\tilde{h}_u. \quad (3.57)$$

To choose the matrix $\tilde{K}$, we use the LQR algorithm on the subsystem (3.57), which has size equal to the number of unstable modes, M. However, to apply these controls, we need to approximate $z = \tilde{h}_u$ based on our observations. We can write our discrete set of observations as $y = \Phi(h-1)$, $\tilde{y} = \tilde{\Phi}\tilde{h} = \tilde{\Phi}_u\tilde{h}_u + \tilde{\Phi}_s\tilde{h}_s$.

We can obtain a good approximation of z by considering a set of ordinary differential equations:

$$\frac{dz}{dt} = (\tilde{J}_u + \tilde{B}_u\tilde{K})z + L(y-\bar{y}) = \left(\tilde{J}_u + \tilde{B}_u\tilde{K} - L\tilde{\Phi}_u\right)z + Ly, \quad \bar{y} = \Phi_u z. \quad (3.58)$$

Here $\bar{y}$ is the expected set of observations based on our current approximation to the system, and the $L(y-\bar{y})$ term indicates a correction based on our actual observations. Once we know z, we can set $\tilde{F} = \tilde{B}\tilde{K}z$. However, we still need to choose the matrix L in order that z will converge rapidly to $\tilde{h}_u$. We define an error term: $\tilde{e} = \tilde{h}_u - z$, and after several substitutions we find that $\tilde{e}$ is governed by

$$\frac{d\tilde{e}}{dt} = Y\tilde{e} - L\Phi_s\tilde{h}_s, \quad Y = \tilde{J}_u - L\tilde{\Phi}_u. \quad (3.59)$$

To obtain rapid convergence of our estimator z towards the true system state, we need the eigenvalues of the matrix Y to have large and negative real part, and we can use the LQR algorithm to obtain a suitable matrix L to achieve this. If the conditions on the eigenvalues of Y are satisfied, it can be proved that the solution z to equation (3.58) converges exponentially to the true coefficients $\tilde{h}_u$ of h as long as the initial guess is sufficiently good. Furthermore,

if the real part of these eigenvalues is sufficiently large (in absolute value), then we can write $Y = \widetilde{Y}/\epsilon$ for small ϵ and, by multiplying (3.59) by ϵ, can obtain a system of equations in the standard singularly perturbed form [129]. This system possesses an exponentially stable fast subsystem (the equation for z) and an exponentially stable slow subsystem (the (stabilised) linearised equation for h), which implies that the system (3.60) below is exponentially stable.

We can rewrite the complete system in real space, to determine the behaviour of the nonlinear initial value problem:

$$h_t + q_x = F(x,t), \tag{3.60a}$$

$$q(x,t) = \frac{h^3}{3}\left(2 - 2h_x \cot\theta + \frac{h_{xxx}}{C}\right) + \frac{8Rh^6 h_x}{15}, \tag{3.60b}$$

$$F(x,t) = \mathcal{F}^{-1}\tilde{B}\tilde{K}z, \tag{3.60c}$$

$$\frac{dz}{dt} = \left(\tilde{J}_u + \tilde{B}_u\tilde{K} - L\tilde{\Phi}_u\right)z + Ly, \tag{3.60d}$$

$$y = \Phi(h-1), \tag{3.60e}$$

where $\mathcal{F}$ is the Fourier transform operator. It can be seen from equations (3.60c)-(3.60e) that the feedback control F is calculated only from those observations of the true system state h attainable through the matrix Φ.

It is necessary to alter, and hence approximate, all of the unstable eigenmodes of the system in order to stabilise the uniform state, and so the size of z must be equal to or greater than the number of unstable modes. We expect to achieve better performance as the number of tracked and stabilised modes is increased. The number of actuators M need not be equal to the number of observers P, and Fig. 3.10 shows the system eigenvalues as P is increased for $M = 5$ (note that P is odd). We find that choosing $P = 7$ gives much faster convergence than $P = 5$, but further increases in P have negligible effect on the eigenvalues. However, nonlinear initial value simulations of the system (3.60) benefit from taking $P = 9$. In Fig. 3.11, we compare nonlinear initial value calculations for $M = 5$, based on $P = 5$ and on full observations. We find, not surprisingly, that much faster convergence is obtained with full observations.

The system (3.60) is presented for the simplified Benney equation (3.3). The analysis can be extended to include cross flow effects present in (3.2) by left-multiplying B by $(I - \partial_x Z_F)$ before computing $\tilde{B}_u$. The Benney control scheme can be implemented in the weighted-

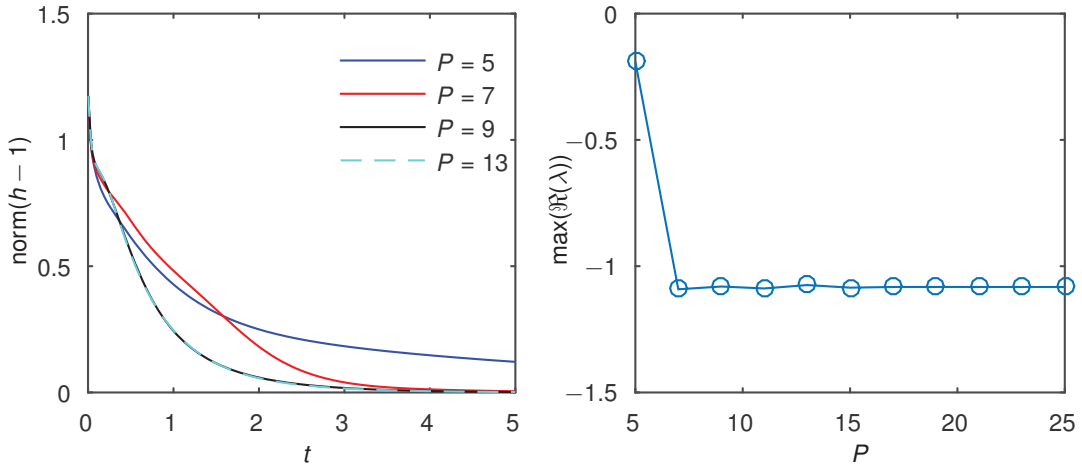

Figure 3.10: Distance between current solution and uniform film state as a function of time for $M = 5$ actuators, with P observers (left) and maximum real part of the eigenvalues of the system (3.60) as a function of P (right). The actuator and observer shapes are as described by (3.49), with $w = 0.1$ and $\xi = 0$. The initial condition is $h = 1 + 0.3\cos(2\pi x/L) + 0.1\sin(4\pi x/L)$, with $L = 30$.

residual equation by simply replacing equation (3.60b) by (3.4), but we cannot be certain that the resulting system will be linearly stable. For our test case, we find that even the linear stability of the uniform state in the weighted-residual equations is sensitive to P, with $P = 5$ stable, but $P = 7$ unstable. A full analysis of the approximately-controlled weighted-residual equation is a topic for future work.

3.4 Controlling to non-uniform solutions with distributed controls

Feedback controls of the form $F = -\alpha(h - H)$ can also be used to drive the system towards non-uniform states, by setting the target state H to be spatially varying. We would like to know whether the state $h = H$ is always reached, and whether this state is stable. Small perturbations about H are always affected by the feedback controls, and so α will change the linear stability properties of the state H. As $F = 0$ when $h = H$, the system can only remain in this state if $h = H$ is an exact solution of the equations in the absence of suction. We will discuss the system dynamics when H is not an exact solution of the governing equations in Sec. 3.4.3. The extension of the localised actuator control scheme developed in the previous section to stabilise a non-uniform state is a non-trivial task, as discussed in Sec. 3.4.4, and is left for future work.

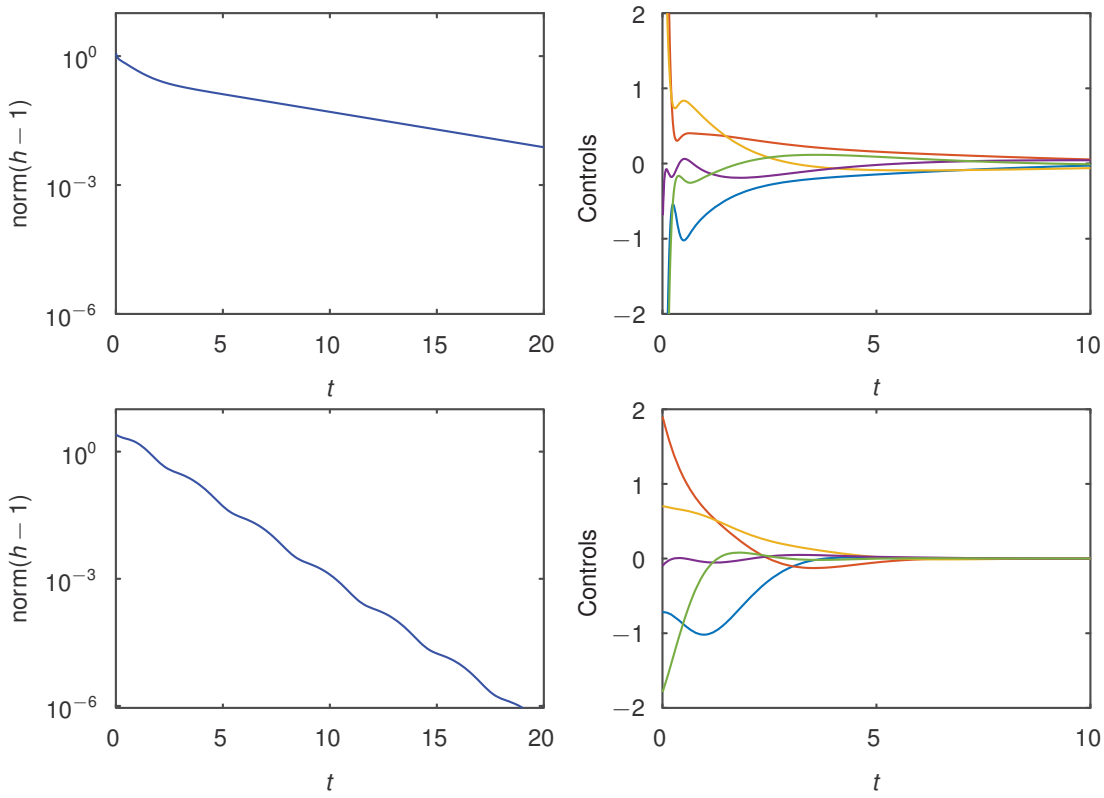

Figure 3.11: Semi-log plot of the distance between the current and flat states (left) and amplitudes of controls as a function of time (right), for $M = 5$. For the upper row of figures, we use $P = 5$ observations, while for the lower row, we use full knowledge of the interface height h.

3.4.1 Travelling waves

The long-wave systems support non-uniform travelling wave solutions, of the form $h = H(x - Ut)$, where U is the propagation speed. Travelling waves undergo bifurcations (see e.g. [165]), and may be stable or unstable in the corresponding moving frame. It is important to note that the shapes and bifurcation structure of travelling waves differ between the models. If the target state H is an exact travelling wave solution to the equations in the absence of suction, then the state H is also a travelling wave solution to the same equations with $F = -\alpha[h - H(\zeta)]$, and thus the application of controls affects the stability but not the shape or speed of the targeted travelling wave.

Fig. 3.12(a) shows an unstable travelling wave solution to the Benney equation. For simplicity, we limit perturbations to those periodic with the same spatial period as the travelling wave. In order to compute the stability of travelling waves, we transform to the frame

moving at speed U, and then identify x with ζ. For the Benney equation, the generalised eigenvalue problem (3.41) becomes

$$\lambda\hat{h} = \{U\partial_\zeta - \partial_\zeta Z_h - [I - \partial_\zeta Z_F]\alpha\}\,\hat{h}. \tag{3.61}$$

We note that if $Z_F = 0$, which is the case for the simplified Benney equation (3.3), then the eigenvalues λ are shifted by $-\alpha$, and the eigenvectors of the system are unchanged from those in the absence of controls. However, if we are using the standard Benney equation (3.2) or the weighted-residual system, the effect of α on the eigenvalues is more complicated than a simple shift, and we solve the eigenvalue problem numerically to determine the effect of α on the linear stability properties of the non-uniform travelling waves. Fig. 3.12(b)

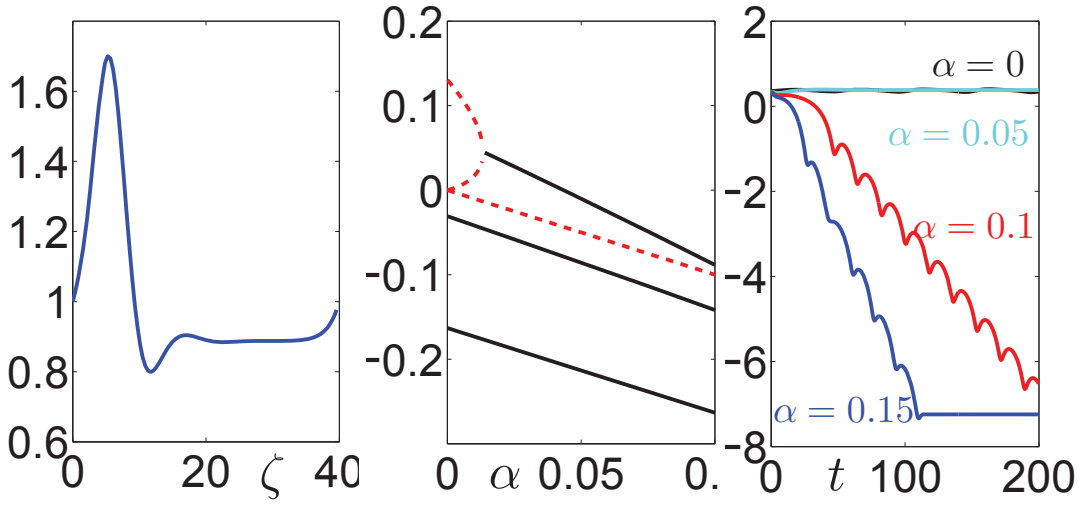

(a) $H(\zeta)$ (b) $\Re(\lambda)$ (c) $\mathrm{norm}(h - H)$

Figure 3.12: (a) A travelling wave solution to the Benney equation, for $R = 2$, $\theta = \pi/4$, $C = 0.05$, $U = 2.82$. (b) The real part of the seven complex eigenvalues with largest real part, as α is increased. Real eigenvalues are shown by red dashed lines, while black solid lines indicate the real part of complex conjugate pairs. Neutral stability occurs at $\alpha = 0.0434$. (c) Results from nonlinear initial value calculations, starting from close to a uniform film, controlling towards the solution shown in (a), for $\alpha = 0$, $\alpha = 0.05$, $\alpha = 0.1$, $\alpha = 0.15$. Convergence to H is only achieved in the two latter cases.

shows the real part of the seven most unstable eigenmodes as a function of α when considering the linear stability of the travelling wave shown in Fig. 3.12(a). When $\alpha = 0$, this travelling wave is unstable, with one eigenmode with a positive real eigenvalue. There are two eigenmodes with eigenvalue zero; one corresponds to varying the mean film thickness,

and the other to translational displacement of the travelling wave. The real part of the most unstable eigenvalue decreases with α, until it collides with another eigenvalue while still in the right half plane. These two eigenvalues then form a complex conjugate pair, which eventually crosses the imaginary axis with a finite imaginary part, stabilising the system for $\alpha > 0.0434$. This stabilisation occurs via a Hopf bifurcation, and so we would expect to observe small-amplitude limit cycles for α just below the critical value. Linear stability alone does not mean that the travelling wave is necessarily an attractor when starting from the uniform state, and indeed initial value calculations starting from the uniform film state, as plotted in Fig. 3.12(c), do not reach the desired travelling wave when $\alpha = 0.05$. However, the system successfully converges to the desired travelling wave when $\alpha = 0.1$, and converges more rapidly when $\alpha = 0.15$. We note that even when the system is converging to the travelling wave, the solution norms show evidence of decaying oscillations.

3.4.2 Non-uniform steady states

We do not know of any non-uniform steady states to the Benney, weighted-residual or Navier–Stokes equations for flow down a planar, unpatterned wall in the absence of suction; instead structures are swept downstream by the underlying flow. However, as discussed in [206], the application of steady non-zero suction gives rise to non-uniform steady states, with their own bifurcation structure and stability properties. Moreover, we can often choose the applied steady suction in order to make a given interface shape into a steady solution of the equations.

In order to include both steady suction and feedback, we use an extension of the controls:

$$F = -\alpha[h(x,t) - H(x)] + S(x). \tag{3.62}$$

Here α is the control parameter, and $S(x)$ is the steady component of F that we are free to specify. If $\alpha = 0$, $S(x)$ must have zero mean to prevent growth in fluid mass, and thus to allow steady solutions.

We choose the following non-uniform steady state as the target state for our calculations:

$$H(x) = 1 + 0.3\cos\left(\frac{2\pi}{L}\right) + 0.2\sin\left(\frac{4\pi}{L}\right) + 0.2\sin\left(\frac{6\pi}{L}\right), \quad L = 30, \tag{3.63}$$

shown in Fig. 3.13, and set $R = 5$, $C = 0.05$, $\theta = \pi/4$. For these parameters, the uniform

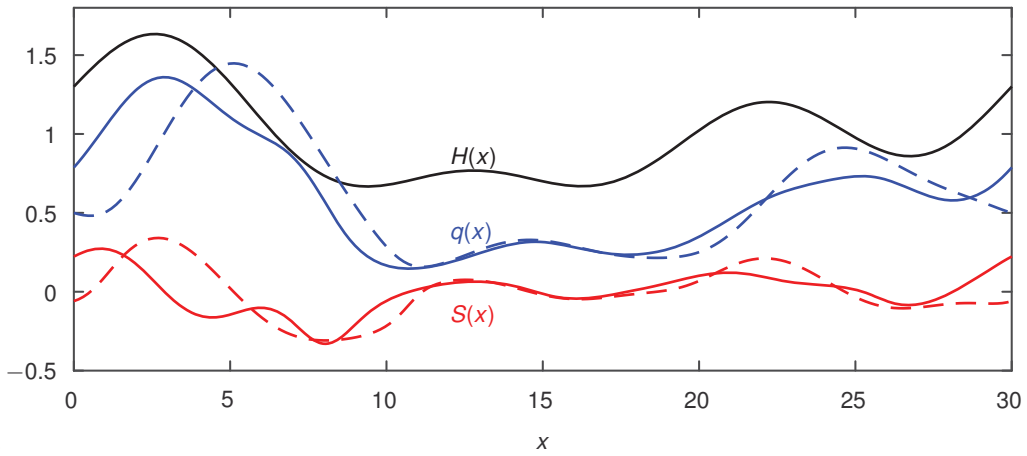

Figure 3.13: Steady flux q and suction S for the steady state (3.63). The solid and dashed lines correspond to Benney and weighted-residual results, respectively.

film state is unstable. The state $h = H$ is not a steady solution of the equations when $S = 0$, but we can calculate $S(x)$ to make it so.

For $h = H$ to be a steady solution of the Benney equation, we have

$$F = S = q_x \tag{3.64}$$

and

$$q = \frac{H^3}{3}\left(2 - 2H_x \cot\theta + \frac{H_{xxx}}{C}\right) R\left(\frac{8H^6 H_x}{15} - \frac{2H^4 F}{3}\right). \tag{3.65}$$

We can rearrange these two equations to obtain a single equation for $S = F$:

$$S + \left(\frac{2RH^4 S}{3}\right)_x = \left[\frac{H^3}{3}\left(2 - 2H_x \cot\theta + \frac{H_{xxx}}{C}\right) + \frac{8RH^6 H_x}{15}\right]_x, \tag{3.66}$$

subject to periodic boundary conditions on $S(x)$. The right hand side of (3.66) is known, and the left hand side is linear in $S(x)$. There is therefore a unique solution for $S(x)$, given $H(x)$, in the Benney model, and the equation has a solution for each smooth, non-zero H. We note that the task of finding a suction profile to enable a particular steady solution is related to inverse topography problems, in which the bottom profile is computed from observations of the interface height [98] or surface velocity [99].

Perhaps unsurprisingly, the linearity with respect to S obtained in (3.66) does not apply

in the weighted-residual model. Instead we must solve

$$F = S = q_x \tag{3.67}$$

and

$$q = \frac{H^3}{3}\left(2 - 2H_x \cot\theta + \frac{H_{xxx}}{C}\right) + R\left(\frac{18q^2H_x}{35} - \frac{34Hqq_x}{35} + \frac{HqF}{5}\right), \tag{3.68}$$

again subject to periodic boundary conditions on S and q. We can use $F = q_x$ to rewrite the second equation as an equation for q alone:

$$q = \frac{H^3}{3}\left(2 - 2H_x \cot\theta + \frac{H_{xxx}}{C}\right) + R\left(\frac{18q^2H_x}{35} - \frac{27Hqq_x}{35}\right), \tag{3.69}$$

but this is nonlinear in the unknown q, and so we cannot guarantee existence or uniqueness of solutions. However, solutions should still exist when H is close to 1, and for the non-uniform state (3.63), we obtain the solution shown in Fig. 3.13.

With the appropriate S for the corresponding model, as shown in Fig. 3.13, numerical solutions of the discretised eigenvalue problems described in Sec. 3.2.6 show that the steady state (3.63) is stable for $\alpha > 1.32$ in the Benney model, and $\alpha > 1.39$ in the weighted-residual model. In both cases, the exchange of stability occurs via a Hopf bifurcation, so that below the critical value of α, we would again expect to observe time-periodic limit cycles.

A second mechanism for exchange of stability involves real eigenvalues passing through zero. In Fig. 3.14, we choose a steady flux $S(x)$ which is known [206] to correspond to two solutions $H(x)$ when $\alpha = 0$, one of which (H_1) is stable, the other (H_2) is unstable with one positive real eigenvalue, and show the results of controlling towards the latter, unstable state, H_2. Each steady state at $\alpha = 0$ gives rise to a solution branch for $\alpha > 0$. The target state H_2 is always a solution, and is stable for $\alpha > 1.92$. For $\alpha < 1.92$, H_2 has a single eigenvalue with positive real part, and this eigenvalue is exactly zero at $\alpha = 1.92$. The exchange of stability via a real eigenvalue passing through zero corresponds to a transcritical bifurcation, and implies the local existence of a second solution branch, which here is the branch that connects back to H_1 at $\alpha = 0$. The second branch diverges as α increases beyond 1.92, here by the minimum film height tending to zero.

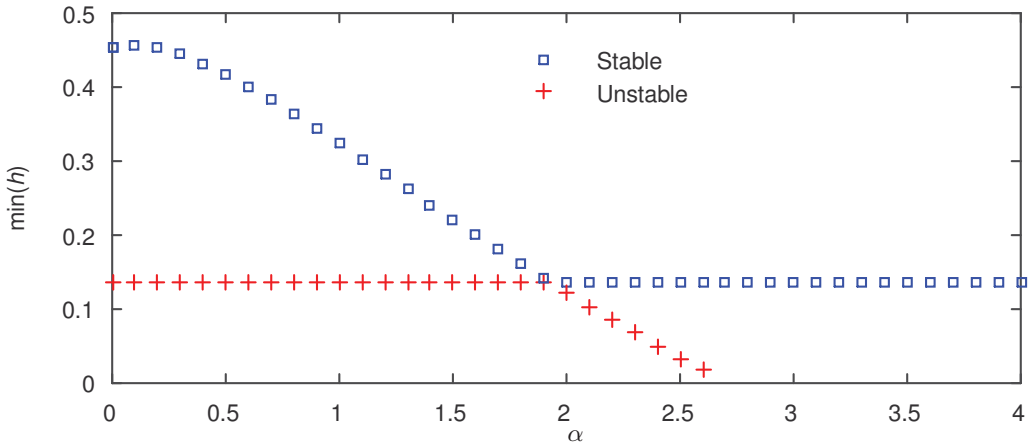

Figure 3.14: Illustration of a transcritical bifurcation that occurs when controlling to an unstable steady state, that has just one positive eigenvalue. Exchange of stability occurs through a transcritical bifurcation at $\alpha = 1.92$, necessitating the existence of another solution branch, which connects to a stable steady solution for the same S at $\alpha = 0$. The second solution branch only persists slightly beyond the transcritical bifurcation, diverging through the minimum layer height vanishing at a finite value of α. The parameters here are $R = 0$, $C = 0.05$, $\theta = \pi/4$, $S = 0.7\cos(2\pi x/10)$, which matches the bifurcation structure for $\alpha = 0$ shown in Fig. 3 of [206].

3.4.3 Controlling towards non-solutions

In the previous subsection, we required that the target state H is an exact solution of the equations, so that the system will remain at $h = H$ if it ever reaches it, and the main questions surround linear stability, which can be directly modified by linear feedback controls. However, in practice, the target state is highly unlikely to be an exact solution, due to discretisation error, imperfectly known parameters, or, more interestingly for our purposes, discrepancies which arise due to calculating travelling waves or the steady flux S according to a low-order model which only approximates the true system. We now investigate robustness to model choice by analysing the behaviour of the system when feedback controls are applied towards a state which is not a solution to the governing equations, and so can never be more than transiently achieved.

We suppose that the system reaches an equilibrium state H^*, which will depend on the target state H, the feedback control strength α, any patterning imposed on the system via S, and the parameters of the uncontrolled system. We usually have a nonlinear system to solve for H^*, which need not have unique solutions. In the Benney equation, the steady state H^*

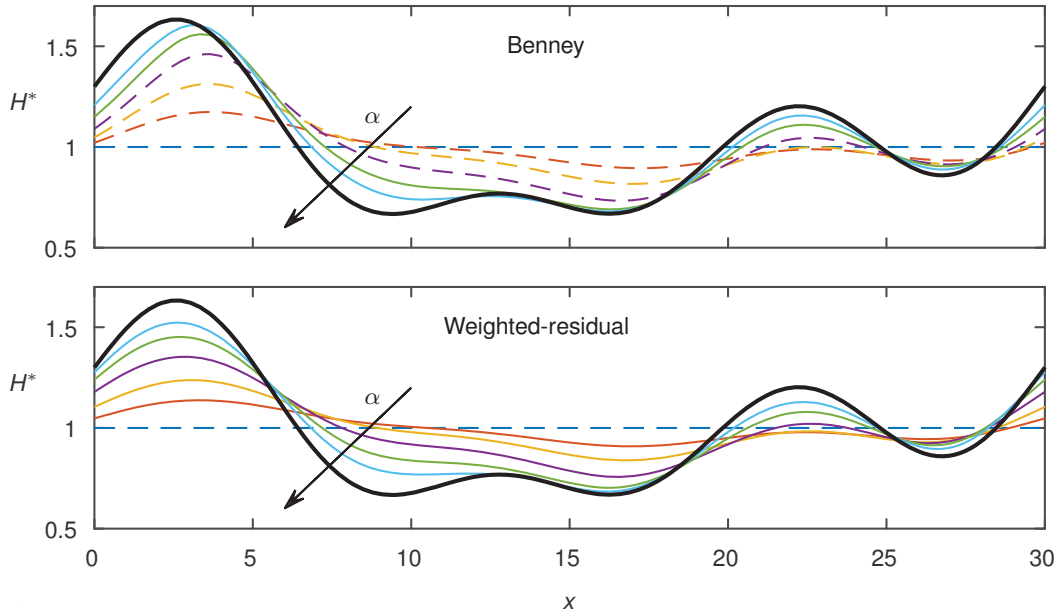

Figure 3.15: Steady solutions to the Benney equation and weighted-residual equations, controlled towards $h = H$ (shown in bold) using the control scheme (3.62), for $\alpha = 0, 0.125, 0.25, 0.5, 1, 2$, and $S = 0$. Here $R = 5$, $C = 0.05$ and $\theta = \pi/4$. Dashed lines indicate unstable solutions.

must satisfy

$$F = -\alpha[H^* - H] + S, \quad F = q_x \tag{3.70}$$

and

$$q = \frac{H^{*3}}{3}\left(2 - 2H_x^* \cot\theta + \frac{H_{xxx}^*}{C}\right) + R\left(\frac{8H^{*6}H_x^*}{15} - \frac{2H^{*4}F}{3}\right). \tag{3.71}$$

These equations are nonlinear in H^*, and can have zero, one, or more solutions. Fig. 3.15 shows steady solutions to the nonlinear Benney system (3.70)-(3.71), and also the corresponding weighted-residual system, for the case $S = 0$, with H given by the large-amplitude, non-uniform state (3.63). We find that for both models, the numerical solutions for H^* tend towards H as α increases, and our linear stability calculations confirm that the states H^* are stable at large α. However, the value of α at which steady states become stable, and also the extent to which the steady states deviate from H at a given α, are dependent on the choice of model.

The linearity of the control scheme means that suction can be interpreted as feedback controls towards the equilibrium state H^*, which is itself dependent on α and the original

target state H. We define $S^* = -\alpha(H^* - H) + S$, so that for general h, we can write

$$F = -\alpha(h - H) + S = -\alpha(h - H^*) + S^*, \tag{3.72}$$

As a result, the system is indistinguishable from controlling to the state H^* with feedback control parameter α and steady suction component S^*.

For large α, we can find a simple asymptotic solution for the steady state H^*. If the system tends towards a bounded steady state as α increases, then F must remain bounded, and so the interface shape H^* must tend towards H. Also, F tends towards $S_0(x)$, which is defined to be the steady flux required to make the desired state H a steady solution of the equations. Thus, without regard to the model details, but assuming only that a bounded steady state H^* exists for large α, we find that this state behaves as

$$H^* = H + \frac{S - S_0}{\alpha} + O\left(\frac{1}{\alpha^2}\right). \tag{3.73}$$

The function S_0, and subsequent terms in the expansion, will depend on the details of the model, but in general we can move the equilibrium state H^* closer to the desired state H by increasing α. In Fig. 3.14, we show a system where there are two steady states for the same parameters, and controls are applied towards one of these states. However, one of the solution branches disappears at a finite α, so that for sufficiently large α, the only steady state remaining is the one described by (3.73). More generally, branch divergence means that unwanted solution branches can be eliminated by increasing the control amplitude.

3.4.4 Control towards non-uniform states with point actuators

In Sec. 3.3 we considered control schemes based on localised observers and actuators that remain fixed in the laboratory frame, and showed that these schemes can be used to stabilise the uniform film state. We then showed in Sec. 3.4 that distributed control schemes can be used to stabilise non-uniform travelling waves, and to create and stabilise non-uniform steady states. However, the extension of the point-actuator control schemes to non-uniform travelling waves and non-uniform steady states faces significant difficulties.

Travelling waves are steady with respect to a moving coordinate $\zeta = x - Ut$, and can be written as $h = H(\zeta)$. However, if the observers and actuators are fixed in the laboratory frame, then these move relative to the travelling wave to be controlled. To calculate

linear stability, we first transform to the moving frame, so that the base state $h = H(\zeta)$ is a steady solution of the controlled equations. However, the evolution of small perturbations is subject to the spatial structure of the control scheme, which in this moving frame is also time-dependent. If the control scheme is spatially periodic in the laboratory frame, then it is both spatially and temporally periodic in the travelling frame, and we must use Floquet multipliers with respect to time to obtain eigenvectors. For a general control scheme, this requires the computation of eigenfunctions that are explicitly dependent on both space and time within periodic boundary conditions, which is left for future work.

Non-uniform steady interface shapes $H(x)$ require a non-zero suction profile $S_0(x)$ in order to be steady solutions of the governing equations. However, if suction must be delivered through a linear combination of M localised actuator shapes, it is very unlikely that the exact profile $S_0(x)$ can be achieved. Thus we will no longer obtain the result that $h \to H(x)$ when strong controls are applied. It is easy to imagine situations where the interface shape appears to be close to the desired state when viewed through localised observers, while diverging significantly at other positions, and so we leave the analysis of this system to future work.

3.5 Discussion

In this chapter, we went one step higher in the hierarchy of models for thin films flowing down inclined planes by analysing the effect of feedback controls on the dynamics of long-wave models derived with the Benney and weighted-residual methodologies. The controls were applied via injection and suction of fluid through the planar wall, with the required injection/suction profile determined in response to observations of the height of the air-fluid interface.

The simplest control scheme we considered was to suppose that the suction profile is applied everywhere in the planar wall and is locally proportional to the deviation of the interface profile from the desired state, so that fluid is injected where the film is particularly thin, and removed from thicker regions. We used linear stability analysis to show that this simple control scheme, governed only by the constant of proportionality α, has a stabilising effect on the uniform film state for positive α in both Benney and weighted-residual models, and also in the Navier–Stokes equations. We calculated the critical value of α needed to stabilise the uniform state to perturbations of all wavelengths, and showed that the control

scheme can significantly increase the critical Reynolds number for the onset of instability.

In a more realistic scenario, injection/suction can only be delivered via a small number of localised actuators, corresponding for example to slots in the planar wall. Likewise, observations of the full state of the solution might not always be available. We considered this case by using M point actuated controls and also a finite number of observations of the interface height, P. The control system requiring the least amount of communication between actuators and observers occurs when each actuator is connected to only one observer, and the applied actuation is proportional to the deviation of the observation from the desired value. For equally spaced actuators, our numerical calculations show that this singly-connected control scheme has a stabilising effect on the uniform film state in both long-wave models. The uniform state becomes more stable as the number of observers and actuators is increased. We investigated the effect of displacing the observer relative to its linked actuator, and found that the observer should ideally be positioned slightly upstream of the actuator to obtain the best results. Displacement between observers and actuators can also be incorporated in the fully distributed case, and we again find that the most efficient stabilisation occurs when the observer is slightly upstream of the actuator.

In principle, we should be able to obtain better system performance by using all available observations to compute the feedback controls. This corresponds to the same methodology used for the Kuramoto-Sivashinsky equation in Chapter 2. The use of point actuators means that the system is no longer translationally invariant, and so the linear stability of the Navier–Stokes equations can no longer be studied by a normal mode analysis. Therefore, we derived the controls for the Benney equation and used the weighted-residuals model as a test case. In the case when observations of the entire interface are available, we used the linear quadratic regulator (LQR) algorithm to find controls that minimise a cost functional defined in terms of the deviation of the film from the flat state and the actuator amplitudes from zero, rather than prescribing the desired eigenvalues of our system. We found that controls calculated using the LQR algorithm for the Benney equation were able to stabilise the uniform state in both the Benney and weighted-residual systems.

For the case where only a small number of observations are available, controls developed under the assumption of full observations can still be implemented by using dynamic observers, and we exploited this strategy to control the Benney system. In this scheme, the Benney system is augmented by a system of ordinary differential equations to create an

evolving approximation of the magnitudes of the unstable eigenmodes, which evolves according to our understanding of the underlying system, with corrections due to the available observations. Our stability and initial value calculations confirm that this approach does indeed stabilise the uniform state in the Benney system. For our test case, we found that increasing the number of observations above the number of unstable modes initially yields a significant increase in the overall convergence rate, but further increases have negligible effect.

To test the robustness of the dynamical observer scheme in a proxy physical setting, we inserted the Benney control scheme into the weighted-residual equations. We found that the uniform state was sometimes stable, but this depended sensitively and non-monotonically on the number of observations used to calculate the controls. The eigenvalues of the Benney and weighted-residual equations behave differently, and so we might expect that the dynamic approximations converge poorly to the true state. However, at least for stabilising the uniform state, we have the option of using the singly-connected control scheme with discrete actuators and observers, which behaves similarly in both long-wave models, and so depends relatively weakly on model details.

The thin-film systems can support non-uniform travelling waves, which propagate down the slope at constant speed. These may be stable or unstable; and we found that the locally proportional (distributed) controls can be used to stabilise unstable travelling waves. The total magnitude of the imposed suction will vanish as the target state is approached if it is an exact solution of the equations, so controls can in principle be used to physically verify the shape of unstable states. If a steady suction profile is applied, the system can support non-uniform steady states [206]. These steady states have their own bifurcation structure, can be stable or unstable, and have a more complicated internal flow than that for a film of uniform thickness. If the suction profile corresponding to a desired steady interface shape is known exactly, we showed that the feedback control scheme can be used to stabilise the steady state in a similar manner to that for stabilising travelling waves.

The shape and speed of travelling waves, and the suction profile corresponding to steady states, differs between the two long-wave models here, and likely also the Navier–Stokes equations. It is therefore unreasonable to assume that the target state is an exact solution of the equations. However, we find that if distributed controls are applied with large positive α towards an arbitrary state that is not an exact solution of the equations, the system will both

move towards that state and become stable as α is increased, irrespective of the model used.

It is somehow unsurprising that simple control schemes can be used to linearly stabilise the uniform state in the Benney equation, as the linear operator is similar to that for the Kuramoto-Sivashinsky (KS) equation studied in Chapter 2. However, the results for the KS equation provide no guarantee on the nonlinear behaviour, or on system dynamics away from long-wave limits, and so our nonlinear initial value calculations and linear stability calculations in the Navier–Stokes equations provide meaningful tests on the use of feedback control for thin film flows.

Chapter 4

Controlling roughening processes in the stochastic KS equation

In this chapter, we generalise the methodology derived in Chapter 2 for the deterministic KS equation to the stochastic KS equation, which models various physical phenomena, such as surface erosion by ion sputtering processes, fluid flow in porous media, fracture dynamics and thin film dynamics under thermal fluctuations.

We use a splitting method in which the original equation is split into a linear stochastic and a nonlinear deterministic equation so that we can apply linear feedback control methods to first stabilise the zero solution of the deterministic part and second to control the roughness of the stochastic linear equation.

We will consider both periodic and point actuated controls. In the latter case, this leads to a matrix problem, which we solve by developing an algorithm that applies basic linear algebra lemmas.

The main results of this chapter are available in [91] and the algorithm in Section 4.3.1 will be presented in [92].

4.1 The sKS equation

We consider the stochastic Kuramoto-Sivashinsky (sKS) equation:

$$u_t = -\nu u_{xxxx} - u_{xx} - uu_x + \sigma\xi(x,t), \tag{4.1}$$

normalised to 2π domains ($x \in [0, 2\pi]$) with $\nu = (2\pi/L)^2 > 0$, where L is the size of the system, with periodic boundary conditions and initial condition $u(x,0) = \phi(x)$. $\xi(x,t)$ denotes Gaussian mean-zero spatiotemporal noise, which is taken to be white in time, and whose strength is controlled by the parameter σ:

$$\langle \xi(x,t)\xi(x',t') \rangle = \mathcal{G}(x-x')\delta(t-t'), \tag{4.2}$$

where $\mathcal{G}(x-x')$ represents its spatial correlation function. We can, in principle, consider the control problem for SPDEs of the form (4.1) driven by noise that is coloured in both space and time. Such a noise can be described using a linear stochastic PDE (Ornstein-Uhlenbeck process) [181].

The noise term can be expressed in terms of its Fourier components as

$$\xi(x,t) = \sum_{k=-\infty}^{\infty} q_k \, \dot{W}_k(t) \, e^{ikx}, \tag{4.3}$$

where $\dot{W}_k(t)$ is a Gaussian white noise in time and the coefficients q_k are the eigenfunctions of the covariance operator of the noise. For example, if $\mathcal{G}(x-x') = \delta(x-x')$ (which corresponds to space-time white noise), we have $q_k = 1$. For the noise to be real-valued, we require that the coefficients q_k verify $q_{-k} = q_k$.

Proofs of existence and uniqueness of solutions to Eq. (4.1) under some appropriate assumptions on $\mathcal{G}$ can be found in [62, 72], for example. In [72], the author also defines the associated Markov semigroup in order to derive sufficient conditions for existence and uniqueness of invariant measures, and presents regularity results on the solutions. Duan and Ervin [62] prove existence and uniqueness of solutions in a similar manner, but by first proving local existence and showing that the solution remains bounded for all $T > 0$; the authors also establish *a priori* estimates for the solution. Yang [231] obtained a pull-back random attractor for the sKS equation and proved that the Hausdorff dimension of a random

attractor for the sKS equation is finite. Furthermore, the author extended these results for the generalisation of the sKS equation that includes the nonlocal term that models the presence of an electric field in [232].

We note that an alternative version of Eq. (4.1) is given by making the change of variable $u = -h_x$ which gives rise to:

$$h_t = -\nu h_{xxxx} - h_{xx} + \frac{1}{2}(h_x)^2 + \sigma\eta(x,t), \tag{4.4}$$

where $\xi(x,t) = \partial_x\eta(x,t)$. The main effect of this transformation is to change the dynamics of the mass of the solution $u_0(t) = \frac{1}{2\pi}\int_0^{2\pi} u(x,t)\,dx$. As a result of this, while both equations have received a lot attention over the last decades, Eq. (4.1) is used in mass-conserved systems such as dynamics of thin liquid films [24, 60, 96, 120, 179], and Eq. (4.4) is used to model surface growth processes such as surface erosion by ion sputtering processes [31, 32, 55, 56, 135, 151, 186].

Our focus will be on the control of the second moment of the solutions to the sKS equation, *i.e.*, its surface roughness, which is given by

$$r(t) = \sqrt{\frac{1}{2\pi}\int_0^{2\pi} \left[u(x,t) - u_0(t)\right]^2\, dx}. \tag{4.5}$$

We note that the solution $u(x,t)$ can be written in terms of its Fourier representation:

$$u(x,t) = \sum_{k\in\mathbb{Z}} \hat{u}_k(t) e^{ikx}, \tag{4.6}$$

where $\hat{u}_k(t)$ are the Fourier components of u and therefore, by making use of Parseval's identity, we can compute the expected value of $r(t)^2$ as follows:

$$\left\langle r(t)^2 \right\rangle = \sum_{k\in\mathbb{Z}} \left\langle \left(\hat{u}_k(t)\right)^2 \right\rangle - \left\langle \left(u_0(t)\right)^2 \right\rangle =: \sum_{k\in\mathbb{Z}} S(k,t) - \left\langle \left(u_0(t)\right)^2 \right\rangle, \tag{4.7}$$

where we have defined the power spectral density $S(k,t) = \left\langle \left(\hat{u}_k(t)\right)^2 \right\rangle$. Therefore, if we can control the Fourier coefficients of the solution u, we can control the surface roughness to evolve to a desired target value r_d, i.e. $\lim_{t\to\infty}\sqrt{\langle r(t)^2\rangle} = r_d$.

The methodology we propose to control the roughness of the sKS solution consists of two main steps. First, using a standard trick from the theory of semilinear parabolic SPDEs,

see e.g. [72], we define w to be the solution of the linear sKS equation:

$$w_t = -\nu w_{xxxx} - w_{xx} + \sigma\xi(x,t), \tag{4.8}$$

and write the full solution u of Eq. (4.1) as $u = w + v$, so that v satisfies

$$v_t = -\nu v_{xxxx} - v_{xx} - vv_x - (vw)_x - ww_x. \tag{4.9}$$

The important point here is to note that the above equation (4.9) is now a deterministic PDE with random coefficients and so we are in a position where we can apply the methodology for nonlinear deterministic PDEs we have presented for the gKS equation in Chapter 2 to stabilise its zero solution - something possible as long as w and its first derivative are bounded in an appropriate sense (see Section 4.2.2 below for a justification of this point). We therefore introduce the controlled equation for v:

$$v_t = -\nu v_{xxxx} - v_{xx} - vv_x - (vw)_x - ww_x + \sum_{n=-l_1}^{l_1} b_n^{det}(x) f_n^{det}(t), \tag{4.10}$$

where $m_1 = 1 + 2l_1$ (with $l_1 = [1/\sqrt{\nu}]$) is the number of controls, and $b_n^{det}(x)$ are the control actuator functions.

Once the zero solution of the equation for v has been stabilised, the second step is to control the roughness of the solution by applying appropriate controls on the linear SPDE (4.8) for w so that the solution is driven towards the desired surface roughness r_d. We will now apply this methodology to the sKS equation, Eq. (4.1) or (4.4), by choosing two different types of controls, namely periodic controls, when the controls are applied throughout the whole domain and point actuated ones, when the control force is applied in a finite number of positions in the domain.

4.2 Periodic controls

We start by deriving the controls in the case when the control actuator functions are distributed throughout the domain and periodic. This is the most common type of controls seen in the literature. We note that, for convenience, we will now be using the Fourier transform of the solution in our analysis . However, the same results are obtained if we use the solution's

Fourier series representation.

4.2.1 Derivation of the controlled equation

From Eq. (4.10), we write

$$v(x,t) = \sum_{k\in\mathbb{Z}} \hat{v}_k e^{ikx}, \tag{4.11}$$

and take inner product with the basis functions e^{ikx} to obtain:

$$\dot{\hat{v}}_k = \left(-\nu k^4 + k^2\right)\hat{v}_k + g_k(v,w) + \sum_{n=-l_1}^{l_1} b_{nk}^{det} f_n^{det}(t), \tag{4.12}$$

with $k \in \mathbb{Z}$, and where dot denotes time derivative. We have introduced $b_{nk}^{det} = \int_0^{2\pi} b_n(x) e^{ikx} dx$ and g_k are functions of the coefficients of v and w - see Appendices B.1 and B.3 for their expressions for the Burgers and KPZ nonlinearities, respectively.

Next we define the following vectors and matrices. We denote $z^v = [z_{s-}\ z_{un}^v\ z_{s+}^v]^T$, where $z_{un}^v = [v_{-l_1}\ \cdots\ v_0\ \cdots\ v_{l_1}]^T$ are the coefficients of the (slow) unstable modes, and $z_{s-}^v = [\cdots\ v_{-l_1-1}]^T$ and $z_{s+}^v = [v_{l_1+1}\ \cdots]^T$ are the coefficients of the (fast) stable modes; we also take $G = [\cdots\ g_k\ \cdots]^T$, $F^{det} = \left[f_{-l_1}^{det}(t)\ \cdots\ f_{l_1}^{det}(t)\right]^T$,

$$A = \begin{bmatrix} A_{s-} & 0 & 0 \\ 0 & A_u & 0 \\ 0 & 0 & A_{s+} \end{bmatrix} \quad \text{and} \quad B^{det} = \begin{bmatrix} B_{s-}^{det} \\ B_u^{det} \\ B_{s+}^{det} \end{bmatrix},$$

where

$$\begin{aligned} A_{s-} &= \mathrm{diag}(\cdots, -(l_1+1)^4\nu + (l_1+1)^2,), \\ A_u &= \mathrm{diag}(0, -(-l_1)^4\nu + (-l_1)^2, \cdots, -l_1^4\nu + l_1^2), \\ A_{s+} &= \mathrm{diag}(-(l_1+1)^4\nu + (l_1+1)^2, \cdots), \end{aligned}$$

and

$$B_{s-}^{det} = \begin{bmatrix} \vdots & \cdots & \vdots \\ b_{-l_1(-l_1-2)}^{det} & \cdots & b_{l_1(-l_1-2)}^{det,s} \\ b_{-l_1(-l_1-1)}^{det} & \cdots & b_{l_1(-l_1-1)}^{det,c} \end{bmatrix},$$

$$B_u^{det} = \begin{bmatrix} b^{det}_{-l_1-l_1} & \cdots & b^{det}_{l_1-l_1} \\ \vdots & \cdots & \vdots \\ b^{det}_{l_1l_1} & \cdots & b^{det}_{l_1l_1} \end{bmatrix}, \quad B_{s+}^{det} = \begin{bmatrix} b^{det}_{-l_1(l_1+1)} & \cdots & b^{det}_{l_1(l_1+1)} \\ b^{det}_{-l_1(l_1+2)} & \cdots & b^{det}_{l_1(l_1+1)} \\ \vdots & \cdots & \vdots \end{bmatrix}.$$

With these definitions we rewrite the infinite system of ODEs (4.12) as:

$$\dot{z}^v = Az^v + G + B^{det}F^{det}. \tag{4.13}$$

The key point now is to note that if there exists a matrix K^{det} such that all the eigenvalues of the matrix $A_u + B_u^{det}K^{det}$ have negative real part, then the controls given by

$$f_n^{det}(t) = K_n^{det}z_{un}^v = K_n^{det}(z_{un}^u - z_{un}^w), \tag{4.14}$$

where K_n^{det} is the $n-$th row of K^{det}, stabilise the zero solution of Eq. (4.10). The proof of this fact follows the same type of Lyapunov argument as for the deterministic KS equation and is justified as long as we have nice bounds on w, something we will demonstrate below. It should be emphasised that in Eq. (4.13) for v we have suppressed the influence of the nonlinearity on the SPDE without assuming knowledge of its value at all times and without changing the fundamental dynamics, in contrast to previous work [106, 110].

The next step is to control the stochastic linear equation for w such that the value of the second moment evolves towards the desired target. To this end, we first write w as

$$w(x,t) = \sum_{k\in\mathbb{Z}} \hat{w}_k(t)e^{ikx}, \tag{4.15}$$

and take the inner product with the basis functions to obtain an infinite system of ODEs verified by the coefficients

$$\begin{aligned} \dot{\hat{w}}_0 &= \xi_0, \\ \dot{\hat{w}}_k &= (-\nu k^4 + k^2)\hat{w}_k + \xi_k, \end{aligned} \tag{4.16}$$

where $k \in \mathbb{Z} - \{0\}$, $\xi_0 = \int_0^{2\pi} \xi(x,t)\, dx$, and $\xi_k = \int_0^{2\pi} \xi(x,t)e^{ikx}\, dx$. The solution to this system is

$$\begin{aligned} \hat{w}_0(t) &= \hat{w}_0(0) + \textstyle\int_0^t \xi_0(t)\, dt, \\ \hat{w}_k(t) &= e^{(-\nu k^4+k^2)t}\hat{w}_k(0) + \textstyle\int_0^t e^{(-\nu k^4+k^2)(t-s)}\xi_k(s)\, ds, \end{aligned} \tag{4.17}$$

and it easily follows that

$$\left\langle \hat{w}_k(t)^2 \right\rangle = -\frac{\sigma^2}{2(-\nu k^4 + k^2)}(1 - e^{-2(\nu k^4 - k^2)t}), \quad k \in \mathbb{Z}. \tag{4.18}$$

We observe that in this case the expected surface roughness only depends on the eigenvalues of the linear operator $\mathcal{L} = -\nu\partial_x^4 - \partial_x^2$; these can be controlled using feedback control to direct the evolution towards the desired value of surface roughness r_d. Hence we introduce the controlled equation for w:

$$w_t = -\nu w_{xxxx} - w_{xx} + \sum_{n=-l_2, n\neq 0}^{l_2} b_n^{rand}(x) f_n^{rand}(t) + \sigma\xi(x,t), \tag{4.19}$$

where $m_2 = 2l_2$ is the number of controls (l_2 needs to be larger than or equal to the number of unstable modes and will be specified later) and we choose the functions $b_n^{rand}(x) = e^{inx}$. We also notice that we do not need to control the eigenvalue corresponding to the constant eigenfunction ($k = 0$), since it does not contribute to the surface roughness.

By truncating the system into N modes (with N sufficiently large so that the contribution from higher modes can be neglected) and taking inner products with the basis functions, we arrive at

$$\begin{aligned} \dot{\hat{w}}_0 &= \xi_0 \\ \dot{\hat{w}}_k &= (-\nu k^4 + k^2)\hat{w}_k + f_k^{rand} + \xi_k, \quad k = -l_2, \ldots, l_2, \\ \dot{\hat{w}}_k &= (-\nu k^4 + k^2)\hat{w}_k + \xi_k, \quad k = -\tfrac{N}{2}, \ldots, -l_2 - 1, l_2 + 1, \ldots, \tfrac{N}{2}. \end{aligned} \tag{4.20}$$

Remark 9. *An important point to note is that because of the choice of periodic functions for b_n^{rand}, the system (4.20) is decoupled. In fact, with such choice of actuator functions, the matrix B_u^{rand} is the identity matrix, and $B_{s\pm}^{rand}$ are zero matrices. As will be shown in Section 4.3, this is not the case for point actuated controls.*

The surface roughness for $m_2 = 2l_2$ controls is therefore given by

$$\left\langle r^2(t) \right\rangle = \sum_{k=-N/2, k\neq 0}^{N/2} \left\langle \hat{u}_k^2(t) \right\rangle = \sum_{k=-l_2, k\neq 0}^{l_2} \left\langle \hat{u}_k^2(t) \right\rangle + \sum_{k=-N/2}^{-l_2-1} \left\langle \hat{u}_k^2(t) \right\rangle + \sum_{k=l_2+1}^{N/2} \left\langle \hat{u}_k^2(t) \right\rangle.$$

If we denote the desired surface roughness as $r_d^2 = \lim_{t\to\infty} \langle r^2(t)\rangle$, we obtain

$$\begin{aligned} r_d^2 &= \sum_{k=-l_2,k\neq 0}^{l_2} -\frac{\sigma^2|q_k|^2}{2\lambda_k} + \sum_{k=-N/2}^{-l_2-1} -\frac{\sigma^2|q_k|^2}{2(-\nu k^4+k^2)} + \sum_{k=l_2+1}^{N/2} -\frac{\sigma^2|q_k|^2}{2(-\nu k^4+k^2)} \\ &= -\frac{\sigma^2}{2}\sum_{k=-l_2,k\neq 0}^{l_2} \frac{|q_k|^2}{\lambda_k} + \underbrace{\sigma^2 \sum_{k=l_2+1}^{N/2} -\frac{|q_k|^2}{-\nu k^4+k^2}}_{\langle r_f^2\rangle}, \end{aligned}$$

where we have used the fact that the coefficients q_k are real with $q_{-k} = q_k$. The chosen eigenvalues for the controlled modes are λ_k, and we take them to be $\lambda_k = \lambda$ for all k to arrive at

$$\lambda = -\frac{\sigma^2 \sum_{k=1}^{l_2} |q_k|^2}{\langle r_d^2\rangle - \langle r_f^2\rangle}. \tag{4.21}$$

To control the surface roughness we therefore define the controls f_k^{rand} such that the new eigenvalues verify the following relation:

$$f_k^{rand} = \left(\lambda + \nu k^4 - k^2\right)\hat{w}_k. \tag{4.22}$$

Finally, putting equations. (4.10) and (4.19) together, yields the controlled equation for the full solution u:

$$u_t = -\nu u_{xxxx} - u_{xx} - uu_x + \xi(x,t) + \sum_{n=-l_1}^{l_1} b_n^{det}(x) f_n^{det}(t) + \sum_{n=-l_2}^{l_2} b_n^{rand}(x) f_n^{rand}(t). \tag{4.23}$$

4.2.2 Proof of applicability of the control methodology

The aim of this subsection is to prove that the solution v can indeed be controlled to zero even though Eq. (4.10) has random coefficients, *i.e.*, the terms $(vw)_x$ and ww_x. We will show that by using a similar argument as used for the proof of existence and uniqueness of solutions of the sKS equation (see [72]), we can apply a Lyapunov-type argument as in the deterministic KS equation.

We use (4.22) to write the solution of Eq. (4.19) as

$$w(t) = e^{\mathcal{A}t}w(x,0) + \sigma\int_0^t e^{\mathcal{A}(t-s)}d\xi(s),$$

where $\mathcal{A} = -(\nu A^2 - A + F)$, $A = -\partial_x^2$ and F is an operator discretised as

$$F = \begin{bmatrix} 0 & 0 & 0 \\ 0 & \mathrm{diag}(\lambda - \nu k^4 + k^2) & 0 \\ 0 & 0 & 0 \end{bmatrix}.$$

We take $\mathcal{G}$ to be a trace class operator, so that it satisfies [72, Assumption (3.1)]. Writing

$$e^{\mathcal{A}(t-s)}\xi(s) = \sigma \sum_{j,k\in\mathbb{Z}} q_k e^{-(\nu k^4 - k^2 + f_k)(t-s)} < e_k, e_j > \beta_k(s) e_j,$$

we have

$$\mathbb{E}[w(t)] = e^{\mathcal{A}t} w(x,0) = 0, \tag{4.24a}$$

$$\begin{aligned} \mathbb{E}[|w(t) - \mathbb{E}[w(t)]|^2] &= \sigma^2 \sum_{j,k\in\mathbb{Z}} \int_0^t e^{-2(\nu k^4 - k^2 + f_k)(t-s)} |q_k|^2 | < e_k, e_j > |^2, \\ &= \sum_{k=-l_2}^{l_2} \frac{\sigma^2 |q_k|^2}{\lambda} + \sum_{|k|\geq l_2} \frac{\sigma^2 |q_k|^2}{2(\nu k^4 - k^2)} = r_d^2, \end{aligned} \tag{4.24b}$$

where we used $< e_k, e_j >= 0$ and $f_k = \lambda + \nu k^4 - k^2$. Since we are assuming that the covariance matrix G is such that assumption (3.1) in [72] is satisfied, we have that $w(t) \in \dot{L}^2(0, 2\pi)$, the space of mean zero L^2 functions, almost surely, for any time t. This also means [181] that there exists a continuous version of w that we shall consider from now on.

Now we define $B(u, v) = uv_x$ and $b(u, v, w) =< B(u, v), w >= \int_0^{2\pi} uv_x w \, dx$ which satisfy the following relations [72, 185]:

$$\|b(u_1, u_2, u_3)\|_{L^2} \leq \|u_1\|_{L^2} \|u_{2,x}\|_{L^\infty} \|u_3\|_{L^2} \leq c\|u_1\|_{L^2} \|Au_2\|_{L^2} \|u_3\|_{L^2}, \tag{4.25a}$$

$$b(u, u, u) = 0, \tag{4.25b}$$

$$b(u_1, u_2, u_2) = b(u_2, u_2, u_1) = -\frac{1}{2} b(u_2, u_1, u_2), \tag{4.25c}$$

$$b(u_1, u_2, u_3) = -b(u_2, u_1, u_3) - b(u_1, u_3, u_2). \tag{4.25d}$$

and ([72, Prop. 2.1]):

$$\|B(u,v)\|_{D(A^{-1})} \leq c\|Au\|_{L^2}\|v\|_{L^2}, \tag{4.26a}$$

$$\|B(z,v)\|_{D(A^{-1})} \leq c\|u\|_{L^2}\|Av\|_{L^2}, \tag{4.26b}$$

$$\|B(z,z)\|_{D(A^{-1})} \leq c\|z\|_{L^2}^2, \tag{4.26c}$$

$$\|B(u,v)\|_{D(A^{-\delta})} \leq c\|u\|_{D\left(A^{\frac{1}{2}-\delta}\right)}\|v\|_{D\left(A^{\frac{1}{2}-\delta}\right)}. \tag{4.26d}$$

On the other hand, we notice that the existence of the matrix K^{det} implies that the operator $\mathcal{L}$ such that $\mathcal{L}v = -\nu v_{xxxx} - v_{xx} - \sum_{n=-l_1}^{l_1} b_n^{det}(x) f_n^{det}(t)$ satisfies $\int_0^{2\pi} v\mathcal{L}v\, dx \leq -a\|v\|_{L^2}^2$ for some positive constant a, which in turn depends on the eigenvalues we choose for the controlled operator. Therefore, multiplying equation (4.10) by v and integrating by parts, yields

$$\begin{aligned}\frac{1}{2}\frac{d}{dt}\|v\|_{L^2}^2 &\leq -a\|v\|_{L^2}^2 - \overbrace{b(v,v,v)}^{=0} - b(v,w,v) - b(v,w,v) - b(w,w,v)\\ &= -a\|v\|_{L^2}^2 + b(w,v,v) + \frac{1}{2}b(w,v,w) \leq -a\|v\|_{L^2}^2 + c\|w\|_{L^2}\|v\|_{L^2}\|Av\|_{L^2}\\ &\quad + \frac{c}{2}\|w\|_{L^2}^2\|Av\|_{L^2} \leq -\left(a - \frac{c}{2}\|w\|_{L^2}^2\right)\|v\|_{L^2}^2 + c\|Av\|_{L^2}^2 + \frac{c}{2}\|w\|_{L^2}^4, \end{aligned} \tag{4.27}$$

where we have used Young's inequality and relations (4.25) and (4.26). The term $c\|Av\|_{L^2}^2$ can be controlled using sufficiently strong controls and the last term in the right-hand-side is a constant that depends on the desired surface roughness and that again can be controlled by choosing large enough eigenvalues. Therefore, by choosing the controls such that a is large enough, $\|v\|_{L^2}^2$ is a Lyapunov function for this system and the zero solution for the controlled equation for v is stable.

4.2.3 Numerical results

We now apply the methodology presented above with periodic controls to the sKS equation with either the Burgers nonlinearity (4.1) or the KPZ nonlinearity (4.4). For simplicity, we consider white noise in both space and time ($q_k = 1$).

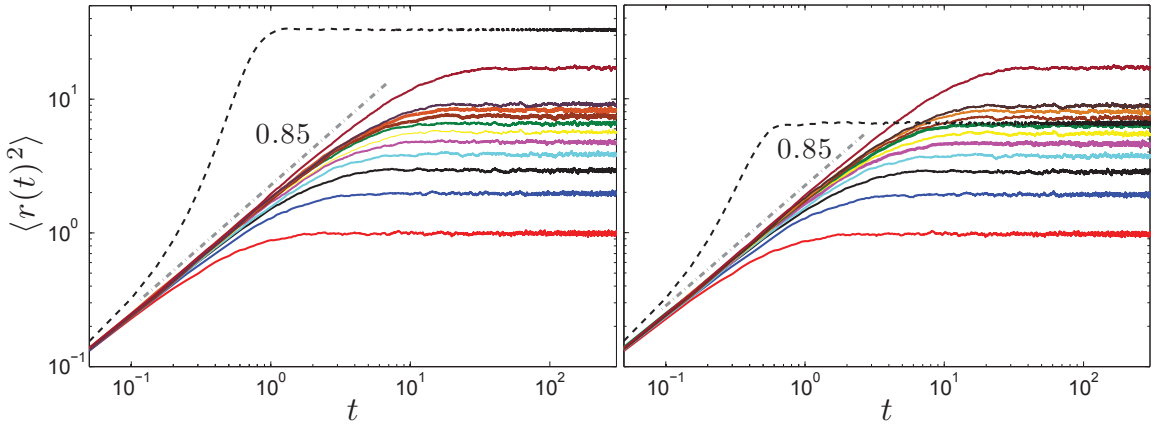

Figure 4.1: Squared value of the surface roughness of the solutions to the sKS equation with Burgers nonlinearity (left) and the KPZ nonlinearity (right) for $\nu = 0.05$, $\sigma = 0.5$ and different values of the desired surface roughness, ranging from 1 to 10, and 20. The dashed lines show the value of the uncontrolled roughness, and the straight dashed-line corresponds to a guide-to-eye line with slope 0.85.

Controlling the roughening process

We solved Eqs. (4.1) and (4.4) for $\nu = 0.05$ and $\sigma = 0.5$, controlling its solutions towards various desired surface roughness values r_d. The results are presented in Fig. 4.1. We observe that in both cases the solution exhibits a power-law behaviour at short times of the form given by Eq. (1.42) until the solution saturates to the desired value of roughness. It is interesting to notice that the exponent in all cases is the same with $\beta \approx 0.43$, independently of the type of nonlinearity and desired surface roughness (note that the exponent in Fig. 4.1 is $\approx 0.85 = 2\beta$, since we are plotting $< r(t)^2 >$). This becomes even clearer if time and surface roughness are rescaled by their saturation values, t_s and r_d, respectively. By noting that $r_d \sim t_s^\beta$, Eq. (1.42) is rewritten as:

$$\frac{\langle r(t) \rangle}{r_d} \sim \begin{cases} x^\beta & \text{if } x \ll 1, \\ 1 & \text{if } x \gg 1, \end{cases} \tag{4.28}$$

where $x = t/r_d^{1/\beta}$. Fig. 4.2 shows that all the different cases presented in Fig. 4.1 collapse into a single curve which is given by the above equation with the universal value $\beta = 0.43$.

We also study the effect of changing the domain, by varying the parameter ν. Fig. 4.3 shows the numerical results obtained when we fix the target value r_d and change the parameter ν. We observe that changing the domain does not change the growth rate (we observe

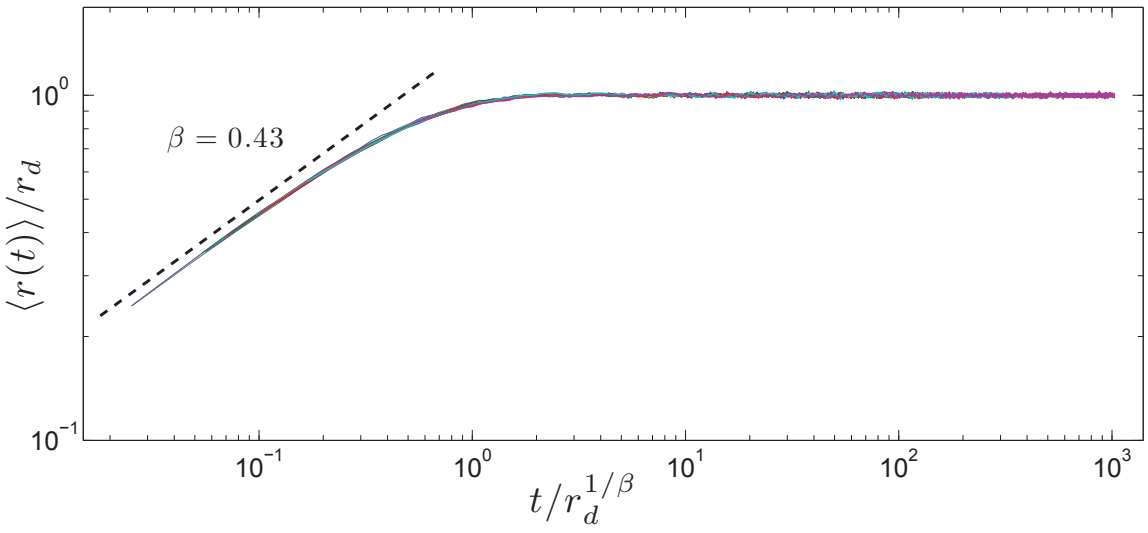

Figure 4.2: Surface roughness rescaled by the target value r_d against the rescaled time $t/r_d^{1/\beta}$ for all cases shown in Fig. 4.1. The dashed line corresponds to a guide-to-eye line with slope 0.43.

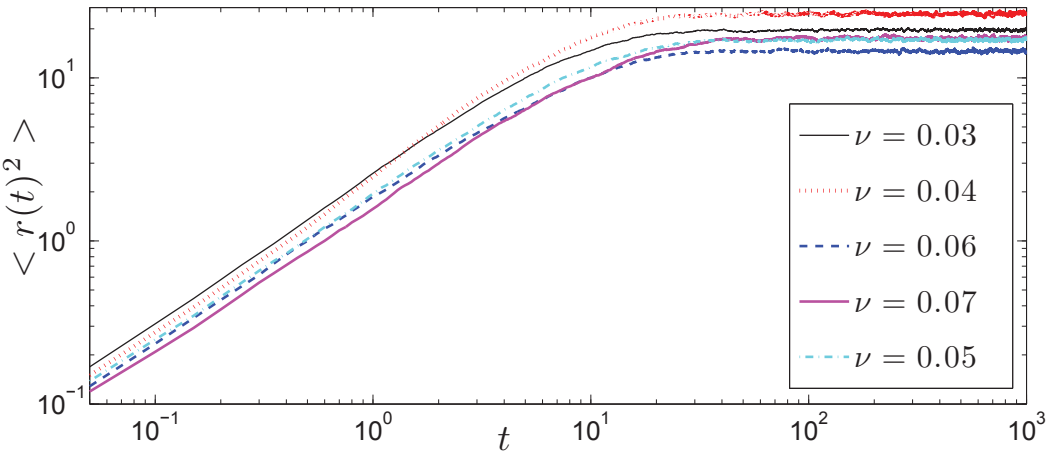

Figure 4.3: Controlled roughness with same target value $r_d^2 = 20$ and different values of ν - the domain size increases as ν decreases.

the same growth exponent $\beta \sim 0.43$) but it does slightly affect the final value of the roughness; more precisely the results indicate that larger domains tend to exhibit larger values of roughness.

Changing the shape of the solution

It is important to emphasise that in addition to controlling the roughness of the solution of the sKS equation, we can also change its shape, something that could have ramifications in

technological applications such as materials processing. We quantify this by considering the surface roughness of the solution as its distance to the desired state. If $\bar{u}(x)$ is the ultimate desired shape of the solution, then the quantity we are trying to control now becomes

$$r(t) = \sqrt{\frac{1}{2\pi}\int_0^{2\pi} \left(u(x,t) - \bar{u}\right)^2 \, dx}. \tag{4.29}$$

Using Parseval's identity we compute the expected value of $r(t)^2$:

$$\left\langle r(t)^2 \right\rangle = \sum_{k\in\mathbb{Z}, k\neq 0} \left\langle \left(u_k(t) - \bar{u}_k\right)^2 \right\rangle. \tag{4.30}$$

To control the shape of the solution, we can therefore control the solution of equation (4.10) for v to the desired shape rather than controlling it to zero. This in turn implies the use of $f_n^{det}(t) = K_n^{det}\left(z_{un}^v - z_{un}^{\bar{u}}\right) = K_n^{det}(z_{un}^u - z_{un}^w - z_{un}^{\bar{u}})$. We use the steady states of the KS equation for the chosen value of ν to define the desired shape $\bar{u}$. Results are shown in Fig. 4.4 for $\nu = 0.5$, where we can see that the solution is fluctuating around the imposed shape.

4.3 Point actuated controls

We now consider controls that are point actuated and not distributed throughout the whole domain, *i.e.* the functions $b_n(x)$ are now given by $b_n(x) = \delta(x - x_n)$, where $\delta(x)$ is the Dirac delta function. By repeating the same procedure as with periodic controls, writing $w = \sum_{k\in\mathbb{Z}} \hat{w}_k e^{ikz}$ and taking the inner product with the eigenfunctions of the linear operator, we obtain an infinite system of linear stochastic ODEs:

$$\begin{aligned} \dot{\hat{w}}_0 &= \xi_0 + \textstyle\sum_{n=1}^m b_n^0 f_n, \\ \dot{\hat{w}}_k &= (-\nu k^4 + k^2)\hat{w}_k + + \textstyle\sum_{n=1}^{m_2} b_n^k f_n + \xi_k, \quad k \neq 0. \end{aligned} \tag{4.31}$$

We can see that the difference between the above system and the periodic controls one given by (4.20) is that now the system is coupled. In fact the coupling matrix is not symmetric, and most importantly, it does not commute with its transpose. Therefore the solution does not follow directly and we cannot easily write the second moment of the coefficients as a function of the eigenvalues as in the previous section. To obtain the controlled equation we thus need to apply a different approach.

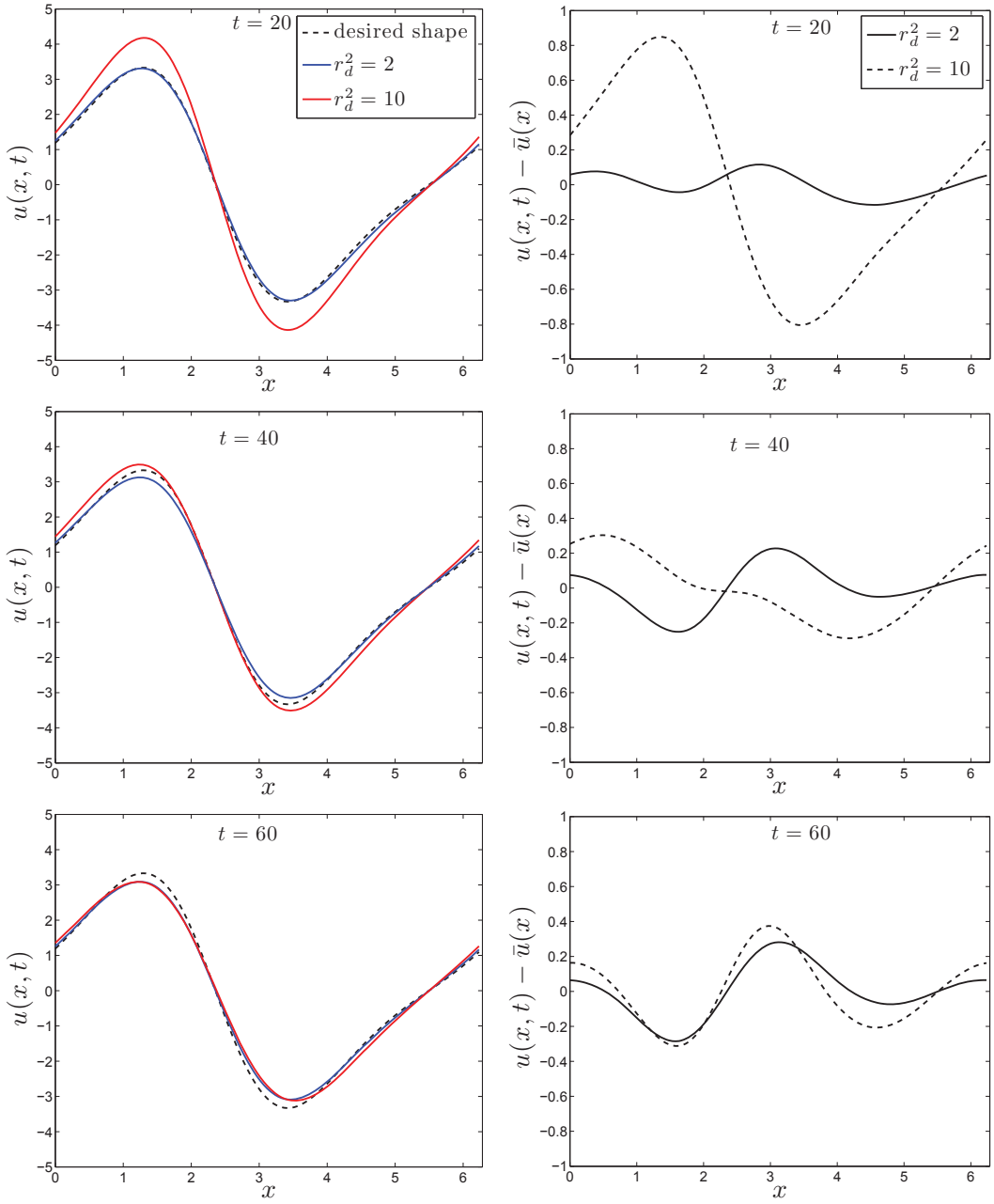

Figure 4.4: Snapshots of the sKS equation solution controlled to the shape of one of the steady states of the KS equation (left panels) and difference between current solution and desired shape for two different desired surface roughness (right panels). Parameters are $\nu = 0.5$, $\sigma = 0.5$, $r_d^2 = 2$ (blue) and $r_d^2 = 10$ (red) with $T = 100$ and $dt = 5 \times 10^{-3}$.

Let the controls $F = [f_1, \cdots, f_m]$ be such that $F = K\hat{w}$ where $\hat{w}$ is a vector containing the Fourier coefficients of w, and the matrix K is to be determined. Since the equations are not decoupled, we cannot multiply by w and integrate to find directly the second moment of the coefficients. However, we can make use of results derived in [116] which provide

simplified formulas for the first and second moments of systems analogous to (4.31). Let Ξ be the vector $\Xi_k = \xi_k$ and $C = A + BK$ where $A = \operatorname{diag} -\nu k^4 + k^2$ and $B_{kn} = b_n^k$, so that we can write the truncated system (4.20) as

$$\dot{\hat{w}} = A\hat{w} + BK\hat{w} + \Xi = C\hat{w} + \Xi.$$

We also assume without loss of generality that $\mathbf{m}(0) = \mathbb{E}(\hat{w}(0)) = 0$ and $\mathbf{P}(0) = \mathbb{E}(\hat{w}(0)\hat{w}(0)^T) = 0$. Then Theorem 4 in [116] states that

$$\mathbf{m}(t) = \mathbb{E}(\hat{w}(t)) = 0 \quad \text{and} \quad \mathbf{P}(t) = \mathbb{E}(\hat{w}(t)\hat{w}(t)^T) = \mathbf{H_1}\mathbf{F}_1^T + \mathbf{F}_1\mathbf{H}_1^T$$

where $\mathbf{F_1}$ and $\mathbf{H_1}$ are the $(1,1)$ and $(1,3)$ blocks of the matrix e^{Mt} where in the case of space-time white noise, M is

$$M = \begin{bmatrix} C & 0 & \frac{\sigma^2}{2}I & 0 \\ 0 & 0 & 0 & 0 \\ 0 & 0 & -C^T & 0 \\ 0 & 0 & 0 & 0 \end{bmatrix},$$

I is an appropriately sized identity matrix and the zeros stand for zero matrices of the appropriate size. We compute e^{Mt} and conclude that

$$\mathbf{F}_1 = e^{Ct},$$

and

$$\begin{aligned}\mathbf{H}_1 =& \frac{\sigma^2}{2}\left[It + (C - C^T)\frac{t^2}{2} + (C^2 - CC^T + (C^T)^2\frac{t^3}{3!}\right] \\ &+ \frac{\sigma^2}{2}\left[(C^3 - C^2C^T + C(C^T)^2 - (C^T)^3\frac{t^4}{4!} + \cdots\right].\end{aligned}$$

Since $\mathbf{F}_1\mathbf{H}_1^T = (\mathbf{H}_1\mathbf{F}_1^T)^T$ and $(\mathbf{H}_1\mathbf{F}_1^T)^T = \mathbf{H}_1\mathbf{F}_1^T$, we have $\mathbf{H}_1\mathbf{F}_1^T + \mathbf{F}_1\mathbf{H}_1^T = 2\mathbf{H}_1\mathbf{F}_1^T$, from

which we obtain

$$\mathbf{P}(t) = \sigma^2 \left(It + (C + C^T)\frac{t^2}{2} + \left(C^2 + 2CC^T + (C^T)^2\right)\frac{t^3}{3!} + \right.$$
$$+ \left(C^3 + 3C^2C^T + 3C(C^T)^2 + (C^T)^3\right)\frac{t^4}{4!} +$$
$$\left. + \left(C^4 + 4C^3C^T + 6C^2(C^T)^2 + 4C(C^T)^3 + (C^T)^4\right)\frac{t^5}{5!} + \cdots \right). \quad (4.32)$$

Remark 10. *In the periodic case, the matrix C is diagonal, so $CC^T = C^TC$, and this is exactly the same as*

$$\mathbf{P}(t) = \sigma^2 \sum_{n=1}^{\infty} \left(C + C^T\right)^{n-1} \frac{t^n}{n!}. \quad (4.33)$$

In addition, when choosing the eigenvalues of C, we can ensure that it is invertible and therefore $C + C^T = 2C$ is also invertible, which gives

$$\mathbf{P}(t) = -\sigma^2 \left(C + C^T\right)^{-1} + \sigma^2 e^{(C+C^T)t}, \quad (4.34)$$

so as $t \to \infty$, $\mathbf{P}(t) \to -\sigma^2 \left(C + C^T\right)^{-1}$ and

$$< r(t)^2 >= \mathrm{tr}(\mathbf{P}(t)) \to \sum_{k \in \mathbb{Z} - \{0\}} -\frac{\sigma^2}{2\lambda_k}, \quad (4.35)$$

where λ_k are the chosen eigenvalues of C, and we recover the same result as before.

It is important to note that the matrix C is not normal, *i.e.* it does not commute with its transpose, and the eigenvalues of $C + C^T$ do not satisfy the useful properties that allow us to get (4.34). However, we are not interested in knowing the full matrix $\mathbf{P}(t)$, but only its trace

$$\mathrm{tr}(\mathbf{P}(t)) = \mathrm{tr}\left(\sigma^2 \left(It + (C + C^T)\frac{t^2}{2} + \left(C^2 + 2CC^T + (C^T)^2\right)\frac{t^3}{3!} + \right.\right.$$
$$+ \left(C^3 + 3C^2C^T + 3C(C^T)^2 + (C^T)^3\right)\frac{t^4}{4!} +$$
$$\left.\left. + \left(C^4 + 4C^3C^T + 6C^2(C^T)^2 + 4C(C^T)^3 + (C^T)^4\right)\frac{t^5}{5!} + \cdots \right)\right). \quad (4.36)$$

By now making use of the linearity of the trace and its continuity to pass it inside the infinite

sum, we get

$$\begin{aligned}\operatorname{tr}(\mathbf{P}(t)) = \sigma^2 \Bigg(&\operatorname{tr}(I)t + \operatorname{tr}(C + C^T)\frac{t^2}{2} + \operatorname{tr}\left(C^2 + 2CC^T + (C^T)^2\right)\frac{t^3}{3!} + \\ &+ \operatorname{tr}\left(C^3 + 3C^2C^T + 3C(C^T)^2 + (C^T)^3\right)\frac{t^4}{4!} + \\ &+ \operatorname{tr}\left(C^4 + 4C^3C^T + 6C^2(C^T)^2 + 4C(C^T)^3 + (C^T)^4\right)\frac{t^5}{5!} + \cdots \Bigg). \quad (4.37)\end{aligned}$$

We also note that, since $\operatorname{tr}(AB) = \operatorname{tr}(BA)$, we have

$$\operatorname{tr}\left(C^2 + 2CC^T + (C^T)^2\right) = \operatorname{tr}\left(C^2 + CC^T + C^TC + (C^T)^2\right) = \operatorname{tr}(C + C^T)^2.$$

Similarly we can prove that the terms multiplied by $\frac{t^n}{n!}$ are of the form $\operatorname{tr}\left((C + C^T)^{n-1}\right)$ and we finally obtain

$$\begin{aligned}\operatorname{tr}(\mathbf{P}(t)) = \sigma^2 \Bigg(&\operatorname{tr}(I)t + \operatorname{tr}(C + C^T)\frac{t^2}{2} + \operatorname{tr}\left(C + C^T\right)^2\frac{t^3}{3!} + \\ &+ \operatorname{tr}\left(C + C^T\right)^3\frac{t^4}{4!} + \operatorname{tr}\left(C + C^T\right)^4\frac{t^5}{5!} + \cdots \Bigg). \quad (4.38)\end{aligned}$$

We proceed by assuming that $C + C^T$ is invertible, so that we can multiply by $I = (C + C^T)^{-1}(C + C^T)$ and add and subtract pertinent terms to obtain

$$\operatorname{tr}(\mathbf{P}(t)) = -\sigma^2 \operatorname{tr}\left(C + C^T\right)^{-1} + \sigma^2 \operatorname{tr}\left(\left(C + C^T\right)^{-1}\sum_{n\in\mathbb{N}}\left(C + C^T\right)^n\frac{t^n}{n!}\right). \quad (4.39)$$

Remark 11. *This does not change the proof provided in Section 4.2.2, it only changes the formula for the covariance so that the bounds are still valid.*

Remark 12. *We emphasise that the following assumptions were made here:*

(a) $C + C^T$ *needs to be invertible.*

(b) In order for the surface roughness to converge to a finite value, we require all of the eigenvalues of $C + C^T$ *to be negative, so that the exponential part disappears.*

4.3.1 Computation of the matrix K

We note in equation (4.39) that we now need to control the trace of $D^{-1} = (C + C^T)^{-1}$ and we can do that by prescribing the eigenvalues of D. Therefore, we can control the surface roughness by finding a matrix K such that the eigenvalues of

$$D = C + C^T = A + BK + A^T + (BK)^T = 2A + BK + K^T B^T \tag{4.40}$$

are a given set $\{\mu_1, \ldots, \mu_N\}$. This is a matrix problem, and even though its structure is similar to that of the well known Sylvester equation [201],

$$AX + XB = C,$$

or the Lyapunov equation [18],

$$AX + XA^T - = C$$

where in both problems we seek for the matrix X, and which have been solved before, there is, to our knowledge, no previous work done for equation (4.40).

Since we only wish to prescribe the eigenvalues of D, rather than knowing all of its entries, we can tackle this problem by using the information provided by the characteristic polynomial, χ_D, of D. We have that

$$\chi_D(t) = \prod_{i=1}^{N}(t - \mu_i) = \sum_{k=0}^{N}(-1)^k \sum_{J:|J|=k} \prod_{j\in J} \mu_j t^{N-k}, \tag{4.41}$$

where J is a subset of $\{1, \ldots, N\}$. Equivalently, we can express χ_D in terms of the sum over all its diagonal minors, *i.e.*

$$\chi_D = \sum_{k=0}^{N}(-1)^k \varsigma_k t^{N-k}, \tag{4.42}$$

where ς_k is the sum over all of the diagonal minors of size k of the matrix $D = 2A + BK + K^T B^T$. This translates into a system of N nonlinear algebraic equations,

$$\varsigma_k = \sum_{J:|J|=k} \prod_{j\in J} \mu_j,$$

for $m \times N$ variables, which are the entries of the matrix K.

We can use a nonlinear solver (e.g., MATLAB's *fsolve*) to obtain the matrix K directly, or obtain closed formulas for ς_k. For the first case, given the structure of the matrix B and the fact that the system is underdetermined, convergence is rather slow when solving the problem directly. We overcome this problem by performing a change of variables: we obtain the SVD decomposition of B by finding matrices X and Y such that $\tilde{B} = XBY^T$ and multiply equation (4.40) by X^T on the left and by X on the right. We then define $\tilde{K} = Y^T K X$, $\tilde{A} = X^T A X$ and $\tilde{D} = X^T D X$, so that we obtain the equation

$$\tilde{D} = 2\tilde{A} + \tilde{B}\tilde{K} + \tilde{K}^T\tilde{B}^T. \tag{4.43}$$

This is of the same form as (4.40), but where the matrix $\tilde{B}$ is diagonal. We find that this accelerates the convergence of the system (for moderate values of N) and we were able to get satisfactory numerical results.

For the latter case, we can apply the Matrix Determinant Lemma (see Appendix A.4) twice to obtain:

$$\begin{aligned}\det(2A + BK + K^T B^T) &= \det(2A + BK)\det(I_m + B^T(2A + BK)^{-1}K^T) \\ &= det(2A)\det(I_m + K(2A)^{-1}B)\det(I_m + B^T(2A + BK)^{-1}K^T).\end{aligned} \tag{4.44}$$

We now use the Woodbury Matrix Identity to expand the inverse in the third determinant around $2A$ and obtain

$$\begin{aligned}\det(2A + BK + K^T B^T) = \det(2A)\det(I_m + K(2A)^{-1}B)\det(I_m + B^T(2A)^{-1}K^T \\ - B^T(2A)^{-1}B(I_m + K(2A)^{-1}B)^{-1}K(2A)^{-1}K^T).\end{aligned} \tag{4.45}$$

When $m = 1$ this formula can be simplified to obtain

$$\det(2A + BK + K^T B^T) = \det(2A)\left((1 + K(2A)^{-1}B)^2 - K(2A)^{-1}BK(2A)^{-1}K^T\right). \tag{4.46}$$

Multiplying this expression out and writing it in component form, we obtain the nonlinear

system of equations

$$\sum_{J:\,|J|=l}\prod_{j\in J}\mu_j = 2^l \sum_{J:\,|J|=l}\prod_{j\in J} a_j \left(1+\sum_{p\in J}\frac{b_p k_p}{a_p}+\sum_{p\in J}\sum_{q\in J\setminus\{p\}}\frac{b_p k_q}{4a_p a_q}(b_q k_p - b_p k_q)\right), \tag{4.47}$$

for $l = 1,\ldots,N$. For $m \geq 2$ we use equation (4.45), which gives an expression for $\det(2A + BK + K^T B^T)$ in terms of determinants of $m \times m$ matrices. We consider this expression for all the principal minors with entries in $J \subset \{1,\ldots,N\}$, considering that the indices of matrix multiplication inside each determinant are also from $j \in J$. Writing equation (4.45) in component form, we notice that the second determinant is given by $\Delta_{(m,J)}$, where

$$\Delta_{(m,J)} := \det(\delta_{ij} + \eta_{ij}^{(J)})_{1\leq i,j\leq m} \tag{4.48a}$$

$$\eta_{ij}^{(J)} := \sum_{l\in J}\frac{k_{il}b_{lj}}{2a_l} \tag{4.48b}$$

$$\beta_{ij}^{(J)} := \sum_{l\in J}\frac{b_{li}b_{lj}}{2a_l}, \tag{4.48c}$$

$$\kappa_{ij}^{(J)} := \sum_{l\in J}\frac{k_{il}k_{jl}}{2a_l}. \tag{4.48d}$$

Using Cramer's rule, we see that the last entry in the third determinant is given by

$$\frac{\sum_{p,q=1}^{m}\beta_{ip}\tau_{pq}\kappa_{qj}}{\Delta_{(m,J)}},$$

where

$$\tau_{pq}^{(J)} := \left(\mathrm{adj}(\delta_{ij}+\eta_{ij})\right)_{pq}. \tag{4.49}$$

We therefore factorise $\frac{1}{\Delta_{(m,J)}}$ out of the determinant, to give the expression:

$$\det_J(2A + BK + K^t B^t) = 2^{|J|}\prod_{j\in J} a_j \frac{\det(\gamma_{pq}^{(m,J)})}{\Delta_{(m,J)}^{m-1}}, \tag{4.50}$$

where

$$\gamma_{ij}^{(m,J)} := \Delta_{(m,J)}(\delta_{ij}+\eta_{ji}) - \sum_{p,q=1}^{m}\beta_{ip}^{(J)}\tau_{pq}^{(J)}\kappa_{qj}^{(J)}. \tag{4.51}$$

We therefore arrive at the following system of nonlinear equations:

$$\sum_{\substack{J\subseteq[N]\\|J|=l}}\prod_{j\in J}\mu_j = 2^l \sum_{\substack{J\subseteq[N]\\|J|=l}}\left(\left(\prod_{j\in J}a_j\right)\frac{\det(\gamma_{ij}^{(m,J)})}{\Delta_{(m,J)}^{m-1}}\right). \tag{4.52}$$

We tested this algorithm for matrices related to the sKS equation and also for randomly generated matrices, obtaining satisfactory results - see Appendix C. We found that this algorithm gives satisfactory results, and also performs faster than solving the system directly using MATLAB's *fsolve* for small N.

4.3.2 Numerical results

We apply the methodology presented in the previous subsection with point actuated controls to the sKS with the Burgers nonlinearity (4.1) (similar results are expected for the KPZ nonlinearity (4.4)).

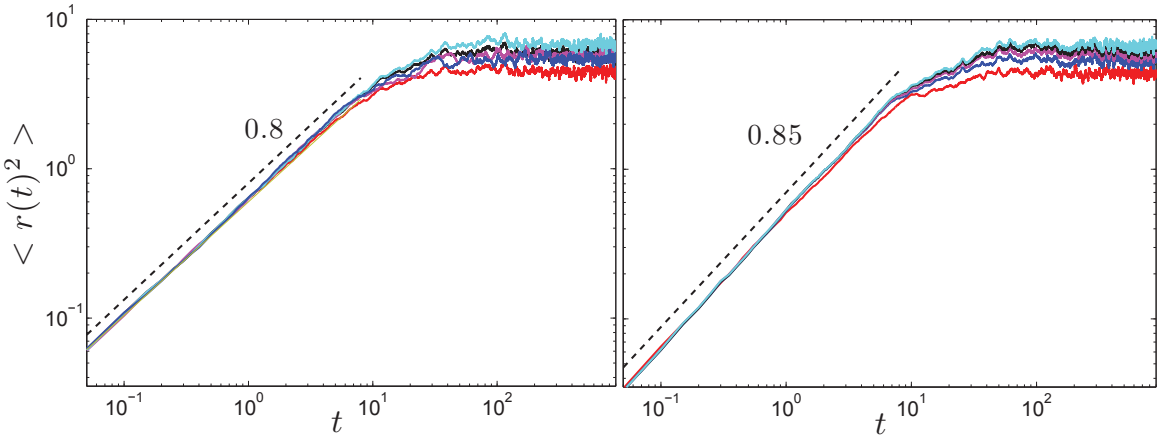

Figure 4.5: Squared value of the surface roughness of the solutions to the sKS equation with Burgers nonlinearity for $\nu = 0.04$, $\sigma = 0.5$ and different values of the desired surface roughness, ranging from 2 to 6. Left: using space time white noise; Right: using coloured noise described by the coefficients $q_k = |k|^{-1}$. We applied $m = 3$ point actuated controls, which were located at the positions $x_1 = \frac{\pi}{3}$, $x_2 = \pi$, $x_3 = \frac{5\pi}{3}$.

We solved Eq. (4.1) for $\nu = 0.4$ and $\sigma = 0.5$. For this value of ν the linear operator has 3 unstable modes and we apply $m = 3$ controls. We note that even though we do not need to control the mode corresponding to the first moment of the solution when using periodic controls, we benefit from doing so in this case, since the matrix D would not be invertible if we allowed for a zero eigenvalue. We consider either space-time white noise ($q_k = 1$) or

coloured noise with $q_k = |k|^{-1}$ (which is chosen to decay at a fast rate so that the system can be truncated at a smaller value of N), and control the solution towards various desired values r_d of the surface roughness.

The results are depicted in Fig. 4.5 where we observe that the solution still exhibits a power-law behaviour with similar exponent as in the periodic case (there we found $\beta \approx 0.43$) until it saturates at the desired value of the surface roughness. We note that even though we obtained satisfactory results for the range of values of r_d^2 selected in Fig. 4.5, further increase of r_d does not lead to the expected saturated results. This may be due to the relatively small system truncation value $N = 21$ that was found necessary in order to obtain convergence of the problem to find the entries of the matrix K. Further work is required in this direction that is beyond the scope of the present study.

4.4 Discussion

In this chapter, we generalise the methodology derived in Chapter 2 for the deterministic KS equation to the stochastic KS equation. We used a splitting method to separate the sKS equation into a linear stochastic PDE, which we use to control the suface roughness, and a nonlinear deterministic PDE with random coefficients. We show that when using periodic controls we can control the deterministic PDE to either zero (which will make us able to choose the surface roughness of the system) or some predetermined shape, given by steady states of the deterministic KS equation, thus allowing us to control the shape of the interface we are modelling. We find that the solution to the controlled problem exhibits a power-law behaviour with exponent $\beta \approx 0.43$, which is not affected by changes in the length of the domain, and is independent of the type of nonlinearity of the sKS equation. Our analytical results are valid for the sKS equation with Burgers nonlinearity, but we show numerically that they can be applied to the sKS equation with KPZ nonlinearity.

When using point actuated feedback controls, the problem becomes considerably harder to solve, due to the fact that the resulting system of linear stochastic ODEs is not decoupled. This leads to the need to solve a new matrix problem, which is similar to a matrix Lyapunov equation, but that to our knowledge has not been solved before. We derived an algorithm to tackle this matrix problem and obtained satisfactory results when controlling towards a range of surface roughness values. However, the complexity of this problem makes it harder to solve for a large N, and therefore we only present results for small N, which is possibly

the reason why we can only control the system towards a small range of surface roughness values. The study of this matrix problem, in particular of extensions to make it efficient for larger N or converge faster to the values of N that it deals with is an interesting problem that we leave for future work.

We believe that our framework offers several distinct advantages over other approaches. First, the controls we derived are linear functions of the solution u, and this in turn decreases the computational cost of their determination. Second, our splitting methodology allows us to deal with the nonlinear term directly rather than including it in the controls, thus rendering the resulting equation essentially linear and easier to handle.

One interesting observation is that feedback control methodologies can be used, in principle, in order to accelerate the convergence of infinite dimensional stochastic systems such as the sKS and the KPZ equations to their steady state. This might prove to be a useful computational tool when analysing the equilibrium properties of such systems, e.g. calculating critical exponents, studying their universality class etc. Accelerating convergence to equilibrium and reducing variance by adding appropriate controls that modify the dynamics while preserving the equilibrium states has already been explored for Langevin-type samplers that are used in molecular dynamics [64, 137]. We plan to return to this issue for the sKS and the KPZ equations in future work.

Chapter 5

Systems of coupled Kuramoto-Sivashinsky type equations

In this chapter we will be concerned with two related problems. In the first part, we will study the problem of controlling and stabilising solutions to systems of coupled Kuramoto-Sivashinsky equations, which are weakly nonlinear models of multiphase flow systems. The case we present was derived in [169] and models the two interfaces between three fluids confined between two parallel inclined planes. The coupling between the two equations is linear and is through the second derivative, but the general case considers coupling also through the fourth order derivatives. We will start by obtaining bounds for the solutions of this system, which we need for the analytical results concerning feedback and optimal control, and then we generalise our results in feedback and optimal control for the gKS equation to this coupled system.

More generally, the coupling is also present via the nonlinear terms and this can cause hyperbolic-elliptic transitions by supporting complex eigenvalues of the nonlinear flux functions, see [168]. This is a harder system to study, and we present an initial attempt to obtain analytical results towards bounding the solutions of these systems, by considering a different type of coupling, which can then be generalised to be nonlinear. This particular system can be seen as a system of conservation laws.

The results concerning the feedback and optimal control of systems of coupled KS equations are published in [89]

5.1 Systems of coupled KS equations and conservation laws

The methodology developed and implemented in Chapter 2 can also be applied to systems of nonlinear coupled PDEs. Of particular interest are systems of coupled Kuramoto-Sivashinsky equations that arise in the weakly nonlinear asymptotic analysis of a three layer flow of immiscible viscous fluids stratified in a channel and driven by gravity and/or a streamwise pressure gradient. Such equations were derived systematically using asymptotic methods in [169].

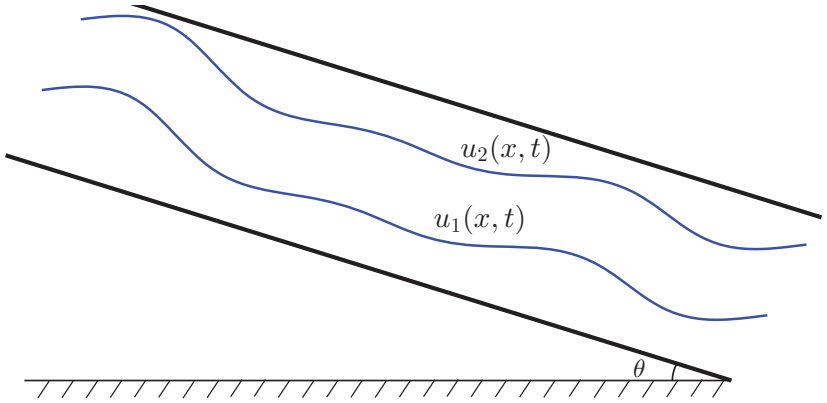

Figure 5.1: Sketch of a three layer flow down an inclined channel. The fluid interfaces are located at $y = u_1(x,t)$ and $y = u_2(x,t)$ and their evolution can be described by systems of PDEs such as (5.1).

The ensuing dynamics is very rich and in fact instabilities can emerge even in the absence of inertia, unlike analogous two-fluid flows. This is due to additional physical parameters, and also because the systems support a resonance mechanism between the two interacting interfaces. As a result, coupled nonlinear systems are mathematically significantly more challenging than scalar PDEs since analytical results on global existence and estimates of solution norms, for example, are poorly understood. Detailed computational results into the complexity of the solutions (especially their zero diffusion limits) of such coupled systems of KS equations can be found in [168].

In this chapter, we will be concerned about two problems regarding these systems. First, we will consider a system of two coupled KS equations, where the coupling is through the second derivatives alone. This is a special case but arises in the derivation of the equations - see [169]. In this case, we were able to obtain bounds on the solutions for the relevant system, System (5.1) below, which will enable us to prove analytical results concerning the

feedback and optimal control for this problem, which are presented in Section 5.2.

More generally, the nonlinear terms are also coupled and can cause hyperbolic-elliptic transitions by supporting complex eigenvalues of the nonlinear flux functions, see [168] where the authors performed extensive numerical computations and found that despite the existence of hyperbolic-elliptic transitions, the solution to the system remains bounded, even in the zero diffusion limit. This motivated us to study the boundedness of this type of systems analytically. We present here a case where there are no second derivatives involved, but both the coupling and the dynamics of each interface are affected via first order derivatives. Even though we were not able to find the desired bounds, we were still able to extend most of the results in [84] to this case and we present these results in Section 5.3.

5.2 Systems of coupled Kuramoto-Sivashinsky equations

We consider systems of coupled Kuramoto-Sivashinsky equations, which were derived in [169] to model three layer flows driven along an inclined channel by gravity and a pressure gradient, such as the one depicted in Fig. 5.1. In the general case, the system allows coupling through first, second, and fourth order derivatives, as well as via the nonlinearities, which are of the form $\beta_{ij}u_{ix}u_{jx}$. This results in a complicated dynamical behaviour: even when the flux matrices governing the system - see [169] for definitions of these matrices - have real and distinct eigenvalues, which correspond to the case when the system is hyperbolic, the interaction between the nonlinearities and, e.g., surface tension terms introduces instabilities, known as Majda-Pego type instabilities [154].

We consider a particular case of these systems, which consist of two coupled Kuramoto-Sivashinsky equations with coupling through the second derivatives alone:

$$\begin{cases} u_{1,t} &= -\nu u_{1,xxxx} - u_{1,xx} - u_1 u_{1,x} - \alpha_1 u_{2,xx} \\ u_{2,t} &= -\nu u_{2,xxxx} - u_{2,xx} - u_2 u_{2,x} - \alpha_2 u_{1,xx}, \end{cases} \tag{5.1}$$

where the equations are valid in the interval $(0, 2\pi)$ with periodic boundary conditions and initial conditions $u_1(x, 0) = u_{10}(x)$ and $u_2(x, 0) = u_{20}(x)$ and $u_{10},\ u_{20} \in \dot{H}^2_p(0, 2\pi)$. This is a simplified version of the general system, which arrives in the derivation. However, it still exhibits very rich dynamics, and its simplicity allows us to obtain analytical results on its solutions; in particular we can bound the solutions and analyse their regularity. We will

use these facts in our analysis of feedback and optimal control for this system.

5.2.1 Bounds on the solutions of System (5.1)

In order to prove any analytical results concerning feedback and optimal control for this problem, we must first obtain bounds on the solutions that enable us to prove that they belong to the relevant functional space, so that we can obtain inequalities such as equation (2.26) or convergence results such as (2.50). We can prove, using the background flow method [50, 159, 218] that the solutions to System (5.1) are bounded:

Proposition 5. *Assume that* $u_{10},\ u_{20} \in \dot{H}^2_p(0, 2\pi)$. *Then there exists a constant* $C_0 = C_0(\nu, \alpha_1, \alpha_2)$ *such that the solutions of System* (5.1) *verify*

$$\|u_1\|_{L^2} + \|u_2\|_{L^2} \leq C_0. \tag{5.2}$$

Proof. We will reproduce the argument in [50] and use the background flow method to find the desired bounds, and therefore only the main steps, and the main differences with the original paper will be presented. We write $U(x,t) = [u_1(x,t)\ u_2(x,t)]^T$, consider a $2\pi-$periodic function $\Phi = [\phi_1(x)\ \phi_2(x)]^T$ and define $V(x,t) = [v_1(x,t)\ v_2(x,t)]^T$ such that $U = V + \Phi$. We can then write the system as

$$V_t = \mathcal{L}V + \mathcal{L}\Phi - F(V, \Phi), \tag{5.3}$$

where

$$\mathcal{L}U = \begin{bmatrix} -\nu u_{1,xxxx} - u_{1,xx} - \alpha_1 u_{2,xx} \\ -\nu u_{2,xxxx} - u_{2,xx} - \alpha_2 u_{1,xx} \end{bmatrix},$$

and

$$F(V, \Phi) = \begin{bmatrix} v_1 v_{1,x} + v_1\phi_{1,x} + \phi_1 v_{1,x} + \phi_1\phi_{1,x} \\ v_2 v_{2,x} + v_2\phi_{2,x} + \phi_2 v_{2,x} + \phi_2\phi_{2,x} \end{bmatrix}.$$

Multiplying the equation by V^T in the left and integrating in space, we obtain:

$$\frac{1}{2}\frac{d}{dt}\|V\|^2 = \frac{1}{2}\frac{d}{dt}\int_0^{2\pi} v_1^2 + v_2^2\, dx = \int_0^{2\pi} V^T\mathcal{L}V + V^T\mathcal{L}\Phi - V^T F(V, \Phi)\, dx.$$

We first simplify the nonlinearity:

$$\int_0^{2\pi} V^T F(V,\Phi)\,dx = \int_0^{2\pi} \left(v_1^2 v_{1,x} + v_2^2 v_{2,x}\right)\,dx + \int_0^{2\pi} \left(v_1^2\phi_{1,x} + v_1\phi_1 v_{1,x} + v_1\phi_1\phi_{1,x} + v_2^2\phi_{2,x} + v_2\phi_2 v_{2,x} + v_2\phi_2\phi_{2,x}\right)\,dx. \quad (5.4)$$

The terms given by $v_i^2 v_{i,x},\ i = 1, 2$ vanish due to periodicity. We can also simplify the terms given by $v_i\phi_i v_{i,x}$ to obtain

$$\int_0^{2\pi} V^T F(V,\Phi)\,dx = \frac{1}{2}\int_0^{2\pi} \left(v_1^2\phi_{1,x} + v_2^2\phi_{2,x}\right)\,dx + \int_0^{2\pi} \left(v_1\phi_1\phi_{1,x} + v_2\phi_2\phi_{2,x}\right)\,dx. \quad (5.5)$$

We now define, for $A,\ B$ and $\Phi \in \dot{H}_p^2(0,2\pi)$, $\gamma \in \mathbb{R}$,

$$(A,B)_{\gamma\Phi} = \int_0^{2\pi} (A'')^T B''\,dx - \int_0^{2\pi} (A')^T \begin{bmatrix} 1 & \alpha_1 \\ \alpha_2 & 1 \end{bmatrix} B'\,dx + \gamma\int_0^{2\pi} A^T \begin{bmatrix} \Phi_1' & 0 \\ 0 & \Phi_2' \end{bmatrix} B\,dx, \quad (5.6)$$

where the prime denotes derivative with respect to x, so that we can write, after integrating by parts,

$$\frac{1}{2}\frac{d}{dt}\int_0^{2\pi} \left(v_1^2 + v_2^2\right)\,dx = -(V,V)_{\Phi/2} - (V,\Phi)_{\Phi}.$$

First step: Antisymmetric case

We consider, for now, that the solutions for system (5.1) are antisymmetric and define the quadratic forms

$$\begin{aligned} R_{\gamma\Phi}(U) &= (U,U)_{\gamma\Phi}, \\ Q(U) &= \tfrac{\nu}{4}\textstyle\int_0^{2\pi}(U'')^T(U'')\,dx + \frac{(1+\sqrt{\alpha_1\alpha_2})^2}{4\nu}\int_0^{2\pi} U^T U\,dx. \end{aligned} \quad (5.7)$$

Following [50], we want to prove that

$$R_{\gamma\Phi}(V) \geq Q(V) \quad (5.8)$$

and

$$R_{\gamma\Phi}(\Phi) \leq C_1(\nu,\alpha_1,\alpha_2), \quad (5.9)$$

and therefore

$$\limsup_{t\to\infty} \|V(\cdot,t)\| \leq C_2(\nu,\alpha_1,\alpha_2) \tag{5.10}$$

where C_1 and C_2 are constants that depend on ν, α_1 and α_2.

Equation (5.10) follows from (5.8) and (5.9) by using Young's inequality with an appropriate choice of ϵ and the definitions of $R(V)$ and $Q(V)$, and choosing $\gamma \geq \frac{1}{4}$, much like the proof presented in [50].

We can write V and Φ in terms of the eigenfunctions of the linear operator of System (5.1) - see Appendix D. Since V is antisymmetric, we can write

$$V(x) = i\sum_{k\in\mathbb{Z}} v_k e^{ikx} \begin{bmatrix} \sqrt{\alpha_1} \\ \sqrt{\alpha_2} \end{bmatrix}$$

where $v_k = v_k(t)$. We have $v_0 = 0$ and $v_k = -v_{-k}$ so that the solution is real valued and has mean zero. Moreover,

$$\Phi(x) = i\sum_{k\in\mathbb{Z}} \Phi_k e^{ikx} \begin{bmatrix} \sqrt{\alpha_1} \\ \sqrt{\alpha_2} \end{bmatrix},$$

and writing $\varphi_k = k\Phi_k$ (notice that $\varphi_{-k} = \varphi_k$), we can write Φ':

$$\Phi'(x) = -\sum_{k\in\mathbb{Z}} \varphi_k e^{ikx} \begin{bmatrix} \sqrt{\alpha_1} \\ \sqrt{\alpha_2} \end{bmatrix}.$$

Proof of the bounds

We have, using similar arguments to those in [50],

$$\begin{aligned}
&\int_0^{2\pi} V^T \begin{bmatrix} \Phi_1' & 0 \\ 0 & \Phi_2' \end{bmatrix} V \, dx = \\
&\quad = \int_0^{2\pi} \sum_{j,k,l\in\mathbb{Z}} v_j v_k \varphi_l \begin{bmatrix} \sqrt{\alpha_1} & \sqrt{\alpha_2} \end{bmatrix} \begin{bmatrix} \sqrt{\alpha_1} & 0 \\ 0 & \sqrt{\alpha_2} \end{bmatrix} \begin{bmatrix} \sqrt{\alpha_1} \\ \sqrt{\alpha_2} \end{bmatrix} e^{i(j+k+l)x} \, dx = \\
&\quad = \underbrace{\left(\alpha_1^{3/2} + \alpha_2^{3/2}\right)}_{K_1} \sum_{j+k+l=0} v_j v_k \varphi_l = 2K_1 \sum_{j,k\in\mathbb{N}} v_j v_k \left(\varphi_{|j+k|} - \varphi_{|j-k|}\right).
\end{aligned} \tag{5.11}$$

Similarly,

$$\int_0^{2\pi} (V'')^T (V'')\, dx = \int_0^{2\pi} \sum_{j,k\in\mathbb{Z}} j^2k^2 v_j v_k e^{i(j+k)x}(\alpha_1+\alpha_2)\, dx = 2(\alpha_1+\alpha_2)\sum_{j>0}(j^2 v_j)^2, \tag{5.12}$$

and

$$\begin{aligned}\int_0^{2\pi} (V')^T \begin{bmatrix} 1 & \alpha_1 \\ \alpha_2 & 1 \end{bmatrix} (V')\, dx &= \int_0^{2\pi} \sum_{j,k\in\mathbb{Z}} jk v_j v_k e^{i(j+k)x} \left[\sqrt{\alpha_1}\ \sqrt{\alpha_2}\right] \begin{bmatrix} 1 & \alpha_1 \\ \alpha_2 & 1 \end{bmatrix} \begin{bmatrix} \sqrt{\alpha_1} \\ \sqrt{\alpha_2} \end{bmatrix} dx \\ &= \sum_{j+k=0} jk v_j v_k (\alpha_1+\alpha_2)\left(1+\sqrt{\alpha_1\alpha_2}\right) = 2(\alpha_1+\alpha_2)\left(1+\sqrt{\alpha_1\alpha_2}\right)\sum_{j>0} j^2 v_j^2, \end{aligned} \tag{5.13}$$

and therefore

$$\begin{aligned}(V,V)_{\gamma\Phi} &= 2\overbrace{(\alpha_1+\alpha_2)}^{K_2}\sum_{j\in\mathbb{N}}\left(\nu j^4 - j^2(1+\sqrt{\alpha_1\alpha_2})\right) v_j^2 + 2\gamma K_1 \sum_{j,k\in\mathbb{N}} v_j v_k \left(\varphi_{|j+k|} - \varphi_{|j-k|}\right) = \\ &= 2\left[\sum_{j\in\mathbb{N}}\left[K_2\left(\nu j^4 - j^2(1+\sqrt{\alpha_1\alpha_2})\right) + K_1\gamma\varphi_{2j}\right] v_j^2 + 2\gamma K_1 \sum_{j>k>0} v_j v_k \left(\varphi_{|j+k|} - \varphi_{|j-k|}\right)\right]. \end{aligned} \tag{5.14}$$

In order to obtain equation (5.8), we need to bound this quantity from below and we do that by choosing the appropriate function Φ. We consider $\gamma \geq \frac{1}{4}$ and define

$$\varphi_{2j} = \frac{4K_2}{\nu K_1}(1+\sqrt{\alpha_1\alpha_2})^2,$$

so that we obtain

$$\begin{aligned} K_2\left(\nu j^4 - j^2(1+\sqrt{\alpha_1\alpha_2})\right) + K_1\gamma\varphi_{2j} &= K_2\left[\left(\nu j^4 - j^2(1+\sqrt{\alpha_1\alpha_2})\right) + \frac{4\gamma}{\nu}(1+\sqrt{\alpha_1\alpha_2})^2\right] \\ &\geq \frac{K_2}{2}\left(\nu j^4 + \frac{(1+\sqrt{\alpha_1\alpha_2})^2}{\nu}\right) =: \tau_j^2. \end{aligned} \tag{5.15}$$

Now we set $w_j = v_j\tau_j$ so that we have

$$R_{\gamma\Phi} = (V,V)_{\gamma\Phi} \geq \sum_{j\in\mathbb{N}} w_j^2 + 2\gamma \sum_{j>k>0} w_k \frac{\varphi_{|j+k|} - \varphi_{|j-k|}}{\tau_j\tau_k} w_j = (w,(I+2\gamma\Gamma)w) \quad (5.16)$$

where I is the identity function. If we prove that

$$(w,(I+2\gamma\Gamma),w) = (w,w) + 2(w,\gamma\Gamma w) \geq \frac{1}{2}(w,w),$$

we obtain estimate (5.8). For this, we need to choose the remaining coefficients of Φ in order to verify that the norm of the operator $2\gamma\Gamma$ is less that $\frac{1}{2}$, which, considering that $\gamma \geq \frac{1}{4}$. means that

$$\|\Gamma\|_2^2 = \sum_{j>k>0} \left| \frac{\varphi_{|j+k|} - \varphi_{|j-k|}}{\tau_j\tau_k} \right|^2 < \frac{1}{16}. \quad (5.17)$$

Furthermore, if, when choosing the coefficients φ_k of Φ, we also minimise $(\Phi,\Phi)_{\gamma\Phi}$, we obtain estimate (5.9) and the proof (for the case of antisymmetric functions) is complete.

In order to keep the norm of Φ finite, we cannot have constant coefficients φ_k. In fact, the coefficients need to decrease sufficiently fast with k. Therefore, we choose, for a constant M that we will define later,

$$\varphi_j = \begin{cases} \frac{4K_2}{\nu K_1}(1+\sqrt{\alpha_1\alpha_2})^2, & 1 \leq |j| \leq 2M \\ \frac{4K_2}{\nu K_1}(1+\sqrt{\alpha_1\alpha_2})^2 f(\frac{|j|}{2M} - 1), & 2M \leq |j| \end{cases}, \quad (5.18)$$

where f is a non-increasing C^1 function satisfying $f(0) = 1$, $f'(0) = 0$, $f \geq 0$, $\sup|f'| < 1$ and

$$\int_0^\infty (1+x^2)|f(x)|^2\,dx < \infty. \quad (5.19)$$

Using this definition for φ_j, we can easily check that $|\varphi_{j-k} - \varphi_{j+k}| = 0$, if $j+k \leq 2M$, and, using the mean value theorem and $\sup|f'| < 1$,

$$|\varphi_{j-k} - \varphi_{j+k}| = \frac{4K_2}{\nu K_1}(1+\sqrt{\alpha_1\alpha_2})^2 \left| f\left(\frac{|j-k|}{2M} - 1\right) - f\left(\frac{|j+k|}{2M} - 1\right)\right| \leq \frac{4K_2}{\nu K_1}(1+\sqrt{\alpha_1\alpha_2})^2 \frac{k}{M}, \quad \forall j > k. \quad (5.20)$$

Now we can bound the norm of Γ:

$$\|\Gamma\|_2^2 \leq \frac{16K_2^2}{M^2\nu^2K_1^2}(1+\sqrt{\alpha_1\alpha_2})^2 \sum_{j>k>0} \frac{k^2}{\tau_j^2\tau_k^2}.$$

We have

$$\sum_{j>k>0} \frac{k^2}{\tau_j^2\tau_k^2} = \sum_{k=1}^{\infty}\sum_{j=k+1}^{\infty} k^2\tau_k^{-2}\tau_j^{-2} = \sum_{k=1}^{M} k^2\tau_k^{-2} \sum_{j=2M-k+1}^{\infty} \tau_j^{-2} + \sum_{k=M+1}^{\infty} k^2\tau_k^{-2} \sum_{j=k+1}^{\infty} \tau_j^{-2}. \tag{5.21}$$

Taking integrals as upper bounds for the sums, and using similar arguments as in [50, 217], we obtain, for $k \leq M$,

$$\sum_{j=2M-k+1}^{\infty} \tau_j^{-2} \leq \int_{2M-k}^{\infty} \tau_j^{-2}\, dj \leq \frac{2}{3\nu K_2}\frac{1}{M^3}, \tag{5.22}$$

and for $k > M$,

$$\sum_{j=k+1}^{\infty} \tau_j^{-2} \leq \int_{k}^{\infty} \tau_j^{-2}\, dj \leq \frac{2}{3\nu K_2}\frac{1}{k^3}, \tag{5.23}$$

so equation (5.21) becomes

$$\sum_{j>k>0} \frac{k^2}{\tau_j^2\tau_k^2} \leq \frac{2}{3}(\nu K_2)^{-1}M^{-3}\sum_{k=1}^{M} k^2\tau_k^{-2} + \frac{2}{3}(\nu K_2)^{-1}\sum_{k=M+1}^{\infty} k^{-1}\tau_k^{-2}. \tag{5.24}$$

Using the same argument again,

$$\sum_{k=1}^{M} k^2\tau_k^{-2} \leq \int_0^M k^2\tau_k^{-2}\, dk \leq \int_0^{\infty} k^2\tau_k^{-2}\, dk \leq \frac{2}{K_2}\int_0^{\infty} \left(\nu^2k^4 + (1+\sqrt{\alpha_1\alpha_2})^2\right)^{-1/2} dk. \tag{5.25}$$

For $a > 0$, this is

$$\begin{aligned}\frac{2}{K_2}\int_0^a \left(\nu^2k^4 + (1+\sqrt{\alpha_1\alpha_2})^2\right)^{-1/2} dk + \frac{2}{K_2}\int_a^{\infty} \left(\nu^2k^4 + (1+\sqrt{\alpha_1\alpha_2})^2\right)^{-1/2} dk \\ \leq \frac{2}{K_2}\int_0^a (1+\sqrt{\alpha_1\alpha_2})\, dk + \frac{2}{K_2}\int_a^{\infty} \frac{1}{\nu k^2}\, dk = \frac{2a(1+\sqrt{\alpha_1\alpha_2})}{K_2} + \frac{2}{a\nu K_2}.\end{aligned} \tag{5.26}$$

For the other integral, we obtain

$$\sum_{k=M+1}^{\infty} k^{-1}\tau_k^{-2} \leq \int_M^{\infty} k^{-1}\tau_k^{-2}\,dk = \frac{2}{K_2}\int_M^{\infty}\left(\nu k^5 + (1+\sqrt{\alpha_1\alpha_2})^2\,k\right)^{-1}\,dk \\ \leq \frac{2}{K_2}\int_M^{\infty}\frac{1}{\nu k^5}\,dk = \frac{1}{2K_2\nu}M^{-4}. \quad (5.27)$$

Adding equations (5.22)-(5.27) together, we arrive at

$$\|\Gamma\|_2^2 \leq \frac{32}{3\nu^3 K_1^2 M^5}(1+\sqrt{\alpha_1\alpha_2})^2\left[\left(a(1+\sqrt{\alpha_1\alpha_2})+\frac{1}{a\nu}\right)+\frac{1}{4\nu M}\right], \quad (5.28)$$

and choosing $a = \nu^{-1/2}(1+\sqrt{\alpha_1\alpha_2})^{-1/2}$ yields

$$\|\Gamma\|_2^2 \leq \frac{8(1+\sqrt{\alpha_1\alpha_2})^2}{3\nu^4 K_1^2 M^6}\left[8\nu^{1/2}(1+\sqrt{\alpha_1\alpha_2})^{1/2}M+1\right]. \quad (5.29)$$

Since the right-hand side of equation (5.29) is a positive and monotonically decreasing function of M, we can choose M such that $\|\Gamma\|_2^2 \leq \frac{1}{16}$, which proves (5.8).

To prove (5.9), we notice that

$$(\Phi,\Phi)_{\gamma\Phi} = (\Phi,\Phi)_0 = 2K_2\sum_{j\in\mathbb{N}}\left(\nu j^4 - j^2(1+\sqrt{\alpha_1\alpha_2})\right)\left(\frac{\varphi_j}{j}\right)^2 \leq 2\nu K_2\sum_{j\in\mathbb{N}} j^2\varphi_j^2. \quad (5.30)$$

Using our definition of φ, and taking integrals as upper bounds for the sums again, we obtain

$$(\Phi,\Phi)_{\gamma\Phi} \leq \frac{32K_2^3}{\nu K_1^2}(1+\sqrt{\alpha_1\alpha_2})^4\left[\frac{8}{3}M^3 + \int_{2M}^{\infty} f^2\left(\frac{|j|}{2M}-1\right)j^2\,dj\right]. \quad (5.31)$$

Now we change variables to $k = \frac{j}{2M} - 1$, so that we can use equation (5.19):

$$(\Phi,\Phi)_{\gamma\Phi} \leq \frac{256K_2^2}{\nu K_1}(1+\sqrt{\alpha_1\alpha_2})^4 M^3\left[\frac{1}{3} + \int_0^{\infty} f^2(k)\,(1+k)^2\,dk\right]. \quad (5.32)$$

Since $\int_0^{\infty} f^2(k)\,(1+k)^2\,dk < \infty$, we can certainly bound $(\Phi,\Phi)_0$ by a constant that only depends on ν, α_1 and α_2.

Second step: The general case

In the general case, the solution is no longer antisymmetric, and therefore the functions V and Φ are not antisymmetric either. To overcome this, we define the following set of

translation invariant functions

$$S = \{\psi \ : \ \exists a \text{ such that } \psi(x) = \Phi(x+a)\},$$

and define

$$F[U] = \text{dist}^2(U, S) = \inf_{\psi \in S} \|U - \psi\|_2^2 = \|U(x,t) - \Phi_a(x)\|_2^2, \tag{5.33}$$

where $\Phi_a(x) = \Phi(x+a(t))$, and $a(t)$ is chosen such that Φ_a realises the infimum in equation (5.33). This means that $dF/da|_{a=a(t)} = 0$, which is equivalent, because of the periodicity of Φ, to

$$\int_0^{2\pi} U^T \Phi_a' dx \Big|_{a=a(t)} = 0,$$

or even

$$\int_0^{2\pi} V^T \Phi_a' dx \Big|_{a=a(t)} = 0, \tag{5.34}$$

where we write $U(x,t) = V(x,t) + \Phi_{a(t)}(x)$. Equation (5.1) becomes

$$V_t + \Phi_a' \frac{da}{dt} = \mathcal{L}V + \mathcal{L}\Phi_a - F(V, \Phi_a) \tag{5.35}$$

Multiplying equation (5.35) by V on the left and integrating, we obtain

$$\begin{aligned} \frac{1}{2}\frac{d}{dt}\int_0^{2\pi} v_1^2 + v_2^2 \, dx + \frac{da}{dt}\int_0^{2\pi} v_1\phi_{a,1}' + v_2\phi_{a,2}' \, dx = \\ = \int_0^{2\pi} V^T\mathcal{L}V + V^T\mathcal{L}\Phi_a \, dx - \int_0^{2\pi} V^T F(V, \Phi_a) \, dx \end{aligned} \tag{5.36}$$

Noticing that $F[U] = \|V\|_2^2$, the above equation becomes

$$\begin{aligned} \frac{1}{2}\frac{d}{dt}F[U] = \frac{1}{2}\frac{d}{dt}\int_0^{2\pi} v_1^2 + v_2^2 \, dx = \int_0^{2\pi} V^T\mathcal{L}V + V^T\mathcal{L}\Phi_a - \frac{1}{2}\int_0^{2\pi} \left(v_1^2\phi_{1a,x} + v_2^2\phi_{2,x}\right) \, dx \\ - \int_0^{2\pi} \left(v_1\phi_1\phi_{1,x} + v_2\phi_2\phi_{2,x}\right) \, dx - a'(t)\int_0^{2\pi} v_1\phi_{a,1}' + v_2\phi_{a,2}' \, dx. \end{aligned} \tag{5.37}$$

The last term of this equation is zero, due to equation (5.34). So we can write equation (5.37) in terms of our functional defined in equation (5.6) as

$$\frac{1}{2}\frac{d}{dt}F[U] = -(V,V)_{\frac{1}{2}\Phi_a} - (V, \Phi_a)_{\Phi_a}.$$

We want to prove a result similar to the antisymmetric case. Let $W = [w_1\, w_2]^T \in (\dot{H}^2_p(0, 2\pi))^2$; we can decompose W in the following way:

$$W(x) = W(0) + \underbrace{\frac{1}{2}\left[W(x) + W(-x) - 2W(0)\right]}_{W_s(x)} + \underbrace{\frac{1}{2}\left[W(x) - W(-x)\right]}_{W_a(x)},$$

where W_s is an even $2\pi-$periodic function of x that verifies $W_s(0) = 0$ and W_a is an odd $2\pi-$periodic function of x. Let us consider

$$\mathcal{T}[f](x) = \begin{cases} f(x), & \text{if } x \in [0, \pi], \\ -f(x) & \text{if } x \in (\pi, 2\pi]. \end{cases}$$

For simplicity, we assume that all the functions are $\pi-$periodic instead of $2\pi-$periodic, and then $\mathcal{T}[W_s]$ is an odd $2\pi-$periodic function. We also have that $R_{\alpha\Phi_a}(W_s) = R_{\alpha\Phi_a}(\mathcal{T}[W_s])$ and $Q(W_s) = Q(\mathcal{T}[W_s])$ and therefore bounds (5.8) and (5.9) hold for both W_s and W_a. Since it can be easily shown that

$$R_{\alpha\Phi_a}(W) = R_{\alpha\Phi_a}(W_a) + R_{\alpha\Phi_a}(W_s) \tag{5.38}$$

and

$$Q(W) = Q(W_a) + Q(W_s) - \frac{\pi(1 + \sqrt{\alpha_1\alpha_2})}{2\nu} W^2(0), \tag{5.39}$$

we have

$$R_{\alpha\Phi_a}(W) \geq Q(W) + \frac{\pi(1 + \sqrt{\alpha_1\alpha_2})}{2\nu} W^2(0) \geq Q(W),$$

which means that the bounds we obtained for antisymmetric functions holds in the general case. □

Prop. 5 proves that the solutions to System (5.1) are bounded in $(\dot{L}^2_p(0, 2\pi))^2$. However, we need them to be bounded in $\dot{H}^1_p$ and $\dot{H}^2_p$ in order to extract the necessary L^∞ bounds. The proof of this fact will be given in Prop. 6 below.

Proposition 6. *Under the same assumptions as in Prop. 5, there exist constants C_1 and C_2, which are functions of ν, α_1 and α_2, such that*

$$\|u_{1,x}\|_{L^2} + \|u_{2,x}\|_{L^2} \leq C_1, \tag{5.40}$$

and

$$\|u_{1,xx}\|_{L^2} + \|u_{2,xx}\|_{L^2} \leq C_2. \tag{5.41}$$

Proof. If we multiply equation (5.1) by U^T_{xxxx} on the left and integrate by parts, we obtain

$$\begin{aligned}\frac{1}{2}\frac{d}{dt}\left(\|u_{1,xx}\|_2^2 + \|u_{2,xx}\|_2^2\right) + \nu\left(\|u_{1,xxxx}\|_2^2 + \|u_{2,xxxx}\|_2^2\right) = \\ = -\int_0^{2\pi} \left[(u_{1,xx} + \alpha_1 u_{2,xx} + u_1 u_{1,x})u_{1,xxxx} + (u_{2,xx} + \alpha_2 u_{1,xx} + u_2 u_{2,x})u_{2,xxxx}\right]\, dx.\end{aligned} \tag{5.42}$$

Using Young's, Hölder's, Triangle, and Nirenberg-Gagliardo interpolation inequalities, we can estimate the right-hand side integral as follows:

$$\begin{aligned}-\int_0^{2\pi} &\left[(u_{1,xx} + \alpha_1 u_{2,xx})u_{1,xxxx} + (u_{2,xx} + \alpha_2 u_{1,xx})u_{2,xxxx}\right] \\ &\leq \|u_{1,xx} + \alpha_1 u_{2,xx}\|_2 \|u_{1,xxxx}\|_2 + \|u_{2,xx} + \alpha_2 u_{1,xx}\|_2 \|u_{2,xxxx}\|_2 \\ &\leq \epsilon_1 \|u_{1,xxxx}\|_2^2 + \frac{\epsilon_1^{-1}}{4}\|u_{1,xx} + \alpha_1 u_{2,xx}\|_2^2 + \epsilon_1 \|u_{2,xxxx}\|_2^2 + \frac{\epsilon_1^{-1}}{4}\|u_{2,xx} + \alpha_2 u_{1,xx}\|_2^2 \\ &\leq \epsilon_1(\|u_{1,xxxx}\|_2^2 + \|u_{2,xxxx}\|_2^2) + \frac{\epsilon_1^{-1}}{4}\left((1+\alpha_2)\|u_{1,xx}\|_2^2 + (1+\alpha_1)\|u_{2,xx}\|_2^2\right),\end{aligned} \tag{5.43}$$

and, for $i = 1, 2$,

$$\begin{aligned}-\int_0^{2\pi} u_i u_{i,x} u_{i,xxxx}\, dx &\leq \|u_i\|_\infty \|u_{i,x}\|_2 \|u_{i,xxxx}\|_2 \leq \sqrt{2}\|u_i\|_2^{1/2}\|u_{i,x}\|_2^{3/2}\|u_{i,xxxx}\|_2 \\ &\leq \sqrt{2C_0}\|u_{i,x}\|_2^{3/2}\|u_{i,xxxx}\|_2 \leq \sqrt{2C_0}\left(C_2\|u_{i,xx}\|_2^{1/2}\|u_i\|_2^{1/2}\|\right)^{3/2}\|u_{i,xxxx}\| \\ &\leq \sqrt{2}C_0^{5/4}C_p^{3/2}\|u_{i,xx}\|_2^{3/4}\|u_{i,xxxx}\|_2 \leq \sqrt{2}C_0^{5/4}C_p^{3/2}\left(\epsilon_2\|u_{i,xxxx}\|_2^2 + \frac{\epsilon_2^{-1}}{4}\|u_{i,xx}\|_2^{3/2}\right) \\ &\leq \sqrt{2}C_0^{5/4}C_p^{3/2}\left(\epsilon_2\|u_{i,xxxx}\|_2^2 + \frac{\epsilon_2^{-1}}{4}\left(\frac{3}{4}\|u_{i,xx}\|_2^2 + \frac{1}{4}\right)\right).\end{aligned} \tag{5.44}$$

where C_0 is the constant obtained in Prop. 5 and C_p is the Poincaré constant (that comes from the Poincaré inequality). Defining $A_1 = \sqrt{2}C_0^{5/4}C_p^{3/2}$ and $A_2 = \frac{\sqrt{2}}{16}\epsilon_2^{-1}C_0^{5/4}C_p^{3/2}$ yields

$$-\int_0^{2\pi} u_i u_{i,x} u_{i,xxxx}\, dx \leq \epsilon_2 A_1 \|u_{i,xxxx}\|_2^2 + 3A_2\|u_{i,xx}\|_2^2 + A_2$$

and we obtain

$$\frac{1}{2}\frac{d}{dt}\left(\|u_{1,xx}\|_2^2+\|u_{2,xx}\|_2^2\right)+\nu\left(\|u_{1,xxxx}\|_2^2+\|u_{2,xxxx}\|_2^2\right)$$
$$\leq(\epsilon_1+\epsilon_2 A_1)\left(\|u_{1,xxxx}\|_2^2+\|u_{2,xxxx}\|_2^2\right)+$$
$$\left(\frac{\epsilon_1^{-1}}{4}(1+\max(\alpha_1,\alpha_2))+3A_2\right)\left(\|u_{1,xx}\|_2^2+\|u_{2,xx}\|_2^2\right)+A_2. \quad (5.45)$$

Choosing ϵ_1 and ϵ_2 such that $\epsilon_1+\epsilon_2 A_1\leq\nu$, and defining $A_3=\frac{\epsilon_1^{-1}}{4}(1+\max(\alpha_1,\alpha_2))+3A_2$, we obtain

$$\frac{1}{2}\frac{d}{dt}\left(\|u_{1,xx}\|_2^2+\|u_{2,xx}\|_2^2\right)\leq A_3\left(\|u_{1,xx}\|_2^2+\|u_{2,xx}\|_2^2\right)+A_2.$$

From here, we just need to apply Gronwall's inequality to conclude that $\|U_{xx}(\cdot,t)\|_2$ is bounded in a finite time interval. Using Poincaré's inequality, we conclude that $\|U_x(\cdot,t)\|_2$ is also bounded in that interval and therefore $U(\cdot,t)\in\dot{H}_p^2(0,2\pi)\times\dot{H}_p^2(0,2\pi)$. Theorem 2.3 in [218] guarantees that this interval is infinite. □

Using these bounds, we can easily conclude, by using the Sobolev embedding theorem, that

$$\|U\|_\infty\leq C\|U\|_{H^2},\quad \|U_x\|_\infty\leq C\|U_x\|_{H^1}, \quad (5.46)$$

where C is a constant (different in each case), which are the bounds we need for our analytical results.

Remark 13. *In the general case presented in [169], the coupling is linear but it is also allowed to act through the fourth derivatives. This presents an extra difficulty by adding terms that depend on j^4 multiplying by $(\alpha_1+\alpha_2)$ in equation* (5.12)*. We believe, however, that a similar result can be proved for the case when the coupling comes only through the fourth order derivatives (i.e. there is a non-diagonal negative definite fourth order viscosity matrix), and having these bounds, it should be possible to obtain bounds for the fully coupled system, with non-diagonal second as well fourth order viscosity matrices.*

Our goal here is only to prove the applicability of the methods we derived in Chapter 2 for systems of coupled Kuramoto-Sivashinsky equations, and therefore we only studied the simplest case, and leave the more general case for future work.

5.2.2 Feedback control for the coupled KS equations

Since Equations (5.1) are coupled linearly and we obtained the necessary bounds on its solutions, we can now derive analogous results to the ones presented in Chapter 2 for the scalar Kuramoto-Sivashinsky equation. First, we can prove that it is possible to stabilise any steady state solution (either the zero solution or any nontrivial steady state) for this system. We proceed in the same way as for the scalar KS equation and write the controlled system

$$\begin{cases} u_{1,t} &= -\nu u_{1,xxxx} - u_{1,xx} - u_1 u_{1,x} - \alpha_1 u_{2,xx} + \sum_{j_1=1}^{m} b_{j_1}(x) f_{j_1}(t), \\ u_{2,t} &= -\nu u_{2,xxxx} - u_{2,xx} - u_2 u_{2,x} - \alpha_2 u_{1,xx} + \sum_{j_2=1}^{m} b j_2(x) f_{j_2}(t), \end{cases} \tag{5.47}$$

where $b_{j_k}(x) = \delta(x - x_{j_k})$. Defining

$$U(x,t) = \begin{bmatrix} u_1(x,t) \\ u_2(x,t) \end{bmatrix} = \sum_{n=1}^{\infty} \begin{bmatrix} u_{1n}^s(t) \\ u_{2n}^s(t) \end{bmatrix} \frac{\sin(nx)}{\sqrt{\pi}} + \sum_{n=0}^{\infty} \begin{bmatrix} u_{1n}^c(t) \\ u_{2n}^c(t) \end{bmatrix} \frac{\cos(nx)}{\sqrt{\pi}}, \tag{5.48}$$

and taking the inner product with the functions $\frac{1}{\sqrt{2\pi}}$, $\frac{\sin(nx)}{\sqrt{\pi}}$ and $\frac{\cos(nx)}{\sqrt{\pi}}$ yields the following infinite system of ODEs

$$\begin{cases} \dot{u}_{in}^s &= \left(-\nu n^4 + n^2\right) u_{in}^s + \alpha_i n^2 u_{jn}^s + g_{in}^s + \sum_{j_i=1}^{m} b_{j_i n}^s f_{j_i}(t) \quad n = 1, \ldots, \infty, \\ \dot{u}_{in}^c &= \left(-\nu n^4 + n^2\right) u_{in}^c + \alpha_i n^2 u_{jn}^c + g_n^c + \sum_{j_i=1}^{m} b_{j_i n}^c f_{j_i}(t) \quad n = 0, \ldots, \infty, \end{cases} \tag{5.49}$$

where $i, j = 1, 2$, $i \neq j$, and the functions b and g are defined in Chapter 2. We truncate the system at N modes and define

$$z^U = \left[u_{10}^c \; u_{11}^s \; u_{11}^c \; \cdots \; u_{1N}^s \; u_{1N}^c \; u_{20}^c \; u_{21}^s \; u_{21}^c \; \cdots \; u_{2N}^s \; u_{2N}^c\right]^T,$$

$$G = \left[0 \; g_{11}^s \; g_{11}^c \; \cdots \; g_{1N}^s \; g_{1N}^c \; 0 \; g_{21}^s \; g_{21}^c \; \cdots \; g_{2N}^s \; g_{2N}^c\right]^T,$$

$$F = \left[f_{11}(t) \; f_{12}(t) \; \cdots \; f_{1m}(t) \; f_{21}(t) \; f_{22}(t) \; \cdots \; f_{2m}(t)\right]^T.$$

Next we write

$$A = \begin{bmatrix} A_0 & A_1 \\ A_2 & A_0 \end{bmatrix}, \qquad B = \begin{bmatrix} B_1 \\ B_2 \end{bmatrix},$$

where

$$A_0 = \operatorname{diag}(0, -\nu + 1, -\nu + 1, \cdots, -\nu n^4 + n^2, -\nu n^4 + n^2, \cdots),$$

$$A_i = \mathrm{diag}(0, \alpha_i, \alpha_i, \cdots, \alpha_i n^2, \alpha_i n^2, \cdots)$$

and

$$B_i = \begin{bmatrix} b^c_{1_i 0} & b^c_{2_i 0} & \cdots & b^c_{m_i 0} \\ b^s_{1_i 1} & b^s_{2_i 1} & \cdots & b^s_{m_i 1} \\ b^c_{1_i 1} & b^c_{2_i 1} & \cdots & b^c_{m_i 1} \\ \vdots & \vdots & \cdots & \vdots \end{bmatrix},$$

for $i = 1, 2$. Hence the infinite system of ODEs can be written as

$$\dot{z}^U = Az^U + G + BF. \tag{5.50}$$

We can prove a result similar to Proposition 1.

Proposition 7. *Let* $\bar{U} = \begin{bmatrix} \bar{u}_1 \\ \bar{u}_2 \end{bmatrix}$ *be an unstable steady state solution of* (5.1)*, and let* $l = l_1 + l_2$ *be the number of unstable eigenvalues of the linearised system, i.e.* $l_1^2 < \frac{1+\sqrt{\alpha_1\alpha_2}}{\nu} < (l_1+1)^2$ *and* $l_2^2 < \frac{1-\sqrt{\alpha_1\alpha_2}}{\nu} < (l_2+1)^2$*. If* $m = 2(l+1)$ *and there exists a matrix* K *such that all of the eigenvalues of the matrix* $A + BK$ *have negative real part, then the state feedback controls*

$$[f_{11}(t)\ f_{12}(t)\ \cdots\ f_{1m}(t)\ f_{21}(t)\ f_{22}(t)\ \cdots\ f_{2m}(t)]^T = F = K(z^U - z^{\bar{U}}), \tag{5.51}$$

stabilise this nontrivial steady state solution of system (5.1)*.*

The proof of this result follows the same steps as the proof of Proposition 1, by replacing the matrices that discretise all of the terms and reordering the modes so that the unstable eigenmodes appear first. The estimates throughout the proof are obtained by left-multiplying the resulting equation for a perturbation V on the left by V and integrating, and thus we prove that $\mathcal{E}(V) = \|V\|_2^2 = \|v_1\|_2^2 + \|v_2\|_2^2$ is a Lyapunov function for the obtained system.

We present in Figs. 5.2 and 5.3 the numerical results of the stabilisation of the zero solution and a steady state solution, respectively, for system (5.1) with $\nu = 0.5$, $\alpha_1 = 0.8$ and $\alpha_2 = 0.5$. In both figures, we used random initial conditions, and $m = 4$ equidistant controls to control each solution, corresponding physically to applying 4 controls in each wall. Upper panels correspond to the uncontrolled solution, and lower panels correspond to the stabilised solution. We clearly observe in both figures the fast stabilisation of the desired

steady state.

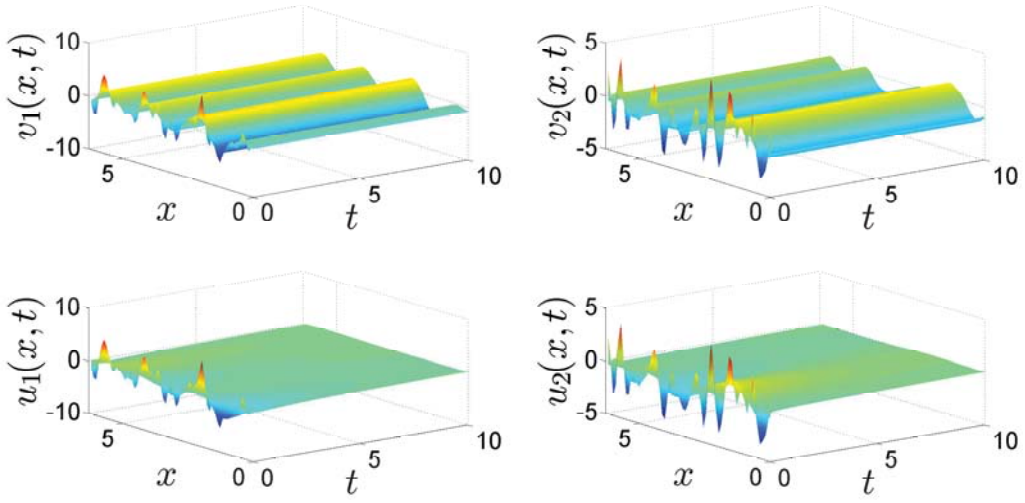

Figure 5.2: Uncontrolled solution (v_i, $i = 1, 2$) and controlled zero solution (u_i, $i = 1, 2$) of the system of coupled KS equations for $\nu = 0.5$, $\alpha_1 = 0.8$ and $\alpha_2 = 0.5$.

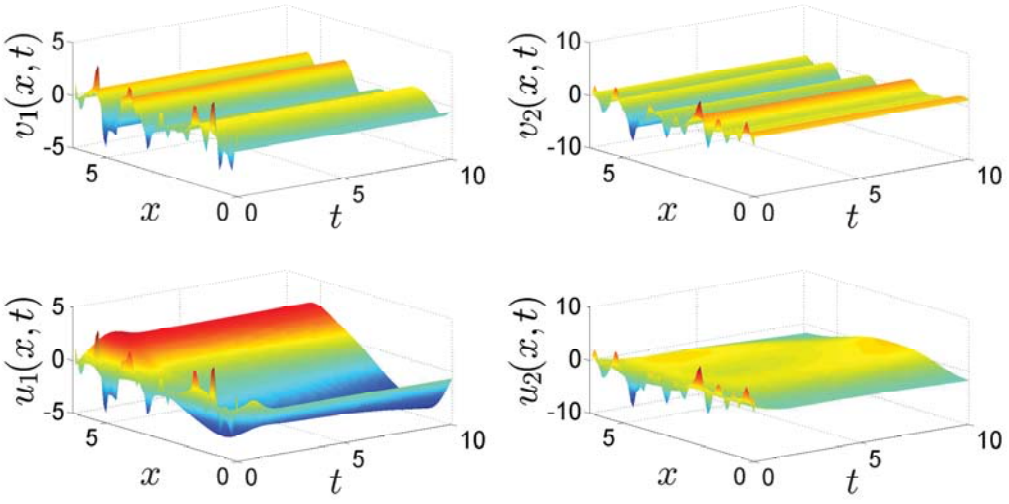

Figure 5.3: Uncontrolled solution (v_i, $i = 1, 2$) and stabilised steady state solution (u_i, $i = 1, 2$) of the system of coupled KS equations for $\nu = 0.5$, $\alpha_1 = 0.8$ and $\alpha_2 = 0.5$.

5.2.3 Optimal control for the system of coupled KS equations

Similarly to the scalar KS equation, we can consider the problem of controlling an arbitrary steady state $\bar{U} = [\bar{u}_1\ \bar{u}_2]^T$ in an optimal way. Here we will generalise the proof of existence

of an optimal control for this system of coupled Kuramoto-Sivashinsky equations.

We introduce the cost functional

$$\begin{aligned}\mathcal{C}(U,F) = \; & \frac{1}{2}\int_0^T \left(\|u_1(\cdot,t)-\bar{u}_1\|_{L^2}^2 + \|u_2(\cdot,t)-\bar{u}_2\|_{L^2}^2\right)\, dt \\ & + \frac{1}{2}\left(\|u_1(\cdot,T)-\bar{u}_1\|_{L^2}^2 + \|u_2(\cdot,T)-\bar{u}_2\|_{L^2}^2\right) \\ & + \frac{\gamma}{2}\int_0^T \left(\|f_1(x,t)\|_{L^2}^2 + \|f_2(x,t)\|_{L^2}^2\right)\, dt.\end{aligned} \tag{5.52}$$

The optimisation problem that we have to solve takes the form

$$\text{minimise} \quad \mathcal{C}(U,F) \tag{5.53a}$$

$$\text{subject to} \quad u_{1,t} + \nu u_{1,xxxx} + u_{1,xx} + u_1 u_{1,x} + \alpha_1 u_{2,xx} = f_1(x,t), \tag{5.53b}$$

$$u_{2,t} + \nu u_{2,xxxx} + u_{2,xx} + u_2 u_{2,x} + \alpha_2 u_{1,xx} = f_2(x,t), \tag{5.53c}$$

$$u_i(x,0) = u_{0,i}(x), \quad i=1,2, \tag{5.53d}$$

$$\frac{\partial^j u_i}{\partial x^j}(x+2\pi) = \frac{\partial^j u_i}{\partial x^j}(x), \quad j=0,1,2,3, \;\; i=1,2, \tag{5.53e}$$

$$f_i \in F_{ad}, \;\; i=1,2. \tag{5.53f}$$

Here, $u_{0,i} \in \dot{H}_p^2(0,2\pi)$ and F_{ad} is a bounded, closed and convex subset of $L^2((0,2\pi)\times(0,T))$.

We can prove the following theorem.

Theorem 2. *If $F_{ad} \subset L^2((0,T);\dot{L}^2(0,2\pi))$, the optimal control problem* (5.53a)-(5.53f) *has at least one optimal control $F^* = [f_1^*\; f_2^*]^T$ with associated optimal state $U^* = [u_1^*\; u_2^*]^T$.*

Sketch of the proof.

The proof follows the same steps as that of Theorem 1 for the scalar KS equation. For the coupled system, we need to consider the state space $X = \left(H^1(0,T;\dot{H}_p^2(0,2\pi))\right)^2 \times (F_{ad})^2$, and redefine $e(\cdot,\cdot;\cdot,\cdot)$:

$$e(u_1,u_2;f_1,f_2) = \begin{bmatrix} u_{1,t} + \nu u_{1,xxxx} + u_{1,xx} + u_1 u_{1,x} + \alpha_1 u_{2,xx} - f_1(x,t) \\ u_{2,t} + \nu u_{2,xxxx} + u_{2,xx} + u_2 u_{2,x} + \alpha_2 u_{1,xx} - f_2(x,t) \\ u_1(\cdot,0) - u_{0,1}(x) \\ u_2(\cdot,0) - u_{0,2}(x) \end{bmatrix}. \tag{5.54}$$

The rest of the proof follows Theorem 1, but accounting for the fact that for every $t \in [0,T]$

we have $U^*(\cdot,t) \in \left(\dot{H}^2_p(0,2\pi)\right)^2$, and then $U^*(\cdot,t) \in (C([0,2\pi]))^2$ and therefore if $\varphi_i \in X$, $(u_i^*\varphi_i)(\cdot,t) \in L^2([0,2\pi])$ for $i = 1,2$.

Finally, we also need the estimates in Proposition 5 to establish that $\|u^n_{i,x}\|_{L^2}$ is bounded, and since H^2 is compactly embedded in L^2, we deduce that

$$\int_0^T \int_0^{2\pi} (u_i^n - u_i^*)u^n_{i,x}\varphi_i \, dx \, dt \leq \|u_i^n - u_i^*\|_{L^2}\|u^n_{i,x}\|_{L^2}\|\varphi_i\|_{L^\infty} \xrightarrow[n\to\infty]{} 0 \; \forall \varphi_i \in \dot{H}^2_p(\Omega). \tag{5.55}$$

Remark 14. *For the general case, when coupling is allowed to act through the fourth derivatives also, since these are still linear, all the feedback and optimal control results presented in this section are valid, as long as the solutions of the corresponding system and their derivatives are bounded in* $(\dot{H}^2_p(0,2\pi))^2$. *Even though we were not able to obtain these bounds, we performed numerical experiments that suggest that we can achieve stabilisation in this case.*

We do not present numerical results for the problem of optimising the position of the control actuators, but we expect to obtain similarly satisfactory results in this case also.

5.3 Systems of conservation laws in the vanishing viscosity limit

In this section, we will consider a different particular case of multiphase flows driven along an inclined channel, which is given by systems of the form

$$U_t + f(U)_x + \mathcal{A}U_x + IU_{xxxx} = 0, \tag{5.56}$$

for $x \in (0,L)$, $t > 0$ and spatially periodic boundary conditions. We have that $U = [u_1 \; u_2]^T$, $\mathcal{A}$ is a matrix of coefficients, I is the identity matrix and $f(U) = \frac{1}{2}[u_1^2 \; u_2^2]^T$. We note we can write it as $U_t + (f(U) + AU + IU_{xxx})_x$.

This is a particular case of the mixed hyperbolic-elliptic systems studied in detail in [168]. It is the particular case presented in Section 4 of this reference, in which the authors performed extensive numerical studies which suggest that, despite the existence of hyperbolic-elliptic transitions, the solutions of System (5.56) exhibit vanishing viscosity limits. This means that the solutions remain bounded despite the existence of elliptic regions, which is due to the existence of linear terms in the flux function, that we include here with the nonzero matrix $\mathcal{A}$. This motivated us to study the boundedness of the solutions to

System (5.56) analytically.

The background flow method used for the particular case studied in the previous section is not straightforward to use here, since the existence of first order derivatives introduces complex eigenvalues, associated with complicated eigenfunctions. The fact that there is no second derivative term also complicates the analysis. Therefore, we are going to adapt the techniques presented in [84] to this case.

In [84], the authors obtain bounds for the scalar Kuramoto-Sivashinsky equation using the entropy method. They first prove that one can write the KS equation as an entropy solution of a perturbed Burgers equation, and then use properties of these solutions (namely, the existence of a viscosity solution for the Burgers equation, associated with the entropy solution) to prove the desired bounds. Most of the results on [84] extend naturally to systems of coupled KS equations, and we will present these below. However, the concept of viscosity solutions does not extend to higher dimensions, which is the reason we cannot conclude that the solutions to System (5.56) are bounded. We will finish this section with ideas of how to overcome this difficulty.

5.3.1 *A priori* energy bounds

Following [84] we start by obtaining energy bounds for System (5.56). We can obtain bounds for $\int_0^L u_1^4 + u_2^4 \, dx$, which is the norm of U in L^4. We notice that we can use these bounds of U for each of its components separately, by using the fact that $\int_0^L u_i^4 \, dx \leq \int_0^L u_1^4 + u_2^4 \, dx$.

If we multiply equation (5.56) in the left by U^T and integrate by parts (using the periodicity of U), we obtain

$$\frac{d}{dt}\int_0^L \frac{u_1^2 + u_2^2}{2} \, dx + \int_0^L \left(u_{1,xx}^2 + u_{2,xx}^2\right) \, dx = -\int_0^L \left(A_{12}u_1u_{2,x} + A_{21}u_2u_{1,x}\right) \, dx. \quad (5.57)$$

Using Young's inequality and Poincaré's inequality, we can write for $i, j = 1, 2$, $i \neq j$,

$$-\int_0^L u_i u_{j,x} \leq \frac{1}{2\epsilon}\int_0^L u_i^2 \, dx + \frac{\epsilon}{2}\int_0^L u_{j,x}^2 \, dx \leq \frac{1}{2\epsilon_{ij}}\int_0^L u_i^2 \, dx + C_L\frac{\epsilon_{ij}}{2}\int_0^L u_{j,xx}^2 \, dx,$$

where C_L is the constant from the Poincaré's inequality and depends on L. Choosing ϵ_{ij}

appropriately (and noticing it is different in the two cases), we obtain

$$\frac{d}{dt}\int_0^L \frac{u_1^2+u_2^2}{2}\,dx \le \frac{C_L}{2}\max(A_{12}^2,A_{21}^2)\int_0^L \frac{u_1^2+u_2^2}{2}\,dx, \tag{5.58}$$

which proves that for $T>0$ and $s\ge 0$ we have

$$\sup_{t\in(s,s+T)}\int_0^L \left(u_1^2+u_2^2\right)\,dx \le C\exp\left(\frac{T}{2}C_L^2\max(A_{12}^2,A_{21}^2)\right)\int_0^L \left(u_1^2(s)+u_2^2(s)\right)\,dx, \tag{5.59}$$

where C is a constant. On the other hand, if we apply Hölder's inequality to (5.57), followed by Poincaré's inequality and Young's inequality with ϵ, we obtain

$$\frac{d}{dt}\int_0^L u_1^2+u_2^2\,dx+\int_0^L \left(u_{1,xx}^2+u_{2,xx}^2\right)\,dx \le \max(A_{12}^2,A_{21}^2)C_L^2\int_0^L \left(u_1^2+u_2^2\right)\,dx. \tag{5.60}$$

Integrating in time, we obtain

$$\begin{aligned}\int_0^L \left(u_1^2(T)+u_2^2(T)\right)\,dx+\int_0^T\int_0^L \left(u_{1,xx}^2+u_{2,xx}^2\right)\,dx \le \\ \le \int_0^L \left(u_1^2(0)+u_2^2(0)\right)\,dx+\frac{\max(A_{12}^2,A_{21}^2)C_L^2}{2}\int_0^T\int_0^L \left(u_1^2+u_2^2\right)\,dx\end{aligned}$$

which, using equation (5.59), proves that for $T>0$ and $s\ge 0$ we have

$$\int_s^{s+T}\int_0^L \left(u_{1,xx}^2+u_{2,xx}^2\right)\,dx \le C\exp\left(\frac{T}{2}C_L^2\max(A_{12}^2,A_{21}^2)\right)\int_0^L \left(u_1^2(s)+u_2^2(s)\right)\,dx. \tag{5.61}$$

Finally, this also implies that

$$\int_s^{s+T}\int_0^L \left(u_{1,x}^2+u_{2,x}^2\right)\,dx \le C\exp\left(\frac{T}{2}C_L^2\max(A_{12}^2,A_{21}^2)\right)\int_0^L \left(u_1^2(s)+u_2^2(s)\right)\,dx. \tag{5.62}$$

Furthermore, we also need estimates in $|u_{i,x}|^3$. We obtain these by observing that

$$\sup_{x\in(0,L)}|u_{i,x}| \le C\left(\int_0^L u_{i,x}^2\,dx\right)^{\frac{1}{4}}\left(\int_0^L u_{i,xx}^2\,dx\right)^{\frac{1}{4}}$$

and therefore

$$\int_0^L |u_{i,x}|^3\,dx \le C\left(\int_0^L u_{i,x}^2\,dx\right)^{1+\frac{1}{4}}\left(\int_0^L u_{i,xx}^2\,dx\right)^{\frac{1}{4}}$$
$$\le C\left(\int_0^L u_i^2\,dx\right)^{\frac{1}{2}}\left(\int_0^L u_{i,x}^2\,dx\right)^{\frac{1}{4}}\left(\int_0^L u_{i,xx}^2\,dx\right)^{\frac{3}{4}}, \quad (5.63)$$

where we have used periodicity of u and Hölder's inequality in

$$\int_0^L u_x^2\,dx = -\int_0^L uu_{xx}\,dx.$$

This yields

$$\int_0^T\int_0^L |u_{1,x}|^3 + |u_{2,x}|^3\,dx\,dt \le C\left(\sup_{t\in(0,T)}\int_0^L u_1^2+u_2^2\,dx\right)^{\frac{1}{2}}\times$$
$$\times\left(\int_0^T\int_0^L u_{1,x}^2+u_{2,x}^2\,dx\right)^{\frac{1}{4}}\left(\int_0^T\int_0^L u_{1,xx}^2+u_{2,xx}^2\,dx\right)^{\frac{3}{4}}, \quad (5.64)$$

and we can apply the previous estimates. We summarise our *a priori* estimates in Prop. 8 below.

Proposition 8. *If $U=[u_1\ u_2]^T$ is a solution of System* (5.56)*, then for $T>0$ and $s\ge 0$ we have*

$$\sup_{t\in(s,s+T)}\int_0^L \left(u_1^2+u_2^2\right)\,dx \le C\exp\left(\frac{T}{2}C_L^2\max(A_{12}^2,A_{21}^2)\right)\int_0^L \left(u_1^2(s)+u_2^2(s)\right)\,dx,$$

$$\int_s^{s+T}\int_0^L \left(u_{1,xx}^2+u_{2,xx}^2\right)\,dx\,dt \le C\exp\left(\frac{T}{2}C_L^2\max(A_{12}^2,A_{21}^2)\right)\int_0^L \left(u_1^2(s)+u_2^2(s)\right)\,dx,$$

$$\int_s^{s+T}\int_0^L \left(u_{1,x}^2+u_{2,x}^2\right)\,dx\,dt \le C\exp\left(\frac{T}{2}C_L^2\max(A_{12}^2,A_{21}^2)\right)\int_0^L \left(u_1^2(s)+u_2^2(s)\right)\,dx.$$

and

$$\left(\int_s^{s+T}\int_0^L \left(|u_{1,x}|^3+|u_{2,x}|^3\right)\,dx\,dt\right)^{\frac{2}{3}} \le C\exp\left(\frac{T}{2}C_L^2\max(A_{12}^2,A_{21}^2)\right)\int_0^L \left(u_1^2(s)+u_2^2(s)\right)\,dx.$$

where C is a constant that is different in each case.

5.3.2 Uniform integrability of solutions

We will now prove uniform integrability of solutions to system (5.56), that is, that the L^4 integral of U is bounded by its L^2 integral. In order to do that, we define

$$V = \begin{bmatrix} \frac{1}{2}u_1^2 \\ \frac{1}{2}u_2^2 \\ \frac{1}{3}u_1^3 + \frac{A_{11}}{2}u_1^2 + u_1u_{1,xxx} - u_{1,x}u_{1,xx} + A_{12}u_1u_2 \\ \frac{1}{3}u_2^3 + \frac{A_{22}}{2}u_2^2 + u_2u_{2,xxx} - u_{2,x}u_{2,xx} + A_{21}u_2u_1 \end{bmatrix}$$

and $H = [h_1\, h_2]^T$ such that

$$\begin{cases} h_{1,t} &= -\left(\frac{1}{2}u_1^2 + A_{11}u_1 + u_{1,xxx} + A_{12}u_2\right) + g(t), \\ h_{2,t} &= -\left(\frac{1}{2}u_2^2 + A_{22}u_2 + u_{2,xxx} + A_{21}u_1\right) + g(t), \\ h_{1,x} &= u_1, \\ h_{2,x} &= u_2, \end{cases} \tag{5.65}$$

where $g(t) = \frac{1}{2}\int_0^L \left(u_1^2(x,t) + u_2^2(x,t)\right)\, dx$. We have that

$$(\partial_t, \partial_t, \partial_x, \partial_x) \cdot V = -\left(u_{1,xx}^2 + u_{2,xx}^2\right) + A_{12}u_{1,x}u_2 + A_{21}u_{2,x}u_1, \tag{5.66}$$

where $\cdot$ denotes inner product, and

$$\begin{aligned} V\cdot(h_{1,t}, h_{2,t}, h_{1,x}, h_{2,x}) = \frac{1}{12}\left(u_1^4 + u_2^4\right) + \frac{1}{2}\left(u_1^2u_{1,xxx} + u_2^2u_{2,xxx}\right) + \frac{1}{2}\left(A_{12}u_1^2u_2 + A_{21}u_2^2u_1\right) \\ + \frac{g}{2}\left(u_1^2 + u_2^2\right) - u_1u_{1,x}u_{1,xx} - u_2u_{2,x}u_{2,xx}. \end{aligned} \tag{5.67}$$

Now, let $\zeta \in C_c^\infty((0,\infty))$, where $C_c^\infty((0,\infty))$ is the space of infinitely differentiable functions with respect to time with compact support. We have, integrating by parts and using Equation (5.66),

$$\begin{aligned} \int_0^\infty \int_0^L V \cdot (h_{1,t}, h_{2,t}, h_{1,x}, h_{2,x})\, dx\, \zeta\, dt = -\int_0^\infty \int_0^L \left(-u_{1,xx}^2 + A_{12}u_2u_{1,x}\right) h_1\, dx\, \zeta\, dt \\ -\int_0^\infty \int_0^L \left(-u_{2,xx}^2 + A_{21}u_1u_{2,x}\right) h_2\, dx\, \zeta\, dt - \int_0^\infty \int_0^L \frac{1}{2}\left(u_1^2h_1 + u_2^2h_2\right)\, dx\, \zeta_t\, dt. \end{aligned} \tag{5.68}$$

On the other hand, using (5.67) directly gives

$$\int_0^\infty \int_0^L V \cdot (h_{1,t}, h_{2,t}, h_{1,x}, h_{2,x})\ dx\, \zeta\, dt = \frac{1}{12}\int_0^\infty \int_0^L \left(u_1^4 + u_2^4\right)\ dx\, \zeta\, dt + \frac{1}{4}\int_0^\infty \left(\int_0^L u_1^2 + u_2^2\, dx\right)^2 \zeta\, dt + \frac{1}{2}\int_0^\infty \int_0^L \left(u_1^2 u_{1,xxx} + u_2^2 u_{2,xxx}\right)\ dx\zeta\, dt + \frac{1}{2}\int_0^\infty \int_0^L u_1 u_2 \left(A_{12}u_1 + A_{21}u_2\right)\ dx\, \zeta\, dt - \int_0^\infty \int_0^L \left(u_1 u_{1,x} u_{1,xx} + u_2 u_{2,x} u_{2,xx}\right)\ dx\, \zeta\, dt, \tag{5.69}$$

where we used the definition of $g(t)$. Now we notice that, integrating by parts and using the periodicity of u, we have

$$\int_0^L \left(\frac{1}{2}u_i^2 u_{i,xxx} - u_i u_{i,x} u_{i,xx}\right)\ dx = -2\int_0^L u_i u_{i,x} u_{i,xx}\, dx = \int_0^L u_{i,x}^3\, dx, \quad i = 1, 2.$$

Substituting this in (5.69) and putting (5.68) and (5.69) together, we obtain

$$\begin{aligned} &\frac{1}{12}\int_0^\infty \int_0^L \left(u_1^4 + u_2^4\right)\ dx\, \zeta\, dt + \frac{1}{4}\int_0^\infty \left(\int_0^L u_1^2 + u_2^2\, dx\right)^2 \zeta\, dt + \int_0^\infty \int_0^L \left(u_{1,x}^3 + u_{2,x}^3\right)\ dx\, \zeta\, dt \\ &= -\frac{1}{2}\int_0^\infty \int_0^L u_1 u_2 \left(A_{12}u_1 + A_{21}u_2\right)\ dx\, \zeta\, dt + \int_0^\infty \int_0^L \left(u_{1,xx}^2 - A_{12}u_2 u_{1,x}\right) h_1\, dx\, \zeta\, dt \\ &+ \int_0^\infty \int_0^L \left(u_{2,xx}^2 - A_{21}u_1 u_{2,x}\right) h_2\, dx\, \zeta\, dt - \int_0^\infty \int_0^L \frac{1}{2}\left(u_1^2 h_1 + u_2^2 h_2\right)\ dx\, \zeta_t\, dt. \end{aligned} \tag{5.70}$$

We will use this identity to prove uniform integrability of U. We first normalise H so that $\int_0^T \int_0^L h_i\, dx\, dt = 0$, $i = 1, 2$. Since u_i, $i = 1, 2$, has zero mean, we have

$$\frac{d}{dt}\int_0^L h_1 + h_2\, dx = -\int_0^L \frac{1}{2}\left(u_1^2 + u_2^2\right)\ dx + g(t) = 0,$$

which means that

$$\int_0^L (h_1 + h_2)\ dx = 0, \qquad 0 \le t \le T.$$

This leads to

$$\sup_{x\in(0,L)} |h_i| \le \int_0^L |h_{i,x}|\, dx = \int_0^L |u_i|\, dx \le \left(L\int_0^L u_i^2\, dx\right)^{\frac{1}{2}},$$

where we used Hölder's inequality in the last step, and therefore

$$\sup_{x\in(0,L),\,t\in(0,T)} |h_i| \le \left(L \sup_{t\in(0,T)} \int_0^L u_i^2(t)\,dx \right)^{\frac{1}{2}}, \quad i=1,2. \tag{5.71}$$

Choosing $\zeta(t) = \chi_{(0,T)}(t)$, which is 1 in $t \in (0,T)$ and 0 elsewhere, we obtain

$$\begin{aligned}
\frac{1}{12}\int_0^T\int_0^L \left(u_1^4+u_2^4\right)\,dx\,dt &+ \frac{1}{4}\int_0^T \left(\int_0^L u_1^2+u_2^2\,dx\right)^2\,dt + \int_0^T\int_0^L \left(u_{1,x}^3+u_{2,x}^3\right)\,dx\,dt \\
&= \frac{1}{2}\int_0^T\int_0^L u_1u_2\left(A_{12}u_1+A_{21}u_2\right)\,dx\,dt + \int_0^T\int_0^L \left(u_{1,xx}^2 - A_{12}u_2u_{1,x}\right)h_1\,dx\,dt \\
&\qquad + \int_0^T\int_0^L \left(u_{2,xx}^2 - A_{21}u_1u_{2,x}\right)h_2\,dx\,dt \\
&- \frac{1}{2}\left(\int_0^L \left(u_1^2(T)h_1(T)+u_2^2(T)h_2(T)\right)\,dx - \int_0^L \left(u_1^2(0)h_1(0)+u_2^2(0)h_2(0)\right)\,dx\right).
\end{aligned} \tag{5.72}$$

Now we use inequality (5.71) to obtain

$$\begin{aligned}
\frac{1}{12}\int_0^T\int_0^L \left(u_1^4+u_2^4\right)\,dx\,dt &\le \int_0^T\int_0^L \left(|u_{1,x}|^3+|u_{2,x}|^3\right) + \frac{|u_1u_2|}{2}\left(A_{12}|u_1|+A_{21}|u_2|\right)\,dx\,dt \\
&\qquad + \left(L\int_0^L \sup_{t\in(0,T)} \left(u_1^2(t)+u_2^2(t)\right)\,dx\right)^{\frac{1}{2}} \times \\
\times \left[\int_0^T\int_0^L \left(u_{1,xx}^2+u_{2,xx}^2+A_{12}|u_2u_{1,x}|+A_{21}|u_1u_{2,x}|\right)\,dx\,dt + \left(\sup_{t\in(0,T)}\int_0^L u_1^2(t)+u_2^2(t)\,dx\right)\right].
\end{aligned} \tag{5.73}$$

We now use Hölder's, Young's and Poincaré's inequalities to obtain

$$A_{ij}\int_0^L |u_ju_{i,x}|\,dx \le \frac{A_{ij}}{2}\left(C_L\int_0^L u_{i,x}^2\,dx + \int_0^L u_{j,x}^2\,dx\right) \tag{5.74}$$

and

$$A_{ij}\int_0^L |u_i^2u_j|\,dx \le \frac{1}{24}\int_0^L u_i^4\,dx + 6A_{ij}^2C_L\int_0^L u_{j,x}^2\,dx. \tag{5.75}$$

Substituting (5.74) and (5.75) in (5.73), we arrive at

$$\frac{1}{24}\int_0^T\int_0^L \left(u_1^4+u_2^4\right)\,dx\,dt \le \int_0^T\int_0^L \left(|u_{1,x}|^3+|u_{2,x}|^3\right)\,dx\,dt$$
$$+3C_L\max\left(A_{12}^2,A_{21}^2\right)\int_0^T\int_0^L \left(u_{1,x}^2+u_{2,x}^2\right)\,dx\,dt+\left(L\int_0^L \sup_{t\in(0,T)}\left(u_1^2(t)+u_2^2(t)\right)\,dx\right)^{\frac{1}{2}}\times$$
$$\times\left[\sup_{t\in(0,T)}\int_0^L \left(u_1^2(t)+u_2^2(t)\right)\,dx+\int_0^T\int_0^L \left(u_{1,xx}^2+u_{2,xx}^2+C_1u_{1,x}^2+C_2u_{2,x}^2\right)\,dx\,dt\right], \tag{5.76}$$

where $C_1=\frac{A_{12}C_L+A_{21}}{2}$ and $C_2=\frac{A_{12}+A_{21}C_L}{2}$. Using Prop. 8 and translation invariance in time, we obtain the following result:

Proposition 9. *Let $L\gg 1$ and let U be a solution of* (5.56)*. Then, for all $s\ge 0$ and $T>0$,*

$$\int_s^{s+T}\int_0^L \left(u_1^4+u_2^4\right)\,dx\,dt \le CL^{\frac{1}{2}}\left(\exp\left(\frac{T}{2}C_L^2\max(A_{12}^2,A_{21}^2)\right)\int_0^L \left(u_1^2(s)+u_2^2(s)\right)\,dx\right)^{\frac{3}{2}},$$

where C is a constant that depends on $A_{12},\ A_{21}$ and C_L.

5.3.3 Hölder continuity, compactness and strong convergence

We now consider H as defined in (5.65), with $g(t)=0$ and define

$$M=\exp\left(\frac{T}{2}C_L^2\max(A_{12}^2,A_{21}^2)\right)\int_0^L \left(u_1^2(s)+u_2^2(s)\right)\,dx \tag{5.77}$$

to obtain, for a given $t_0\in(0,T)$ and $x_1,\ x_2\in(0,L)$,

$$|h_i(t_0,x_1)-h_i(t_0,x_2)| \le \int_{x_1}^{x_2}|u_i(x,t_0)|\,dx \le |x_1-x_2|^{\frac{1}{2}}\left(\sup_{t\in(0,T)}\int_0^L u_i^2(x,t)\,dx\right)^{\frac{1}{2}}$$
$$\le |x_1-x_2|^{\frac{1}{2}}\left(\sup_{t\in(0,T)}\int_0^L u_1^2(x,t)+u_2^2(x,t)\,dx\right)^{\frac{1}{2}} \le M^{\frac{1}{2}}|x_1-x_2|^{\frac{1}{2}}$$

and therefore the functions h_i, $i = 1, 2$ are Hölder continuous in space. We can also prove Hölder continuity in time, by defining $\varphi_\delta(s) = \frac{1}{\delta}\varphi\left(\frac{s}{\delta}\right)$, where

$$\varphi(s) = \frac{1}{C}\chi_{(-1,1)}(s)e^{-\frac{1}{1-s^2}},$$

so that $\int_{\mathbb{R}} \varphi_\delta(s)\, ds = 1$. We have, for a given $x_0 \in (x-\delta, x+\delta)$,

$$\begin{aligned}\left|\int_{\mathbb{R}} \varphi_\delta(x-x_0)h_i(x,t)\, dx - h_i(x_0,t)\right| &= \left|\int_{\mathbb{R}} \varphi_\delta(x-x_0)\left(h_i(x,t)-h_i(x_0,t)\right)\, dx\right| \\ \leq \int_{\mathbb{R}} \varphi_\delta(x-x_0)|h_i(x,t)-h_i(x_0,t)|\, dx &\leq M^{\frac{1}{2}}\int_{\mathbb{R}} \varphi_\delta(x-x_0)|x-x_0|^{\frac{1}{2}}\, dx \leq M^{\frac{1}{2}}\delta^{\frac{1}{2}},\end{aligned} \tag{5.78}$$

so, by adding and subtracting terms of the form $\int_{\mathbb{R}} \varphi_\delta(x-x_0)h_i(x,t_j)\, dx$, $j = 1, 2$, and using equation (5.78), we have, for $i = 1, 2$,

$$|h_i(x_0,t_1) - h_i(x_0,t_2)| \leq 2M^{\frac{1}{2}}\delta^{\frac{1}{2}} + \left|\int_{t_1}^{t_2}\int_{\mathbb{R}} \varphi_\delta(x-x_0)h_{i,t}\, dx\right|. \tag{5.79}$$

We now use the definition of H and integration by parts to obtain, for $i, j = 1, 2$, $i \neq j$,

$$\begin{aligned}\left|\int_{t_1}^{t_2}\int_{\mathbb{R}} \varphi_\delta(x-x_0)h_{i,t}\, dx\right| &\leq |t_1-t_2|\frac{1}{2}\sup|\varphi_\delta| \sup_{t\in(0,T)}\int_0^L u_i^2(x,t)\, dx \\ &\quad + |t_1-t_2|\left(\int_{\mathbb{R}} \varphi_{\delta,xxx}^2(x-x_0)\, dx\right)^{\frac{1}{2}}\left(\int_0^L u_i^2\, dx\right)^{\frac{1}{2}} \\ &\quad + |t_1-t_2|\left(\int_{\mathbb{R}} \varphi_\delta^2(x-x_0)\, dx\right)^{\frac{1}{2}}\left(A_{ii}\left(\int_0^L u_i^2\, dx\right)^{\frac{1}{2}} + A_{ij}\left(\int_0^L u_j^2\, dx\right)^{\frac{1}{2}}\right).\end{aligned} \tag{5.80}$$

Now, since $\sup|\varphi_\delta| = \frac{1}{\delta}$, $\int_{\mathbb{R}} \varphi_\delta^2\, dx \leq \sup|\varphi_\delta| \int_{\mathbb{R}} \varphi_\delta\, dx = \frac{1}{\delta}$ and $\int_{\mathbb{R}} \varphi_{\delta,xxx}^2\, dx = \delta^{-7}$, we obtain

$$\left|\int_{t_1}^{t_2}\int_{\mathbb{R}} \varphi_\delta(x-x_0)h_{i,t}\, dx\right| \leq |t_1-t_2|\left(\delta^{-1}M + \delta^{-7/2}M^{1/2} + A_{ii}\delta^{-1/2}M^{1/2} + A_{ij}\delta^{-1/2}M^{1/2}\right),$$

and therefore we have

$$|h_i(x_0,t_1) - h_i(x_0,t_2)| \leq 2M^{1/2}\delta^{1/2} + |t_1-t_2|\left(\delta^{-1}M + \delta^{-\frac{7}{2}}M^{\frac{1}{2}} + (A_{ii}+A_{ij})\delta^{-\frac{1}{2}}M^{\frac{1}{2}}\right).$$

Choosing $\delta = \max\left(|t_1-t_2|^{2/3}M^{1/3}, |t_1-t_2|^{1/4}, |t_1-t_2|(A_{ii}+A_{ij})\right)$ we arrive at

$$|h_i(x_0,t_1)-h_i(x_0,t_2)| \le C\left(M^{\frac{2}{3}}|t_1-t_2|^{\frac{1}{3}} + M^{\frac{1}{2}}|t_1-t_2|^{\frac{1}{8}} + M^{\frac{1}{2}}|t_1-t_2|^{\frac{1}{2}}(A_{ii}+A_{ij})^{\frac{1}{2}}\right).$$

Using translation invariance in time, we prove the following result:

Proposition 10. *Let U be a solution to* (5.56) *and H be defined in* (5.65) *with $g(t) = 0$. Then h_i, $i = 1, 2$, verifies*

$$\begin{aligned}&|h_i(x_1,t_1) - h_i(x_2,t_2)| \le \\ &\le C\left(M^{\frac{1}{2}}\left(|x_1-x_2|^{\frac{1}{2}} + |t_1-t_2|^{\frac{1}{8}} + |t_1-t_2|^{\frac{1}{2}}(A_{ii}+A_{ij})^{\frac{1}{2}}\right) + M^{\frac{2}{3}}|t_1-t_2|^{\frac{1}{3}}\right), \quad (5.81)\end{aligned}$$

for all $x_1, x_2 \in \mathbb{R}$, $s \ge 0$, $T > 0$ and $t_1, t_2 \in (s, s+T)$, where M is defined in (5.77).

Boundedness in an initial layer

We choose any $0 < T \le 1$, introduce the function

$$f(s) = f_1(s)+f_2(s) = \int_s^{s+T}\int_0^L u_1^2(x,s+T)\,dx\,dt + \int_s^{s+T}\int_0^L u_2^2(x,s+T)\,dx\,dt \quad (5.82)$$

and use Prop. 8 to show that f is comparable with $\int_0^L u_1^2(x,s) + u_2^2(x,s)\,dx$:

$$\begin{aligned}T\int_0^L u_1^2(x,s+T) + u_2^2(x,s+T)\,dx &= \int_s^{s+T}\int_0^L u_1^2(x,s+T) + u_2^2(x,s+T)\,dx\,dt \\ &\le C_1\int_s^{s+T}\int_0^L u_1^2(x,t) + u_2^2(x,t)\,dx\,dt = C_1 f(s), \quad (5.83)\end{aligned}$$

where C_1 is a constant. Using Hölder's inequality, adding the positive quantity u_i^4, $i = 1, 2$, when necessary and using Proposition 9, we obtain

$$\begin{aligned}f(s) &\le L^{\frac{1}{2}}T^{\frac{1}{2}}\left[\left(\int_s^{s+T}\int_0^L u_1^4\,dx\,dt\right)^{\frac{1}{2}} + \left(\int_s^{s+T}\int_0^L u_2^4\,dx\,dt\right)^{\frac{1}{2}}\right] \\ &\le CL^{\frac{3}{4}}T^{\frac{1}{2}}\exp\left(\frac{T}{2}C_L^2\max\left(A_{12}^2, A_{21}^2\right)\right)^{\frac{3}{4}}\left(\int_0^L u_1^2(x,s) + u_2^2(x,s)\,dx\right)^{\frac{3}{4}}, \quad (5.84)\end{aligned}$$

where, again, C is a constant. Now, using (5.83) we have that

$$\int_0^L u_1^2(x,s)+u_2^2(x,s)\,dx = -f'(s)+\int_0^L u_1^2(x,s+T)+u_2^2(x,s+T)\,dx \\ \leq -f'(s)+C_1T^{-1}f(s), \quad (5.85)$$

and using (5.84) we obtain the differential inequality

$$f(s)\leq L^{\frac{3}{4}}T^{\frac{1}{2}}C_2\left(-f'(s)+C_1T^{-1}f(s)\right)^{\frac{3}{4}},$$

where $C_2=C(T,C_L,A_{12},A_{21})$ is a constant. Defining $h(s)=e^{-C_1s/T}f(s)$, we obtain

$$e^{C_1s/T}h(s)\leq C_2L^{3/4}T^{1/2}\left(-e^{C_1s/T}h'(s)\right)^{3/4},$$

or

$$\left(\frac{3}{h^{1/3}(s)}\right)'=-\frac{h'(s)}{h^{4/3}(s)}\geq C_3\frac{e^{C_1s/(3T)}}{LT^{2/3}}.$$

We integrate to obtain

$$\frac{1}{h^{1/3}(s)}\geq\frac{1}{h^{1/3}(s)}-\frac{1}{h^{1/3}(0)}\geq C_4\frac{T^{1/3}}{C_2L}\left(e^{C_2s/(3T)}-1\right),$$

or

$$h(s)\leq C_4\frac{L^3}{T\left(e^{C_2s/(3T)}-1\right)^3}.$$

Going back to f, this yields

$$\int_0^L u_1^2(x,s+T)+u_2^2(x,s+T)\,dx\leq\frac{C_1}{T}f(s)\leq C_5\frac{L^3}{T^2}\frac{e^{C_2s/T}}{\left(e^{C_2s/(3T)}-1\right)^3}, \quad (5.86)$$

for $0<T\leq 1$ and $s\geq 0$. Now, if $t\leq 1$, we choose $s=T=t/2$ so that

$$\int_0^L u_1^2(x,t)+u_2^2(x,t)\,dx\leq C\frac{L^3}{t^2}, \quad (5.87)$$

where C is a constant and if $t>1$ we choose $T=1/2$ and $s=t-1/2$ so that

$$\int_0^L u_1^2(x,t)+u_2^2(x,t)\,dx\leq CL^3. \quad (5.88)$$

This proves the following:

Proposition 11. *If U is a solution to* (5.56)*, there exists a constant $C > 0$ such that*

$$\int_0^L u_1^2(t) + u_2^2(t)\, dx \leq CL^3 \left(1 + \frac{1}{t^2}\right), \qquad \forall t > 0.$$

Weak convergence of the solution to (5.56)

We will now prove that the solutions to System (5.56) converge weakly to a vector valued function, $\hat{U}$, and identify this limit. We consider a sequence of domain lengths $\{L_n\}_{n\in\mathbb{N}}$ such that $L_n \overset{n\to\infty}{\longrightarrow} \infty$, let U_n be a solution to (5.56) in the domain $(0, L_n)$ and let $\hat{U}_n$ be the correspondent rescaled solution to the spatial domain $(0, 1)$, *i.e.*, $x = L\hat{x}$, $t = \hat{t}$ and

$$\hat{U} = \frac{1}{L} U\left(\hat{x}, \hat{t}\right). \tag{5.89}$$

We aim to show that there exists a subsequence of $\left\{\hat{U}_n\right\}_{n\in\mathbb{N}}$ associated with $\{L_n\}_{n\in\mathbb{N}}$ that converges strongly to some limit $\hat{U}$ in a suitable space and to identify this limit. In order to do that, we choose the temporal domain $t \in (T^{-1}, T)$, $T > 1$, and notice that Proposition 11 implies that, for $i = 1, 2$,

$$\int_0^{L_n} u_{n,i}^2(T^{-1})\, dx \leq \int_0^{L_n} u_{n,1}^2(T^{-1}) + u_{n,2}^2(T^{-1})\, dx \leq CL_n^3 T^2 \leq C^* L_n^3, \tag{5.90}$$

where C^* is a constant that is independent of n but depends on T. We also have, from Proposition 9 and Equation (5.90),

$$\begin{aligned}
&\int_{T^{-1}}^{T}\int_0^{L_n} u_{n,i}^4\, dx\, dt = \int_{T^{-1}}^{T}\int_0^{L_n} \left(u_{n,1}^4 + u_{n,2}^4\right)\, dx\, dt \\
&\leq CL_n^{\frac{1}{2}} \left(\exp\left(\frac{T}{2} C_{L_n}^2 \max(A_{12}^2, A_{21}^2)\right) \int_0^{L_n} \left(u_{1,n}^2(T^{-1}) + u_{2,n}(T^{-1})\right)\, dx\right)^{\frac{3}{2}} \leq CL_n^5,
\end{aligned}$$

and using the rescaling above, we obtain

$$\int_{T^{-1}}^{T}\int_0^1 \hat{u}_{n,i}^4\, d\hat{x}\, d\hat{t} \leq \int_{T^{-1}}^{T}\int_0^1 \left(\hat{u}_{n,1}^4 + \hat{u}_{n,2}^4\right)\, d\hat{x}\, d\hat{t} \leq C.$$

This means that both $\{\hat{u}_{1,n}\}_{n\in\mathbb{N}}$ and $\{\hat{u}_{2,n}\}_{n\in\mathbb{N}}$ are bounded sequences in L^4 and therefore there exist functions $\hat{u}_1$, $\hat{u}_2$ and subsequences, again labelled by $\hat{u}_{1,n}$ and $\hat{u}_{2,n}$ that are weakly

convergent to $\hat{u}_1$ and $\hat{u}_2$ respectively, that is

$$\begin{aligned}
\hat{u}_{i,n} &\rightharpoonup \hat{u}_i \quad \text{in } L^4((T^{-1},T);\dot{L}^4_p([0,1])),\\
\hat{u}^2_{i,n} &\rightharpoonup \overline{\hat{u}_i} \quad \text{in } L^2((T^{-1},T);L^2_p([0,1])),\\
\hat{u}^3_{i,n} &\rightharpoonup \overline{\hat{u}_i} \quad \text{in } L^{4/3}((T^{-1},T);L^{4/3}_p([0,1])),\\
\hat{u}^4_{i,n} &\overset{*}{\rightharpoonup} \overline{\hat{u}_i} \quad \text{in } \left(C^0([T^{-1},T];C^0_p([0,1]))\right)^*,
\end{aligned} \tag{5.91}$$

for $i = 1, 2$, where the second, third and fourth weak convergences are up to oscillations - see Appendix A.1. Furthermore, $\hat{u}_i$ has mean zero. Using the rescaling, equation (5.56) becomes

$$\hat{U}_{n,\hat{t}} + \left(f(\hat{U}_n) + \frac{\mathcal{A}}{L_n}\hat{U}_n + \frac{I}{L_n^4}\hat{U}_{n,\hat{x}\hat{x}\hat{x}} \right)_{\hat{x}} = 0, \quad \hat{x} \in (0,1),\, t > 0 \tag{5.92}$$

and the weak convergence of the solution for $n \to, \infty$ yields the distributional identity

$$\begin{aligned}
\hat{u}_{1,\hat{t}} + \left(\tfrac{1}{2}\overline{\hat{u}_1^2}\right)_{\hat{x}} &= 0,\\
\hat{u}_{2,\hat{t}} + \left(\tfrac{1}{2}\overline{\hat{u}_2^2}\right)_{\hat{x}} &= 0,
\end{aligned} \tag{5.93}$$

which we can write as

$$\hat{U}_{\hat{t}} + \left(\frac{\hat{U}^2}{2}\right)_{\hat{x}} \tag{5.94}$$

We now define the function $a(U) = \frac{1}{2}(u_1^2 + u_2^2)$ so that $\nabla a = U$. Taking the inner product of ∇a with equation (5.56) we obtain

$$\begin{aligned}
\left(\frac{u_1^2+u_2^2}{2}\right)_t + \left(\frac{u_1^3+u_2^3}{3}\right)_x &+ u_1u_{1,xxxx} + u_2u_{2.xxxx}\\
&+ A_{11}u_1u_{1,x} + A_{12}u_1u_{2,x} + A_{21}u_2u_{1,x} + A_{22}u_2u_{2,x} = 0,
\end{aligned} \tag{5.95}$$

where A_{ij}, $i, j = 1, 2$ are the entries of the matrix $\mathcal{A}$. We note that

$$uu_{xxxx} = (uu_{xxx})_x - u_xu_{xxx} = (uu_{xxx})_x - (u_xu_{xx})_x + u_{xx}^2,$$

and therefore we obtain

$$\left(\frac{u_1^2+u_2^2}{2}\right)_t+\left(\frac{u_1^3+u_2^3}{3}+\frac{A_{11}u_1^2+A_{22}u_2^2}{2}+u_1u_{1,xxx}-u_{1,x}u_{1,xx}+u_2u_{2,xxx}-u_{2,x}u_{2,xx}\right.$$
$$\left.+(A_{12}+A_{21})u_1u_2\right)_x=-u_{1,xx}^2-u_{2,xx}^2+A_{12}u_2u_{1,x}+A_{21}u_1u_{2,x}$$
$$=-u_{1,xx}^2-u_{2,xx}^2-\frac{u_1^2}{4}-\frac{u_2^2}{4}-A_{12}^2u_{1,x}^2-A_{21}^2u_{2,x}^2+\left(\frac{u_2}{2}+A_{12}u_{1,x}\right)^2+\left(\frac{u_1}{2}+A_{21}u_{2,x}\right)^2$$
$$\leq\left(\frac{u_2}{2}+A_{12}u_{1,x}\right)^2+\left(\frac{u_1}{2}+A_{21}u_{2,x}\right)^2. \quad (5.96)$$

We now consider equation (5.96) for the sequence of domains $\{L_n\}_{n\in\mathbb{N}}$ and its solutions $\{U_n\}_{n\in\mathbb{N}}$ and define a sequence of measures $\{\mu_n\}_{n\in\mathbb{N}}$:

$$\mu_n:=\mu_{1,n}+\mu_{2,n}=-u_{1,n,xx}^2-\frac{u_{2,n}^2}{4}-A_{12}^2u_{1,n,x}^2+\left(\frac{u_{2,n}}{2}+A_{12}u_{1,n,x}\right)^2+$$
$$-u_{2,n,xx}^2-\frac{u_{1,n}^2}{4}-A_{21}^2u_{2,n,x}^2+\left(\frac{u_{1,n}}{2}+A_{21}u_{2,n,x}\right)^2$$
$$\leq\left(\frac{u_{2,n}}{2}+A_{12}u_{1,n,x}\right)^2+\left(\frac{u_{1,n}}{2}+A_{21}u_{2,n,x}\right)^2. \quad (5.97)$$

We extend the rescaling (5.89) to the measures, by defining

$$\hat{\mu}_n=\frac{\mu_n}{L_n^2}. \quad (5.98)$$

We notice that this changes inequality (5.97); we now have

$$\hat{\mu}_n\leq\left(\frac{\hat{u}_{2,n}}{2}+\frac{A_{12}}{L_n}\hat{u}_{1,n,x}\right)^2+\left(\frac{u_{1,n}}{2}+\frac{A_{21}}{L_n}\hat{u}_{2,n,x}\right)^2.$$

We use Triangle inequality to obtain

$$\int_{T^{-1}}^{T}\int_0^1|\hat{\mu}_n|\,d\hat{x}\,d\hat{t}=L_n^{-3}\int_{T^{-1}}^{T}\int_0^L|\mu_n|\,dx\,dt$$
$$\leq C_1L_n^{-3}\int_{T^{-1}}^{T}\int_0^L u_{1,n,xx}^2+u_{2,n,xx}^2+u_{1,n}^2+u_{2,n}^2+u_{1,n,x}^2+u_{2,n,x}^2,$$

where C_1 is a constant that depends on A_{12} and A_{21}. Using Prop. 8 in all of the terms, we obtain

$$\int_{T^{-1}}^{T}\int_0^1|\hat{\mu}_n|\,d\hat{x}\,d\hat{t}\leq C_1C_2L_n^{-3}\int_{T^{-1}}^{T}u_n^2(T^{-1})\,dt,$$

where C_2 is a constant that depends on the constants obtained from Prop. 8. We finally use equation (5.90) and obtain

$$\int_{T^{-1}}^{T}\int_{0}^{1} |\hat{\mu}_n|\, d\hat{x}\, d\hat{t} \leq C_1 C_2 L_n^{-3} C L_n^3 = C^*, \tag{5.99}$$

for a constant C^*, which proves that the sequence of measures $\{\hat{\mu}_n\}_{n\in\mathbb{N}}$ is bounded, and this means that it has a weakly-$*$ convergent subsequence:

$$\hat{\mu}_n \overset{*}{\rightharpoonup} \hat{\mu} \quad \text{in } \left(C^0\left([T^{-1},T]; C_p^0([0,1])\right)\right)^*. \tag{5.100}$$

We can now apply the rescaling (5.89) to equation (5.96) and obtain

$$\left(\frac{\hat{u}_{1,n}^2+\hat{u}_{2,n}^2}{2}\right)_{\hat{t}} + \left(\frac{\hat{u}_{1,n}^3+\hat{u}_{2,n}^3}{3} + \frac{A_{11}\hat{u}_{1,n}^2 + A_{22}\hat{u}_{2,n}^2}{2L_n} + \frac{A_{12}+A_{21}}{L_n}\hat{u}_{1,n}\hat{u}_{2,n}\right)_{\hat{x}} + \frac{1}{L_n^4}\sum_{i=1,2}\left(\hat{u}_{i,n}\hat{u}_{i,n,\hat{x}\hat{x}\hat{x}} - \hat{u}_{i,n,\hat{x}}\hat{u}_{i,n,\hat{x}\hat{x}}\right)_{\hat{x}} = \hat{\mu}_n,$$

or

$$\left(\frac{\hat{u}_{1,n}^2+\hat{u}_{2,n}^2}{2}\right)_{\hat{t}} + \left(\frac{\hat{u}_{1,n}^3+\hat{u}_{2,n}^3}{3} + \frac{A_{11}\hat{u}_{1,n}^2 + A_{22}\hat{u}_{2,n}^2}{2L_n} + \frac{A_{12}+A_{21}}{L_n}\hat{u}_{1,n}\hat{u}_{2,n}\right)_{\hat{x}} + \frac{1}{L_n^4}\left(\frac{\hat{u}_{1,n}^2+\hat{u}_{2,n}^2}{2}\right)_{\hat{x}\hat{x}\hat{x}\hat{x}} - \frac{4}{L_n^2}\left(\hat{u}_{1,n,x}^2+\hat{u}_{2,n,\hat{x}}^2\right)_{\hat{x}\hat{x}} = \hat{\mu}_n, \tag{5.101}$$

where we left the last term in the left hand side partially rescaled, following [84]. This is because then we can bound the sequence $\left\{u_{i,n,x}^2\right\}_{n\in\mathbb{N}}$, $i=1,2$ in the following way:

$$\int_{T^{-1}}^{T}\int_{0}^{1} \hat{u}_{i,n,x}^2\, d\hat{x}\, d\hat{t} = L_n^{-3}\int_{T^{-1}}^{T}\int_{0}^{L} u_{i,n,x}^2\, dx\, dt \leq C L_n^{-3}\int_{0}^{L} u_{i,n}^2(T^{-1})\, dx \leq C, \tag{5.102}$$

where C is a constant and we used Prop. 8 and inequality (5.90). We can similarly bound the term $\int_{T^{-1}}^{T}\int_{0}^{1} u_{1,n}u_{2,n}\, d\hat{x}\, d\hat{t}$. This proves that all of the terms involving $\hat{u}$ in Equation (5.101) are bounded and therefore possess a weakly convergent subsequence. This allows us to pass to the limit $n\to\infty$, when $L_n\to\infty$, which gives us the distributional equation for the limit $\hat{U}$:

$$\left(\frac{\overline{\hat{u}_1^2}+\overline{\hat{u}_2^2}}{2}\right)_{\hat{t}} + \left(\frac{\overline{\hat{u}_1^3}+\overline{\hat{u}_2^3}}{3}\right)_{\hat{x}} = \hat{\mu}. \tag{5.103}$$

We have now identified the limit towards which the solutions of System (5.56) converge weakly. It remains to show that the convergence is strong. Once we have shown that, we will also have ruled out oscillations, and therefore shown that the solutions of System (5.56) are equivalent to the entropy solution of the following modified system of Burgers equations:

$$\hat{u}_{1,t} + \left(\frac{\hat{u}_1^2}{2}\right)_{\hat{x}} = 0 \tag{5.104a}$$

$$\hat{u}_{2,t} + \left(\frac{\hat{u}_2^2}{2}\right)_{\hat{x}} = 0 \tag{5.104b}$$

$$\left(\frac{\hat{u}_1^2 + \hat{u}_2^2}{2}\right)_t + \left(\frac{\hat{u}_1^3 + \hat{u}_2^3}{3}\right)_{\hat{x}} \leq \left(\frac{\hat{u}_{2,n}}{2} + \frac{A_{12}}{L_n}\hat{u}_{1,n,x}\right)^2 + \left(\frac{u_{1,n}}{2} + \frac{A_{21}}{L_n}\hat{u}_{2,n,x}\right)^2. \tag{5.104c}$$

Remark 15. *We notice that since all the weak convergence and boundedness resultses are valid for u_i and h_i individually, we can use the same techniques to prove the convergence of eah μ_i individually obtaining:*

$$\begin{array}{ll} \left(\frac{\overline{\hat{u}_1^2}}{2}\right)_{\hat{t}} + \left(\frac{\overline{\hat{u}_1^3}}{3}\right)_{\hat{x}} & = \hat{\mu}_1, \\ \left(\frac{\overline{\hat{u}_2^2}}{2}\right)_{\hat{t}} + \left(\frac{\overline{\hat{u}_2^3}}{3}\right)_{\hat{x}} & = \hat{\mu}_2. \end{array} \tag{5.105}$$

Strong convergence of the solutions to (5.56)

In order to prove strong convergence of the solutions to (5.56) to entropy solutions of (5.104), we will follow [84] and use a standard compensated compactness argument based on the div-curl structure of (5.56). We define H_n associated with the sequence $\{L_n\}_{n\in\mathbb{N}}$ of domain lengths and the correspondent solutions $\{U_n\}_{n\in\mathbb{N}}$ using (5.65) with $g(t) = 0$, again normalised so that

$$\int_{T^{-1}}^{T}\int_0^L h_{i,n}\, dx\, dt = 0. \tag{5.106}$$

We rescale H: $H_n = L_n^2 \hat{H}_n$, so that equations (5.65) become

$$\left\{\begin{array}{lcl} \hat{h}_{1,n,\hat{t}} & = & -\left(\frac{1}{2}\hat{u}_{1,n}^2 + \frac{1}{L_n}\left(A_{11}\hat{u}_{1,n} + A_{12}\hat{u}_{2,n}\right) + \frac{1}{L_n^4}\hat{u}_{1,n,\hat{x}\hat{x}\hat{x}}\right), \\ \hat{h}_{2,n,\hat{t}} & = & -\left(\frac{1}{2}\hat{u}_{2,n}^2 + \frac{1}{L_n}\left(A_{22}\hat{u}_{2,n} + A_{21}\hat{u}_{1,n}\right) + \frac{1}{L_n^4}\hat{u}_{2,n,\hat{x}\hat{x}\hat{x}}\right), \\ \hat{h}_{1,n,\hat{x}} & = & \hat{u}_{1,n}, \\ \hat{h}_{2,n,\hat{x}} & = & \hat{u}_{2,n}. \end{array}\right. \tag{5.107}$$

Repeating the proof of Prop. 10 for the rescaled equation, we obtain

$$|\hat{h}_{i,n}(x_1,t_1)-\hat{h}_{i,n}(x_2,t_2)| \leq \\ \leq C\left(|x_1-x_2|^{\frac{1}{2}}+|t_1-t_2|^{\frac{1}{2}}(A_{ii}+A_{ij})^{\frac{1}{2}}+|t_1-t_2|^{\frac{1}{3}}+L_n^{-\frac{1}{2}}|t_1-t_2|^{\frac{1}{8}}\right), \quad (5.108)$$

which means that the sequence of functions $\left\{\hat{h}_{i,n}\right\}_{n\in\mathbb{N}}$, $i=1,2$ is equicontinuous. From equation (5.106) we know that it is also uniformly bounded and therefore we can apply the Ascoli-Arzelá theorem - see Appendix A.1 - and prove strong convergence of $\hat{H}$:

$$\hat{h}_{i,n} \xrightarrow[n\to\infty]{} \hat{h}_i, \qquad \text{in } C^0\left([T^{-1},T];C_p^0([0,1])\right). \quad (5.109)$$

Using (5.91), the system (5.107) turns into the distributional identity

$$\begin{cases} \hat{h}_{1,\hat{t}} &= -\frac{\overline{\hat{u}_1^2}}{2}, \\ \hat{h}_{2,\hat{t}} &= -\frac{\overline{\hat{u}_2^2}}{2}, \\ \hat{h}_{1,\hat{x}} &= \hat{u}_1, \\ \hat{h}_{2,\hat{x}} &= \hat{u}_2. \end{cases} \quad (5.110)$$

We now recall equation (5.70) with $g(t)=0$. We have, after rescaling some of the terms,

$$\frac{1}{12}\int_{T^{-1}}^{T}\int_0^1\left(\hat{u}_{1,n}^4+\hat{u}_{2,n}^4\right)\,d\hat{x}\,\zeta\,d\hat{t}+L_n^{-5}\int_{T^{-1}}^{T}\int_0^L\left(u_{1,n,x}^3+u_{2,n,x}^3\right)\,dx\,\zeta\,dt \\ +\frac{L_n^{-5}}{2}\int_{T^{-1}}^{T}\int_0^L u_{1,n}u_{2,n}\left(A_{12}u_{1,n}+A_{21}u_{2,n}\right)\,dx\,\zeta\,dt=-\int_{T^{-1}}^{T}\int_0^1\hat{\mu}_{1,n}\hat{h}_{1,n}\,d\hat{x}\,\zeta\,d\hat{t} \\ -\int_{T^{-1}}^{T}\int_0^1\hat{\mu}_{2,n}\hat{h}_{2,n}\,d\hat{x}\,\zeta\,d\hat{t}-\int_{T^{-1}}^{T}\int_0^1\frac{1}{2}\left(\hat{u}_{1,n}^2\hat{h}_{1,n}+\hat{u}_{2,n}^2\hat{h}_{2,n}\right)\,d\hat{x}\,\zeta_t\,d\hat{t}. \quad (5.111)$$

We can bound the term involving $|u_{i,n,x}|^3$ using Prop. 8 and equation (5.90), in the same way as in [84]:

$$L_n^{-5}\int_0^\infty\int_0^L\left(|u_{1,n,x}|^3+|u_{2,n,x}|^3\right)\,dx\,\zeta\,dt\leq CL_n^{-\frac{1}{2}}.$$

In order to be able to pass to the limit, we need the terms of the form $u_{i,n}^2u_{j,n}$ to converge

weakly. This can be shown using Hölder's inequality

$$L_n^{-5}\int_0^L u_{i,n}^2 u_{j,n}\,dx \le L_n^{-5}\left(\int_0^L u_{i,n}^4\,dx\right)^{\frac{1}{2}}\left(\int_0^L u_{j,n}^2\,dx\right)^{\frac{1}{2}} \tag{5.112}$$

combined with Prop. 9 and Prop. 8:

$$\begin{aligned} L_n^{-5}\int_{T^{-1}}^T\int_0^L u_{i,n}^2 u_{j,n}\,dx &\le L_n^{-5}\left(\int_{T^{-1}}^T\int_0^L u_{1,n}^4+u_{2,n}^4\,dx\right)^{\frac{1}{2}}\left(\sup_{t\in(T^{-1},T)}\int_0^L u_{1,n}^2+u_{2,n}^2\,dx\right)^{\frac{1}{2}}\\ &\le L_n^{-5}CL_n^{\frac{1}{4}}\left(\int_0^L u_{1,n}^2(T^{-1})+u_{2,n}^2(T^{-1})\,dx\right)^{\frac{3}{4}}\left(\int_0^L u_{1,n}^2(T^{-1})+u_{2,n}^2(T^{-1})\,dx\right)^{\frac{1}{2}}\\ &\le C^*L_n^{-5}(L_n^3)^{\frac{3}{4}}(L_n^3)^{\frac{1}{2}} = C^*L_n^{-1}, \end{aligned} \tag{5.113}$$

where C^* is a constant that depends on T and on the constants obtained from the various inequalities. Therefore we can pass to the limit in equation (5.111) and obtain

$$\begin{aligned} \frac{1}{12}\int_{T^{-1}}^T\int_0^1\left(\overline{\hat{u}_1^4}+\overline{\hat{u}_2^4}\right)\,d\hat{x}\,\zeta\,d\hat{t} = &-\int_{T^{-1}}^T\int_0^1\hat{\mu}_1\hat{h}_1\,d\hat{x}\,\zeta\,d\hat{t}-\int_{T^{-1}}^T\int_0^1\hat{\mu}_2\hat{h}_2\,d\hat{x}\,\zeta\,d\hat{t}\\ &-\int_{T^{-1}}^T\int_0^1\frac{1}{2}\left(\overline{\hat{u}_1^2}\hat{h}_1+\overline{\hat{u}_2^2}\hat{h}_2\right)\,d\hat{x}\,\zeta_t\,d\hat{t}. \end{aligned}$$

Using equation (5.105), we obtain

$$\begin{aligned} \frac{1}{12}\int_{T^{-1}}^T\int_0^1\left(\overline{\hat{u}_1^4}+\overline{\hat{u}_2^4}\right)\,d\hat{x}\,\zeta\,d\hat{t} = &-\int_{T^{-1}}^T\int_0^1\left[\left(\frac{\overline{\hat{u}_1^2}}{2}\right)_{\hat{t}}+\left(\frac{\overline{\hat{u}_1^3}}{2}\right)_{\hat{x}}\right]\hat{h}_1\,d\hat{x}\,\zeta\,d\hat{t}\\ &-\int_{T^{-1}}^T\int_0^1\left[\left(\frac{\overline{\hat{u}_2^2}}{2}\right)_{\hat{t}}+\left(\frac{\overline{\hat{u}_2^3}}{2}\right)_{\hat{x}}\right]\hat{h}_2\,d\hat{x}\,\zeta\,d\hat{t}-\int_{T^{-1}}^T\int_0^1\frac{1}{2}\left(\overline{\hat{u}_1^2}\hat{h}_1+\overline{\hat{u}_2^2}\hat{h}_2\right)\,d\hat{x}\,\zeta_t\,d\hat{t}. \end{aligned}$$

The rest of the proof follows [84] exactly: f we write $(\hat{u}_{i,n}-\hat{u}_i)^4 = \hat{u}_{i,n}^4-4\hat{u}_{i,n}^3\hat{u}_i+6\hat{u}_{i,n}^2\hat{u}_i^2-4\hat{u}_{i,n}\hat{u}_i^3+\hat{u}_i^4$ and use the distributional identity (5.110), we can prove that each $\hat{u}_{i,n}$ converges to $\hat{u}_i$ in norm in L^4, which means that the solutions to System (5.56) converge strongly to the solution of the modified System (5.104).

5.3.4 Boundedness of the solutions to a system of inviscid Burgers equations

We now turn to a special case of equation (5.104), when the measure is actually zero valued:

$$\hat{u}_{1,t} + \left(\frac{\hat{u}_1^2}{2}\right)_{\hat{x}} = 0 \tag{5.114a}$$

$$\hat{u}_{2,t} + \left(\frac{\hat{u}_2^2}{2}\right)_{\hat{x}} = 0 \tag{5.114b}$$

$$\left(\frac{\hat{u}_1^2 + \hat{u}_2^2}{2}\right)_t + \left(\frac{\hat{u}_1^3 + \hat{u}_2^3}{3}\right)_{\hat{x}} \leq 0. \tag{5.114c}$$

We notice that in this case, the equations are decoupled. This means that essentially we have two independent systems of Burgers equations and the proof of boundedness of this system follows the same argument as the one given in [84, Prop. 2.3]. The proof is based on defining H as in equation (5.65) and exploring the div-curl structure of the system to prove uniform integrability and *a priori* energy estimates for its solutions. We then only need to repeat the proof of Prop. 11 for this case, to prove that there exists a constant C such that the solution the solutions of (5.114) rescaled to $x \in (0, 1)$ satisfy

$$\int_0^1 \hat{u}_1^2(\hat{x}, \hat{t}) + \hat{u}_2^2(\hat{x}, \hat{t})\, d\hat{x} \leq \frac{C}{t},$$

for all $t > 0$.

Equivalence between System (5.104) and a system of inviscid Burgers equations

The last step of the proof of boundedness of the solutions to System (5.104) would be to use the bounds on System (5.114) to our advantage. In the scalar KS equation case, it is possible to show ([138, Cor. 2.5], [84, Thm. 2.2]) that solutions of the system corresponding to (5.104) are also solutions to the system corresponding to (5.114). However, the proof uses the fact that, for scalar equations, the existence of an entropy solution of a system implies the existence of a viscosity solution for an associated system, a fact which is not possible to show in our case.

A proof of this fact would provide us with the last tool we would need for proving that the solutions to system (5.56) are bounded and therefore we believe that this is a project of interest, to study in the future. Possible ways of addressing it would be to use the generalisation of viscosity solutions for systems of equations [143] or to make use of a Green's function of the linear operator, if it exists.

5.4 Discussion

In this chapter we have analysed two particular cases of the general system of coupled Kuramoto-Sivashinsky equations that was studied in [168, 169]. These systems are weakly nonlinear models for three layer flows of immiscible viscous fluids stratified in a channel and driven by gravity and/or a streamwise pressure gradient. Due to the additional complexity that comes from the coupling, either through linear terms (first, second or fourth order derivatives) or the nonlinearities, the dynamics of these systems is very rich and in fact instabilities can emerge even in the absence of inertia, unlike analogous two-fluid flows. As a result, analytical results on global existence and estimates of solution norms, for example, are poorly understood.

We therefore started by looking at the possible bounds of the solutions to these systems. Computational studies in [168] suggest that the solutions to these systems are bounded and that these bounds do not depend on the domain length L. We took two particular cases: the first, simpler, case is the most similar to the scalar Kuramoto-Sivashinsky equation studied in Chapter 2 - the coupling comes only through the second order derivatives; and the second is a more realistic model for three layer flows in the vanishing viscosity limit, where there are no second order derivatives, and instead the coupling is via first order derivatives.

In the first case, we used the well-known background flow method ([50, 159]), which was the first successful method to obtain bounds for the scakar KS equation. This consists in defining a function Φ, called the background flow, in an appropriate manner, and using its properties, associated with a Lyapunov type argument to obtain bounds on the solutions to the equation/system of equations and its derivatives. The bounds obtained with this method are not optimal, but nevertheless they gives us an insight not only on the boundedness of the solutions but also on their regularity, given appropriate regularity in the initial conditions. We were successful in obtaining bounds for the particular case presented here, and anticipate that the same method can be used in the case where the coupling is through even order derivatives

(either fourth order, or second and fourth order simultaneously).

Having these bounds on the solutions to System (5.1) and its derivatives, we were in a position where we could generalise our results for the scalar KS equation presented in Chapter 2 to this case. We proved that we can stabilise all the solutions to System (5.1), either the zero solution or any steady state or travelling wave solution. We show results for the first two cases and anticipate similar numerical results for travelling waves. Finally, we also show how to extend the proof of existence of an optimal (distributed) control for this problem, by extending the proof of Theorem 1 to systems of coupled KS equations. We did not generalise the algorithm presented in Section 2.4.2 to this case, but we expect it to work similarly well here too.

In the second case, the coupling through the first derivatives makes the system harder to analyse using the background flow method, due to the existence of complex eigenvalues associated with complicated eigenfunctions. We therefore used the entropy method presented in [84] for the scalar KS equation. This method uses the fact that we can write the KS equation as a perturbation of an inviscid Burgers equation. This equation possesses an entropy solution and this fact, together with the fact that modified systems of the same form are all equivalent, is crucial for the proof of the bounds. We found that we can extend most of the results presented in this reference to our case, but we cannot prove the equivalence between different systems of entropy solutions to the Burgers equations. This is the only remaining step to prove boundedness of System (5.56) and we leave it for future work.

More generally, the nonlinear terms are also coupled and can cause hyperbolic-elliptic transitions by supporting complex eigenvalues of the nonlinear flux functions, see [168]. The study of this case would be a nice extension of the results proved in Section 5.3.

Chapter 6

Conclusions

This chapter provides a summary of the work presented in this thesis. We discuss the results obtained in each chapter, for weakly nonlinear models, long-wave models and stochastic equations. Finally, we discuss possible future directions for each problem.

6.1 Summary of results and main findings

In this thesis, we studied the problem of controlling the solutions of various nonlinear PDE models that describe the evolution of the free interface in thin liquid films flowing down inclined planes. We use a variety of models, ranging from weakly nonlinear models such as the Kuramoto-Sivashinsky equation and reduced-order long-wave models (Benney equation and weighted-residual model) and, when possible, the 2-D Navier–Stokes equaions; and also add the effects of noise. The problem is addressed analytically, and when this is not possible we perform extensive numerical calculations using spectral methods or finite differences for the space discretisation and a second order BDF method for time-stepping.

For the particular case of weakly nonlinear models (the KS equation and its generalisations), it is possible to obtain analytical results on the controllability of the whole range of regimes that the equations allow. We show, using a Lyapunov argument, that we can use point actuated controls to drive the solution of this equation towards any desired state: the zero solution, nontrivial steady states, and travelling wave solutions. If we allow the controls to have a distributed component, we can also drive the system towards any periodic state of our choosing. We have also shown that the controls are robust with respect to uncertainty in the parameters of the model, and also to small changes in the number of control actuators we apply. Finally, we prove the existence of a distributed optimal control and propose an algorithm based on gradient descent methods to compute the optimal positions of the control actuators. We note that we assumed that complete information about the solution of the gKS equation is available in these models. This is not realistic, but we feel that this would be a trivial generalisation of [7], and therefore decided not to do it here and apply it to the long-wave models instead.

Due to the complicated nonlinearities present in the long-wave models, it is not possible to obtain analytical results on controllability of the fully nonlinear systems and therefore we started by considering distributed controls, which are proportional to the deviation between the current state and the desired state of the system. We performed a linear stability analysis to show that this simple control scheme has a stabilising effect on the uniform film state in both Benney and weighted-residual models, and also in the Navier–Stokes equations. Furthermore, we found that proportional controls can also be used to stabilise unstable travelling waves and non-uniform steady states. We proceeded to apply the controls in nonlinear simulations and found that the controls indeed stabilise the fully nonlinear system. In the

more realistic scenario, where the controls can only be delivered via a small number of localised actuators and full observations of the full state of the solution are not available, we use dynamic observers to estimate the full solution and use this estimate for the design of the controls. We find that this point actuated control strategy is quite efficient for the stabilisation of the flat solution, but not immediately generalisable for nontrivial solutions.

We then proceeded to study the control of these equations in the presence of noise. The models we consider are variations of the stochastic Kuramoto-Sivashinsky equation, arising in thin films with thermal fluctuations or surface roughening by ion sputtering processes. For these equations, the goal is usually to be able to control some face value such as its surface roughness. We proposed a splitting method that turns the nonlinear stochastic PDE into a linear stochastic PDE coupled to a nonlinear deterministic PDE with random coefficients. We show that using this method we can use periodic controls to drive the system to a trajectory that has any desired surface roughness and furthermore we can also control its shape. When using point actuated feedback controls, the problem is harder to solve but we show that we can still drive the system to a range of desired surface roughness values. In order to solve this problem, we also had to formulate and solve a matrix problem, similar to a matrix Lyapunov equation and we developed an algorithm to do so.

Finally, we studied systems of coupled Kuramoto-Sivashinsky equations. We considered two particular cases of a general system of conservation laws: in the first case, we were able to obtain bounds on the solutions of the system, and also on their derivatives. This in turn allowed us to extend the results obtained for the generalised Kuramoto-Sivashinsky equation to this problem: we proved that we can use point actuated feedback controls to stabilise the full range of solutions to this system and exemplified it with numerical simulations. Furthermore, we extended the proof of existence of optimal controls to this case. In the second particular case, the proof of boundedness of the solutions is considerably harder, due to the nature of the coupling. We were able to generalise most of the results available for the scalar KS equation when using the entropy method to bound its solutions, and the only thing we fail to show is the equivalence between two systems of inviscid Burgers equations.

6.2 Current and future work

One of the objectives of this thesis was to design a control system that is valid in the full 2-D Navier–Stokes equations and therefore can be used in thin film experiments. While we have

derived controls that are effective at least in the linear stability analysis of these equations, there are still a few obstacles we need to overcome before we can be sure that the controls will work in a physical system and that we would like to be able to address.

First of all, it would be interesting and useful to investigate analytically the effect of the feedback controls derived here on nonlinear stability and blow up phenomena in the Benney equation and the weighted-residual model. We also do not know that the controls will stabilise the solutions in nonlinear simulations of the Navier–Stokes equations, and therefore applying our controls in Direct Numerical Simulations (DNS) of the Navier–Stokes equations is something we wish to do in the future. Another barrier to the application of these controls is that real experiments are nearly always performed in channels with rigid bounding side walls. Side walls are responsible for the appearance of curved wave fronts [224] even for channels much wider than the fluid depth, and the stability boundary can be surprisingly sensitive [175] to the conditions governing the three-phase contact line where air, liquid and wall meet. Furthermore, if the control actuation is applied close to the walls, we might also expect complex interactions.

Our analysis has also assumed either a domain of infinite extent in the streamwise direction or periodic boundary conditions. However, experiments are actually performed on a wall of finite extent. Fluid enters the domain at an inlet at which periodic perturbations can be applied. It then takes some distance for the waves to reach their fully developed state, and eventually the fluid is allowed to fall from the plane at the outlet. This case is a more realistic possibility for future work, and in fact it has already been studied for weakly nonlinear models including the KS equation and also the well-known Korteweg-de-Vries (KdV) equation (see, e.g., [38], where the authors explore the controllability of the system using both distributed controls and controls acting in the inlet, or both in the inlet and outlet walls). For practical implementation, we would envisage observing the interface in the developed region, and also applying feedback there. It is therefore important that feedback is quickly applied, so that it is able to take effect before waves pass out of the region of interest. We note that it is possible to simulate the whole system, including inflow and outflow regions, in both Navier–Stokes and long-wave computations.

In addition to exploring the effects of side walls and inlet and outlet regions, future work could also include assessing the effect of noise and uncertainty in the long-wave and Navier–Stokes models, either in a similar manner to what was done in Chapter 2 for the robustness

study of the controls applied to the Kuramoto-Sivashinsky equation, or by considering versions of the long-wave models that include the effects of noise. These were derived for the case when the noise is provenient from thermal fluctuations in [60, 96].

Other interesting case studies would be to consider numerical experiments incorporating restrictions on the control scheme to reflect latency in flow visualization, data processing, and the application of feedback, but overall, we are hopeful that practical implementation of feedback control for thin film flow can soon be achieved.

6.2.1 Using temperature as the actuation method

The focus of the current work was on using feedback controls applied via blowing and suction at the wall, but the methodology developed here could be extended to other types of actuation, such as substrate heating, which would be easier to implement in practice. This is a subject that we are actively exploring.

In this case, we wish to apply the controls via prescribing the temperature or heat flux at the wall, which will in turn react to the evolution of the fluid flow, ideally to observations of its interface. The first step is, therefore, to derive evolution equations that account for nonuniform wall temperature that varies in both space and time. Non isothermal flows introduce extra non dimensional parameters, such as the Péclet number, that measures the relative importance between convection and diffusion of the temperature, the Biot number, which measures how temperature is lost to the wall and/or the air, and the Marangoni number, which prescribes how the evolution of the temperature affects surface tension and therefore the evolution of the interface.

The first problem we encounter is that in this case we cannot restrict ourselves to first order long-wave models. For example, the first order Benney equation does not even account for the effects of large Péclet numbers on the temperature evolution equation and therefore will not give accurate results. Furthermore, in the weighted-residual model we find that for large Péclet numbers, prescribing distributed proportional controls stabilise long-waves but have a destabilising effect in short waves, and therefore we run the risk of obtaining an ill-posed model. Trevelyan and Kalliadasis [210] developed a high-order Galerkin projection model for the temperature equation which solves this problem for constant heating at the wall and we are studying variations of this model to account for spatiotemporal variation of the prescribed temperature. We obtained several models, using a Benney-type approach, as well

as a weighted-residual approach and a single integral approach. In the latter case, we obtain an equation for the evolution of the interface temperature in which the wall temperature only appears as a forcing term and which gives satisfactory results for the case of a flat film which is decoupled from the evolution of the interface temperature. This can be achieved by setting the Marangoni number to zero.

We aim to generalise this model to nonuniform films and to the case when the system is fully coupled, and to validate our models with direct numerical simulations. Once this is done, we can study the effects of different types of controls in this model. There are still a few challenges in the derivation of these controls: the first one being the fact that temperature is advected within the fluid, and therefore heating effects are felt downstream of its actuation. This is particularly important for point actuated heating. Furthermore, there is a time lag between the actuation and the instant when the interface feels the effects of the controls. We can see these as shifts, in time and space, and take them into account on the derivation of the controls: the first shift needs to be taken into account in the position of the control actuators and the time shift needs to be taken care of via, e.g., delayed control effects [158].

This is work in progress, in collaboration with Dr Alice Thompson, Dr Michael Dallaston and Dr Fabian Denner.

6.2.2 Non-normal operators

Another characteristic of the linear operators of the PDEs we considered is that they are mostly self-adjoint, or at least normal operators. We have seen in the context of the stochastic Kuramoto-Sivashinsky equation that non-normal operators can lead to complications in the analysis of stochastic systems, and in fact this is also true for deterministic systems. It is known [22] that non-normal operators are responsible for transient growth similar to that obtained from nonlinear interactions and this lead to the study of generalised stability theory [69, 70] and optimal perturbations [59, 71].

Non-normal operators arise, for example, in the modelling of a counter-current gas-liquid film flow. Models for this particular physical phenomenon were derived by Tseluiko and Kalliadasis [215], where the authors obtain a weakly nonlinear model of the interface, by isolating the gas problem. They obtain a modified Kuramoto-Sivashinsky equation with an extra dispersion term (which is given in terms of its Fourier representation) that gives rise to the non-normal aspect of the operator. This problem was studied numerically in [140] and

the study of its absolute and convective instabilities can be found in [221]. In the case of co-current gas-liquid flow, the problem was studied experimentally in [235].

This is an interesting future problem, to which we expect our control methodology to extend naturally.

References

[1] G. Akrivis, D. Papageorgiou, and Y.-S. Smyrlis. On the analyticity of certain dissipative-dispersive systems. *B. Lond. Math. Soc.*, 45:52–60, 2013.

[2] G. Akrivis, D. T. Papageorgiou, and Y.-S. Smyrlis. Linearly implicit methods for a semilinear parabolic system arising in two-phase flows. *IMA J. Numer. Anal.*, 31:299–321, 2011.

[3] G. Akrivis, D. T. Papageorgiou, and Y.-S. Smyrlis. Computational study of the dispersively modified Kuramoto-Sivashinsky equation. *SIAM J. Sci. Comput.*, 34(3):A729–A813, 2012.

[4] M. Alava, M. Dubé, and M. Rost. Imbibition in disordered media. *Adv. Phys.*, 53(2):83–175, 2004.

[5] M. Amaouche, H. Ait Abderrahmane, and L. Bourdache. Hydromagnetic thin film flow: Linear stability. *Phys. Rev. E*, 88:023028, 2013.

[6] B. Anderson. The inverse problem of stationary covariance generation. *J. Stat. Phys.*, 1(1):133–147, 1969.

[7] C. Antoniades and P. D. Christofides. Integrating nonlinear output feedback control and optimal actuator/sensor placement for transport-reaction processes. *Chem. Eng. Sci.*, 56:4517–4535, 2001.

[8] A. Armaou and P. D. Christofides. Feedback control of the Kuramoto-Sivashinsky equation. *Physica D*, 137:49–61, 2000.

[9] A. Armaou and P. D. Christofides. Wave supression by nonlinear finite-dimensional control. *Chem. Eng. Sci.*, 55:2627–2640, 2000.

[10] A. Armaou and P. D. Christofides. Dynamic optimization of dissipative PDE systems using nonlinear order reduction. *IEEE Decis. Contr. P.*, 2:2310–2316, December 2002.

[11] D. Auerbach, C. Grebogi, E. Ott, and J. A. Yorke. Controlling chaos in high dimensional systems. *Phys. Rev. Lett.*, 69(24):3479–3482, December 1992.

[12] S. Bagheri, D. Henningson, J. Hoepffner, and P. Schmid. Input-output analysis and control design applied to a linear model of spatially developing flows. *Appl. Mech. Rev.*, 62:020803, 2009.

[13] S. G. Bankoff. Stability of liquid flow down a heated inclined plane. *Int. J. Heat Mass Tran.*, 14:377–385, 1971.

[14] A.-L. Barabasi and H. E. Stanley. *Fractal Concepts in Surface Growth*. Cambridge University Press, 1995.

[15] A. Barbagallo, G. Dergham, D. Sipp, P. Schmid, and J.-C. Robinet. Closed-loop control of unsteadiness over a rounded backback facing step. *J. Fluid Mech.*, 703:326–362, 2012.

[16] B. Barker, M. A. Johnson, P. Noble, L. M. Rodrigues, and K. Zumbrun. Stability of periodic Kuramoto-Sivashinsky waves. *Appl. Math. Lett.*, 25:824–829, 2012.

[17] B. Barker, M. A. Johnson, P. Noble, L. M. Rodrigues, and K. Zumbrun. Nonlinear modulational stability of periodic traveling-wave solutions of the generalized Kuramoto-Sivashinsky equation. *Physica D*, 258:11–46, 2013.

[18] R. H. Bartels and G. W. Stewart. Solution of the matrix equation $AX + XB = C$ [F4]. *Commun. ACM*, 15(9):820–826, 1972.

[19] S. Beeler, H. Tran, and H. Banks. Feedback control method for nonlinear systems. *J. Optimiz Theory App*, 107(1):1–33, 2000.

[20] T. B. Benjamin. Wave formation in laminar flow down an inclined plane. *J. Fluid Mech.*, 2:554–573, 1957.

[21] D. J. Benney. Long waves on liquid films. *J. Math. Phys.*, 45:150–155, 1966.

[22] A. Bertozzi and M. Brenner. Linear stability and transient growth in driven contact lines. *Phys. Fluids*, 9:530–539, 1997.

[23] M. Block, B. Schmittmann, and E. Schöll. Controlling surface morphologies by time-delayed feedback. *Phys. Rev. B*, 75:233414, 2007.

[24] D. Blömker, C. Gugg, and M. Raible. Thin-film growth models: roughness and correlation functions. *Eur. J. Appl. Math.*, 13:385–402, 2002.

[25] M. G. Blyth and A. P. Bassom. Flow of a liquid layer over heated topography. *Proc. R. Soc. A*, 468:4067–4087, 2012.

[26] M. G. Blyth and C. Pozrikidis. Effect of surfactant on the stability of film flow down an inclined plane. *J. Fluid Mech.*, 521:241–250, 2004.

[27] S. Boccaletti, C. Grebogi, Y.-C. Lai, H. Mancini, and D. Maza. The control of chaos: theory and applications. *Phys. Rep.*, 329(3):103 – 197, 2000.

[28] A. Borzi and V. Schulz. *Computational optimization of systems governed by partial differential equations*. SIAM, 2012.

[29] E. Bouchbinder, I. Procaccia, S. Santucci, and L. Vanel. Fracture surfaces as multiscaling graphs. *Phys. Rev. Lett.*, 96:055509, Feb 2006.

[30] J. Bronski and T. Gambill. Uncertainty estimates and L_2 bounds for the Kuramoto-Sivashinsky equation. *Nonlinearity*, 19:2023–2039, 2006.

[31] J. Buceta, J. Pastor, M. A. Rubio, and F. J. de la Rubia. The stochastic Kuramoto-Sivashinsky equation: a model for compact electrodeposition growth. *Phys. Lett. A*, 235:464–468, 1997.

[32] J. Buceta, J. Pastor, M. A. Rubio, and F. J. de la Rubia. Small scale properties of the stochastic stabilized Kuramoto-Sivashinsky equation. *Physica D*, 113:166–171, 1998.

[33] C. Byrnes, D. Gilliam, C. Hu, and V. Shubov. Zero dynamics boundary control for regulation of the Kuramoto-Sivashinsky equation. *Math. Comput. Model*, 52:875–891, 2010.

[34] N. Carreno and E. Cerpa. Local controllability of the stabilized Kuramoto-Sivashinsky system by a single control acting on the heat equation.

[35] E. Cerpa. Null controllability and stabilization of the linear Kuramoto-Sivashinsky equation. *Commun. Pure Appl. Ana.*, 9(1):91–102, 2010.

[36] E. Cerpa. Boundary control of Korteweg-de Vries and Kuramoto-Sivashinsky PDEs. *Encyclopedia of Systems and Control*, pages 88–93, 2015.

[37] E. Cerpa, P. Guzmán, and A. Mercado. On the control of the linear Kuramoto-Sivashinsky equation. *ACTA DE RESUMENES LXXXIII Encuentro Anual Sociedad de Matemática de Chile*, page 183, 2015.

[38] E. Cerpa and A. Mercado. Local exact controllability to the trajectories of the 1-D Kuramoto-Sivashinsky equation. *J. Differ. Equ.*, 250:2024–2044, 2011.

[39] E. Cerpa, A. Mercado, and A. Pazoto. On the boundary control of a parabolic system coupling KS-KdV and heat equations. *Sci. Sin. A-Math. P A T*, 22:55–74, 2012.

[40] E. Cerpa, A. Mercado, and A. Pazoto. Null controllability of the stabilized Kuramoto-Sivashinsky system with one distributed control. *SIAM. J. Control Optim.*, 53(3):1543–1568, 2015.

[41] D. J. Christini *et al.* Nonlinear-dynamical arrhythmia control in humans. *Proc. Natl. Acad. Sci. U.S.A*, 98(10):5827–5832, 2001.

[42] P. D. Christofides. Feedback control of the Kuramoto-Sivashinsky equation. *IEEE Decis. Contr. P.*, pages 4646–4651, 1998.

[43] P. D. Christofides. *Nonlinear and Robust Control of PDE Systems*. Birkhauser, 2000.

[44] P. D. Christofides and A. Armaou. Global stabilization of the Kuramoto-Sivashinsky equation via distributed output feedback control. *Syst. Control Lett.*, 39:283–294, 2000.

[45] E. K. Chu. A pole-assignment algorithm for linear state feedback. *Syst. Control Lett.*, 7:289–299, 1986.

[46] E. K. Chu. Optimization and pole assignment in control system design. *Int. J. Appl. Math. Comp.*, 11(5):1035–1053, 2001.

[47] F. Clarke. *Functional analysis, calculus of variations and optimal control*. Springer, 2013.

[48] B. Cohen, J. Krommes, W. Tang, and M. Rosenbluth. Non-linear saturation of the dissipative trapped ion mode by mode coupling. *Nucl. Fusion*, 16:971–992, 1976.

[49] P. Collet, J.-P. Eckmann, H. Epstein, and J. Stubbe. Analyticity for the Kuramoto-Sivashinsky equation. *Physica D*, 67:321–326, 1993.

[50] P. Collet, J.-P. Eckmann, H. Epstein, and J. Stubbe. A global attracting set for the Kuramoto-Sivashinsky equation. *Commun. Math. Phys.*, 152:203–214, 1993.

[51] P. Constantin, C. Foias, B. Nicolaenko, and R. Temam. *Integral Manifolds and Inertial Manifolds for Dissipative Partial Differential Equations*. Springer - New York, 1989.

[52] I. Corwin. The Kardar-Parisi-Zhang equation and universality class. *Random Matrices: Theory and Appl.*, 1:1130001, 2012.

[53] A. Coward, D. T. Papageorgiou, and Y.-S. Smyrlis. Nonlinear stability of oscillatory core-annular flow: a generalized Kuramoto-Sivashinsky equation with time periodic coefficients. *Z. Angew. Math. Phys.*, 46:1–39, 1995.

[54] R. V. Craster and O. K. Matar. Dynamics and stability of thin liquid films. *Rev. Mod. Phys.*, 81:1131–1198, 2009.

[55] A. Cuerno, H. A. Makse, S. Tomassone, S. T. Harrington, and H. E. Stanley. Stochastic erosion for surface erosion via ion sputtering: Dynamical evolution from ripple morphology to rough morphology. *Phys. Rev. Lett.*, 75:4464–4467, 1995.

[56] R. Cuerno and A.-L. Barabasi. Dynamic scaling of ion-sputtered surfaces. *Phys. Rev. Lett.*, 74(23):4746–4749, 1995.

[57] R. Curtain. Invariance concepts in infinite dimensions. *SIAM J. Control Optim.*, 24(5):1009–1030, 1986.

[58] R. Curtain. Robust stabilization of infinite dimensional systems by finite dimensional controllers. *Syst. Control Lett.*, 7:41–47, 1986.

[59] T. DelSole. The necessity of optimal perturbations. 2003.

[60] J. A. Diez and A. G. González. Metallic-thin-film instability with spatially correlated thermal noise. *Phys. Rev. E*, 93:013120, 2016.

[61] E. Doedel and B. Oldman. *AUTO-07P: Continuation and Bifurcation Software for Ordinary Differential Equations.* Concordia University. Documentation and source code available at http://cmvl.cs.concordia.ca/auto/, 2009.

[62] J. Duan and V. J. Ervin. On the stochastic Kuramoto-Sivashinsky equation. *Nonlinear Analysis*, 44:205–216, 2001.

[63] S. Dubljevic. Model predictive control of Kuramoto-Sivashinsky equation with state and input constraints. *Chem. Eng. Sci*, 65:4388–4396, 2010.

[64] A. B. Duncan, T. Lelievre, and G. A. Pavliotis. Variance reduction using nonreversible Langevin samplers. *J. Stat. Phys.*, 2016.

[65] M. G. el Hak. *Flow Control Passive, Active, and Reactive Flow Management*. Cambridge University Press, 2007.

[66] J. Elezgaray, G. Berkooz, and P. Holmes. Large-scale statistics of the Kuramoto-Sivashinsky equation: A wavelet-based approach. *Phys. Rev. E*, 54:224–230, Jul 1996.

[67] N. Fabbiane, O. Semeraro, S. Bagheri, and D. Henningson. Adaptive and model-based control theory applied to convectively unstable flows. *Appl. Mech. Rev.*, 66:060801, 2014.

[68] A. Farhat, E. Lunasin, and E. S. Titi. Abridged continuous data assimilation for the 2D Navier-Stokes equations utilizing measurements of only one component of the velocity field. *J. Math. Fluid Mech.*, 18:1–23, 2016.

[69] B. Farrell and P. Ioannou. Generalized stability theory. Part I: Autonomous operators. *J. Atmos. Sci.*, 53(14):2025–2040, 1996.

[70] B. Farrell and P. Ioannou. Generalized stability theory. Part II: Nonautonomous operators. *J. Atmos. Sci.*, 53(14):2041–2053, 1996.

[71] B. Farrell and P. Ioannou. Optimal perturbations of uncertain systems. *Stoch. Dynam.*, 2(3):395–402t, 2002.

[72] B. Ferrario. Invariant measures for a Stochastic Kuramoto-Sivashinsky equation. *Stoch. Anal. Appl.*, 26(2):379–407, 2008.

[73] J. M. Floryan, S. H. Davis, and R. E. Kelly. Instabilities of a liquid film flowing down a slightly inclined plane. *Phys. Fluids*, 30:983, 1987.

[74] M. Frankel and V. Roytburd. Dissipative dynamics for a class of nonlinear pseudo-differential equations. *J. Evol. Equ.*, 8:491–512, 2008.

[75] M. Frankel and V. Roytburd. Stability for a class of nonlinear pseudo-differential equations. *Appl. Math. Lett.*, 21:425–430, 2008.

[76] T. Friederich and M. Kloker. Localized blowing and suction for direct control of the crossflow secondary instability. *AIAA Paper 4394*, 2008.

[77] T. Friederich and M. Kloker. Control of the secondary cross-flow instability using localized suction. *J. Fluid Mech.*, 706:470–495, 2012.

[78] U. Frisch, Z. S. She, and O. Thual. Viscoelastic behaviour of cellular solutions to the Kuramoto-Sivashinsky model. *J. Fluid Mech.*, 168:221–240, 1986.

[79] P. Gao. Optimal distributed control of the Kuramoto-Sivashinsky equation with pointwise state and mixed control-state constraints. *IMA J Math. Control I*, dnv010, 2015.

[80] P. Gao, M. Chen, and Y. Li. Observability estimates and null controllability for forward and backward linear stochastic Kuramoto-Sivashinsky equations. *SIAM J. Control Optim.*, 53(1):475–500, 2015.

[81] P. H. Gaskell, P. K. Jimack, M. Sellier, H. M. Thompson, and M. C. T. Wilson. Gravity-driven flow of continuous thin liquid films on non-porous substrates with topography. *J. Fluid Mech.*, 509:253–280, 2004.

[82] Gaurav and V. Shankar. Stability of gravity-driven free-surface flow past a deformable solid at zero and finite Reynolds number. *Phys. Fluids*, 19:024105, 2007.

[83] R. Gharraei, M. Hemayatkhah, S. B. Islami, and E. Esmaeilzadeh. An experimental investigation on the developing wavy falling film in the presence of electrohydrodynamic conduction phenomenon. *Exp. Therm. Fluid Sci.*, 60:35–44, 2015.

[84] L. Giacomelli and F. Otto. New bounds for the Kuramoto-Sivashinsky equation. *Commun. Pure Appl. Math.*, 58:0297–0318, 2005.

[85] B. Gjevik. Occurence of finite-amplitude surface waves on falling liquid films. *Phys. Fluids*, 13:1918–1925, 1970.

[86] A. Glezer and M. Amitay. Synthetic jets. *Annu. Rev. Fluid Mech.*, 34:503Ű529, 2002.

[87] K. Glover, R. Curtain, and J. Partington. Realisation and approximation of linear infinite-dimensional systems with error bounds. *SIAM J. Control Optim.*, 26(4):863–898, 1988.

[88] M. Goldman, M. Josien, and F. Otto. New bounds for the inhomogenous Burgers and the Kuramoto-Sivashinsky equations. *Commun. Part. Diff. Eq.*, 40:2237–2265, 2015.

[89] S. N. Gomes, D. T. Papageorgiou, and G. A. Pavliotis. Stabilizing non-trivial solutions of the generalized Kuramoto-Sivashinsky equation using feedback and optimal control. *IMA J Appl Math, first published online March 17, 2016 doi:10.1093/imamat/hxw011*, 2016.

[90] S. N. Gomes, M. Pradas, S. Kalliadasis, D. T. Papageorgiou, and G. A. Pavliotis. Controlling spatiotemporal chaos in in active dissipative-dispersive nonlinear systems. *Phys. Rev. E*, 92:022912, 2015.

[91] S. N. Gomes, M. Pradas, S. Kalliadasis, D. T. Papageorgiou, and G. A. Pavliotis. Controlling roughening processes in the stochastic Kuramoto-Sivashinsky equation. *Submitted to Physica D*, 2016.

[92] S. N. Gomes and S. J. Tate. Solution of a Lyapunov type matrix equation arising in the control of stochastix partial differential equations. *Submitted to IMA J. Appl. Math.*, 2016.

[93] J. Goodman. Stability of the Kuramoto-Sivashinsky equation and related systems. *Commun. Pure Appl. Math.*, 47:293–306, 1994.

[94] C. Grebogi, E. Ott, and J. A. Yorke. Chaos, strange attractors, and fractal basin boundaries in nonlinear dynamics. *Science*, 238(4827):632–638, 1987.

[95] R. O. Grigoriev. Contact line instability and pattern selection in thermally driven liquid films. *Phys. Fluids*, 15(6):1363–1374, 2003.

[96] G. Grün, K. Mecke, and M. Rauscher. Thin-film flow influenced by thermal noise. *J Stat Phys*, 122(6):1261–1294, 2006.

[97] M. Hairer. Solving the KPZ equation. *Ann. Math.*, 178(2):559–664, 2013.

[98] C. Heining and N. Aksel. Bottom reconstruction in thin-film over topography: Steady solution and linear stability. *Phys. Fluids*, 21:083605, 2009.

[99] C. Heining, T. Pollak, and M. Sellier. Flow domain identification from free surface velocity in thin inertial films. *J. Fluid Mech.*, 720:338–356, 2013.

[100] M. Hinze and K. Kunisch. Second order methods for optimal control of time-dependent fluid flow. *SIAM. J. Control Optim.*, 40(3):925–946, 2001.

[101] A. Hooper and R. Grimshaw. Nonlinear instability at the interface between two fluids. *Phys. Fluids*, 28:37–45, 1985.

[102] R. A. Horn and C. R. Johnson. *Matrix Analysis*. Cambridge University Press, 1985.

[103] R. A. Horn and C. R. Johnson. *Topics in Matrix Analysis*. Cambridge University Press, 1991.

[104] C. Hu and R. Temam. Robust control of the Kuramoto-Sivashinsky equatiion. *Dynam. Cont. Dis. Ser. B*, 8:315–338, 2001.

[105] G. Hu, O. G, and P. D. Christofides. Stochastic modeling and simultaneous regulation of surface roughness and porosity in thin film deposition. *Ind. Eng. Chem. Res.*, 48:6690–6700, 2009.

[106] G. Hu, Y. Lou, and P. D. Christofides. Dynamic output feedback covariance control of stochastic dissipative partial differential equations. *Chem. Eng. Sci*, 63:4531–4542, 2008.

[107] G. Hu, Y. Lou, and P. D. Christofides. Model parameter estimation and feedback control of surface roughness in a sputtering process. *Chem. Eng. Sci*, 63:1800–1816, 2008.

[108] G. Hu, G. Orkoulas, and P. D. Christofides. Modeling and control of film porosity in thin film deposition. *Chem. Eng. Sci*, 64:3668–3682, 2009.

[109] G. Hu, G. Orkoulas, and P. D. Christofides. Regulation of film thickness, surface roughness and porosity in thin film growth using deposition rate. *Chem. Eng. Sci*, 64:3903–3913, 2009.

[110] L. Hu and X. Mao. Almost sure exponential stabilisation of stochastic systems by state-feedback control. *Automatica*, 44:465–471, 2008.

[111] L. Huang, P. Huang, and R. LeBeau. Numerical study of blowing and suction control mechanism on NACA0012 airfoil. *J. Aircraft*, 41(5):1005–1013, 2004.

[112] J. Hyman and B. Nicolaenko. The Kuramoto-Sivashinsky equation: a bridge between PDEs and dynamical systems. *Physica D*, 18:113–126, 1986.

[113] J. Hyman, B. Nicolaenko, and S. Zaleski. Order and complexity in the Kuramoto-Sivashinsky model of weakly turbulent interfaces. *Physica D*, 23:256–292, 1986.

[114] L. Illing, D. J. Gauthier, and R. Roy. Controlling optical chaos, spatio-temporal dynamics, and patterns. volume 54 of *Advances In Atomic, Molecular, and Optical Physics*, pages 615 – 697. Academic Press, 2007.

[115] J. Il'yashenko. Global analysis of the phase portrait for the Kuramoto-Sivashinsky equation. *J. Dyn. Differ. Equ.*, 4:585–615, 1992.

[116] J. Jimenez. Simplified formulas for the mean and variance of linear stochastic differential equations. *Appl. Math. Lett.*, 49:12–19, 2015.

[117] M. Jolly, I. Kevrekidis, and E. Titi. Approximate inertial manifolds for the Kuramoto-Sivashinsky equation: analysis and computations. *Physica D*, 44:38–60, 1990.

[118] M. S. Jolly, R. Rosa, and R. Temam. Evaluating the dimension of an inertial manifold for the Kuramoto-Sivashinsky equation. *Adv. Differential Equations*, 5(1-3):31–66, 2000.

[119] S. Kalliadasis, A. Kiyashko, and E. Demekhin. Marangoni instability of a thin liquid film heated from below by a local heat source. *J. Fluid Mech.*, 475:377–408, 2003.

[120] S. Kalliadasis, C. Ruyer-Quil, B. Scheid, and M. G. Velarde. *Falling Liquid Films*, volume 176. Springer Series on Applied Mathematical Sciences, Springer-Verlag Berlin Heidelberg, 2012.

[121] S. K. Kalpathy, L. F. Francis, and S. Kumar. Thermally induced delay and reversal of liquid film dewetting on chemically patterned surfaces. *J. Colloid Interf. Sci.*, 408:212–219, 2013.

[122] M. Kardar, G. Parisi, and Y.-C. Zhang. Dynamic scaling of growing interfaces. *Phys. Rev. Lett.*, 56:889–892, Mar 1986.

[123] J. Kautsky, N. K. Nichols, and P. V. Dooren. Robust pole assignment in linear state feedback. *Int. J. Control*, 41(5):1129–1155, 1985.

[124] T. Kawahara. Formation of saturated solitons in a nonlinear dispersive system with instability and dissipation. *Phys. Rev. Lett.*, 51:381–382, 1983.

[125] T. Kawahara and S. Toh. Nonlinear dispersive periodic waves in the presence of instability and damping. *Phys. Fluids*, 28:1636–1638, 1985.

[126] T. Kawahara and S. Toh. Pulse interactions in an unstable dissipative-dispersive nonlinear system. *Phys. Fluids*, 31(8):2103–2111, August 1988.

[127] I. G. Kevrekidis, B. Nicolaenko, and J. C. Scovel. Back in the saddle again: a computer assisted study of the Kuramoto-Sivashinsky equation. *SIAM J. Appl. Math.*, 50(3):760–790, June 1990.

[128] T. Kobayashi. Adaptive stabilization of the Kuramoto-Sivashinsky equation. *Int. J. Syst. Sci.*, 33(3):175–180, 2002.

[129] P. Kokotovic, H. K. Khalil, and J. O'Reilly. *Singular perturbation methods in control: analysis and design*. Academic Press, 1986.

[130] J. Krug. Origins of scale invariance in growth processes. *Adv. Phys.*, 46(2):139–282, 1997.

[131] K. Kunisch and S. Volkwein. Control of the Burgers equation by a reduced-order approach using proper orthogonal decomposition. *J. Optimiz Theory App*, 102(2):345–371, August 1999.

[132] Y. Kuramoto. Diffusion-induced chaos in reaction systems. *Prog. Theor. Phys. Supp.*, 64:346–367, 1978.

[133] Y. Kuramoto and T. Tsuzuki. On the formation of dissipative structures in reaction-diffusion systems. *Prog. Theor. Phys.*, 54:687–699, 1975.

[134] Y. Kuramoto and T. Yamada. Turbulent state in chemical reaction. *Prog. Theor. Phys.*, 56:679, 1976.

[135] K. B. Lauritsen, R. Cuerno, and H. A. Makse. Noisy Kuramoto-Sivashinsky equation for an erosion model. *Phys. Rev. E*, 54(4):3577–3580, 1996.

[136] C. Lee and H. T. Tran. Reduced-order based feedback control of the Kuramoto-Sivashinsky equation. *J. Compu. Appl. Math.*, (173):1–19, 2005.

[137] T. Lelievre, F. Nier, and G. A. Pavliotis. Optimal non-reversible linear drift for the convergence to equilibrium of a diffusion. *J. Stat. Phys.*, 152(2):237–274, 2013.

[138] C. D. Lellis, F. Otto, and M. Westdickenberg. Minimal entropy conditions for Burgers equation. *Quarterly Appl. Math.*, 62:687–700, 2004.

[139] K. Levenberg. A method for the solution of certain non-linear problems in least squares. *Quarterly Appl. Math.*, 2:164–168, 1944.

[140] T.-S. Lin, D. Tseluiko, and S. Kalliadasis. Numerical study of a non-local weakly nonlinear model for a liquid film sheared by a turbulent gas. *Procedia IUTAM*, 11:98–109, 2014.

[141] J. L. Lions. *Optimal Control of Systems Governed by Partial Differential Equations*. Berlin: Springer-Verlag, 1971.

[142] J. Liu and J. P. Gollub. Onset of spatially chaotic waves on flowing films. *Phys. Rev. Lett.*, 70:2289–2292, 1993.

[143] W. Liu, Y. Yang, and G. Lu. Viscosity solutions of fully nonlinear parabolic systems. *J. Math. Anal. Appl.*, 281:362–381, 2003.

[144] W.-J. Liu and M. Krstić. Stability enhancement by boundary control in the Kuramoto-Sivashinsky equation. *Nonlinear Anal.-Theor*, 43:485–507, 2001.

[145] J. Löber and H. Engel. Controlling the position of traveling waves in reaction-diffusion systems. *Phys. Rev. Lett.*, 112:148305, Apr 2014.

[146] Y. Lou and P. Christofides. Feedback control of surface roughness using stochastic PDEs. *AIChE Journal*, 51(1):345–352, 2005.

[147] Y. Lou and P. D. Christofides. Estimation and control of surface roughness in thin film growth using kinetic Monte-Carlo models. *Chem. Eng. Sci*, 58:3115–3129, 2003.

[148] Y. Lou and P. D. Christofides. Feedback control of growth rate and surface roughness in thin film growth. *AIChE Journal*, 49(8):2099–2113, 2003.

[149] Y. Lou and P. D. Christofides. Optimal actuator/sensor placement for nonlinear control of the Kuramoto-Sivashinsky equation. *IEEE T. Contr. Syst. T.*, 11(5):737–745, September 2003.

[150] Y. Lou and P. D. Christofides. Feedback control of surface roughness in sputtering processes using the stochastic Kuramoto-Sivashinsky equation. *Comput. Chem. Eng.*, 29:741–759, 2005.

[151] Y. Lou and P. D. Christofides. Nonlinear feedback control of surface roughness using a stochastic PDE: Design and application to a sputtering process. *Ind. Eng. Chem. Res.*, 45:7177–7189, 2006.

[152] Y. Lou, G. Hu, and P. D. Christofides. Model predictive control of nonlinear stochastic partial differential equations with application to a sputtering process. *AIChE Journal*, 54(8):2065–2081, 2008.

[153] Y. Lou, G. Hu, and P. D. Christofides. Model predictive control of nonlinear stochastic PDEs: Application to a sputtering process. *2009 American Control Conference*, 2009.

[154] A. Majda and R. Pego. Stable viscosity matrices for systems o conservation laws. *J. Differ. Equ.*, 56:229–262, 1985.

[155] P. Manneville. *Macroscopic Modeling of Turbulent Flows*, volume 230. Lecture Notes in Physics, Springer-Verlag Berlin Heidelberg, 1985.

[156] D. W. Marquardt. An algorithm for least-squares estimation of nonlinear parameters. *J. Soc. Ind. Appl. Math.*, 11(2):431–441, 1963.

[157] D. Michelson and G. Sivashinsky. Nonlinear analysis of hydrodynamic instability in laminar flames- II. numerical experiments. *Acta Astronaut.*, 4:1207–1221, 1977.

[158] W. Michiels and S.-. Niculescu. *Stability, control, and computaiton for time-delay systems: An eigenvalue-based approach*, volume 27. SIAM, second edition, 2014.

[159] B. Nicolaenko, B.Scheurer, and R. Temam. Some global dynamical properties of the Kuramoto-Sivashinsky equations: nonlinear stability and attractors. *Physica D*, 16:155–183, 1985.

[160] M. Nicoli, R. Cuerno, and M. Castro. Unstable nonlocal interface dynamics. *Phys. Rev. Lett.*, 102:256102, Jun 2009.

[161] J. Nocedal and S. J. Wright. *Numerical Optimization*. Springer, second edition, 2006.

[162] W. Nusselt. Der Wärmeaustausch und Berieselungskühler. *Z. Ver. Deut. Indr.*, 67:206–210, 1923.

[163] K. A. Ogden, S. J. D. D'Alessio, and J. P. Pascal. Gravity-driven flow over heated, porous, wavy surfaces. *Phys. Fluids*, 23:122102, 2011.

[164] A. Or, R. Kelly, L. Cortelezzi, and J. Speyer. Control of long-wavelength Marangoni-Bénard convection. *J. Fluid Mech.*, 387:321–341, 1999.

[165] A. Oron and O. Gottlieb. Subcritical and supercritical bifurcations of the first- and second-order Benney equations. *J. Eng. Math.*, 50:121–140, 2004.

[166] E. Ott, C. Grebogi, and J. A. Yorke. Controlling chaos. *Phys. Rev. Lett.*, 64(11):1196–1199, March 1990.

[167] F. Otto. Optimal bounds on the Kuramoto-Sivashinsky equation. *J. Funct. Anal.*, 257:2188–2245, 2009.

[168] E. S. Papaefthymiou and D. T. Papageorgiou. Vanishing viscosity limits of mixed hyperbolic-elliptic systems arising in multilayer channel flows. *Nonlinearity*, 28:1607–1631, 2015.

[169] E. S. Papaefthymiou, D. T. Papageorgiou., and G. A. Pavliotis. Nonlinear interfacial dynamics in stratified multilayer channel flows. *J. Fluid Mech*, 734:114–143, 2013.

[170] D. T. Papageorgiou, C. Maldarelli, and D. Rumschitzki. Nonlinear interfacial stability of core-annular film flow. *Phys. Fluids A*, 2:340–352, 1990.

[171] D. T. Papageorgiou, G. C. Papanicolaou, and Y.-S. Smyrlis. Modulational stability of periodic solutions of the Kuramoto-Sivashinsky equation. *NATO ASI Series Singularities in Fluids, Plasmas and Optics*, 404:255–263, 1993.

[172] D. T. Papageorgiou and Y.-S. Smyrlis. The route to chaos for the Kuramoto-Sivashinsky equation. *Theor. Comp. Fluid. Dyn.*, 3:15–42, 1991.

[173] C. Park and T. Nosoko. Three-dimensional wave dynamics on a falling film and associated mass transfer. *AIChE J.*, 49(11):2715–2727, 2003.

[174] T. Pollak and N. Aksel. Crucial flow stabilization and multiple instability branches of gravity-driven films over topography. *Phys. Fluids*, 25:024103, 2013.

[175] T. Pollak, A. Haas, and N. Aksel. Side wall effects on the instability of thin gravity-driven films – from long-wave to short-wave instability. *Phys. Fluids*, 23:094110, 2011.

[176] C. Pozrikidis. The flow of a liquid film along a periodic wall. *J. Fluid Mech.*, 188:275–300, 1988.

[177] M. Pradas and A. Hernández-Machado. Intrinsic versus superrough anomalous scaling in spontaneous imbibition. *Phys. Rev. E*, 74:041608, Oct 2006.

[178] M. Pradas, S. Kalliadasis, and D. Tseluiko. Binary interactions of solitary pulses in falling liquid films. *IMA J. Appl. Math.*, 77:408–419, 2012.

[179] M. Pradas, G. A. Pavliotis, S. Kalliadasis, D. T. Papageorgiou, and D. Tseluiko. Additive noise effects in active nonlinear spatially extended systems. *Eur. J. Appl. Math.*, 23:563–591, 2012.

[180] M. Pradas, D. Tseluiko, S. Kalliadasis, D. T. Papageorgiou, and G. A. Pavliotis. Noise induced state transitions, intermittency, ans universality in the noisy Kuramoto-Sivashinsky equation. *Phys. Rev. Lett.*, 106:060602–, 2011.

[181] G. D. Prato and J. Zabczyk. *Stochastic equations in infinite dimensions*. Encyclopedia of mathematics and its applications. Cambridge University Press, second edition, 2014.

[182] I. Procaccia, M. H. Jensen, V. S. L'vov, K. Sneppen, and R. Zeitak. Surface roughening and the long-wavelength properties of the Kuramoto-Sivashinsky equation. *Phys. Rev. A*, 46:3220–3224, Sep 1992.

[183] J. Quastel and H. Spohn. The one-dimensional KPZ equation and its universality class. *J. Stat. Phys.*, 160:965–984, 2015.

[184] S. Rasoulian and L. Ricardez-Sandoval. Stochastic nonlinear model predictive control applied to a thin film deposition process under uncertainty. *Chem. Eng. Sci*, 140:90–103, 2016.

[185] J. C. Robinson. *Infinite-Dimensional Dynamical Systems. An introduction to dissipative parabolic PDEs and the theory of global attractors*. Cambridge University Press, 2001.

[186] M. Rost and J. Krug. Anisotropic Kuramoto-Sivashinsky equation for surface growth and erosion. *Phys. Rev. Lett.*, 75(21):3894–3897, 1995.

[187] C. Ruyer-Quil and P. Manneville. Improved modeling of flows down inclined planes. *Eur. Phys. J. B*, 15:357–369, 2000.

[188] R. Sakthivel and H. Ito. Non-linear robust boundary control of the Kuramoto-Sivashinsky equation. *IMA J Math. Control I*, 24:47–55, 2007.

[189] B. Scheid, A. Oron, P. Colinet, U. Thiele, and J. C. Legros. Nonlinear evolution of nonuniformly heated falling liquid films. *Phys. Fluids*, 14:4130, 2002.

[190] M. Schörner, D. Reck, and N. Aksel. Does the topography's specific shape matter in general for the stability of film flows? *Phys. Fluids*, 27:042103, 2015.

[191] G. R. Sell and Y. You. *Dynamics of Evolutionary Equations*, volume 143 of *Applied Mathematical Sciences*. Springer, 2002.

[192] T. Shinbrot, C. Grebogi, E. Ott, and J. A. Yorke. Using small perturbations to control chaos. *Nature*, 363:411–417, June 1993.

[193] T. Shlang and G. I. Sivashinsky. Irregular flow of a liquid film down a vertical column. *J. Phys.*, 43:459–466, 1982.

[194] G. Sivashinsky. Instabilities, pattern formation, and turbulence in flames. *Annu. Rev. Fluid Mech.*, 15:179–199, 1983.

[195] G. I. Sivashinsky. Nonlinear analysis of hydrodynamic instability in laminar flames - I. Derivation of basic equations. *Acta Astronaut.*, 4:1177–1206, 1977.

[196] G. I. Sivashinsky and D. M. Michelson. On irregular wavy flow of a liquid film down a vertical plane. *Prog. Theor. Phys.*, 63:2112–2114, 1980.

[197] Y.-S. Smyrlis and D. T. Papageorgiou. Predicting chaos for infinite dimensional dynamical systems: The Kuramoto-Sivashinsky equation, a case study. *P. Natl. Acad. Sci. USA*, 88:11129–11132, December 1991.

[198] J. E. S. Socolar, D. W. Sukow, and D. J. Gauthier. Stabilizing unstable periodic orbits in fast dynamical systems. *Phys. Rev. E*, 50(4):3245–3248, October 1994.

[199] J. Soriano, A. Mercier, R. Planet, A. Hernández-Machado, M. A. Rodríguez, and J. Ortín. Anomalous roughening of viscous fluid fronts in spontaneous imbibition. *Phys. Rev. Lett.*, 95:104501, Aug 2005.

[200] B. Sun. Maximum principle for optimal boundary control of the Kuramoto-Sivashinsky equation. *J Frankl Inst*, 347:467–482, 2010.

[201] J. J. Sylvester. Sur l'equation en matrices $px = xq$. *C. R. Acad. Sci. Paris*, 99:67–71 and 115–116, 1984.

[202] E. Tadmor. The well-posedness of the Kuramoto-Sivashinsky equation. *SIAM J. Math. Anal.*, 17(4):884–893, July 1986.

[203] R. Temam. *Infinite-Dimensional Dynamical Systems in Mechanics and Physics*. Springer Verlag, 1988.

[204] U. Thiele, B. Goyeau, and M. G. Velarde. Stability analysis of thin film flow along a heated porous wall. *Phys. Fluids*, 21:014103, 2009.

[205] A. B. Thompson, S. N. Gomes, G. A. Pavliotis, and D. T. Papageorgiou. Stabilising falling liquid film flows using feedback control. *Phys. Fluids*, 28:012107, 2016.

[206] A. B. Thompson, D. Tseluiko, and D. T. Papageorgiou. Falling liquid films with blowing and suction. *J. Fluid Mech.*, 787:292–330, 2016.

[207] N. Tiwari, A. Awasthi, and J. Davis. Linear stability analysis of thin liquid film flow over a heterogeneously heated substrate. *Phys. Fluids*, 26:042105, 2014.

[208] L. Trefethen. *Spectral Methods in Matlab*. SIAM, 2000.

[209] C. Tretter. *Spectral theory of block operator matrices and applications*. Imperial College Press, 2008.

[210] P. Trevelyan and S. Kalliadasis. Wave dynamics on a thin-liquid film falling down a heated wall. *J. Eng. Math.*, 50:177–208, 2004.

[211] F. Troltzsch. *Optimal Control of Partial Differential Equations: Theory, Methods and Applications*. American Mathematical Society, 2010.

[212] D. Tseluiko, M. G. Blyth, and D. T. Papageorgiou. Stability of film flow over inclined topography based on a long-wave nonlinear model. *J. Fluid Mech.*, 729:638–671, 2013.

[213] D. Tseluiko, M. G. Blyth, D. T. Papageorgiou, and J.-M. Vanden-Broeck. Effect of an electric field on film flow down a corrugated wall at zero Reynolds number. *Phys. Fluids*, 20:042103, 2008.

[214] D. Tseluiko, M. G. Blyth, D. T. Papageorgiou, and J.-M. Vanden-Broeck. Electrified viscous thin film flow over topography. *J. Fluid Mech.*, 597:449–475, 2008.

[215] D. Tseluiko and S. Kalliadasis. Nonlinear waves in counter-current gas-liquid film flow. *J. Fluid Mech.*, 673:19–59, 2011.

[216] D. Tseluiko and S. Kalliadasis. Weak interaction of solitary pulses in active dispersive-dissipative nonlinear media. *IMA J. Appl. Math.*, 79:274–299, 2014.

[217] D. Tseluiko and D. T. Papageorgiou. Wave evolution on electrified falling films. *J. Fluid Mech*, 556:361–386, 2006.

[218] D. Tseluiko and D. T. Papageorgiou. A global attracting set for nonlocal Kuramoto-Sivashinsky equations arising in interfacial electrohydrodynamics. *Eur. J. Appl. Math.*, 17:677–703, 2007.

[219] D. Tseluiko and D. T. Papageorgiou. Dynamics of an electrostatically modified Kuramoto-Sivashinsky-Korteweg-de Vries equation arising in falling film flows. *Phys. Rev. E*, 82:016322–1–12, 2010.

[220] A. Varshney, S. Pitchaiah, and A. Armaou. Feedback control of dissipative PDE systems using adaptive model reduction. *AIChE J.*, 55(4):906–918, 2009.

[221] R. Vellingiri, D. Tseluiko, and S. Kalliadasis. Absolute and convective instabilities in counter-current gas-liquid film flows. *J. Fluid Mech*, 763:166–201, 2015.

[222] S. Veremieiev, H. M. Thompson, M. Scholle, Y. C. Lee, and P. H. Gaskell. Electrified thin film flow at finite Reynolds number on planar substrates featuring topography. *Int. J. Multiphase Flow*, 44:48–69, 2012.

[223] M. Vlachogiannis and V. Bontozoglou. Experiments on laminar film flow along a periodic wall. *J. Fluid Mech.*, 457:133–156, April 2002.

[224] M. Vlachogiannis, A. Samandas, V. Leontidis, and V. Bontozoglou. Effect of channel width on the primary instability of inclined film flow. *Phys. Fluids*, 22:012106, 2010.

[225] S. Volkwein. Application of the augmented Lagrangian-SQP method to optimal control problems for the stationary Burgers equation. *Comput. Optim. Appl.*, 16:57–81, 2000.

[226] D. Wachsmuth and A. Rösch. How to check numerically the sufficient optimality conditions for infinite-dimensional optimization problems. *Optimal Control of Coupled Systems of Partial Differential Equations*, 158:297–317, 2009.

[227] S. J. Weinstein and K. J. Ruschak. Coating flows. *Ann. Rev. Fluid Mech.*, 36:29–53, 2004.

[228] R. Wittenberg. Dissipativity, analyticity and viscous shocks in the (de)stabilized Kuramoto-Sivashinsky equation. *Phys. Lett. A*, 300:407–416, 2002.

[229] R. Wittenberg and P. Holmes. Scale and space localization in the Kuramoto-Sivashinsky equation. *Chaos*, 9:452–464, 1999.

[230] V. Yakhot. Large-scale properties of unstable systems governed by the Kuramoto-Sivashinksi equation. *Phys. Rev. A*, 24:642–644, Jul 1981.

[231] D. Yang. Random attractors for the stochastic Kuramoto-Sivashinsky equation. *Stoch. Anal. Appl.*, 24:1285–1303, 2006.

[232] D. Yang. Dynamics for the stochastic nonlocal Kuramoto-Sivashinsky equation. *J. Math. Anal. Appl.*, 330:550–570, 2007.

[233] C.-S. Yih. Stability of liquid flow down an inclined plane. *Phys. Fluids*, 6:321–334, 1963.

[234] J. Zabczyk. *Mathematical Control Theory: An Introduction*. Birkhäuser, 1992.

[235] I. Zadrazil and C. Markides. An experimental characterization of liquid films in downwards co-current gas-liquid annular flow by particle image and tracking velocimetry. *Int. J. Multiphase Flow*, 67:42–53, 2014.

[236] E. Zeidler. *Nonlinear functional analysis and its applications I*. Springer-Verlag, 1985.

[237] X. Zhang, G. Hu, G. Orkoulas, and P. D. Christofides. Predictive control of surface mean slope and roughness in a thin film deposition process. *Chem. Eng. Sci*, 65:4720–4731, 2010.

[238] J. Zheng. The bang-bang principle of time optimal controls for the Kuramoto-Sivashinsky-KdV equation with internal control. *Int. J. Robust Nonlin.*, 2015.

Appendices

Appendix A

Background

Throughout this thesis, we use some well-known results in functional analysis, (feedback and optimal) control theory and linear algebra. Here we will state the relevant results, and also the relevant literature concerning these topics.

A.1 Functional analysis

Here we state some basic definitions and properties of functional spaces that will be useful throughout our analysis of the proposed feedback control problems. This will be splitted in three sections: first we define the functional spaces of interest to us, followed by the definition of functional derivatives and finally by the definition and properties of the Hilbert transform operator. Further details can be found in nonlinear functional analysis textbooks, and we suggest [47, 185, 236].

A.1.1 Functional spaces

Throughout this thesis, we make use of the properties of some appropriate functional spaces. We particularly use the following spaces:

- $\dot{L}^2_p(0, 2\pi)$, the space of periodic, mean zero functions $f(x)$ in $L^2(0, 2\pi)$,
- $\dot{H}^s_p$, the periodic, mean zero Sobolev space of order s, which is the space of all functions $f(x)$ in $\dot{L}^2_p(0, 2\pi)$ which possess weak derivatives of order up to s also in $\dot{L}^2_p(0, 2\pi)$.

- $L^2(0,T;X)$ (or $H^s(0,T;X)$), where X is either $\dot{L}^2_p(0,2\pi)$ or $\dot{H}^s_p(0,2\pi)$ is the space of all functions $f(x,t)$ which are L^2 (or H^s) functions of time.

The following inequalities are valid in the aforementioned spaces, for $I=[0,L]$:

Poincaré's inequality: if $u \in \dot{H}^1_p(I)$, then

$$\|u\|_{L^2(0,L)} \leq \frac{L}{2\pi}\|u_x\|_{L_2(0,L)};$$

Gronwall's inequality: Let $x(t) \in \mathbb{R}$ satisfy the differential inequality

$$\frac{dx}{dt} \leq g(t)x + h(t).$$

Then

$$x(t) \leq x(0)e^{G(t)} + \int_0^t e^{G(t)-G(s)}h(s)\,ds,$$

where

$$G(t) = \int_0^t g(s)\,ds.$$

Hölder's inequality: let $1 < p < \infty$ and $\frac{1}{p}+\frac{1}{q}=1$ and suppose that $f \in L^p(I)$ and $g \in L^q(I)$. Then $fg \in L^1(I)$ and

$$\|fg\|_{L^1(I)} \leq \|f\|_{L^p(I)}\|g\|_{L^q(I)};$$

Nirenberg-Gagliardo interpolation inequality: Fix $1 \leq q,r \leq \infty$ and a natural number m and suppose that there exist $\alpha \in \mathbb{R}$ and $j \in \mathbb{N}$ such that

$$\frac{1}{p} = j + \left(\frac{1}{r} - m\right)\alpha + \frac{1-\alpha}{q},$$

with

$$\frac{j}{m} \leq \alpha \leq 1.$$

If $u \in L^q(\mathbb{R})$ and $D^m u \in L^r(\mathbb{R})$, then $D^j u \in L^p(\mathbb{R})$ and there exists a constant C depending only on $m,\ j,\ q,\ r$ and α such that

$$\|D^j u\|_{L^p} \leq C\|D^m u\|^{\alpha}_{L^r}\|u\|^{1-\alpha}_{L^q},$$

where $D^k u$ stands for the $k-$th derivative of u.

We also huse **Young's inequality**: if $a, b \geq 0$ and $p, q > 1$ with $\frac{1}{p} + \frac{1}{q} = 1$, then

$$ab \leq \epsilon a^p + \epsilon^{-\frac{q}{p}} b^q.$$

The **Sobolev embedding theorem** is helpful when obtaining L^∞ bounds. For functions of one variable, it reads: Let Ω be a bounded C^k domain in $\mathbb{R}$ and suppose that $u \in H^k(\Omega)$.

(a) if $k < \frac{1}{2}$ then $u \in L^{\frac{2}{1-2k}}(\Omega)$ and there exists a constant C such that

$$\|u\|_{L^{\frac{2}{1-2k}}} \leq C\|u\|_{H^k},$$

(b) if $k = \frac{1}{2}$ then $u \in L^p(\Omega)$ for $1 \leq p < \infty$ and for each p there exists a constant $C = C(p)$ such that

$$\|u\|_{L^p} \leq C\|u\|_{H^k},$$

(c) if $k > j + \frac{1}{2}$ then $u \in C^j(\bar{\Omega})$ and there exists a constant C_j such that

$$\|u\|_{C^j(\bar{\Omega})} \leq C_j\|u\|_{H^k}.$$

Since Ω is bounded, it follows trivially that $u \in L^p(\Omega)$ for $1 \leq p \leq \infty$.

For periodic functions, this means, in particular, that: if $u \in H^s(I)$ (where $I = (0, L)$) with $s > \frac{1}{2}$ then $u \in C^0(\bar{I})$ and there exists a constant C_s such that

$$\|u\|_\infty \leq C_s\|u\|_{H^s}.$$

Furthermore, if $s > j + \frac{1}{2}$ then $u \in C^j(\bar{I})$ and

$$\|u\|_{C^j} \leq C\|u\|_{H^s}.$$

The **Ascoli-Arzelá theorem** allows us to extract strongly convergent subsequences from sequences of functions: let X be a compact subset of $\mathbb{R}^{m_1}$ and let $\{f_n\}$ be a sequence of continuous functions from X into $\mathbb{R}^{m_2}$. If f_n is uniformly bounded, that is, there exists a constant M such that

$$\|f_n\|_\infty \leq M, \quad \forall n,$$

and equicontinuous, that is, for every $\epsilon > 0$ there exists a $\delta > 0$, independent of n, such that

$$|x - y| \leq \delta \quad \Rightarrow \quad |f_n(x) - f_n(y)| \leq \epsilon,$$

then $\{f_n\}$ has a subsequence that converges uniformly in X.

Finally, we also use some properties of **weak and weak-* convergence**. We say that a sequence $\{x_n\}$ of elements of a Banach space X converges weakly to $\hat{x} \in X$, and write $x_n \rightharpoonup \hat{x}$ if $f(x_n) \to f(\hat{x})$ for every $f \in X^*$, where X^* is the dual space of X. It is known that:

- strong convergence implies weak convergence, and weak limits are unique,
- bounded sequences have a weakly convergence subsequence,
- linear functionals f of weakly convergent sequences $\{x_n\}$ converge weakly to $f(\hat{x})$.

The concept of weak-* convergence is useful for elements of the dual space X^*: a sequence $\{f_n\}$ of elements in X^* converges weakly-* to $\hat{f} \in X^*$, and write $f_n \overset{*}{\rightharpoonup} \hat{f}$, if $f_n(x) \to \hat{f}(x)$, $\forall x \in X$. It is known that weak-* limits are unique, weak convergence implies weak-* convergence, and if X is reflexive, weak-* convergence implies weak convergence.

In Chapter 5, we prove that nonlinear (continuous) functionals f of the sequences $u_{i,n}$ (e.g. $u_{i,n}^2$), converge to a correspondent function $\overline{f(\hat{u}_n)}$ (e.g. $\overline{\hat{u}_n^2}$). These functions are defined using the **Young measure** associated with the sequence. These are defined as follows: let $\{u_n\}_{n=1}^{\infty}$ be a bounded sequence of L^∞ functions. Then there exists a subsequence $\{u_{n_j}\}_{j=1}^{\infty} \subset \{u_n\}_{n=1}^{\infty}$ and for almost every x a Borel probability measure μ_x on $\mathbb{R}$ such that for each $f \in C(\mathbb{R})$ we have $f(u_{n_j}) \overset{*}{\rightharpoonup} \int_{\mathbb{R}} f(y) d\mu_x(y)$ in L^∞. The measures μ_x are called the Young measures generated by the sequence $\{u_n\}_{n=1}^{\infty}$.

A.1.2 Functional derivatives

In the context of optimal control for systems governed by PDEs (see below), in order not only to obtain solutions for these problems, but also to be able to prove existence of such solutions and study their regularity properties, there is the need to generalise the notion of derivative of a real-valued function to that of functional derivatives. Here we state the definition of Fréchet and Gâteaux derivatives, which generalise the derivative of a real-valued function and the classical directional derivative, respectively.

In what follows, we will use the *little-o notation*: for a function $r \in U \subset X \to Y$,

$$r(h) = o(\|h\|) \Leftrightarrow \frac{r(h)}{\|h\|} \xrightarrow[\|h\|\to 0]{} 0,$$

$$r(h) = o(1) \Leftrightarrow r(h) \xrightarrow[\|h\|\to 0]{} 0.$$

Let X and Y be two normed spaces and let $f : U(u_0) \subset X \to Y$, where $u_0 \in X$ and $U(u_0)$ is a neighbourhood of u_0 and is an open subset of X. We say that f is *Fréchet differentiable in* u_0 if there exists a linear operator $F : X \to Y$ such that

$$f(u_0 + h) - f(u_0) = Fh + o(\|h\|) \tag{A.1}$$

for $h \in X$. If F exists, it is called Fréchet derivative of f at u_0 and we write $f'(u_0) := F$. Alternatively, we can also write

$$\lim_{\substack{u \to u_0 \\ u \neq u_0}} \frac{\|f(u) - f(u_0) - (F(u_0), u - u_0)\|_Y}{\|u - u_0\|_X} = 0 \tag{A.2}$$

for $u \in X$ and where $\|\cdot\|_X$ represents the norm in X and $(\cdot, \cdot)$ is the corresponding inner product.

Similarly, f is *Gâteaux differentiable at* u_0 if there exists a linear operator $F : X \to Y$ such that

$$f(u_0 + th) - f(u_0) = tFh + o(t) \tag{A.3}$$

for all $h \in X$ such that $\|h\| = 1$. In this case, F is called the Gâteaux derivative of f at u_0, and we also write $f'(u_0) := F$. As for the case of real-valued functions, if a Fréchet (or Gâteaux) derivative exists for all $u_0 \in U$, then $f' : U \subset X \to L(X, Y)$, $u \mapsto f'(u)$, where $L(X, Y)$ is the space of all linear functions from X to Y, is called the Fréchet (or Gâteaux) derivative of f in U.

We notice that Gâteaux differentiability is a weaker concept than Fréchet differentiability in the sense that it does not imply continuity. Furthermore, a Fréchet differentiable function is always Gâteaux differentiable, but the converse is not always true.

The usual properties of derivatives of real-valued functions are easily generalised for Fréchet derivatives - see [47] for details. We can also use these definitions to generalise the

notion of second (and higher order) derivatives, which would be useful, for instance, if we were interested to find sufficient conditions for existence of optimal controls.

A.1.3 Hilbert transform

The Hilbert transform operator is defined by

$$\mathcal{H}[u](x) = \frac{1}{\pi} PV \int_{-\infty}^{\infty} \frac{u(\xi)}{x-\xi}\, d\xi, \tag{A.4}$$

where PV means that the integral is understood in the sense of Cauchy principal value. It is a linear, invertible and bounded operator in both the Lebesgue space $L^2(\mathbb{R})$ and the Sobolev spaces $H^k(\mathbb{R})$.

In the periodic space $\dot{L}^2_p(0, 2\pi)$ (or $\dot{H}^k_p(0, 2\pi)$), it is defined instead by

$$\mathcal{H}[u](x) = \frac{1}{2\pi} PV \int_0^{2\pi} u(\xi) \cot\left(\frac{x-\xi}{2}\right)\, d\xi.$$

We note some of its properties, wich are useful to our analysis:

$$\partial_x \circ \mathcal{H} = \mathcal{H} \circ \partial_x \tag{A.5a}$$

$$\mathcal{H}^{-1} = -\mathcal{H} \tag{A.5b}$$

$$\int u(x)\mathcal{H}[v](x)\, dx = -\int v(x)\mathcal{H}[u](x)\, dx \tag{A.5c}$$

$$\mathcal{F}[\mathcal{H}[u]](k) = -i\,\mathrm{sign}(\mathcal{R}(k))\mathcal{F}[u](k). \tag{A.5d}$$

From Equation (A.5d) we can deduce that $\mathcal{H}[\sin](x) = -\cos(x)$ and $\mathcal{H}[\cos](x) = \sin(x)$.

A.2 Control theory

Here we state some basic definitions from control theory and outline two of the available algorithms for pole placement; further details can be found in [234]. We consider the linear system

$$\dot{z} = Az + Bu, \quad y = Cz, \tag{A.6}$$

where A, B and C are $N \times N$, $N \times M$ and $M \times P$ matrices, respectively. We will say that a matrix A is stable if all its eigenvalues have negative real part.

We will call the system (A.6), or the pair (A, B), controllable if there exists a matrix K such that $A + BK$ is stable. If the system is controllable, we can always obtain the state z^* by taking $u = K(z - z^*)$, regardless of initial conditions. Similarly, we say that system (A.6), or the pair (A, C), is detectable if there exists a matrix L such that $A + LC$ is stable. If the pair (A, C) is detectable, then (A^T, C^T) is controllable.

The Kalman Rank condition gives a necessary and sufficient condition on A and B for controllability, and therefore detectability. This condition states that the system (A.6) is controllable if and only if $\mathrm{rank}[A|B] = N$, where

$$[A|B] = [B \; AB \; A^2B \; \cdots \; A^{N-1}B]$$

is a $N \times NM$ matrix obtained by writing consecutively the columns of the matrices $A^{n-1}B$, $n = 1, \ldots, N$.

The natural choice when constructing controls based on the observations y would be to choose a matrix K such that the matrix $A + BKC$ is stable. Controls that can be written in the form $u = Ky$ are called *static output feedback controls*. However, for nontrivial B and C, it is not possible, in general, to construct a matrix K so that $A + BKC$ is stable. This difficulty motivates the construction of the *dynamic observers* presented in Sec. 3.3.4.

A.2.1 Pole placement algorithms

We used two different algorithms to compute the matrix K associated with the stabilisation of the chosen solutions to our PDEs and we summarise them here.

MATLAB's command place

MATLAB's command place is designed for the system

$$\frac{dz}{dt} = Az + Bu, \quad u = Kz, \tag{A.7}$$

where z and u are vectors, the matrices A and B are given and we wish to compute a matrix K such that the eigenvalues of $A + BK$ are a given set $p = \{\lambda_1, \ldots, \lambda_N\}$. The algorithm is based on [123] and requires that if the eigenvalues in p are complex then they must be complex conjugates and also that their multiplicity cannot exceed that of the rank of B (or

equivalently to our case, the number of control inputs).

The solution to this problem is not unique, and this algorithm computes the matrix K which minimises the condition number of the matrix X of eigenvectors of $A + BK$. This means that K also minimises the sensitivity of the closed-loop poles to perturbations in the matrices A or B, which allowed us to prove the robustness results in Section 2.2.2.

This algorithm was our first choice when dealing with the stabilisation of the solutions to weakly nonlinear models, since it allows us to choose the eigenvalues of the stabilised system. This was necessary since we needed to make sure that inequalities such as the one in Equation (2.26) were verified. If there is no need to specify the eigenvalues of the closed-loop system, then algorithms such as the LQR algorithm are more adequate.

The LQR algorithm

The Linear-Quadratic Regulator (LQR) algorithm is designed for system (A.7), but in this case the goal is to choose the matrix K in order to minimise the cost κ defined by

$$\kappa = \int_0^\infty \left(z^T U z + u^T V u\right)\, \mathrm{d}t, \tag{A.8}$$

where U and V are given symmetric, positive definite matrices that define the relative cost associated with different solution components. A minimiser K of the cost (A.8) subject to the system (A.7) is strongly connected to a solution, if it exists, of an algebraic Riccati equation:

$$U + PJ + J^T P - PBV^{-1}B^T P = 0, \tag{A.9}$$

in which the unknown P is a nonnegative definite matrix. If $\tilde{P}$ is a solution to (A.9) and $\tilde{P} - P$ is negative definite for all other solutions P, then $\tilde{P}$ is called a minimal solution to (A.9) and $K = -V^{-1}B^T\tilde{P}$ minimises the cost functional (A.8). Furthermore, in [234], it is proved that if the pair (A, B) is controllable and $U = C^T C$, where the pair (A, C) is observable then the algebraic Ricatti equation (A.9) has exactly one solution P, and the matrix $A - BV^{-1}B^T P$ is stable.

MATLAB's LQR algorithm requires that the pair (A, B) is controllable and (U, A) has no unobservable modes on the imaginary axis. These conditions are equivalent to the uniqueness of solutions of (A.9), which means that the matrix P is unique. It then computes the matrix K by solving the associated Riccati equation (A.9) and outputs both K, the matrix P

and the eigenvalues of the closed-loop system.

A.3 Optimal control of PDEs

Here we state some basic results from the theory of optimal control of PDEs that are useful for the construction of our algorithm to find the optimal position of the point actuators. This is an area that has seen considerable progress in the last decade, and for a comprehensive study of the most general results on this field see [141, 211]. There, one can find proof of existence of an optimal control for general PDEs, as well as uniqueness of such controls in the case when the problem is convex. These results assume that the nonlinearities present in the problem are Lipschitz continuous and Fréchet differentiable. We adapted the proof of existence of an optimal control to the case when the nonlinearity is of the form uu_x in Chapter 2.

The problem we considered can be generally written in the form

$$\begin{aligned}
\text{minimise} \quad & \mathcal{C}\,(u, f) && \text{(A.10a)}\\
\text{subject to} \quad & u_t + \mathcal{A}u + \mathcal{N}(u) = f(x,t), && \text{(A.10b)}\\
& u(x,0) = u_0(x) \in \dot{H}^2_p(0, 2\pi), && \text{(A.10c)}\\
& \frac{\partial^j u}{\partial x^j}(x + 2\pi) = \frac{\partial^j u}{\partial x^j}(x), && \text{(A.10d)}\\
& f \in F_{ad}, && \text{(A.10e)}
\end{aligned}$$

where $\mathcal{C}$ is a quadratic cost, $\mathcal{A}$ is a linear operator, $j = 0, 1, \ldots, k$ (k is the highest order derivative present in $\mathcal{A}$), $\mathcal{N}$ is the nonlinearity (which may depend on u_x) and F_{ad} is the space of admissible controls, usually a bounded and convex subset of L^2.

In this case, one can write the cost functional as a function of the control f only, by defining a control-to-state operator $\mathcal{G}$ such that $u = u(f) = \mathcal{G}(f)$. Using this, we can obtain a reduced cost functional

$$\mathcal{J}(f) := \mathcal{C}(\mathcal{G}(f), f) = \mathcal{C}(u, f).$$

Under the correct assumptions on the operators involved, the functional $\mathcal{J}$ is Fréchet differ-

entiable, and therefore we can take its derivative to obtain the variational inequality

$$\mathcal{J}'(\bar{f})(f-\bar{f}) \geq 0, \quad \forall f \in F_{ad}, \tag{A.11}$$

which needs to be verified by any locally optimal control $\bar{f}$. Using the chain rule, one can write the variational inequality (A.11) in terms of $\bar{f}$, $\bar{u} = \mathcal{G}(\bar{f})$ and u, where u is the solution to a linearised version of the state equation, which can be eliminated by means of an adjoint state $p(x,t)$. It can then be proved that the variational inequality (A.11) can be written in the form

$$\int_0^T \int_0^{2\pi} \left(p + \varphi_f(x,t,\bar{u}\bar{f})\right)(f-\bar{f})\, dx\, dt \geq 0, \quad \forall f \in F_{ad}, \tag{A.12}$$

where φ is the component of the cost functional that penalises the controls (usually $\|f\|^2_{L^2}$) and the subscript f means we are taking the Fréchet derivative with respect to f.

We use a simpler way of obtaining the adjoint operator p and the variational inequality (A.12) directly, by looking at $p(x,t)$ as a Lagrange multiplier. We therefore look at the problem as a nonlinear optimisation problem - see [161] - and define the Lagrangian

$$\mathcal{L}(u,p,f) = \mathcal{C}(u,f) - \int_0^T \int_0^{2\pi} (u_t + \mathcal{A}u + \mathcal{N}(u) - f(x,t))\, p(x,t)\, dx\, dt. \tag{A.13}$$

In this context, the first order necessary conditions are knwon as Karush-Kuhn-Tucker (KKT) conditions and are stated in the following way: if $\bar{f}$ and $\bar{u} = \mathcal{G}(\bar{f})$ are a local minimiser of (A.10), then $\bar{u},\ \bar{f}$ and $\bar{p}$ minimise the Lagrangian (A.13) and therefore we have the following:

1. $\bar{u}$ is a solution of $\mathcal{L}_p(\bar{u},\bar{p},\bar{f}) = 0$ which gives the state equation (A.10b),
2. $\bar{p}$ solves the adjoint equation, which is given by $\mathcal{L}_u(\bar{u},\bar{p},\bar{f}) = 0$ and
3. $\bar{f}$ verifies the variational inequality $\mathcal{L}_f(\bar{u},\bar{p},\bar{f}) \geq 0$.

Therefore, by taking the Fréchet derivative of the Lagrangian with respect to u and f we can easily obtain the adjoint equation and the variational inequality that needs to be verified.

Since these are only necessary conditions, there is the possibility that a pair $\bar{u}$, $\bar{f}$ verifying the KKT conditions is not a minimiser of the optimal control problem. We did not come across this difficulty in our computations, but if needed, we can exclude such pairs by

differentiating a second time, and deriving the second order sufficient conditions for a pair $\bar{u}$, $\bar{f}$ to be a minimiser [100, 211, 226].

A.4 Linear Algebra

In order to solve the matrix problem presented in Chapter 4, we made use of the following Lemmas, which can be found in any matrix analysis textbook, *e.g.* [102]:

Lemma 1 (Matrix-Determinant Lemma)**.** *For an invertible $N \times N$ matrix A, and $N \times m$ matrix B and $m \times N$ matrix K, where $m < N$, we have the following identity:*

$$\det(A + BK) = \det(A) \det(I_{m\times m} + KA^{-1}B). \tag{A.14}$$

Corollary 1 (Matrix Determinant Lemma - rank one version)**.** *For an invertible $N \times N$ matrix A and $N \times 1$ vectors* $\mathbf{u}$ *and* $\mathbf{v}$*, we have the following identity:*

$$\det(A + \mathbf{u}\mathbf{v}^t) = \det(A)(1 + \mathbf{v}^t A^{-1}\mathbf{u}). \tag{A.15}$$

If A is not invertible, then we have the following version:

$$\det(A + \mathbf{u}\mathbf{v}^t) = \det(A) + \mathbf{v}^t \operatorname{adj}(A)\mathbf{u}. \tag{A.16}$$

Lemma 2 (Woodbury Matrix Identity)**.** *For an $N \times N$ matrix A, $N \times m$ matrix B and $m \times N$ matrix K, we have the following identity:*

$$(A + BK)^{-1} = A^{-1} - A^{-1}B(I_{m\times m} + KA^{-1}B)^{-1}KA^{-1}. \tag{A.17}$$

Corollary 2 (Sherman Morrison Formula)**.** *Let A be an $N \times N$ matrix and* $\mathbf{u}$ *and* $\mathbf{v}$ *be $N \times 1$ vectors. We have the following expansion of the rank one perturbation of the inverse of the matrix A:*

$$(A + \mathbf{u}\mathbf{v}^t)^{-1} = A^{-1} - \frac{A^{-1}\mathbf{u}\mathbf{v}^t A^{-1}}{1 + \mathbf{v}^t A^{-1}\mathbf{u}}. \tag{A.18}$$

Appendix B

Discretisation of the nonlinear terms

For our numerical methods used in Chapters 2, 4 and 5, we need to discretise the various nonlinear terms appearing in the equations. Consider f, g two functions in $L^2_p(0, 2\pi)$. We can write them as

$$f(x,t) = \frac{f_0(t)}{\sqrt{2\pi}} + \sum_{n=1}^{\infty} f_n^s(t)\frac{\sin(nx)}{\sqrt{\pi}} + \sum_{n=1}^{\infty} f_n^c(t)\frac{\cos(nx)}{\sqrt{\pi}},$$

$$g(x,t) = \frac{g_0(t)}{\sqrt{2\pi}} + \sum_{n=1}^{\infty} g_n^s(t)\frac{\sin(nx)}{\sqrt{\pi}} + \sum_{n=1}^{\infty} u_n^g(t)\frac{\cos(nx)}{\sqrt{\pi}}.$$

We multiply them together to obtain

$$(fg)(x,t) = \frac{b_0}{\sqrt{2\pi}} + \sum_{j=1}^{\infty}\left(a_j(t)\frac{\sin(jx)}{\sqrt{\pi}} + b_j(t)\frac{\cos(jx)}{\sqrt{\pi}}\right), \tag{B.1}$$

where

$$a_j = \frac{1}{2\sqrt{\pi}}\sum_{m+n=j}(f_m^s g_n^c + f_m^c g_n^s) + \frac{1}{2\sqrt{\pi}}\sum_{m-n=j}(f_m^s g_n^c - f_m^c g_n^s - f_n^s g_m^c + f_n^c g_m^s)$$

and

$$b_j = \frac{1}{2\sqrt{\pi}}\sum_{m+n=j}(f_m^c g_n^c - f_m^s g_n^s) + \frac{1}{2\sqrt{\pi}}\sum_{m-n=j}(f_m^s g_n^s + f_m^c g_n^c + f_n^s g_m^s + f_n^c g_m^c).$$

B.1 $\mathcal{N}(u) = uu_x$

We differentiate equation (B.1) with respect to x and use trigonometric identities to find that

$$(fg)_x = \sum_{j=1}^{\infty} c_j(t)\frac{\sin(jx)}{\sqrt{\pi}} + d_j(t)\frac{\cos(jx)}{\sqrt{\pi}},$$

where

$$c_j = \frac{j}{2\sqrt{\pi}} \sum_{m+n=j} (f_n^s g_m^s - f_n^c g_m^c) - \frac{j}{2\sqrt{\pi}} \sum_{m-n=j} (f_n^s g_m^s + f_n^c g_m^c + f_m^s g_n^s + f_m^c g_n^c)$$

and

$$d_j = \frac{j}{2\sqrt{\pi}} \sum_{m+n=j} (f_n^s g_m^c - f_n^c g_m^s) + \frac{j}{2\sqrt{\pi}} \sum_{m-n=j} (f_n^c g_m^s - f_n^s g_m^c - f_m^c g_n^s + f_m^s g_n^c)$$

By replacing $f = u$, $g = \frac{u}{2}$, we obtain

$$uu_x = \left(\frac{u^2}{2}\right)_x = \sum_{n=1}^{\infty} g_n^s(t)\frac{\sin(nx)}{\sqrt{\pi}} + g_n^c(t)\frac{\cos(nx)}{\sqrt{\pi}},$$

where

$$g_n^s = \frac{n}{4\sqrt{\pi}} \sum_{j+k=n} (u_j^c u_k^c - u_j^s u_k^s) + \frac{n}{2\sqrt{\pi}} \sum_{j-k=n} (u_j^c u_k^c + u_j^s u_k^s),$$

$$g_n^c = -\frac{n}{2\sqrt{\pi}} \sum_{j+k=n} u_j^c u_k^s + \frac{n}{2\sqrt{\pi}} \sum_{j-k=n} (u_j^c u_k^s - u_j^s u_k^c).$$

B.2 $\mathcal{N}(u, p) = up_x$

Replacing $f = u$, $g = p_x$ in equation (B.1) , we obtain

$$(up_x) = \frac{g_0}{\sqrt{2\pi}} + \sum_{n=1}^{\infty} g_n^s(t)\frac{\sin(nx)}{\sqrt{\pi}} + g_n^c(t)\frac{\cos(nx)}{\sqrt{\pi}},$$

where

$$g_n^s = \frac{1}{2\sqrt{\pi}} \sum_{j+k=n} k(u_j^s p_k^s - u_j^c p_k^c) + \frac{1}{2\sqrt{\pi}} \sum_{j-k=n} \left(k(u_j^s p_k^s + u_j^c p_k^c) - j(u_k^s p_j^s + u_k^c p_j^c)\right),$$

$$g_n^c = \frac{1}{2\sqrt{\pi}} \sum_{j+k=n} k(u_j^c p_k^s + u_j^s p_k^c) + \frac{1}{2\sqrt{\pi}} \sum_{j-k=n} \left(k(u_j^c p_k^s - u_j^s p_k^c) + j(u_k^c p_j^s - u_k^s p_j^c) \right).$$

B.3 $\mathcal{N}(u) = (u_x)^2$

Finally, replacing $f = g = u_x$ in equation (B.1), we obtain

$$(u_x^2) = \sum_{n=1}^{\infty} g_n^s(t) \frac{\sin(nx)}{\sqrt{\pi}} + g_n^c(t) \frac{\cos(nx)}{\sqrt{\pi}},$$

where

$$g_n^s = -\frac{1}{2\sqrt{\pi}} \sum_{j+k=n} jk(u_j^s u_k^c + u_j^c u_k^s) - \frac{1}{\sqrt{\pi}} \sum_{j-k=n} jk(u_j^c u_k^s - u_j^s u_k^c),$$

$$g_n^c = \frac{1}{2\sqrt{\pi}} \sum_{j+k=n} jk(u_j^s u_k^s - u_j^c u_k^c) + \frac{1}{\sqrt{\pi}} \sum_{j-k=n} jk(u_j^c u_k^c + u_j^s u_k^x).$$

Appendix C

Implementation of the algorithm derived in Section 4.3.1 to solve equation (4.40)

We solved the matrix equation (4.40) by implementing our algorithm in MATLAB. Given a diagonal matrix A, a matrix B and the desired eigenvalues of matrix D, we used a nonlinear solver to solve the system of N equations (4.47) for $m = 1$ and (4.52) for $m > 1$. We note that when only one control is used ($m = 1$), then we have a system of N equations for N unknowns and therefore we use Newton's method. For $m > 1$, the problem is underdetermined and we may use a least-squares method. We use the Levenberg-Marquardt algorithm [139, 156].

We solved the problem for various values of N and m and different matrices A and B. We first give the relevant case for the stochastic Kuramoto-Sivashinsky equation. We wish to maintain the negative eigenvalues and change the positive ones to a value that will allow the prescribed trace for the matrix D. For the purposes of this test, we will have

$$\mu_j = \begin{cases} 2a_j & \text{if } a_j < 0, \\ -a_j & \text{if } a_j > 0, \\ -0.1 & \text{if } a_j = 0. \end{cases} \tag{C.1}$$

We used $\nu = 0.5$, which (if we ignore the zero entry) has two positive entries in matrix A. In this case, it makes sense to use $m = 2$ and we chose $x_1 = \frac{\pi}{3}$ and $x_2 = \frac{5\pi}{3}$.

We make a further implementation of our algorithm. For this implementation we generate a vector $\mathbf{a}$ with N entries randomly distributed, following a Gaussian law with mean zero

and variance 1. We define the initial $\boldsymbol{\mu}_0 = 2\mathbf{a}$ and change 1, 2 or 3 of its elements to obtain the $\boldsymbol{\mu}$ that we require, we then use $m = 1,\ 2$ or 3 controls, respectively, to obtain the matrix K that gives us the desired eigenvalues. We specify below the randomly generated matrix B and vector $\mathbf{a}$ we use.

$$\mathbf{a} = \begin{bmatrix} 1.2616 \\ 0.4754 \\ 1.1741 \\ 0.1269 \\ -0.6568 \\ -1.4814 \\ 0.1555 \\ 0.8186 \\ -0.2926 \\ -0.5408 \\ -0.3086 \\ -1.0966 \\ -0.4930 \\ -0.1807 \\ 0.0458 \\ -0.0638 \\ 0.6113 \\ 0.1093 \\ 1.8140 \\ 0.3120 \end{bmatrix} \qquad B = \begin{bmatrix} 1.8045 & -0.4251 & 0.9421 \\ -0.7231 & 0.5894 & 0.3005 \\ 0.5265 & -0.0628 & -0.3731 \\ -0.2603 & -2.0220 & 0.8155 \\ 0.6001 & -0.9821 & 0.7989 \\ 0.5939 & 0.6125 & 0.1202 \\ -2.1860 & -0.0549 & 0.5712 \\ -1.3270 & -1.1187 & 0.4128 \\ -1.4410 & -0.6264 & -0.9870 \\ 0.4018 & 0.2495 & 0.7596 \\ 1.4702 & -0.9930 & -0.6572 \\ -0.3268 & 0.9750 & -0.6039 \\ 0.8123 & -0.6407 & 0.1769 \\ 0.5455 & 1.8089 & -0.3075 \\ -1.0516 & -1.0799 & -0.1318 \\ 0.3975 & 0.1992 & 0.5954 \\ -0.7519 & -1.5210 & 1.0468 \\ 1.5163 & -0.7236 & -0.1980 \\ -0.0326 & -0.5933 & 0.3277 \\ 1.6360 & 0.4013 & -0.2383 \end{bmatrix}.$$

We then extracted, for each N, the first N rows of $\mathbf{a}$ and B to generate the matrices A and B, respectively. In the case of matrix B, we extract its first column when $m = 1$, the first two columns for $m = 2$ and the three columns when $m = 3$. Finally, the initial guess for the matrix K is the zero matrix, with ones in the position k_{jj}, $j = 1, \ldots, m$. We limit the function count to 5000.

We define two types of error for this problem:

- Error 1 is defined by how far are the obtained eigenvalues μ_k from the prescribed ones

($\bar{\mu}_k$):

$$E_1 = \sqrt{\sum_{k=1}^{N} (\mu_k - \bar{\mu}_k)^2}$$

- Error 2 is defined by how far the obtained trace is from $\sum_{k=1}^{N} \bar{\mu}_k$:

$$E_2 = \left| \mathrm{Tr}(2A + BK + K^t B^t) - \sum_{k=1}^{N} \bar{\mu}_k \right|.$$

Control of the stochastic Kuramoto-Sivashinsky equation

The convergence results for the stochastic Kuramoto-Sivashinsky equation are:

N	2	4	6	8	10	12	14
Run time (s)	0.05	0.16	1.09	4.29	23.30	97.43	495.13
Nr of iterations	10	16	24	18	17	17	18
Function Count	57	162	345	349	415	499	614
E_1	0.0014	0.0688	0.1217	0.0933	0.0880	0.0784	0.1047
E_2	2.6×10^{-9}	2.6×10^{-4}	0.0055	0.0110	0.0165	0.0349	0.0144

Table C.1: Results of the numerical method for the solution of the matrix problem for the sKS equation with $\nu = 0.5$.

Control of randomly generated matrices

For the case $m = 1$, we changed the first entry of $\boldsymbol{\mu}$ to $\mu_1 = 2$, while for $m = 2$ we change the first and second entries as $\mu_1 = 2$, $\mu_2 = 1$. Finally, for $m = 3$ we chose$\mu_1 = 2$, $\mu_2 = 1$, $\mu_3 = 1.5$. We obtained the following results, which are presented in tables 2-4.

Case $m = 1$:

N	4	5	6	7	8	9	10
Run time (s)	2.00	3.47	12.92	37.1	78.77	155.87	317.93
Nr of iterations	395	316	513	665	607	536	490
Function Count	1920	1847	3514	5006	5000	5001	5001
E_1	0.0201	0.0195	0.0188	0.0213	0.0808	0.1145	0.1158
E_2	9.4×10^{-4}	0.0015	0.0033	0.0032	0.0166	0.0284	0.0312

Table C.2: Results of the numerical method for the solution of the general case with $m = 1$.

Case $m = 2$:

N	4	5	6	7	8	9	10
Run time (s)	0.39	0.32	0.54	1.89	3.04	10.47	23.30
Nr of iterations	49	14	11	18	13	19	20
Function Count	475	174	163	297	246	392	454
E_1	0.0179	0.0178	0.0170	0.0185	0.0271	0.0263	0.0251
E_2	7.9×10^{-4}	0.0013	0.0029	0.0027	8×10^{-4}	0.0010	0.0015

Table C.3: Results of the numerical method for the solution of the general case with $m = 2$.

Case $m = 3$:

N	4	5	6	7
Run time (s)	0.56	1.26	2.96	8.23
Nr of iterations	11	13	9	16
Function Count	156	240	205	389
E_1	6.9×10^{-15}	9.8×10^{-15}	6.7×10^{-15}	6.6×10^{-15}
E_2	1.78×10^{-15}	1.8×10^{-15}	1.8×10^{-15}	$< 10^{-16}$

N	8	9	10
Run time (s)	14.74	36.51	75.15
Nr of iterations	12	17	17
Function Count	337	518	572
E_1	4.9×10^{-15}	1×10^{-14}	3.1×10^{-14}
E_2	8.9×10^{-16}	4.4×10^{-16}	1.8×10^{-15}

Table C.4: Results of the numerical method for the solution of the general case with $m = 3$.

The high level of accuracy for the sKS equation is explained through the fact that the matrix B has a regular structure and there are repeated eigenvalues. We observe that the algorithm converges faster when the distance between the diagonal entries of $2A$ and the required eigenvalues is small. There may be difficulties in wanting to make a perturbation that is too large, and this idea would still need to be quantified.

It is noteworthy that the performance of our algorithm improves when m increases. This is due to the fact that for larger m we have an increased number of degrees of freedom, which makes our algorithm more versatile in terms of obtaining the correct eigenvalues.

Appendix D

Eigenvalues and eigenfunctions of System (5.1)

To obtain the eigenvalues and eigenfunctions of System (5.1), we will consider the linear system

$$\left\{ \begin{array}{rcl} u_{1,t} & = & -\nu u_{1,xxxx} - u_{1,xx} - \alpha_1 u_{2,xx} \\ u_{2,t} & = & -\nu u_{2,xxxx} - u_{2,xx} - \alpha_2 u_{1,xx}, \end{array} \right. \tag{D.1}$$

in the interval $(0, 2\pi)$, with periodic boundary conditions and initial conditions $u_1(x,0) = u_{10}(x)$ and $u_2(x,0) = u_{20}(x)$ and $u_{10},\ u_{20} \in \dot{H}^2_p(0,2\pi)$.

We assume that the solution of System (D.1) is of the form

$$U(x,t) = \left[\begin{array}{c} u_1(x,t) \\ u_2(x,t) \end{array} \right] = \sum_{k\in\mathbb{Z}} \left[\begin{array}{c} a_1 \\ a_2 \end{array} \right] e^{\lambda t + ikx} = e^{\lambda t + ikx} \underline{\mathrm{a}}. \tag{D.2}$$

Substituting (D.2) in (D.1) we obtain, for each $k \in \mathbb{Z}$

$$\lambda \underline{\mathrm{a}} = \left[\begin{array}{cc} -\nu k^4 + k^2 & \alpha_1 k^2 \\ \alpha_2 k^2 & -\nu k^4 + k^2 \end{array} \right] \underline{\mathrm{a}} = L \underline{\mathrm{a}}. \tag{D.3}$$

λ is then an eigenvalue of matrix L and verifies:

$$(-\nu k^4 + k^2 - \lambda)^2 - \alpha_1 \alpha_2 k^4 = 0.$$

The solutions to this equation are

$$\lambda_{\pm} = -\nu k^4 + k^2(1 \pm \sqrt{\alpha_1 \alpha_2}). \tag{D.4}$$

The eigenfunctions associated to these eigenvalues verify the equation $(L - \lambda I)\underline{a} = 0$, or

$$\left\{ \begin{array}{rcl} \left[-\nu k^4 + k^2 - (-\nu k^4 + k^2(1 \pm \sqrt{\alpha_1 \alpha_2}))\right] a_1 + \alpha_1 k^2 a_2 & = & 0 \\ \alpha_2 k^2 a_1 + \left[-\nu k^4 + k^2 - (-\nu k^4 + k^2(1 \pm \sqrt{\alpha_1 \alpha_2}))\right] a_2 & = & 0 \end{array} \right.$$

$$\Leftrightarrow \left\{ \begin{array}{rcl} \pm\sqrt{\alpha_1 \alpha_2} a_1 & = & \alpha_1 a_2 \\ \pm\sqrt{\alpha_1 \alpha_2} a_2 & = & \alpha_2 a_1 \end{array} \right.$$

And a particular solution to this equation is

$$\left[\begin{array}{c} a_1 \\ a_2 \end{array} \right] = \left[\begin{array}{c} \sqrt{\alpha_1} \\ \pm\sqrt{\alpha_2} \end{array} \right].$$

This means that, for each $k \in \mathbb{Z}$, the eigenvalue $\lambda_{k+} = -\nu k^4 + k^2 \left(1 + \sqrt{\alpha_1 \alpha_2}\right)$ is associated with the eigenfunction $e^{ikx} \left[\begin{array}{c} \sqrt{\alpha_1} \\ \sqrt{\alpha_2} \end{array} \right]$ and the eigenvalue $\lambda_{k-} = -\nu k^4 + k^2 \left(1 - \sqrt{\alpha_1 \alpha_2}\right)$ is associated with the eigenfunction $e^{ikx} \left[\begin{array}{c} \sqrt{\alpha_1} \\ -\sqrt{\alpha_2} \end{array} \right]$.

In the more general case when the coupling is also through the fourth order derivatives,

$$\left\{ \begin{array}{rcl} u_{1,t} & = & -\nu u_{1,xxxx} - u_{1,xx} - u_1 u_{1,x} - \alpha_1 u_{2,xx} - \beta_1 u_{2,xxxx} \\ u_{2,t} & = & -\nu u_{2,xxxx} - u_{2,xx} - u_2 u_{2,x} - \alpha_2 u_{1,xx} - \beta_2 u_{1,xxxx}, \end{array} \right. \tag{D.5}$$

we can still compute the relevant eigenvalues and eigenfunctions, and these are

$$\lambda_{\pm} = -\nu k^4 + k^2(1 \pm \sqrt{(\alpha_1 - \beta_1 k^2)(\alpha_2 - \beta_2 k^2)}) \tag{D.6}$$

associated with the eigenfunctions

$$e^{ikx} \left[\begin{array}{c} \sqrt{\alpha_1 - \beta_1 k^2} \\ \pm\sqrt{\alpha_2 - \beta_2 k^2} \end{array} \right].$$